Faculty of Engineering of the University of Porto



Design of a heat pump for domestic hot water using natural refrigerant transcritical CO_2

Daniel Alexandre Meira Ferreira

Master in Mechanical Engineering

Major Fluids and Energy

Supervisor at FEUP: Carlos Pinho

Supervisor at RACE: Nuno João Moreira

Porto, July 2022

Abstract

The present work focuses on the designing of a transcritical CO_2 heat pump and on studying the main parameters that can affect its performance. In order to accomplish that, the primary objective was to develop a thermodynamic model that would allow simulating, through EES software, the operation of the heat pump. In addition, it is also studied the potential of an NH_3 heat pump for domestic hot water and the main parameters that can affect their performance. Based on the simulation results, a component selection is also made.

Results from the first simulations show that the gas cooler pressure is the control parameter with the highest effect on the performance of the heat pump. For the gas cooler pressure, it is observed that the optimum value increases with an increase in the gas cooler exit temperature of the refrigerant. Besides that, it is shown that even though evaporation temperature has some effect on the optimum value, it can be considered minimal when compared to the influence of the gas cooler exit temperature.

Final simulations are done for both heat pumps using the same thermodynamic cycles. However, the geometric and thermodynamic properties of the selected heat exchangers are used in order to confirm the viability of the components. In addition, using the designed heat exchanger properties allow the influence of the water conditions to be analyzed. The results from these simulations show that the performance of the heat pump is significantly impacted by the temperature of the water entering the gas cooler. Specifically, if the water inlet temperature is increased then the COP value declines. COP decreases by 21 % when increasing water inlet temperature from 10 to 25 ºC. Since this increase also leads to an increase in the refrigerant outlet temperature of the gas cooler, the optimum pressure is also increased. The influence of the ambient air temperature is also measured. It is shown, as expected, that the ambient air temperature has the biggest effect on the performance of the heat pump. Results indicate that, when varying the ambient air temperature from 10 ºC to 25 ºC, compressor efficiency increases from 70 to 80 % due to the decrease of the pressure ratio, and the COP value increases significantly from 3.508 at 10 ºC to 4.597 at 25 ºC. Finally, the comparison with the NH_3 heat pump shows that the performance of the heat pump is greatly improved by using ammonia as the working fluid. According to the findings, the COP value in the NH_3 arrangement is 35 % higher under the same design parameters. When considering 25 ºC as the ambient air temperature, this value rises by up to 96 %.

Resumo

O presente trabalho centra-se no projeto de uma bomba de calor a CO_2 transcrítico e no estudo dos principais parâmetros que podem afectar o seu desempenho. Para o conseguir, o objectivo principal era desenvolver um modelo termodinâmico que permitisse simular, através do EES, o funcionamento da bomba de calor. Além disso, estudou-se também o potencial de uma bomba de calor a NH_3 para aquecimento de águas sanitárias e os principais parâmetros que podem afectar o seu desempenho. Com base nos resultados da simulação, é também feita uma selecção de componentes.

Os resultados das primeiras simulações mostram que a pressão do arrefecedor de gás é o parâmetro de controlo com maior efeito no desempenho da bomba de calor. Para a pressão do arrefecedor de gás, observa-se que o valor óptimo aumenta consideravelmente com um aumento da temperatura de saída do arrefecedor de gás do CO_2. Além disso, mostra-se que, embora a temperatura de evaporação tenha algum efeito sobre o valor óptimo, pode ser considerada mínima quando comparada com a influência da temperatura de saída do arrefecedor de gás.

As simulações finais são feitas para ambas as bombas de calor utilizando os mesmos ciclos termodinâmicos. No entanto, as propriedades geométricas e termodinâmicas dos permutadores de calor seleccionados são utilizadas a fim de confirmar a viabilidade dos componentes. Além disso, a utilização das propriedades do permutadores de calor selecionados permite analisar a influência das condições da água. Os resultados destas simulações mostram que o desempenho da bomba de calor é significativamente afectado pela temperatura de entrada da água a aquecer, sendo que o COP diminui 21% ao aumentar a temperatura da entrada da água de 10 para 25 ºC. Uma vez que este aumento leva também a um aumento da temperatura de saída do CO_2 do arrefecedor de gás, a pressão óptima é também aumentada. Além disso, demonstra-se que a temperatura do ar ambiente tem o maior efeito sobre o desempenho da bomba de calor. Os resultados indicam que, ao variar a temperatura do ar ambiente de 10 ºC para 25 ºC, a eficiência do compressor aumenta de 70 para 80% devido à diminuição da razão de pressão, e o valor COP aumenta significativamente de 3,508 a 10 ºC para 4,597 a 25 ºC. Finalmente, a comparação com a bomba de calor a NH_3 mostra que o desempenho desta é superior. De acordo com os resultados, o valor COP no sistema NH_3 é 35 % mais elevado sob os mesmos parâmetros de projeto. Ao considerar 25 ºC como temperatura ambiente, este valor aumenta até 96 %.

Acknowledgments

First of all, I would like to thank all people that are part of RACE SA for the opportunity to develop this project with their continuous cooperation.

To my supervisor at RACE, Engineer João Moreira, thank you for your patience and for all the help, knowledge, and experience you have given.

I thank the technicians who were willing to help in the selection of the various components, as well as in the supply of the technical reports of the same.

To my supervisor at FEUP, Professor Carlos Pinho, for the tireless mentorship from the first moment to the last. Without the knowledge and experience, the realization of this dissertation would have been much more difficult.

A warm thank you to all the friends that these years have brought me. For all the fun times, but also for all the help that such a journey requires. You have given me the greatest laughter and the greatest emotions, and I am honored to finish this journey by your side.

Finally, the most special thank you has to go to my family. Mom, dad, and brother, thank you for guiding me through this journey right from the beginning. If today I am able to finish this goal, I owe it completely to you and your support. It was thanks to your education and affection that this path became possible.

Table of Contents

Abstract ..... **i**
Resumo ..... **iii**
Acknowledgments ..... **v**
List of figures ..... **x**
List of tables ..... **xiv**
Nomenclature ..... **xv**
1. Introduction **1**
1.1. Current energy context 1
1.1.1. Decarbonized energy 1
1.1.2. Energy access and sustainable development 4
1.1.3. Economic activity correlation 7
1.1.4. Energy in the buildings sector 8
1.2. Use of carbon dioxide (CO_2) as working fluid in heat pump 9
1.3. Company RACE 11
1.4. Objectives of the dissertation 12
1.5. Structure of the dissertation 13
2. Literature review **15**
2.1. Refrigeration and heat pump cycles 15
2.2. Lorentz cycle 18
2.3. Transcritical versus subcritical CO_2 cycle 19
2.4. Working fluids for heat pumps 24
2.4.1. CO_2 (R744) thermodynamic properties 24
2.4.2. Comparison between refrigerants 25
3. State-of-the-art CO_2 transcritical heat pump **33**
3.1. Market overview 33
3.2. Energy sources 33
3.2.1. Air source heat pump (ASHP) 34
3.2.2. Water source heat pump (WSHP) 34
3.2.3. Ground source heat pump (GSHP) 34
3.3. Transcritical CO_2 cycle modifications 35
3.3.1. Internal heat exchanger 36
3.3.2. Multistage compression 37
3.3.3. Ejector 38
3.3.4. Vortex tube expansion 39
3.3.5. Expander 39
3.3.6. Flash gas bypass 40
3.3.7. Parallel compression 41
3.3.8. Comparison between configurations 41
3.4. Application areas 42
3.5. NH_3 research 43
4. Component design **45**

4.1. Compressor 45
4.2. Heat exchangers 47
4.2.1. Gas cooler 48
4.2.2. Evaporator 50
4.2.3. Internal heat exchanger 51
4.3. Expansion device 52
4.4. Accessories 53
4.4.1. Suction line accumulator 53
4.4.2. Oil separator 53
4.4.3. Oil receiver 54
4.4.4. Filters 54
4.4.5. Check valves 55
4.4.6. Sight glass 55
4.5. Issues related to component design 55
4.5.1. Throttling loss 55
4.5.2. Pressure drop 56
5. Simulation of cycles 57
5.1. CO_2 thermodynamic model 57
5.1.1. Compressor 57
5.1.2. Gas cooler 58
5.1.3. Evaporator 59
5.1.4. Expansion valve 60
5.1.5. Internal heat exchanger 60
5.1.6. Perfomance 61
5.2. CO_2 conventional cycle 61
5.3. CO_2 cycle with IHX 64
5.4. CO_2 cycles simulation analysis 66
5.4.1. Gas cooler optimal pressure 66
5.5. NH_3 conventional cycle 72
5.6. NH_3 cycle with IHX 76
5.7. NH_3 cycles simulation analysis 78
5.8. Comparison between CO_2 and NH_3 simulations 79
6. Component selection 83
6.1. Transcritical CO_2 system 83
6.1.1. Compressor 83
6.1.2. System piping 85
6.1.3. Gas cooler 89
6.1.4. Evaporator 90
6.1.5. Internal heat exchanger (IHX) 90
6.1.6. Expansion valve 91
6.1.7. Accessories 93
6.1.8. Economic analysis 97
6.2. Subcritical NH_3 system 98
6.2.1. Compressor 98

6.2.2. Piping 99
6.2.3. Condenser 100
6.2.4. Evaporator 100
6.2.5. Desuperheater 101
6.2.6. Expansion valve 101
6.2.7. Accessories 101
6.2.8. Economic analysis 102
6.3. Dimensions and refrigerant charge 102
6.3.1. CO_2 heat pump 103
6.3.2. NH_3 heat pump 104
6.4. Control system 105
7. CO_2 heat pump simulation with selected components 107
7.1. Gas cooler 107
7.2. Results and discussion 109
7.2.1. Water inlet temperature 109
7.2.2. Ambient air temperature 111
7.3. Comparison with NH_3 heat pump 113
8. Domestic hot water heating 115
8.1. CO_2 heat pump water storage 115
8.2. DHW requirements 117
9. CO_2 system diagram 119
10. Conclusions 121
11. Further studies 125
References 127
Appendices 138
A. Comparison with other refrigerants 138
B. Other software results 139
C. Components full reports 140
D. Catalogs 162
E. Pressure drop 166
F. EES simulation results for the thermodynamic cycles 173
G. Results for EES simulations with components properties 174
H. EcoCute technical report 176
I. CO_2 system diagram 177
J. EES simulation codes 178

List of figures

Figure 1.1: Global energy demand: actual vs predicted [1]. 1
Figure 1.2: CO_2 emissions from energy and industrial processes from 2000 to 2030 [8]. 3
Figure 1.3: Final energy consumption in the EU in TWh [9]. 3
Figure 1.4: Evolution of the share of different energy sources [8]. 4
Figure 1.5: Current and projected evolution of electricity as a share of total final consumption [8] 4
Figure 1.6: Use of different energy sources in the different sectors [9]. 4
Figure 1.7: Current and projected annual average change in percentage points. 6
Figure 1.8: Gross domestic product and electricity use growth rates from 2011 to 2015 [22]. 7
Figure 1.9: Global share of buildings and construction final energy and emissions in 2019 [24]. 8
Figure 1.10: Main categories of technologies in the end-use subsector for buildings [29]. 9
Figure 1.11: Logo of RACE S.A. company [38]. 11
Figure 2.1: Schematic diagrams of (a) power cycles and (b) refrigeration and heat pump cycles [39]. 15
Figure 2.2: *T-s* and *P-h* diagrams for the ideal vapor-compression refrigeration cycle [40]..... 17
Figure 2.3: *T-s* diagram for the actual vapor-compression refrigeration cycle [40]. 17
Figure 2.4: *T-s* diagram of the ideal Lorentz cycle [43]. 18
Figure 2.5: *P-h* diagrams for (a) subcritical cycle (b) transcritical cycle. 20
Figure 2.6: Comparison between the heat rejection curve for R-134a and CO_2 [49]..... 21
Figure 2.7: Comparison of the pinch point for different gas cooler pressures [46]. 21
Figure 2.8: *COP* value for different gas cooler pressures and gas cooler exit temperatures [51]. 23
Figure 2.9: Influence of the optimum gas cooler pressure on the heating capacity and compressor work [55]. 23
Figure 2.10: c_p and density values for different temperatures and pressures [58]. 24
Figure 2.11: Prandtl number value for different temperatures and pressures [58]. 24
Figure 2.12: Phase diagram for carbon dioxide (CO_2) [44]. 27
Figure 2.13: Refrigerant flammability classes [63]. 27
Figure 2.14: Volumetric refrigerating capacity comparison for R744 and other refrigerants [74]. 31
Figure 3.1: Main transcritical CO_2 cycle possible modifications. 36
Figure 3.2: $T - s$ diagram and schematic of the transcritical CO_2 cycle with the IHX addition [90]. 37
Figure 3.3: *P-h* diagram comparison of the transcritical CO_2 cycle with and without the IHX [55]. 37
Figure 3.4: Transcritical CO_2 multistage cycle with intercooler: (a) schematic and (b) *P-h* diagram (HP: high pressure, LP: low pressure) [94]. 38
Figure 3.5: Transcritical CO_2 ejector cycle: (a) schematic (b) *P-h* diagram [97]. 39
Figure 3.6: Transcritical CO_2 vortex tube expansion cycle: (a) schematic (b) *P-h* diagram [86]. 39
Figure 3.7: Schematic of the transcritical CO_2 cycle with an expander working (a) independently or (b) coaxially with the compressor [98]. 40
Figure 3.8: *P-h* diagram for the transcritical CO_2 cycle with an expander [55]. 40

Figure 3.9: $P-h$ diagram and schematic of the transcritical CO_2 cycle with flash tank bypass [86]. 41
Figure 3.10: *P-h* diagram and schematic of the transcritical CO_2 cycle with parallel compression [86]. 41
Figure 3.11: COP improvement of the different configurations [86]. 42
Figure 3.12: Optimum discharge pressure reduction of the different configurations [86]. 42
Figure 3.13: Main application areas for heat pump transcritical CO_2 cycle. 43
Figure 4.1: Main types of compressors. 46
Figure 4.2: SWEP brazed plate heat exchanger configuration [107]. 49
Figure 4.3: Plates with low theta pattern ($L\theta$) and high theta pattern ($H\theta$) and the different possible plate pattern conjugations [42]. 49
Figure 4.4: Schematic of the finned tube evaporator [109]. 51
Figure 4.5: Finned-tube evaporator with aluminum fins and copper tubes. 51
Figure 5.1: Schematic of the gas cooler model. 59
Figure 5.2: Schematic of the evaporator model. 59
Figure 5.3: Conventional CO_2 cycle: (a) *T-s* diagram (b) *P-h* diagram. 63
Figure 5.4: Schematic of the transcritical CO_2 cycle with the IHX addition [89]. 64
Figure 5.5: Transcritical CO_2 cycle with IHX: (a) *T-s* diagram (b) *P-h* diagram. 65
Figure 5.6: Effect of gas cooler pressure on COP of the IHX cycle at various gas cooler CO_2 exit temperatures $Tgce$. 67
Figure 5.7: Effect of gas cooler pressure on *COP* of the IHX cycle at various evaporation temperatures T_{evap}. 67
Figure 5.8: Influence of T_{gce} and T_{evap} on the optimal gas cooler pressure according to Equation (5.16). 68
Figure 5.9: Gas cooler outlet temperature T_{gce} influence on gas cooler optimal pressure ($P_{gc,opt}$) and *COP* with the addition of the IHX. 69
Figure 5.10: Evaporation temperature (T_{evap}) influence on gas cooler optimal pressure $P_{gc,opt}$ and *COP* with the addition of the IHX. 70
Figure 5.11: Schematic of the conventional NH_3 cycle. 73
Figure 5.12: Conventional NH_3 cycle: (a) *T-s* diagram (b) *P-h* diagram. 75
Figure 5.13: NH_3 cycle with IHX: (a) *T-s* diagram (b) *P-h* diagram. 76
Figure 5.14: COP dependence of $Tcond$ for different IHX efficiencies and the conventional configuration. 77
Figure 5.15: *COP* dependence on T_{evap} for the conventional and the IHX configurations. 79
Figure 5.16: *COP* and mass flow rate dependence of the evaporation temperature for the NH_3 and CO_2 configurations. 80
Figure 5.17: *COP* and T_{disch} values for different superheat and evaporation temperatures. 81
Figure 6.1: BITZER ECOLINE+ compressor [133]. 84
Figure 6.2: BITZER software selection output [131]. 84
Figure 6.3: SWEP B4TH gas cooler. 90
Figure 6.4: EEV software system results [137]. 92
Figure 6.5: CCMT4 mechanical and geometric properties [137]. 92
Figure 6.6: Danfoss CCMT 4 expansion valve [138]. 92
Figure 6.7: Technical drawing of the Danfoss CCMT 4 expansion valve [138]. 92

Figure 6.8: ESK technical data report for FA-CDH suction line accumulators [139]. 93
Figure 6.9: FA-CDH prototype [139]. 93
Figure 6.10: FA-CDH technical drawing [139]. 93
Figure 6.11: Dimension represented in Figure 6.10 [139]. 93
Figure 6.12: Temprite oil separator model 135A [141]. 95
Figure 6.13: Technical drawing of model 135A with the respective components [141]. 95
Figure 6.14: Carly's table of dimensions for the filter drier BCY-P14 487 [143]. 96
Figure 6.15: Technical dimensions of the filter drier [143]. 96
Figure 6.16: Core reference for the chosen shell [142]. 97
Figure 6.17: ESK catalog for available check valves for transcritical CO_2 operation [144]. 97
Figure 6.18: BITZER model W4NA. 99
Figure 6.19: Bitzer software outputs for the NH_3 compressor. 99
Figure 6.20: Example of a multiple EcoCute HPWH installation for a dormitory [145]. 104
Figure 6.21: Dimension of Y-Frame EcoCute HPWH [145]. 104
Figure 7.1: Q_{gc} and *COP* dependence on $T_{w,i}$ (T_{evap} = 0 ℃ and P_{gc} = 86 bar). 110
Figure 7.2: T_{gce}, T_{disch}, T_{suc} for four different $T_{w,i}$ (T_{evap} = 0 ℃ and P_{gc} = 86 bar). 110
Figure 7.3: $P_{gc,opt}$ and m_{CO2} dependence on $T_{w,i}$ (T_{evap}=0 ℃). 111
Figure 7.4: COP dependence on P_{gc} for four different $T_{w,i}$ (T_{evap}=0 ℃). 111
Figure 7.5: Q_{gc}, Q_{evap}, W_{comp} and *COP* dependence on T_{amb} (P_{gc} = 86 bar). 112
Figure 7.6: T_{gce}, T_{disch}, T_{suc} dependence on T_{amb} (P_{gc} = 86 bar). 112
Figure 7.7: p_r and η_{comp} dependence on T_{amb} (P_{gc} = 86 bar). 113
Figure 7.8: Difference between the values of Q_{gc}, Q_{evap}, W_{comp} and *COP* at different T_{amb} at optimal P_{gc} and at (P_{gc} = 86 bar) for different evaporation temperatures. 113
Figure 7.9: *COP* dependence on ambient temperature for the NH_3 and CO_2 configurations. 114
Figure 7.10: P_{evap}, P_{cond}, p_r dependence on ambient temperature for NH_3 and CO_2 configurations. 114
Figure 8.1: Schematic diagram of the system of DHW accumulation [150]. 117
Figure 9.1: Schematic of the CO_2 heat pump with the designed components (AutoCAD software). 119
Figure A.1: Properties of the most used refrigerants in heat pumps. 138
Figure B.1: Simple CO_2 one-stage plant software results [154]. 139
Figure C.1: CO_2 BITZER compressor 4GTE-20K (page 1/2). 141
Figure C.2: CO_2 BITZER compressor 4GTE-20K (page 2/2). 142
Figure C.3: CO_2 SWEP gas cooler B4THx90 (page 1/2). 143
Figure C.4: CO_2 SWEP gas cooler B4THx90 (page 2/2). 144
Figure C.5: CABERO evaporator CO2-ACHS S (page 1/2). 145
Figure C.6: CABERO evaporator CO2-ACHS S (page 2/2). 146
Figure C.7: CO_2 SWEP IHX B18Lx30 (page 1/2). 147
Figure C.8: CO_2 SWEP IHX B18Lx30 (page 2/2). 148
Figure C.9: CO_2 EEV Danfoss CCMT 4 (page 1/2). 149
Figure C.10: CO_2 EEV Danfoss CCMT 4 (page 2/2). 150
Figure C.11: CO_2 oil separator Temprite 135A (page 1/2). 151
Figure C.12: CO_2 oil separator Temprite 135A (page 2/2). 152
Figure C.13: NH_3 compressor Bitzer W4NA-K (page 1/2). 153

Figure C.14: NH_3 compressor BITZER W4NA-K (page 2/2)..... 154
Figure C.15: NH_3 condenser SWEP B10TSHx40 (page 1/3)..... 155
Figure C.16: NH_3 condenser SWEP B10TSHx40 (page 2/3)..... 156
Figure C.17: NH_3 condenser SWEP B10TSHx40 (page 3/3)..... 157
Figure C.18: NH_3 desuperheater SWEP B5THx18 (page 1/2)..... 158
Figure C.19: NH_3 desuperheater SWEP B5THx18 (page 2/2)..... 159
Figure C.20: NH_3 EEV Danfoss AKVA 10-7 (page 1/2)..... 160
Figure C.21: NH_3 EEV Danfoss AKVA 10-7 (page 2/2)..... 161
Figure D.1:Carly catalog for the selection of the cores for the filter drier..... 162
Figure D.2: ESK catalog for NH_3 liquid receivers..... 163
Figure D.3: ESK catalog for NH_3 suction line accumulators..... 164
Figure D.4: Temprite catalog for the selection of NH_3 oil separator..... 165
Figure E.1: Danfoss Coolselector2 NH_3 piping selection report (page 1/6)..... 167
Figure E.2: Danfoss Coolselector2 NH_3 piping selection report (page 2/6)..... 168
Figure E.3: Danfoss Coolselector2 NH_3 piping selection report (page 3/6)..... 169
Figure E.4: Danfoss Coolselector 2 NH_3 piping selection report (page 4/6)..... 170
Figure E.5: Danfoss Coolselector 2 NH_3 piping selection report (page 5/6)..... 171
Figure E.6: Danfoss Coolselector 2 NH_3 piping selection report (page 6/6)..... 172
Figure H.1: EcoCute technical report [145]..... 176
Figure I.1: CO_2 system diagram with the selected components..... 177
Figure J.1: EES simulation code for the CO_2 conventional heat pump cycle..... 180
Figure J.2: EES simulation code for the CO_2 with IHX heat pump cycle..... 183
Figure J.3: EES simulation code for the NH_3 conventional heat pump cycle..... 186
Figure J.4: EES simulation code for the NH_3 with IHX heat pump cycle..... 189
Figure J.5: EES simulation code and procedure control for determination of the outlet temperature of the heat exchangers based on waterside temperatures (CO_2 IHX configuration)..... 192
Figure J.6: EES simulation code and procedure control for determination of the outlet temperature of the heat exchangers based on waterside temperatures (NH_3 conventional configuration)..... 195

List of tables

Table 3.1: Current commercial market heat pumps for R744 and R717 and respective characteristics 33
Table 4.1: Characteristics of the different types of compressors 47
Table 5.1: 50 kW simulation inputs 63
Table 5.2: 50 kW simulation outputs 63
Table 5.3: State points simulation results (50 kW configuration) 64
Table 5.4: 50 kW with IHX simulation inputs 65
Table 5.5: 50 kW with IHX simulation outputs 65
Table 5.6: State points simulation results (50 kW with IHX configuration) 66
Table 5.7: Optimal gas cooler pressure results from the simulation iteration ($Tevap = 0\ ºC$) .. 69
Table 5.8: Different parameters values for different gas cooler pressures and IHX efficiencies . 71
Table 5.9: Conventional NH_3 cycle 50 kW simulation inputs 75
Table 5.10: Conventional NH_3 cycle 50 kW simulation outputs 75
Table 5.11: NH_3 cycle state points simulation results (50 kW configuration) 75
Table 5.12: Conventional NH_3 cycle 50 kW with IHX simulation inputs 77
Table 5.13: Conventional NH_3 cycle 50 kW with IHX simulation outputs 77
Table 5.14: NH_3 cycle state points simulation results (50 kW with IHX configuration) 77
Table 6.1: Compressor inputs in the BITZER software 83
Table 6.2: Recommended velocities for the different pipelines [118] 87
Table 6.3: CO_2 heat pump piping selection 89
Table 6.4: Gas cooler SWEP software inputs 89
Table 6.5: Gas cooler SWEP software outputs 89
Table 6.6: IHX SWEP software inputs 91
Table 6.7: IHX SWEP software outputs 91
Table 6.8: Temprite software inputs for the selection of the oil separator 94
Table 6.9: Chosen cores for the filters [142] 97
Table 6.10: Economical analysis for the CO_2 transcritical heat pump 98
Table 6.11: EES simulation results for the NH_3 configuration with a heat load of 58.4 kW 99
Table 6.12: NH_3 heat pump piping selection (Coolselector 2) 100
Table 6.13: Economic analysis for the NH_3 heat pump 102
Table 6.14: CHP-80Y EcoCute model dimensions and characteristics [145] 103
Table 7.1: COP value for the CO_2 and NH_3 and the calculated improvement 114
Table E.1: Selection of piping sizes for CO_2 heat pump 166
Table F.1: Parameters results from the EES simulations of different gas cooler capacities 173
Table G.1: EES simulation results for Tw, i =10, 15, 20 and 25 ºC 174
Table G.2: CO_2 heat pump simulation results for ambient temperatures from -5 to 25 ºC 174
Table G.3: NH_3 heat pump simulation results for ambient temperatures from -5 to 25 ºC 175

Nomenclature

Abbreviations	
ASHP	Air Source Heat Pump
BPHE	Brazed Plate Heat Exchanger
CFCs	Chlorofluorocarbons
COP	Coefficient Of Perfomance
DHW	Domestic Hot Water
DX	Direct Expansion
EEV	Electronic Expansion Valve
EU	European Union
HCs	Hydrocarbons
HCFCs	Hydrochlorofluorocarbons
HFCs	Hydrofluorocarbons
HFOs	Hydrofluoro-olefins
HPWH	Heat Pump Water Heater
GDP	Gross Domestic Product
GHG	Greenhouse Gas
GIEC	Gross Inland Energy Consumption
GSHP	Ground Source Heat Pump
GWP	Global Warming Potential
IEA	International Energy Agency
IHX	Internal heat exchanger
IPCC	Intergovernmental Panel on Climate Change
LMTD	Log Mean Temperature Difference
MEV	Mechanic Expansion Valve
NZE	Net Zero Emissions
NZEBs	Net Zero Energy Buildings
OECD	Organization for Economic Cooperation and Development
ODP	Ozone Depletion Potential
PA	Paris Agreement
SDGs	Sustainable Development Goals
SGHX	Suction Gas Heat Exchanger

SLA	Suction Line Accumulator
TEV	Thermostatic Expansion Valve
UNFCCC	United Nations Framework Convention on Climate Change
WSHP	Water Source Heat Pump

Symbol	**Description**	**Unit**
A	Heat transfer surface area	m^2
c_p	Isobaric specific heat capacity	kJ/(kgK)
COP	Coefficient of Perfomance	-
D	Diameter	m
f	Darcy factor	-
h	Convective heat transfer coefficient	$kW/(m^2K)$
h	Specific enthalpy	J/kg
L	Length	m
$LMTD$	Logarithmic mean temperature difference	K
$\dot{m}$	Mass flow rate	kg/s
N	Rotation speed	RPM
p	Pressure	kPa
p_r	Pressure ratio	-
$\dot{Q}$	Thermal power	kW
$\dot{W}$	Work rate	kW
s	Specific entropy	kJ/(kgK)
T	Temperature	ºC/K
u	Fluid velocity	m/s
U	Overall heat transfer coefficient	$kW/(m^2K)$
v	Specific volume	m^3/kg
V	Volume	m^3
$\dot{V}$	Swept volume (compressor)	m^3/s
VRC	Volumetric refrigerating capacity	kJ/m^3
Greek Symbols		
Δ	Difference	-
ε	Effectiveness	-
η	Efficiency	-
μ	Kinematic viscosity	m^2/s

ρ	Density	kg/m^3
Dimensionless Numbers		
Nu	Nusselt number	-
Pr	Prandtl number	-
Re	Reynolds number	-
Subscripts		
cond	Condensation	
comp	Compressor	
disch	Discharge	
disp	Displacement	
dsh	Desuperheater	
ev	Evaporator	
evap	Evaporation	
gc	Gas cooler	
gce	Gas cooler exit	
heat	Heat load	
hp	High pressure	
HP	Heat pump	
i	Inlet	
lp	Low pressure	
LZ	Lorentz	
o	Outlet	
opt	Optimum	
r	Refrigerant	
rec	Recommended	
R	Refrigeration	
s	Isentropic	
sc	Subcool	
sh	Superheat	
suc	Suction	
v	Volumetric	
w	Water	

1. Introduction

1.1. Current energy context

1.1.1. Decarbonized energy

The two main questions that have been influencing the organization, planning, and structuring of each current country in the past few decades are the use of energy and how to achieve energy self-sufficiency. Energy demands rise year after year, due not just to the increased global population, but also to economic and technical advancement, as well as an increased desire for comfort levels. Increasing energy consumption naturally necessitates more production. It is therefore important that this increase is made through energy-efficient solutions. Figure 1.1 shows the annual change in energy demand and compares it to the predicted. As it was stated, the figure shows a positive change in the last decades. However, it is important to notice that in 2020 there was a decrease in primary energy consumption, the largest recession since the end of World War II. The imposition of lockdowns, due to the extraordinary conditions imposed by the pandemic situation of COVID-19, drove oil demand to a collapse, justifying the negative change in primary energy consumption [1].

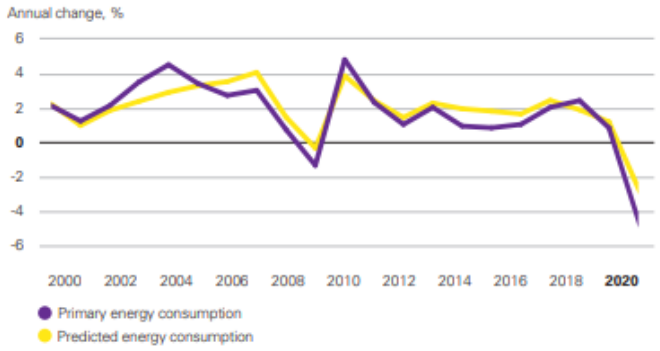


Figure 1.1: Global energy demand: actual vs predicted [1].

At the same time, there has been an increasing understanding of the implications of energy usage on climate change. Notice that climate change also is connected with sea-level rise and attendant coastal land loss, changes in growing seasons and soil moisture retention, changes in storm frequency and ferocity, and the spread of diseases such as malaria [2]. So, it is possible to understand that climate change has repercussions in all aspects of life and that is the reason why such awareness has been raised in order to tackle this problem. It is clear that problems, such as

global warming and the destruction of the ozone layer need urgent measures that promote the reduction of the agents that contribute to the deterioration of the current situation.

As it is known, and even though fossil fuels are expected to continue to dominate the energy supply throughout the next years due to mainly greater energy density, a decrease in the specific amount of carbon emitted per unit of primary energy consumed, i.e., decarbonization, is the main goal for the imminent future of energy use and production. As a result, lowering greenhouse gas (GHG) emissions from electricity, transportation, and industry is critical. In addition, most European countries are looking to invest in energy-saving and renewable energy so that they are less dependent on fossil fuels, with overcharged prices [3].

The two first main attempts to decrease environment-threatening substances were the Montreal Protocol established in 1987 against substances that deplete the ozone layer and the Kyoto Protocol in 1997 for reducing greenhouse gas emissions [4]. Even though there was some success in these protocols, it was still not enough to reverse the fast-paced climate change. In order to set stricter regulations, a group of policies between some of the most energy-consuming countries was set. Following the Paris climate conference (COP21) in December 2015 and eighteen years after the Kyoto Protocol, under the United Nations Framework Convention on Climate Change (UNFCCC) the Paris Agreement (PA) was signed, being the first universal, legally binding global climate change agreement. As of November 2021, 194 states and the European Union have signed the Agreement, including China and the United States, the countries with the first and second-largest CO_2 emissions [5]. Among other agreements, its main goal is to limit global warming to below 2 ºC, and the more ambitious 1.5 ºC.

It is important then to understand if the PA has succeeded in its mission. Although a lot more has to be done regarding climate change so that the goals of the PA are achieved, the following years after the PA have induced high developments in low-carbon, or even zero-carbon, solutions, and new markets, especially in the power and transport sectors. However, the correlation between increased wealth and the increased energy consumption is extremely powerful [6]. Therefore, the impact of these policies to reduce energy demand and CO_2 has not been successful enough and the regulations tend to be highly contested and limited [6]. One example is the set price for CO_2 emissions in the PA, which is considered to be especially low, and consequently, not fulfilling the purpose of raising the effort and pace towards decarbonization. Even with these lowlights, it is estimated that the existence of the PA stopped what would be a nonstop growth to

3 ℃ by 2100 [7]. In Figure 1.2, the CO_2 emissions from energy and industrial processes are displayed. As it is shown, to be consistent with the 1.5 ℃ goal, global net CO_2 emissions from these processes need to decline by about 37 % by 2300 when compared to 2010 levels. The net-zero analysis differs once it considers both that the emission will again rise following the pandemic situation and also the lead times associated with financing and implementing the required changes to the different energy systems, essential to achieve decarbonization [8]. It is also relevant to note that the Net Zero Emissions (NZE) approach aims to reach net-zero CO_2 emissions, as it is stated by the International Energy Agency (IEA) [9].

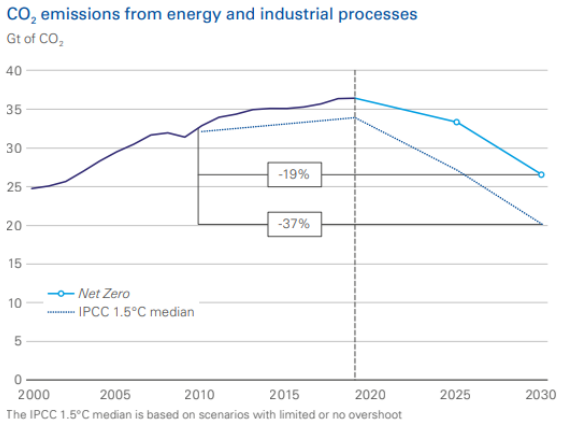


Figure 1.2: CO_2 emissions from energy and industrial processes from 2000 to 2030 [8].

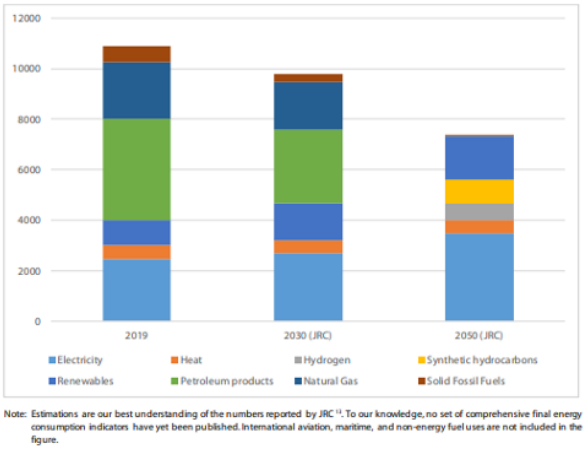


Figure 1.3: Final energy consumption in the EU in TWh [9].

Final energy consumption in the twenty-seven European Union (EU) countries achieve a total of 11000 TWh in 2019, as it is shown in Figure 1.3. About 35 % of this energy was provided by oil and 20 % by electricity, with coal and natural gas also having great percentages [10]. The percentage in production from electricity proves that, for the last decades, there has been a gradual shift in energy demand. The hydrocarbons have been declining noticeably, which has been accompanied by a quick expansion in renewables and electrification. This tendency is set to be even more noticeable until 2050, as can be seen in Figure 1.4. The tendency displayed in the graph shows the necessity for coal to be phased out. The same requirement happens with large volumes of natural gas, even though some natural gas can be replaced with a diversity of other methane sources, such as bio-methane [10].

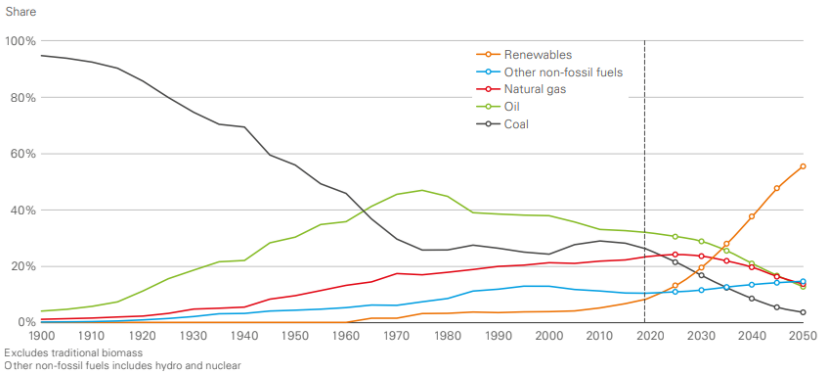


Figure 1.4: Evolution of the share of different energy sources [8].

Figure 1.5 shows the evolution of the share of electricity uses as final energy. The rise in electricity demand affects all three end-use sectors: industry, transportation, and buildings. The graph displays three different approaches to predicting the evolution of energy consumption. The increased growth in the *Accelerated* and *Net Zero* lines is due to the transport sector, predicting that road transportation will become increasingly electrified [8]. These two approaches are broadly in line with the goals of the PA and the Intergovernmental Panel on Climate Change (IPCC). The *New Momentum* line represents the most cautious scenario. Figure 1.6 shows the indicative pathway for the evolution of the demand of the different energy sectors.

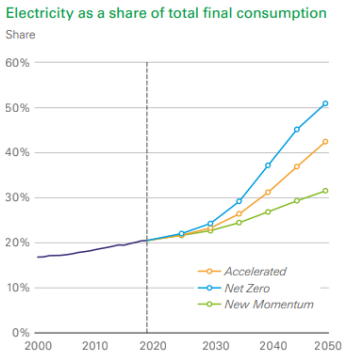


Figure 1.5: Current and projected evolution of electricity as a share of total final consumption [8]

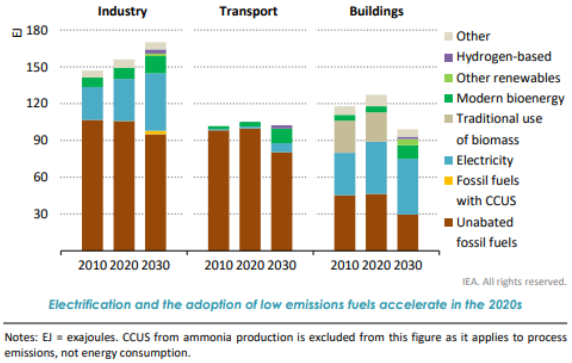


Figure 1.6: Use of different energy sources in the different sectors [9].

1.1.2. Energy access and sustainable development

The signing of the PA got the focus of the participating countries mainly turned into climate change. However, the agreement also stipulates another important goal that should accompany the

energy transition expected for the next decades. It is stated that the response to climate change should be in "the context of sustainable development and efforts to eradicate poverty". When looking into the goals set in the PA, it can be considered that prioritizing sustainable development and the eradication of poverty is mostly consistent with the efforts to adapt to climate change and achieve a sustainable energy transition [11].

Sustainable development is defined by UNESCO as the "development that meets the needs of the present without compromising the ability of future generations to meet their own needs". Currently, the path to sustainability goes through four main connected dimensions – society, environment, culture, and economy [12]. Looking to fulfill this purpose, in September 2015, almost coincidently with the PA, the United Nations (UN) issued a global agenda for sustainable development, named Sustainable Development Goals (SDGs) [13]. The UN states that "this agenda is a plan of action for people, planet, and prosperity" [14], looking to eradicate poverty "in all its forms and dimensions". At the heart of this agenda are 17 SDGs and 169 goals that must be implemented in all nations, both developed and developing, to be reached by 2030. [15]. Some of these goals go hand in hand with the sustainable energy transition in the PA and also in SDG 13, and the consequent increase in renewable energy generation. One of the goals underlined in the agenda, SDG 7, is described as "ensure access to affordable, reliable, sustainable and modern energy". It focuses on mainly three goals up to 2030 [16]:

- By 2030, ensure universal access to affordable, reliable, and modern energy services;
- By 2030, increase substantially the share of renewable energy in the global energy mix;
- By 2030, double the global rate of improvement in energy efficiency.

Following the implementation of these goals, global electrification has seen a consistent rise from 83 % in 2010 and 89 % in 2017, with 44 countries achieving universal access and 29 others accelerating their electrification rate by at least 2 % annually. Nevertheless, in 2019, 759 million people remained without access to electricity, and 2.6 billion, one-third of the world population, remained without access to clean cooking. The majority of attention is still directed toward Sub-Saharan Africa, where the number of people without electricity has increased in recent years [17]. This shows that a lot more work must be done to achieve the set point for 2030. As is shown in Figure 1.7, an average of 0.86 % average annual increase must be achieved to fulfill

universal access by 2030. Despite the electrification growth above 1 % between 2015 and 2017, achieving the 0.86 % average will be difficult, considering that, in most countries without universal access, advanced progress is seen as a stepping stone towards a full breakthrough [18].

When it comes to the second subgoal of SDG 7, up until 2018, there was a tremendous rise in renewable energy production. More than one-third of the growth in these improvements is attributable to East Asia and its advancements in solar and wind energy, particularly in China. Significant improvements in renewable energy, notably hydropower generation, have benefited Spain as well. Nevertheless, to get in line with the SDG 7 target, the pace of renewable energy generation must increase while, at the same time, stopping total energy demand from increasing through efficiency and conservation [17].

The ratio of gross inland energy consumption (GIEC) to gross domestic product (GDP), determined for a calendar year, is known as the global energy intensity [19]. It is used as a measure to track advancements in world energy efficiency. It is crucial to understand that improvements in energy intensity are stalling and falling short of the 2030 goal. Although the initial goal was to reduce emissions by 2.6 % per year through 2030, these numbers have not been met in recent years. In 2017, it registered an improvement of only 1.7 %, and, in 2018, the improvements got even shorter, recording only 1.2 %. Now this means that from 2019 to 2030 needed to improve by 2.9 % annually to reach the target value [20]. However, advances in both 2019 and 2020, fell short of what was needed, with 2.0 % and 0.5 %. Thus, the following improvements will have to be extra significant so that the goals defined in SDG 7 are met [21].

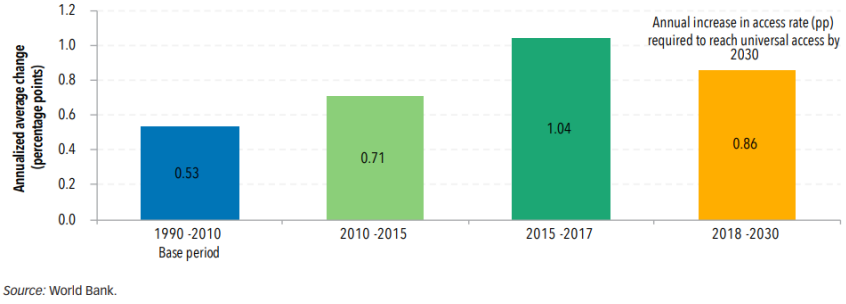


Figure 1.7: Current and projected annual average change in percentage points.

1.1.3. Economic activity correlation

For the last decades, the GDP has been used as an indicator that is intertwined with increases in electricity use, since a higher energy demand tends to generate more goods and services and therefore boost economic growth, i.e., the GDP. Despite this, a number of countries have seen a decoupling of the relationship between economic development and energy demand in recent years [22]. Figure 1.8 shows the growth rates of some of the most significant nations in the world, showing that the United Kingdom and Japan were able to experience economic growth without increasing their electricity consumption while India and Egypt needed to substantially increase their electricity demand in order to experience significant economic growth. This can be justified considering the countries' levels of development, electrification, and income. On the one hand, more developed nations have been successful in making the transition from manufacturing economies to service economies, mostly because of the impressive expansion of the service industries. Naturally, this leads to a less energy-consuming economy. This naturally results in a less energy-intensive economy. Additionally, these nations strive to conserve energy, keep energy intensity below 1 (GIEC/GDP), and hence improve energy efficiency. Countries like the United Kingdom, the United States, Japan, and the majority of the Organization for Economic Cooperation and Development (OECD) members fall into this category. On the other hand, in developing countries restrictions are considerably less demanding to not block the countries' growth, resulting in less efficient energy use (the energy intensity indication is normally above 1), until the country is able to reach the expected standards. These types of fast-growing economies, such as China, India, Brazil, and Egypt, display a large manufacturing sector, which is linked to less efficient technologies and lower-skilled labor. Thus, to achieve greater GDP more energy is required [22, 23].

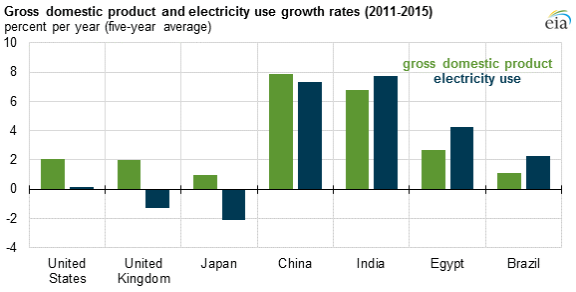


Figure 1.8: Gross domestic product and electricity use growth rates from 2011 to 2015 [22].

1.1.4. Energy in the buildings sector

As was stated before, the buildings sector is responsible for a significant portion of the total global final energy consumption (35 % in 2019) and GHG emissions (38 % in 2019) [24], as it is shown in Figure 1.9, and are, consequently, a great part of the foundation for an energy-efficient and clean future. These numbers vary a lot from country to country, especially when comparing OECD and non-OECD countries due to the different uses of energy that were already discussed previously.

The building sector can be divided into the residential and services sectors (non-residential), both having an alike structure. Non-residential buildings are estimated to be 40 % more energy-intensive than residential structures (250 kWh/m^2 vs. 180 kWh/m^2) [25]. Furthermore, through these two sectors, energy demand is supplementarily divided according to their end-use: space and water heating, appliances (which are further divided into four other categories: refrigeration, cleaning, brown goods such as televisions and computers, and other appliances), lighting, cooking, and space cooling.

Currently, and even though gas energy consumption still represents the highest share of energy use in buildings (about 36 % for EU countries), the electrification of the building sector already puts it close to the gas consumption level at 32 % (for EU countries) [25, 26].

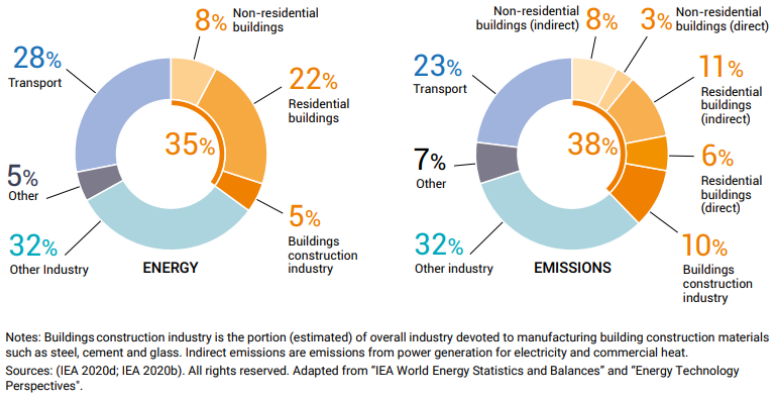


Figure 1.9: Global share of buildings and construction final energy and emissions in 2019 [24].

However, building efficiency requires more than an efficient performance from the equipment installed. It is indispensable that the building is built with superior architecture and engineering designs, providing its occupants with a comfortable and reliable living or work

environment [27]. A quality, optimized construction allows for less energy demand, lowering costs and increasing safety. Thus, better insulation can contribute greatly to an energy-efficient building [28].

The technologies that supply the end-user service demand must be optimized. Figure 1.10 shows a variety of technologies that can be optimized for each end-use sector. Examples include the use of high-efficiency CO_2 heat pumps for space and water heating, which can reduce or eventually eliminate the use of hazardous refrigerants that can result in GHG emissions with low global warming potential (GWP) [27, 29]. The selection of the technology to be used is determined by its efficiency, costs, and policy constraints [29].

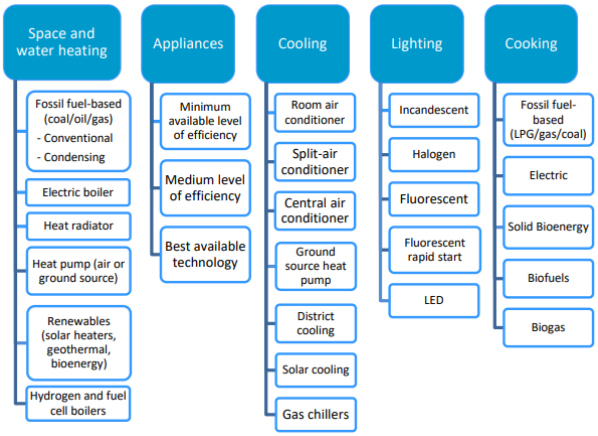


Figure 1.10: Main categories of technologies in the end-use subsector for buildings [29].

1.2. Use of carbon dioxide (CO_2) as working fluid in heat pump

The use of CO_2 for both refrigeration and heat pump purposes has been through a lot of ups and downs ever since the beginnings of mechanical refrigeration at the end of the 19th century. Up to 1950, CO_2, followed by NH_3, dominated the working fluid market and was mainly used in air conditioning and marine refrigeration [30]. However, after World War II, CO_2 and NH_3 began being substituted by the emerging synthetic halocarbons working fluids (mainly R12). They were regarded as the best refrigerants because of their greater efficiency in heating and cooling applications, increased safety (non-toxic and non-flammable), and moderate operating pressure. The usage of these refrigerants enabled the refrigerant application area to be expanded into the commercial and residential sectors [30, 31]. Even though CO_2 was essentially extinct from

refrigeration applications, NH_3 continued to be used in many industrial applications due to its excellent thermodynamic properties [31].

Chlorofluorocarbons (CFCs) came under scrutiny in the late 1980s due to environmental concerns, and the search for viable substitutes advanced quickly. The Norwegian Professor Gustav Lorentzen was the main driver behind the resurgence of natural refrigerants and mainly CO_2. In 1989, Lorentzen et al. [32] introduced an application for an international patent on a transcritical CO_2 cycle system, which aimed to eliminate the capacity and efficiency problems associated with the subcritical CO_2 cycle previous systems. The technology was primarily designed for use in automotive air conditioning applications, which at the time accounted for most emissions. Finally, in 1992, Lorentzen et al. [33] published experimental results that indicated that a transcritical CO_2 system was capable of achieving similar levels of efficiency that an R12 system. These reports launched CO_2 again into the refrigerants market and a lot of research has been done over the last few decades to improve CO_2 systems.

Heat pumps turn renewable energy from the air, earth, or water around them into heat that may be used for hot water and comfort heating. The most widely used refrigeration cycle in heat pump technology often produces three to five times as much useable energy as is required to power the compressor [34]. Additionally, it may be possible to develop a reversible heat pump that may deliver cooling in the summer and heating in the winter. Research into CO_2 heat pump systems allowed the development of transcritical CO_2 heat pump water heaters (HPWH), especially for domestic hot water (DHW), that aimed to substitute fossil fuels and electric boilers and reduce environmental harmfulness. In 2001, Japan launched the first full-scale commercial use of the transcritical system in the form of HPWH [35]. With the ability to produce hot water at 60–90 ºC without the use of electric heaters or boilers, CO_2 HPWH is currently one of the most energy-efficient methods of producing hot water. Thus, large energy savings can be achieved within the buildings sector, such as hotels, residential buildings, etc., with the implementation and management of CO_2 HPWH, together with energy storage technologies [36].

Even though it is heavily used for refrigeration purposes, leading many countries as the working fluid in large refrigeration and cold storage plants, NH_3 heat pumps are still to be made widely available as a commercial option for heating purposes. The main current German manufacturer GEA has only recently reached 150 installations around the world. Danish OEM Saboe has also launched an NH_3 high-temperature heat pump capable of delivering up to 95 ºC as

a heating source [37]. Additionally, several experimental models with limited capacity are being researched for academic purposes. District heating is the main application in use today. The increased interest is due to the excellent thermophysical characteristics and minimal ecological impact inherent to NH_3, which make it very alluring for this area. The main challenge is the lack of readily available suitable parts and potential safety issues. However, these issues can be addressed by utilizing particular materials, like stainless steel, and low refrigerant charges.

1.3. Company RACE

RACE, S.A. – Refrigeration & Air-Conditioning Engineering – company is based in Matosinhos, Portugal, being originated from one of the first companies in this sector, Selfrio S.A. founded in 1985. This company provided technical assistance services, design, manufacture, and construction of refrigeration facilities. With the addition of the HVAC sector in 1992, it was founded Sistavac S.A., owned totally by Selfrio S.A. Only in 2011, with the fusion of these two companies, the company adopted the only name of Sistavac S.A. Finally, in 2017, the company decided to rebrand, adopting the current name of RACE, S.A. The logo of the rebranded company is presented in Figure 1.11 [38].



Figure 1.11: Logo of RACE S.A. company [38].

The company aims to develop new technologies and solutions to achieve innovation in the sectors of refrigeration, climatization, and building efficiency. The company offers both manufacturing and post-sale services. These services are provided by qualified technicians in the respective areas of operation, who have several years of proven experience in maintenance, operation, and repair. All services provided are supervised and accompanied by engineers [38].

At present, RACE has maintenance contracts in various market segments, including industry, distribution, hypermarkets, hospitals, hotels, office buildings, and other large services. Currently, RACE has 75 maintenance technicians and 70 vehicles properly equipped with all the means and tools necessary for the respective activity. It is also important the existence of five delegations, which guarantee national coverage, allowing a rapid and effective response to requests

for assistance. The headquarters are based in Porto, having four other delegations in Coimbra, Lisbon, Estremoz, Algarve, and the Azores. It has about 300 employees and is present not only in Portugal but also in Brazil and Romania, developing engineering projects for the whole world [38].

1.4. Objectives of the dissertation

The previous chapters have highlighted the importance that the development and use of heat pumps using natural refrigerants can have for sustainable energy development. Both the thermophysical characteristics and the excellent environmental character of these refrigerants make a greater implementation a short-term goal.

The aim of this dissertation is the development and analysis of a transcritical CO_2 heat pump for heating domestic hot water, as well as the analysis of a potential implementation of NH_3 as a substitute for CO_2 in that same role. This main objective may be divided into several sub-goals throughout this project:

- Study of the main characteristics of CO_2 transcritical heat pump and comparison with conventional heat pumps;
- Review of the benefiting and undesirable properties of CO_2 and NH_3 as working fluids in heat pumps and comparison with the most used working fluids currently;
- Study of the main design specifications and considerations associated with each component of the heat pump;
- Assessment of existing solutions currently available on the heat pump market;
- Development of a thermodynamic model that makes it possible to simulate the functioning of a heat pump;
- Using EES software, simulation of multiple thermodynamic cycles and analysis of performance results;
- Analysis of the introduction of an internal heat exchanger as a method of improving the performance of the heat pump;
- Dimensioning and selection of components that fit the requirements of each heat pump configuration;
- Simulation and analysis of the operation of the designed heat pump when subject to external property variations.
- Schematic drawing of the CO_2 transcritical heat pump system with the selected components.

1.5. Structure of the dissertation

In order to achieve the above objectives, it was possible to describe the work carried out in ten chapters. In this regard, the following structure was chosen to provide the reader with a consistent line of thought and to assist understanding.

The present chapter, Chapter 1, introduces the subject of the dissertation, outlining its motivation and relevance. An energy context analysis proceeds in order to frame the use of natural refrigerants as working fluids for heat pumps in the current energy transition.

Chapter 2 prepares a theoretical foundation for the realization and comprehension of the work done in the subsequent chapters. A brief review of the standard refrigeration and heat pump cycles is done, as well as the distinctions between the transcritical and subcritical cycles. Furthermore, a study of the characteristics of CO_2 and NH_3 is presented so that a comparison with conventional working fluids can be established.

Chapter 3 discusses the current state of the technology under consideration. First, data on the existing market for CO_2 and NH_3 is gathered. Furthermore, the different energy sources that can be used for heat pumps are discussed. Finally, a study on various possible modifications to improve the performance of the heat pump is done.

In Chapter 4, several ideas, and studies about the design of the heat pump components are presented.

Chapter 5 lists, first, the various thermodynamic models of the heat pump components. EEs software is used to run several simulations to ascertain the heat pump operating parameters. These simulations are done to analyze the potential benefits of the introduction of the internal heat exchanger and establish a foundation for component selection.

In Chapter 6, based on suggestions from RACE S.A. members, the selection of components is made and economic analysis of the two configurations is conducted.

In Chapter 7, after the selection of the components, the simulation codes are changed to fit the effects that both water temperature and ambient air temperature may have on the performance of the heat pumps. The results are presented, and an analysis of these effects is made. Moreover, a comparison between the performance of the CO_2 heat pump and the NH_3 is conducted.

Chapter 8 focuses on the design of the domestic hot water storage and consumption structure. An estimation of the domestic hot water requirement is also done.

Chapter 9 presents a schematic diagram for the CO_2 heat pump system.

Chapter 10 is a brief text that summarizes the complexity of the heat pump. The suggestions are used for further studies.

Finally, in the Appendixes more detailed reports, catalogs, and results regarding the subjects of the chapters can be found.

2. Literature review

2.1. Refrigeration and heat pump cycles

Naturally, heat transfer occurs from a higher temperature environment to a lower temperature environment. When put into a power cycle, this type of phenomenon can deliver a net work transfer of energy. For that to happen, then the heat transfer to the system from the hot environment, Q_H, must be greater than the heat transfer out of the system to the cold environment, Q_L, and the difference between these two will result in work output, $\dot{W}_{net,out}$ [39, 40]:

$$\dot{W}_{net,o} = \dot{Q}_H - \dot{Q}_L \tag{1.1}$$

Nevertheless, in some cases, the aim is to extract heat from a lower temperature environment and deliver it to a higher temperature environment. Following Clausius's statement of the second law of thermodynamics and contrary to the previous case, with this type of system, designated by either a refrigerant cycle or a heat pump cycle, is not possible to have a work output out of it. Instead, the system requires a net work input, $\dot{W}_{cycle}$ [39, 40]:

$$\dot{W}_{net,in} = \dot{Q}_H - \dot{Q}_L \tag{1.2}$$

Figure 2.1 shows a schematic of the difference between the two systems described previously.

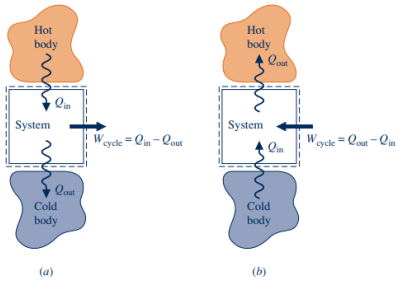


Figure 2.1: Schematic diagrams of (a) power cycles and (b) refrigeration and heat pump cycles [39].

Despite the refrigeration and the heat pump cycles being equal, their objectives differ. On the one hand, the refrigeration cycle or refrigerator seeks to maintain the temperature extracting the heat gain, so that the system's temperature stays lower than the ambient temperature. Discharging this heat to a higher temperature environment is not the purpose of the refrigerator, but a need to achieve refrigeration. The objective of the heat pump cycle, on the other hand, is to provide high-temperature heat to the environment or to keep the temperature above its surroundings [39].

This difference is explicit when calculating the coefficient of performance (COP) for each system [40]:

$$COP_R = \frac{Desired\ output}{Required\ input} = \frac{Cooling\ effect}{Work\ input} = \frac{\dot{Q}_L}{\dot{W}_{net,in}}\ (Refrigerator) \tag{1.3}$$

$$COP_{HP} = \frac{Desired\ output}{Required\ input} = \frac{Heating\ effect}{Work\ input} = \frac{\dot{Q}_H}{\dot{W}_{net,in}}\ (Heat\ pump) \tag{1.4}$$

By manipulating Equations (1.3) and (1.4), the following relation, for fixed values of $\dot{Q}_L$ and $\dot{Q}_H$, between the two COP can be achieved:

$$COP_{HP} = COP_R + 1 \tag{1.5}$$

This relation demonstrates that the COP_{HP} will always be above the unit. Thus, in the worst-case scenario, the energy value provided to the space to be warmed $\dot{Q}_H$, balances the energy value consumed by the heat pump $\dot{W}_{net,in}$. Since part of the heat provided by the heat pump can be lost through piping, or other parts of the heat pump, the COP_{HP} might end up being slightly lower than the unit, especially when the air temperature is very low [40]. Figure 2.2 shows the ideal vapor-compression refrigeration cycle, which is mostly used for refrigerators, air-conditioning systems, and heat pumps. It is formed by four processes [40]:

- 1-2: Isentropic compression in a compressor;
- 2-3: Isobaric (high-pressure) heat rejection in a condenser;
- 3-4: Throttling in an expansion device (typically an expansion valve);

- 4-1: Isobaric (low-pressure) heat absorption in an evaporator.

However, it is known that the ideal case is not possible to obtain in practical systems due to irreversibilities that occur in the different components. Firstly, there are pressure losses in both the condenser and the evaporator, which increase compression work. Secondly, it is difficult to control the state of the refrigerant so precisely that it will leave the evaporator and enter the compressor as a saturated vapor. Alternatively, the refrigerant is slightly superheated. Likewise, at the exit of the condenser, it is difficult to achieve saturated liquid. As a result, the refrigerant is subcooled before it enters the throttling valve. This can, however, be useful, increasing the cooling effect. Moreover, the compressor is considered to be internally reversible in the ideal cycle, which is naturally not achievable, mainly due to frictional effects increasing the entropy. As a consequence, compression work will be higher. In addition, heat exchange due to temperature differences in both the evaporator and condenser contributes to losses increase. Lastly, the throttling process in the expansion device is also heavily responsible for energy losses. It is relevant to notice that, even though heat exchanging and compressor losses are dependent on the equipment used and are considered inexistent in an idealized cycle, both throttling and vapor superheating losses, even tough superheating can be useful, still exist and reduce their COP. These last two losses are dependent on the refrigerant used [40, 41]. This all means that the actual vapor compression cycle will differ greatly from the ideal cycle as it is shown in Figure 2.2 and Figure 2.3.

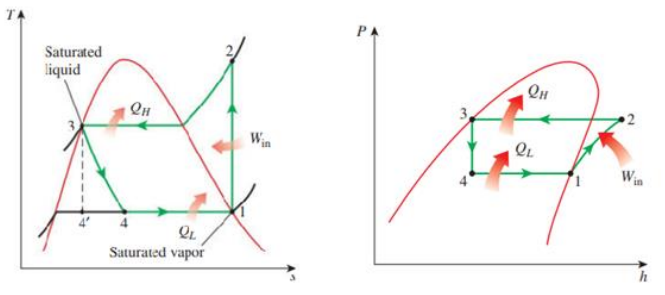


Figure 2.2: *T-s* and *P-h* diagrams for the ideal vapor-compression refrigeration cycle [40]

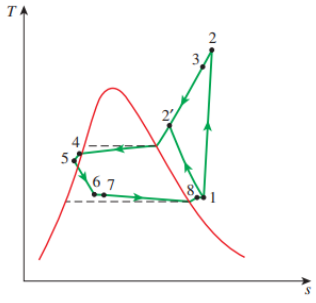


Figure 2.3: *T-s* diagram for the actual vapor-compression refrigeration cycle [40].

It is relevant to understand that the complexity of the vapor-compression cycle is normally higher than the previous figures. In the conventional process, the vapor is assumed as dry and saturated. However, it is useful and convenient to allow the refrigerant to stay longer at the

evaporator to allow superheating and, therefore, avoid the carry-over of liquid refrigerant into the compressor, where, due to its incompressibility, can induce serious damage. The inverse analysis can be made for the condenser. Even though it is ideally considered that the liquid leaving the heat rejection process is liquid saturated, the pressure drop throughout the diverse components before the expansion valve, such as pipes, filters, etc., causes the formation of some vaporized refrigerant in gas form. This is often named flash gas. To avoid this problem, the condensed liquid should, previously to the expansion process, suffer subcooling either in the condenser or via the addition of another component, for example, a suction gas heat exchanger (SGHX), which will be explained in the following chapters [42].

2.2. Lorentz cycle

In contrast to subcritical cycles, where the Carnot cycle is employed as a comparison term, this cycle is not the most suitable for a theoretical comparison when dealing with transcritical cycles. This is due to the fact that heat rejection in a transcritical cycle happens at a gliding temperature and is not constant as in a subcritical cycle. Since the fluid is at a state above the critical point there is no phase change at constant temperature and all heat is sensible heat. The most adequate theoretical cycle to utilize for comparison is the ideal Lorentz cycle. This cycle is divided into the same steps as a convention vapor compression cycle, except for heat rejection not being isothermal [43]. The ideal Lorentz cycle *T-s* diagram is shown in Figure 2.4.

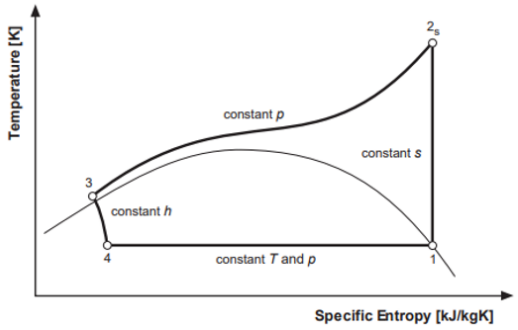


Figure 2.4: *T-s* diagram of the ideal Lorentz cycle [43].

In order to establish a comparison method, it is needed to define COP value for this cycle [43]:

$$COP_{LZ} = \frac{T_m}{T_m - T_0} \tag{1.6}$$

where

$$T_m = \frac{T_{2s} - T_3}{\ln\left(\frac{T_{2s}}{T_3}\right)} \tag{1.7}$$

From Equations (1.6) and (1.7) it results:

$$COP_{LZ} = \frac{T_{2s} - T_3}{(T_{2s} - T_3) - T_0 \times \ln\left(\frac{T_{2s}}{T_3}\right)} \tag{1.8}$$

where T_0 is the heat source temperature and T_m is the average temperature throughout the heat rejection.

The Lorentz efficiency η_{LZ} can then be used to compare the transcritical CO_2 heat pump performance to its theoretical maximum:

$$\eta_{LZ} = \frac{COP_{HP}}{COP_{LZ}} \tag{1.9}$$

2.3. Transcritical versus subcritical CO_2 cycle

In Figure 2.5, it is shown the *P-h* diagrams for both of the refrigeration cycles commonly used for CO_2: subcritical and transcritical. The subcritical cycle functions such as a typical vapor compression cycle. It follows that when CO_2 or other subcritical refrigerants are used in the subcritical state in a conventional cycle, the efficiencies are low and not profitable, due to the low heat rejection enthalpy achieved when condensation occurs near the critical point. One option for reducing irreversible heat losses involves using multiple stages, which means greater expenses. Contrary to this case, for transcritical cycles, the system works above the critical point,

i.e. with supercritical CO_2 at the high-pressure part of the cycle, which allows for a single compression stage from low to high temperatures. As a result, working pressures can be up to 130 bar, significantly greater than in the majority of standard refrigeration cycles. Subsequently, these high pressures may enhance safety risks and therefore require more robustly designed components. Despite the fact that the lack of these components was in part responsible for the first fall of CO_2 use as a refrigerant, currently, devices that meet these requirements have already been developed. Still, the high volumetric capacity of CO_2 (3 to 10 times higher than other halogenated refrigerants) together with great heat transfer properties, such as high vaporization heat and specific heat, allow for smaller piping diameters and flow areas, reducing costs [30]. Thus, even though a larger pipe thickness is required due to the high pressures, the overall piping material is reduced. Although the functions of the compressor, evaporator, and expansion valve remain the same, as in any traditional compression vapor cycle, in a transcritical cycle, the compressor raises the vapor pressure beyond the operating fluid critical pressure, enhancing the capacity of heat rejection through single-phase sensible cooling. In this case, there is no condensation, and the vapor decreases its temperature while maintaining its phase. For this reason, the component where the heat rejection takes place is known as a high-pressure gas cooler instead of a condenser. Therefore, in the transcritical cycle, the CO_2 cooling process is not in the phase-change region, contrary to the subcritical cycle. Thus, there are no saturation conditions, and the gas cooler pressure and temperature are independent [31, 44, 45].

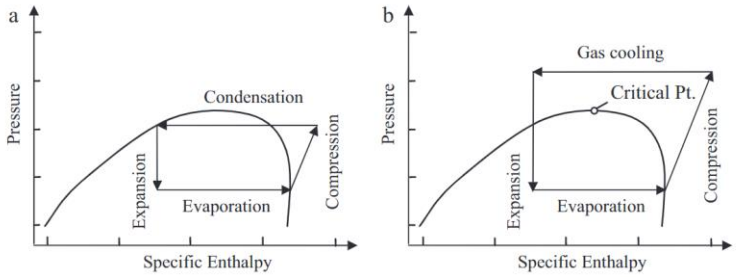


Figure 2.5: *P-h* diagrams for (a) subcritical cycle (b) transcritical cycle.

In Figure 2.6 it can be observed a *T-s* diagram for a specific application in a transcritical CO_2 heat pump. The water line represents the heating process of the inlet water at 5 °C and the outlet of the gas cooler at 70 °C. This process is parallel to what happens in a subcritical system. Although, heat rejection is achieved very differently. While in a subcritical system there is a step that corresponds to the condensation, the transcritical CO_2 curve inversely matches the water curve, which accounts for more homogeneous heat rejection. Consequently, the average

temperature of CO_2 throughout heat rejection is significantly lower. This process is normally characterized as a temperature glide and is due to a continuous increase in density from a vapor state to a liquid-like dense gas state and a non-monotonic variation of the specific heat for supercritical CO_2. This highly increases efficiency for processes that need a large temperature increase, creating the least entropy. A higher temperature glide generally increases the COP value of the system. To allow this, counter-flow heat exchange in the gas cooler is required [30, 46, 47]. Additionally, there is a point along the curve where the temperature difference between the two fluids is at its smallest. That point is designated as a pinch point [46]. Normally, on transcritical systems, that point is achieved at the inlet of the water and outlet of the refrigerant. However, as is shown in Figure 2.7, if the gas cooler pressure is not high enough the pinch point can happen, for example, in the refrigerant inlet of the gas cooler. This is mainly subject to the heat capacity of the fluids. If $\dot{m}_{CO2}c_{p,CO2} > \dot{m}_w c_w$ the temperature change of the refrigerant will be smaller than that of the water. If the opposite happens, then the temperature change for CO_2 will be higher [46]. In subcritical systems, the pinch point happens at the saturated vapor state of the refrigerant. Naturally, the temperature difference at the pinch point is dependent on several factors, being the main ones, heat transfer area, or effectiveness of the gas cooler. These mentioned characteristics of the heat rejection process allow that, in a CO_2 transcritical HPWH, water can be very efficiently heated in one pass at the gas cooler [46, 48].

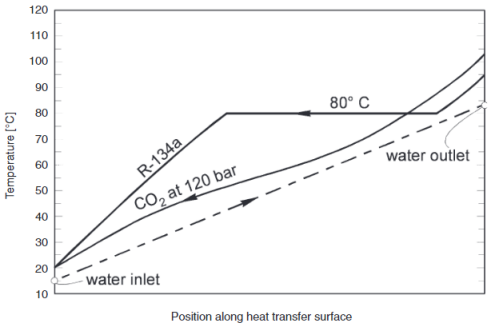


Figure 2.6: Comparison between the heat rejection curve for R-134a and CO_2 [49].

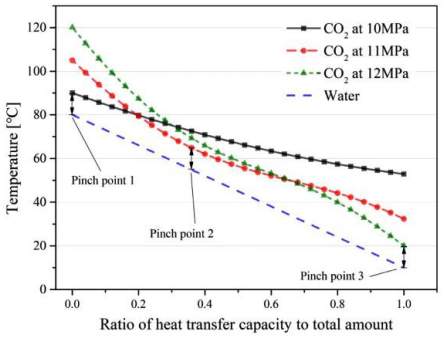


Figure 2.7: Comparison of the pinch point for different gas cooler pressures [46].

In order to achieve optimal conditions for the transcritical cycle, regulation of the high pressure at the gas cooler is mandatory. As mentioned previously, following the fact that the transcritical system does not work in the phase change region, it is possible to establish either a constant gas cooler pressure or exit temperature, controlling the remaining one. For instance, if the

operating pressure is raised then both the heating effect and the compression work increase. As a result, the gas cooler outlet temperature may be used to calculate an optimal pressure, which will lead to the highest possible value for the COP. Figure 2.8 shows the evolution of the discharge pressure and the COP for different gas cooler exit temperatures. This exit temperature varies with the size of the gas cooler and the external fluid inlet temperature [31, 50]. For an established cooler outlet temperature, initially, the increase in gas cooler pressure translates into an increase in COP, due to a greater increase in the heating capacity over energy input for the compressor. At a particular pressure, designated as optimum pressure, the COP reaches a maximum value. If the pressure continues to be increased, the COP begins to reduce since the compressor work increase is higher [51]. This high dependence of the system's performance on gas cooler pressure is mainly connected to the slope of the isotherms near the critical point. As seen in Figure 2.9, the slope of the isotherms reaches an almost flat evolution at certain pressures. If those pressures are selected as gas cooler pressures this leads to a much larger enthalpy decrease at the gas cooler exit (3 to 3') than the increase at the gas cooler entrance (2 to 2'), thus increasing the overall enthalpy difference at the gas cooler without significantly increasing the compressor work. Subsequently the COP value increases [52]. Besides that, Figure 2.8 also shows that the optimal gas cooler pressure increases with the gas cooler exit temperature, and the COP of the cycle decreases. Most of the systems work with supercritical CO_2 at operating pressures close to 100 bar, which is considerably higher than typical operating pressures for traditional hydrofluorocarbons (HFCs) and ammonia systems [53]. Gas cooler pressure is generally chosen for optimum COP unless larger capacity is required, which case a higher pressure would be selected [54].

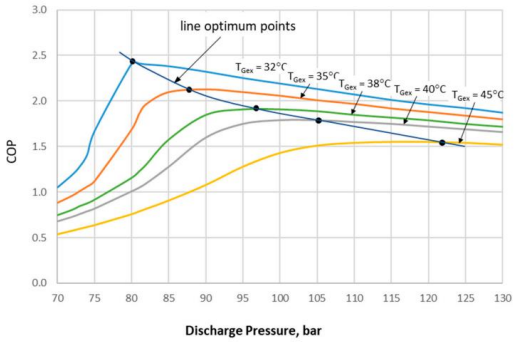


Figure 2.8: *COP* value for different gas cooler pressures and gas cooler exit temperatures [51].

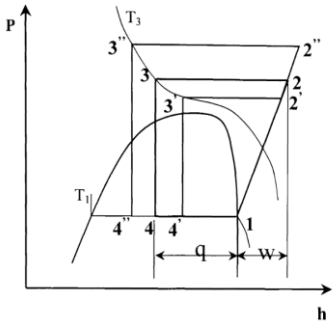


Figure 2.9: Influence of the optimum gas cooler pressure on the heating capacity and compressor work [55].

Another advantage of the transcritical CO_2 cycle is that the evaporating temperature has a small impact on heating capacity and COP, allowing the CO_2 system to retain a high heating capacity at low ambient temperatures. This is especially important for HPWH since heat is extracted from the ambient air which is extremely fluctuant throughout the year.

When considering heat rejection at supercritical state CO_2, another factor must be addressed. In an isobaric process and near the critical point, CO_2 experiences rapid variations in physical properties, such as enthalpy, specific heat, density, conductivity, and viscosity. As a consequence of these variations, the heat transfer coefficient is highly unstable close to the critical point. This effect is more pronounced in the pseudocritical temperature T_{pc}, which is the temperature at which the specific heat, for a given pressure, reaches its maximum [56, 57]. This variation is shown in Figure 2.10, which demonstrates the variation of the specific heat and the density of CO_2 with temperatures of 40, 80, and 90 bar. Due to the importance of the Prandtl number Pr for heat transfer, its variation with supercritical temperature and pressure is also shown in Figure 2.11. The graphics show that the specific heat and Pr maximum values decrease significantly with an increase in pressure. Pr also increases with pressure from temperatures slightly higher than the supercritical temperature and decreases with pressure for temperatures until the supercritical temperature. In addition, the graph shows that the pseudocritical temperature increases for superior supercritical pressure. Relatively to density, when compared to lower pressures, supercritical pressures provide a smoother fall when increasing temperature. For 40 bar, all properties maintain a practically constant value for temperatures higher than the boiling point at that pressure.

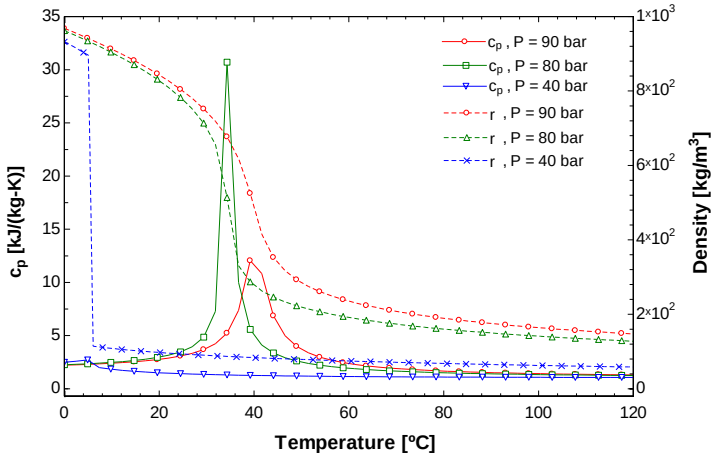


Figure 2.10: c_p and density values for different temperatures and pressures [58].

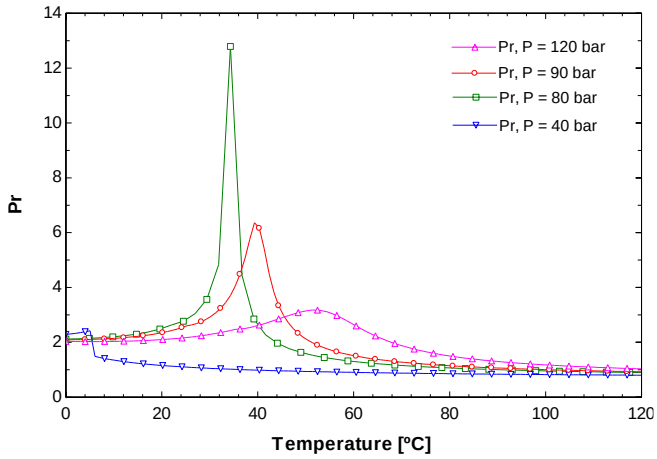


Figure 2.11: Prandtl number value for different temperatures and pressures [58].

2.4. Working fluids for heat pumps

2.4.1. CO_2 (R744) thermodynamic properties

In the atmosphere there is about 0.04 % (v/v) of CO_2 [54]. Thus, being a naturally occurring substance, cheap, readily available, not poisonous in any common concentration, and nonflammable, CO_2 is a very recurrent solution to many technologies used in climatization.

When observing Figure 2.12, two essential states should be noted, when working with CO_2 (ASHRAE official designation R744) [49]. At the triple point, which occurs at 5.2 bar and -56.6 ºC, the three phases of CO_2 coexist (dry ice, gaseous, and liquid). Below the pressure at this point, there is no liquid phase, meaning that, at atmospheric pressure, solid CO_2 sublimes directly

to the gaseous phase. Another crucial point is the critical point, which appears at 73.8 bar and 31 ℃. At this point, the gaseous and the liquid phases become similar and there is no visible boundary between the two phases. The refrigerant then becomes a supercritical fluid above this point and the latent heat of vaporization concept is not appliable, which leads to the supercritical fluid behaving completely different when compared to the subcritical fluid. When heat is removed, while it is above the critical temperature and pressure, no phase change will take place, and, consequently, the fluid will decrease its temperature (a subcritical fluid maintains its temperature constant throughout a phase change) and exchange sensible heat (not latent heat like the subcritical fluid). This is a very compelling characteristic of refrigerant fluid, since, in a refrigeration system, supercritical R744 will not condense but just cool. Of all other commonly used refrigerants, R744 is the only one that has such a low critical temperature, benefiting it in some specific applications [49, 54].

On the one hand, subcritical CO_2 operates as a normal refrigeration cycle, below the CO_2 critical point, which requires the use of a cascade-type system, using another type of fluid as the primary fluid. On the other hand, using transcritical (or supercritical) CO_2 does not allow condensation and therefore no latent heat will be exchanged. Therefore, it does not require an individual system for condensation. However, it works at much higher temperatures and pressures.

2.4.2. Comparison between refrigerants

The choice of the working fluid plays a crucial part in how efficient and successful the functioning of the heat pump system turns out to be. Furthermore, multiple factors must be attentively studied to select long-term sustainable solutions. To achieve this, Danfoss adopted the 7 Force Model that grouped these into three key criteria: affordability, environment, and safety. It is essential to specify the qualities a refrigerant should have in order to balance these three factors [59]. Firstly, low life cycle cost and medium to high availability are mandatory so that the fluid is easily accessible. Chemically, the fluid must be stable, miscible with lubricants, and compatible with the construction material used, so that little wear is made on the components, achieving long-term reliability, and should not be either toxic or flammable. Finally, as was stated previously, regulations on the use of refrigerants have been heavily increased to reduce their environmental impact. Therefore, the fluid must display low ozone depletion potential (ODP) and GWP [2, 31, 40, 53, 60].

In order to optimize heat pump operation, transport and thermodynamic properties of the chosen refrigerant must be heavily considered. The refrigerant must present an appropriate critical point and boiling point, and low vapor heat capacity. To prevent possible leakage and air infiltrations, evaporation pressure should be higher than atmospheric pressure. High thermal conductivity and low viscosity lead to smaller heat exchangers, because of a greater transfer coefficient. Higher latent heat of vaporization considerably lowers the need for a large mass flow rate of the refrigerant. Simultaneously, this leads to less compressor displacement and lower power consumption. Preferably, the pressure ratio should be low as it leads the compressor to higher volumetric efficiency, reducing its required work. Finally, a low-pressure drop is also desirable. This may be achieved by choosing a refrigerant with low viscosity [61].

The classification regarding inflammability and toxicity is of particular significance and it is stated in ASHRAE Standard 34, *Designation and Safety Classification of Refrigerants*. ASHRAE assigns an identifying reference letter, which designates the toxicity class, and a number, which designates refrigerants flammability. Concerning toxicity, refrigerants may be attributed to class A or B [50, 53, 62]:

- Class A: refrigerants that have not exhibited toxicity at concentrations less than or equal to 400 ppm (v/v);
- Class B: refrigerants that have exhibited toxicity at concentrations below 400 ppm (v/v).

Regarding inflammability, refrigerants can be distributed into four different classes [50, 53, 62]:

- Class 1: refrigerants that don’t show flame propagation when tested in air at 21 ℃ and 101 kPa;
- Class 2: refrigerants that exhibit a lower flammability limit of more than 0.10 kg/m^3 at 21 ℃ and 101 kPa and heat of combustion of less than 19 kJ;
- Class 2L: this subclass indicates lower flammability refrigerants with a very slow-burning velocity (<10 cm/s);
- Class 3: highly flammable refrigerants, which have a lower flammability limit of less than or equal to 0.10 kg/m^3 at 21 ℃ and 101 kPa or heat of combustion greater than or equal to 19 kJ/kg.

As was stated before, the refrigerant must not be either toxic or flammable. This leads to the perfect classification to be A1, which translates into no flame propagation and low toxicity. This distribution of the majority of available refrigerants is shown in Figure 2.13.

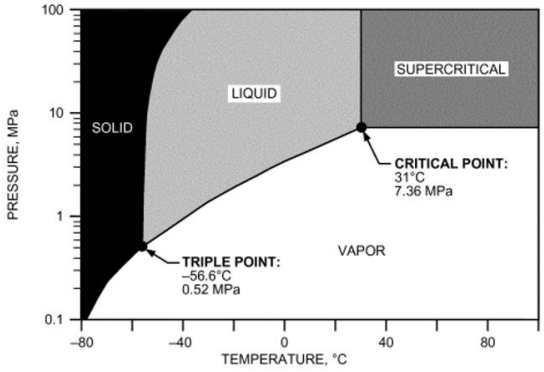


Figure 2.12: Phase diagram for carbon dioxide (CO_2) [44].

Flammability					
	higher	A3	R290, R1270, R601, R600, R600a, E170	B3	
	lower	A2	R142b, R152a, R365mfc, SES36, R1234ze(Z)	B2	
		A2L	R1234ze(E), R1234yf	B2L	R717
	no flame propagation	A1	**R113, R114, R124, R134a, R236fa,R227ea, R1336mzz(Z), R1336mzz(E), R1233zd(E), R1224yd(Z), R718, R744**	B1	R123, R21, R245ca, R245fa
			lower		higher
			Toxicity		

Figure 2.13: Refrigerant flammability classes [63].

Given the above, it is important to understand that no refrigerant is capable of owning all of these properties and, therefore, the choice of the refrigerant is bound to be a compromise that satisfies as much as possible the purpose of the fluid.

The main classification regarding refrigerants concerns their chemical composition and it is divided into six common current categories:

- Chlorofluorocarbons (CFCs): CFCs were introduced as second-generation refrigerants, solving problems such as toxicity, material incompatibility, and flammability. However, thanks to environmental issues related to ozone layer depletion and global warming, their commercialization and production were banned following 60 years of market domination. Some examples were R12, R114, and R502 [53, 62].
- Hydrochlorofluorocarbons (HCFCs): HCFCs, mainly represented by R22, appeared with the addition of hydrogen atoms. Despite their shorter atmospheric lifetime (about 13 years), the chlorine atoms still pose a threat to the ozone layer. Thus, their production is being phased out [2, 64].
- Hydrofluorocarbons (HFCs): HFCs are the third generation of fluorine-based gases. Since there is no chlorine in their structure, these refrigerants are considered to have zero ODP, which makes them strong candidates. However, HFCs present a relatively high GWP (a

hundred times higher than that of CO_2). Consequently, and even though they are currently the greenhouse gases that are expanding the fastest, many nations have reached an agreement to reduce HFCs emissions. The most relevant refrigerants belonging to this category are R410A, R134a, R152a, R245fa, and R32 [2, 62, 65].

- Hydrocarbons (HCs): HCs are organic compounds, such as R290, R1270, or R600. They present a short atmospheric life, which results in a very low GWP, and normally come at a low cost due to lower energy consumption. Their main problem is related to their high flammability, which limits their use in low-power applications such as domestic refrigeration [65, 66].
- Hydrofluoro-olefins (HFOs): HFOs belong to the fourth generation of fluorine-based gases, which appeared in the 2010s. When compared to the HFCs structure, the difference concerns the double bond between the carbon atoms, which results in a short atmospheric life. The first HFO developed was the R1234yf and it aims to potentially replace R134a and R114 in domestic refrigeration and mobile air conditioning applications. Along with a very low GWP, it presents zero ODP. However, their mild flammability and much higher cost of manufacturing are drawbacks to more regular use. Another typical developed HFO is the R1234ze [2, 67, 68].
- Inorganic natural refrigerants: these include ammonia (R717), water (R718), and carbon dioxide (R744) and result from a biochemical process that occurs in nature. Thus, they do not deplete the ozone layer and have nearly zero GWP. Moreover, they present high efficiency which contributes even more to their environmentally safe status [2, 65, 68].

At this time, there are a few diverse options regarding which refrigerant to use. Figure A.1 in Appendix A shows the main refrigerants currently used and their main properties. Based on the values displayed, a general review can be made regarding each property.

Due to the environmental concerns and current regulations in force, the first criteria that should be considered are the ODP and GWP. Most of the refrigerants currently in use present zero ODP so that is not a differentiating characteristic. However, GWP varies considerably according to the chosen fluid. With an ODP of 0 and a GWP of 1, CO_2 is one of the most environmentally friendly refrigerants. The newer HFOs and HCs also present almost negligible GWP values. Despite not preventing its current use, due to their high GWP, the use of HFCs is being reduced [67].

Concerning safety issues, the flammability of the HCs, such as R600a or R290, is the main obstacle for a more prominent use, when compared to neither toxic nor flammable R744 (A1). Together with CO_2, R134a also presents an excellent safety grade.

As previously stated, the substantially lower critical temperature of CO_2 is the main differential factor since it allows heat rejection as a single-phase process. Besides that, several thermophysical properties make CO_2 even more favorable [55]:

- Heat pump size requirements are usually reduced due to the high density (30 times as high as R717 and 3 times as R410A) and pressure. High density also reduces compressor work input;
- Heat transfer coefficients and heat exchanger effectiveness benefit from the high specific heats;
- Moderately high latent heat of vaporization compared to other refrigerants, reducing the necessary CO_2 flow rate for certain cooling and heat capacities;

Even though suction and discharge pressure differences are substantially greater (fourteen times as high as R134a and five times as high as R410A), CO_2 compressors are generally able to operate with lower pressure ratios than those working with HFC refrigerants. The pressure ratio of a transcritical cycle ranges from 2 to 4, although HFC cycles can show pressure ratios of up to 8 [61, 69]. All of this implies that CO2 compressors should, in theory, be able to operate more efficiently. Still, some other issues, such as greater leakage and reduced volumetric efficiency need to be considered before making that assumption. These problems are mainly a consequence of increased pressure and heat loss. In addition, CO_2 also is easily compatible with typical machine construction materials, such as copper and stainless steel. Standard lubricants may also be used when working with CO_2. Both these features contribute to avoiding the high wearing of the heat pump components [61, 69].

Even though R717 has been successfully used in refrigeration technology, especially food processing, for over 150 years, only lately, has NH_3 risen as a valuable option for heat pumps [67]. It leads to smaller systems and operates at lower pressures than CO_2 (operating pressures are similar to those of HFCs and HCs), together with a zero GWP and zero ODP [67, 70]. Some of the few disadvantages it presents are its toxicity and flammability levels, together with a pungent odor. Currently, it is evaluated as a B2L refrigerant, which means that it has high toxicity and some flammability. TLV (Threshold Limit Value) $= 50$ ppm (v/v). IDLH (Immediately dangerous to

life or health) = 300 ppm (v/v) [67]. This implies that, besides requiring close monitoring and highly skilled workers, most of the time, a NH_3 heat pump needs to be installed outside of the building, in a special facility, or through indirect systems [61, 71]. In addition, it is not compatible with either copper or brass, the most common material for components in residential systems, which means that only welded steel pipes can be used, increasing initial installation costs. Thus, the major drawback regarding the use of R717 is related to the lack of components able to provide long-term operation, together with specific design issues [71]. R717 causes high discharge temperatures, which is undesirable for most refrigeration systems as it leads to the need for multi-staging. However, for hot water heating applications, high temperatures following the compression may be advantageous.

Despite the inconveniences stated above, its remaining thermodynamic properties, such as high latent heat and high thermal conductivity, and low energy requirements are ideal for a working fluid for refrigerators and heat pumps. Specifically, the high enthalpy of vaporization allows the flow rate in ammonia systems to be significantly lower than in CO_2 and other conventional refrigerant-based systems. This leads to NH_3 often being acknowledged as the most efficient refrigerant [61, 70, 71, 72].

It is noteworthy to acknowledge that not necessary to have a condensation temperature higher than that of the water outlet's desired temperature (heat sink temperature), as heat in the de-superheating region may be able to achieve the desired output. For the same heating effect, if the suction temperature at the compressor is maintained constant, a higher condensation temperature means the percentage of heat transferred in the condensation region drops, but in the de-superheating region increases. This occurs because R717 presents a very high discharge temperature when compared to the condensation temperature at a given discharge pressure [70].

Figure 2.14 shows that the volumetric refrigerating capacity of R744 is significantly higher than any other common refrigerant used for refrigerating systems. This is due to the higher vapor density. When compared to R717, it can be up to 8 times the capacity for the same temperature [73]. However, for higher temperatures, R717 is capable of maintaining high volumetric refrigerating capacity while R744 drops after 22 ºC so that the capacity is null at the critical point [74].

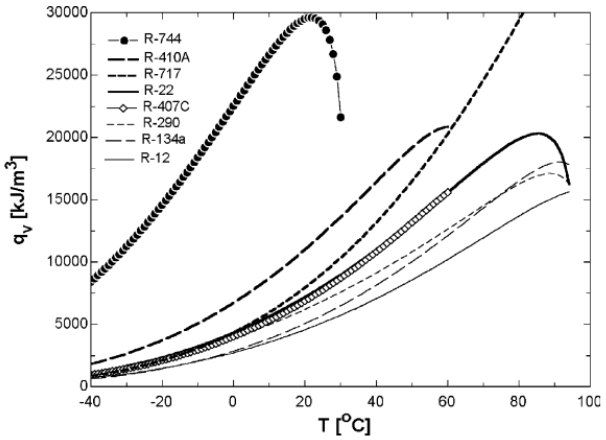


Figure 2.14: Volumetric refrigerating capacity comparison for R744 and other refrigerants [74].

3. State-of-the-art CO_2 transcritical heat pump

3.1. Market overview

Currently, several heat pump models are developed with great ease, being a technology with a great evolution in the last decades. Most current heat pump producers already offer CO_2 solutions along with other fluids. Table 3.1 shows some current commercially available models along with their main features. It should be noted that, as has been said previously, a wide range of capacities are available at the moment. Denso of Japan was the first manufacturer to develop an HPWH using the transcritical cycle of CO_2 with their model EcoCute. That model started development in 1999 in collaboration with Gustav Lorentzen and was introduced in 2001 [75].

Table 3.1: Current commercial market heat pumps for R744 and R717 and respective characteristics

Model	Manufacturer	Type	Working fluid	Heating Capacity	Max. Heating Temperature	COP	Ref.
EcoCute	Denso	Air-to-water	R744	6.0 kW	90 ºC	3.2	[48]
Vitocal 252-A	Viessman	Air-to-water	R744	12 kW	70 ºC	5.3	[76]
unimoAW	Mayekawa	Air-to-water	R744	74 kW	90 ºC	4.2	[77]
CHP	Revere	Air-to-water	R744	5 to 80 kW	90 ºC	3.9	[78]
Ecosirocco	Mayekawa	Air-to-air	R744	123 kW	120 ºC	5.5	[79]
Q-ton	Mitsubishi	Air-to-water	R744	30 kW	90 ºC	4.7	[80]
HeatPAC	SABROE	Water-to-water	R717	310-2075 kW	75 ºC	6.0	[81]

3.2. Energy sources

Heat pumps are considered a very efficient technology and therefore play a big part in reducing energy demand and GHG emissions. The possibility of using natural refrigerants allows heat pumps to have an environmentally friendly system and at the same time generate higher thermal outputs than the mechanical energy input necessary for their functioning. Moreover, a variety of energy sources can be used, the main ones being air sources, ground sources, and water sources. This diverse range of input options results in the rapid and continuous development of new and optimized solutions looking for the most efficient technology [82]. It is important, however, to acknowledge the differences between the energy sources stated above.

3.2.1. Air source heat pump (ASHP)

Due to their low installation cost and simple operation, together with medium-to-high efficiency, which leads to less primary energy consumption, the most common application of heat pumps uses outdoor air as a heat source, which implies that the evaporator is located on the outside of the building. The major drawback is regarding the variations in the ambient air temperature, which can hurt the system output. Still, as the aforementioned, the evaporating temperature does not as heavily the performance of the transcritical cycle as it happens with subcritical cycles of conventional refrigerants. Moreover, there can be frost formation on the outside of the evaporator when the ambient temperature is considerably low [53, 82].

3.2.2. Water source heat pump (WSHP)

When compared to air, water benefits from high density and approximately four times more specific heat, which leads to greater energy density. Due to this, water is also used in the sinks that are part of a heat pump system. Furthermore, water sources display a shorter temperature range and higher maximum temperatures than environmental air [53, 82].

3.2.3. Ground source heat pump (GSHP)

As an energy source, the ground has been considered one the most efficient. This is mainly due to its environmentally friendly properties, together with the reliability that it offers. It is always available throughout the day, and it offers a mostly constant source temperature, higher than air or water source temperature. The initial cost, however, is considerably high due to the drilling process [53, 82].

When it comes to energy utilization, geothermal energy is one of the most effective. It is thus envisaged that solutions would be improved by employing it as a heat source. In a heat pump system, it is possible for the evaporator to absorb thermal energy from the subsoil rather than from the surrounding air. In order to achieve this, the evaporator must be connected to the subsoil and come into touch with the heat source. This method has the advantage of having a cold source that maintains a nearly constant temperature, which considerably improves the system's effectiveness all year round. As opposed to an ASHP, this means that it is more suited for cold regions. There is a drawback, though, and that has to do with the drilling process expenses [53, 82].

Using an evaporator with horizontally mounted pipes is an effective way to utilize the earth as a heat source. Numerous investigations show that the ground temperature is quite steady below the frost line. Typically, a depth of around 2 meters is sufficient to provide a steady heat source. Because of this, the costs are fair, and the economy and efficiency of this solution are on par with ASHPs. Vertical boreholes can be utilized if the evaporator pipes are positioned vertically, and they can reach depths of 200 meters. In addition, because groundwater maintains a consistent temperature between 8 and 10 °C, it is also a stable solution. All of these techniques deal with seasonal temperature changes while providing a reliable heat supply. Although the groundwater solution has the greatest COP, it can occasionally be challenging to locate areas that produce this source in large enough amounts. Additionally, the design of the vertical borehole also offers a greater COP than the horizontal pipes, but it is not a workable solution for the majority of heat pump projects due to the much higher cost [83].

3.3. Transcritical CO_2 cycle modifications

When working with a natural working fluid such as CO_2, the conventional transcritical cycle may not take full advantage of the favorable heat transfer and thermodynamic properties of the refrigerant. Hence, rather than searching for another fluid that fits the defined cycle, some modifications can be incorporated into the conventional cycle [49]. The goal of these modifications is to lead to improvements in performance efficiency, capacity, and component size, by adapting the system to its requirements. Specifically for the studied cycle, the modifications are mainly focused on reducing exergy losses in the throttling and gas cooling processes. Various authors have suggested and studied a large number of improvements in technologies toward the conventional CO_2 cycle. In particular, Lorentzen et al. [84] highlighted most of them. The main studied modifications of the transcritical CO_2 cycle are shown in Figure 3.1 and presented here. It is important to mention that some modifications are considered for refrigeration cycles instead of heat pump cycles. Since their configuration is quite similar, both areas will be reviewed.

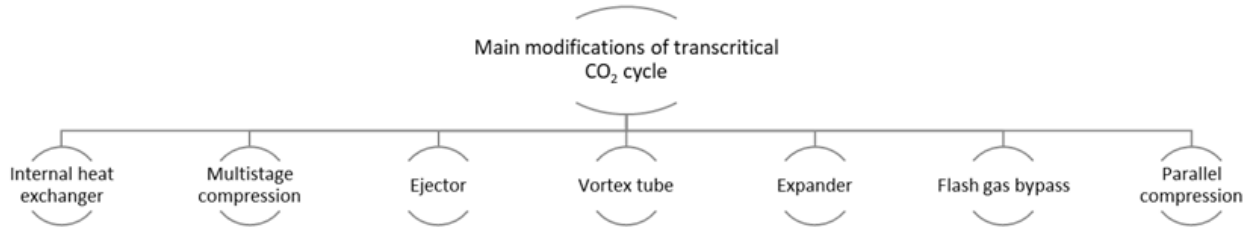


Figure 3.1: Main transcritical CO_2 cycle possible modifications.

3.3.1. Internal heat exchanger

From all the presented possibilities, the introduction of an internal heat exchanger (IHX) is the most commonly used in refrigeration and heat pump systems due to its simplicity and accessibility, while still having a considerable impact on the efficiency and capacity of the transcritical cycle when optimized and used correctly. Many authors have reported benefits in using an additional heat exchanger internally to the cycle. Mu et al. [85] showed that IHX can lower optimal discharge pressure. This allows that, at optimal conditions, high side pressure and low side pressure are closer [86]. Aprea et. al [87] indicated up to 10 % improvements to the COP in a residential application. Finally, by lowering the relatively high irreversibility during the expansion step in the conventional transcritical CO_2 cycle, Boewe et al [88] achieved a 25 % overall improvement. Chen et al [89] observed that a high-efficiency IHX is particularly advantageous for systems operating at pressures less than 95 bar and evaporation temperatures below 5 ºC. At higher pressures, above 110 bar, the IHX efficiency should be lower than 60 %. However, in some cases, the effects on optimal discharge and COP with the addition of the IHX were also found to be marginal [86]. This is largely due to the conflict between the different outcomes of the addition of the IHX. While the IHX increases, in fact, cooling and heating capacity, reducing the mass flow rate necessary, it also increases compressor work due to the increased superheating and increases compressor discharge temperature. Thus, the IHX positive or negative effect on system performance is mostly determined by the working fluid and operating circumstances.

The primary application of an IHX is to eliminate the need for superheating and subcooling in a typical setup. The IHX is also known as SGHX since it is usually placed at the exit of the gas cooler and in the suction line of the compressor. The placement of the IHX is shown in the schematic in Figure 3.2. The heat exchange of the discharge vapor of the gas cooler with the

discharge vapor of the evaporator allows subcooling of the fluid before it enters the expansion valve and, at the same time, superheats the fluid that will enter the compressor. Thus, the additional heat given to the fluid by staying longer at the evaporator is no longer necessary [47].

In short, the addition of this heat exchanger brings three main benefits to the heat pump performance: firstly, it increases enthalpy at the compressor inlet, reducing compressor work, secondly, it guarantees that the fluid is entirely vaporized before entering the compressor, and finally it increases the heat rejected from the high-pressure side, reducing evaporator heat input [69]. All these outcomes are represented in Figure 3.3.

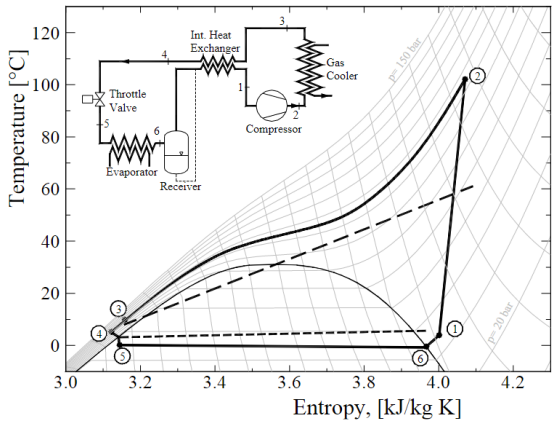


Figure 3.2: $T - s$ diagram and schematic of the transcritical CO_2 cycle with the IHX addition [90].

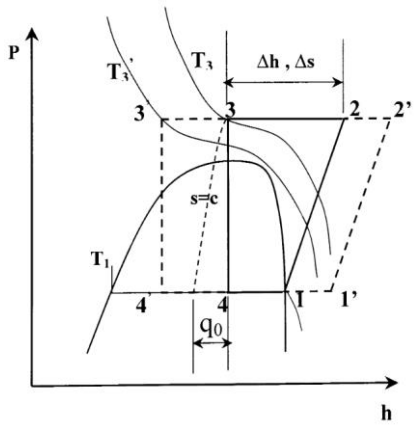


Figure 3.3: *P-h* diagram comparison of the transcritical CO_2 cycle with and without the IHX [55].

3.3.2. Multistage compression

For refrigeration purposes, a multistage compression and intercooling of liquid and vapor refrigerant is a very commonly used technology to improve capacity and COP. It is normally incorporated when the compression ratio is greater than 8 to 10 or the evaporation temperature is as low as -40 to -70 ℃ and a great temperature lift between the source and sink is needed. Multistage compression allows refrigerant heating to happen over two or more different pressures and temperatures, offering great potential applications such as commercial supermarkets refrigeration and air conditioning [91]. Even though it is mainly used for cooling purposes and not a lot of research has been done on its application for heating applications, it can still be useful for domestic water heating, especially in cold climates [92]. Multi-staging is normally unnecessary

for temperatures lift until 80 to 100 °C. This way, the system's complexity is maintained low and with reduced costs [93].

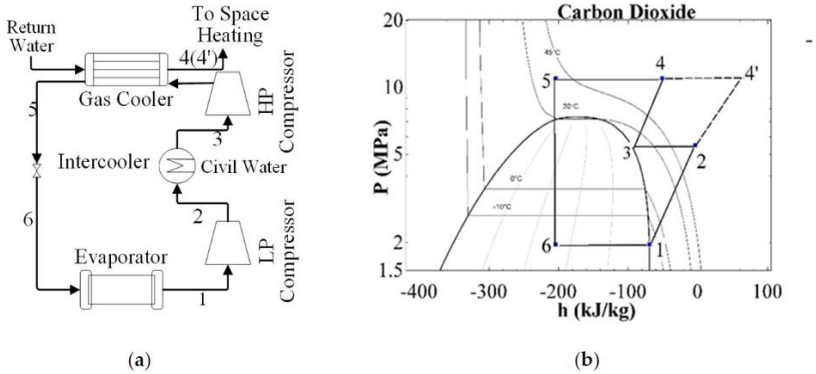


Figure 3.4: Transcritical CO_2 multistage cycle with intercooler: (a) schematic and (b) *P-h* diagram (HP: high pressure, LP: low pressure) [94].

3.3.3. Ejector

A traditional CO_2 transcritical cycle is severely damaged as a result of expansion losses during the expansion device operation because of the significant disparity between the gas cooler pressure and the evaporation pressure [95]. Using an ejector is one of the methods discovered to recycle some of the kinetic energy produced by the expansion process. The ejector increases the pressure for the superheated CO_2 at the inlet of the compressor, reducing the pressure ratio and saving the compressor input power. In addition, by correctly lowering the expansion inlet pressure, throttle loss may be decreased, improving COP [4]. When compared to other solutions regarding the expansion process, the ejector has the advantage of having a simple structure, absence of moving parts, low cost, and low maintenance requirements [96]. Figure 3.5 shows the placement of the ejector and the respective modifications to the *P-h* diagram.

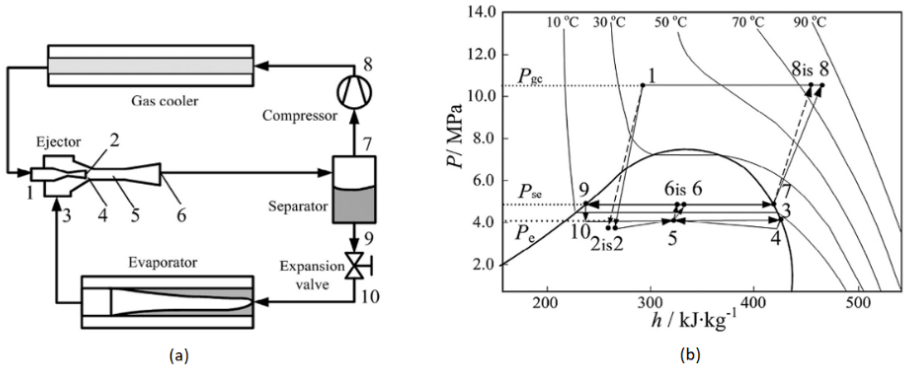


Figure 3.5: Transcritical CO_2 ejector cycle: (a) schematic (b) *P-h* diagram [97].

3.3.4. Vortex tube expansion

A vortex tube can be added to the transcritical CO_2 cycle as an energy separation device, as the inlet fluid for a vortex tube can be divided into two fluids with different heat and temperature. This occurs if the pressure gap between the inlet and outlet is constant. Analogous to the ejector, the introduction of the vortex tube aims at reducing expansion losses after the heat rejection, operating as the expansion valve [91]. This setting is represented in Figure 3.6 together with the respective *P-h* diagram.

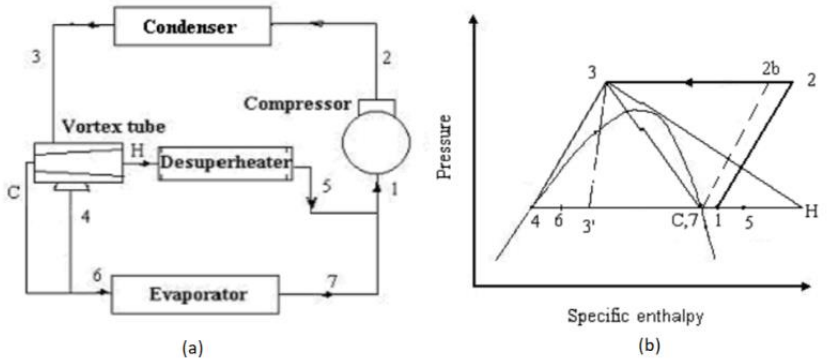


Figure 3.6: Transcritical CO_2 vortex tube expansion cycle: (a) schematic (b) *P-h* diagram [86].

3.3.5. Expander

As it was stated before, throttling losses for the transcritical CO_2 cycle are significantly higher than that of a standard working fluid, since the supercritical fluid is throttled to the two-

phase region. The replacement of the expansion device for a work-producing device such as an expander can lead to improvements in system performance, mainly due to the reduction of expansion losses. In addition, when acting coaxially with the compressor, it can recycle the expansion power, which can reach 25 to 30 % of compressor work input [4]. The schematic related to this modification is shown in Figure 3.7. Similar to what happens with the remaining components, the upside for the use of an expander depends mainly on the isentropic efficiency of the expander as it is shown in the *P-h* diagram of Figure 3.8 [98]. Robinson et al. [99] run a rigorous parametric study and found that an IHX may boost cycle COP if the expander efficiency was just 30%, but it would significantly reduce COP if the expander isentropic efficiency reached 60 % efficiency. Both Yang et al. [100] and Hua et al. [101] registered improvements in exergy and energy performance when using the expander. Even though the introduction shows potential to improve the efficiency of a transcritical system, there is still a necessity to reduce the cost and difficulty associated with its use as well as increase the range of operating conditions for CO_2 expanders [91].

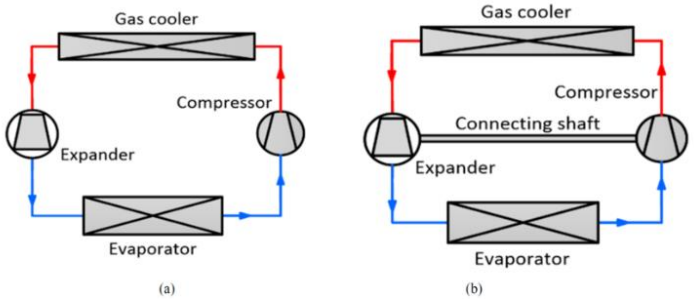


Figure 3.7: Schematic of the transcritical CO_2 cycle with an expander working (a) independently or (b) coaxially with the compressor [98].

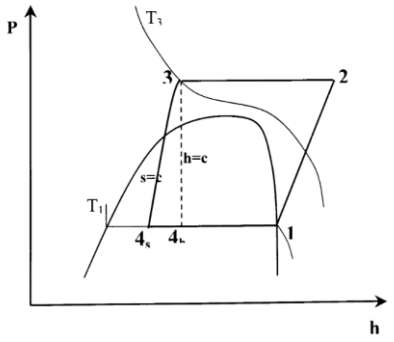


Figure 3.8: *P-h* diagram for the transcritical CO_2 cycle with an expander [55].

3.3.6. Flash gas bypass

The introduction of a flash gas bypass aims at resolving the problem of having two-phase flow entering the evaporators for heat absorption. This results in a vapor state entering the evaporator without having a significant cooling capacity [98]. Although this problem is not unique to CO_2 systems, they are made considerably more prone to it because they use tiny or micro-channel tubes with several passes in the evaporator to try to handle the extremely high pressures. [52]. The technique behind the flash gas bypass is to prevent the vapor state flow from

entering the evaporator by pumping it directly to the compressor suction line. Thus, phase separation occurs at the flash tank. The separate liquid flow follows the conventional line into the evaporator inlet [98]. Figure 3.9 shows both the schematic and *P-h* diagram that results from the addition of the flash gas bypass.

3.3.7. Parallel compression

Parallel compression is a variation of the flash gas bypass technology presented in the previous section. However, instead of using the same compressor for the flash gas as for the evaporator vapor, an auxiliary compressor is utilized to increase flash gas pressure to the discharge pressure. This can also be achieved by using a coupling compressor. When compared to the flash gas bypass conventional configuration, this technology is useful since the compressor mainly compresses the evaporator vapor when both flows are mixed. Hence, the parallel compression configuration is capable of at least achieving the same efficiency as the flash gas bypass configuration. Its maximum efficiency improvement is achieved when dealing with low evaporation temperatures [91, 98]. This configuration is shown in the schematic in Figure 3.10.

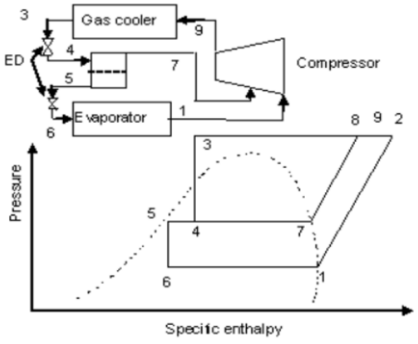


Figure 3.9: $P-h$ diagram and schematic of the transcritical CO_2 cycle with flash tank bypass [86].

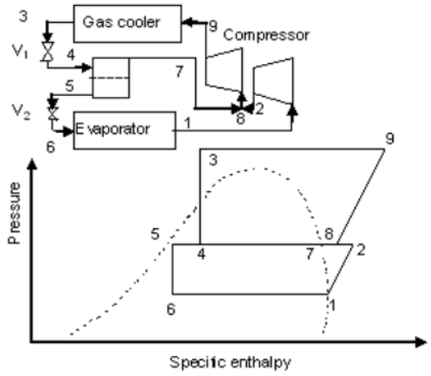


Figure 3.10: *P-h* diagram and schematic of the transcritical CO_2 cycle with parallel compression [86].

3.3.8. Comparison between configurations

A comparison between the various modifications is essentially based on COP improvement and reduction of optimum discharge pressure. Following the results presented in Figure 3.11 and Figure 3.12, it can be concluded that maximum COP improvement and optimum discharge pressure are reached when adopting the turbine/expander configuration, while the minimum is

achieved with the internal heat exchanger. It is noteworthy, however, to state that the introduction of a work recovery device such as a turbine or an expander is heavily costly when compared to an internal heat exchanger. The same applies to CO_2 cycle modifications such as multi-staging, parallel compression, and vortex tube. Once it allows lower investment, while still providing significant COP and discharge pressure improvements, the ejector expansion cycle should be heavily considered. However, since current heat pump configurations are mainly focused on the use of an energy recovery system, in this work, the standard configuration adopted will be the transcritical CO_2 cycle with an IHX located after the outlet of the gas cooler and on the suction line to the compressor [86].

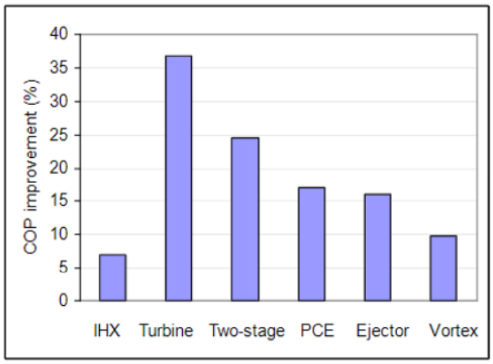


Figure 3.11: COP improvement of the different configurations [86].

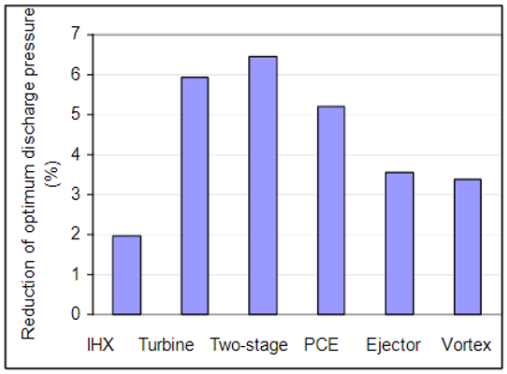


Figure 3.12: Optimum discharge pressure reduction of the different configurations [86].

3.4. Application areas

The beneficial characteristics of CO_2, discussed in Chapter 2.4.2, make it greatly applicable in diverse heat pump applications. For example, a CO_2 heat pump can easily run simultaneously for heating and cooling, which highly increases its performance. The most promising areas for CO_2 heat pump application are provided in the diagram in Figure 3.13. This work analyzes the potential of a CO_2 transcritical heat pump for heating DHW.

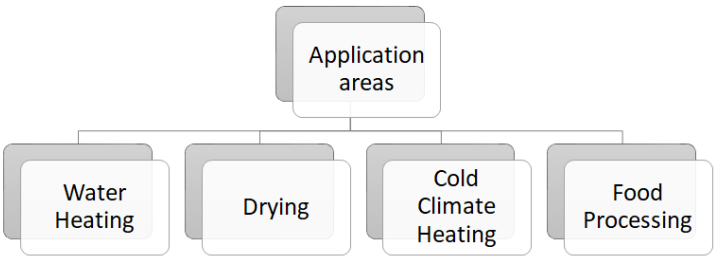


Figure 3.13: Main application areas for heat pump transcritical CO_2 cycle.

3.5. NH_3 research

As was stated previously, the study of NH_3 as a working fluid for heating applications is far less developed than for CO_2, so it is natural that for now there is not plenty of available studies regarding different modifications to the conventional cycle. Due to that and so that a fair comparison between CO_2 and NH_3 configurations can be made, only the conventional and the addition of the IHX will be studied.

Compared to the transcritical CO_2 cycle, NH_3 systems work sub-critically, similar to what happens with most refrigerants. Consequently, condensation temperature is constant and chosen based on the desired water outlet temperature. The condenser pressure is the corresponding saturation pressure. Still, the heating of the water may be achieved throughout different configurations.

4. Component design

4.1. Compressor

The compressor makes up the fundamental part of the heat pump design, as it is the most complex and the most expensive. It can tolerate high discharge pressures, high differential pressures, and high discharge and oil temperatures. This implies that, after years of research and development, compressors have been highly developed for multiple and diverse applications. Due to the high work input, it is also subject to the highest wear [102]. The most effective compressor design lowers suction gas heating, and the suction, valve throttling, and compression losses [55]. Thus, its selection must be taken carefully and with some safety margin. As was mentioned before, the transcritical CO_2 cycle requires extremely high pressures (80 to 130 bar) at the compressor discharge state compared to CFC and HFC systems (10 to 40 bar). There is therefore a chance of numerous mechanical losses and oil leakage. The pressure ratios for a CO_2 system are relatively low, even with the significant pressure differential, which boosts compressor efficiency. As a result, using high-pressure small compressors is a practical choice [55]. Even if the structure, particularly the outer shell, must be thicker, a CO_2 compressor can nevertheless be smaller overall than compressors used for many of the major traditional refrigerants. In reality, studies have shown that a CO_2 compressor can be more compact than an R134a compressor, primarily because the latter has a lower volumetric capacity and a lower gas density [55, 74]. According to Süss et. al [103], CO_2 compressors are able to operate better than those for conventional refrigerants since they have lower pressure ratios. The smaller piping and heat exchangers may also serve to offset the eventual greater cost added by the compressor.

Although Fleming et al [104] found that two-stage compression will be useful in most circumstances in order to optimize these operation parameters, it was also concluded that for DHW, heat pumps with a single-stage compression are competitive with state-of-the-art current technology [55].

Due to the significant role that a compressor plays in the refrigeration cycle, numerous types of compressors have evolved over time to accommodate the widest range of applications. The main types of compressors are displayed in Figure 4.1. Positive displacement compressors and dynamic compressors are the two basic types of compressors. On one hand, in a positive displacement compressor, a volume of gas is trapped inside a closed chamber, and the vapor pressure increases by steadily constricting this space via a compressing device, such as a piston,

scroll, or screw. Dynamic compressors, on the other hand, use an impeller (centrifugal or axial force) to accelerate the gas while compressing the fluid. In the diffuser, the pressure is increased even further. Thus, positive displacement compressors boost pressure by mechanically altering the volume of the working fluid, whereas dynamic compressors do it by mechanically changing the velocity of the working fluid. Additionally, there are two different types of positive displacement systems: reciprocating (where the volume change is achieved by a piston rotating within a cylinder) and rotary (where the refrigerant is compressed within the casing by two rotors) [42, 105].

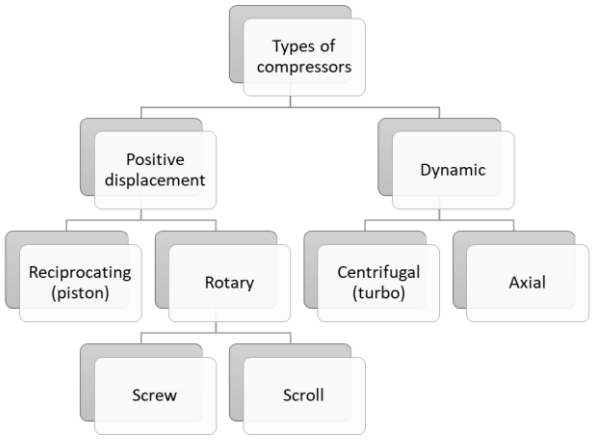


Figure 4.1: Main types of compressors.

Compressors can be characterized not only by their varied operating principles but also by the basic type of construction, as shown in Table 4.1. The distinction between open, semi-hermetic, and hermetic compressors has nothing to do with the type of compressor and everything to do with how the compressor is linked to the drive motor [42].

Table 4.1: Characteristics of the different types of compressors

Type	Size	Type of construction	Characteristics
Open compressor	Large	The motor and compressor are mounted separately. Easy access to the components	No shell cost; high risk of refrigerant leakage;
Semi-hermetic compressor	Medium	The motor and compressor are mounted in a two-piece shell that can be opened. Most components are accessible.	More expensive than the hermetic; considerable risk of refrigerant leakage; use oil pump for lubrication.
Hermetic compressor	Small	The motor and compressor are housed together in a closed shell. Can't be opened for maintenance. In case of failure, the compressor must be replaced.	Very low risk of refrigerant leakage; lubrication by centrifugal force.

Turbo compressors are the best technology among the ones described previously. This sort of compressor, however, is primarily intended for capacities of MW or above. Since the heat pump to be designed will have a heating capacity of up to 250 kW, the use of this pricey technology is not optimal for this application, as there will be considerable friction losses and the speeds employed need to be very high. Scroll and screw compressors are also feasible possibilities and are sometimes used in HPWH. It is crucial to remember that discharge temperatures in the thermodynamic cycle of CO_2 can reach high values, like 150 ºC, which makes it challenging to lubricate adequately for the proper operation of this type of compressor. Reciprocating/piston compressors address the aforementioned difficulties despite incurring the highest wear on the contact between the rings and the cylinder walls. They are also very efficient at preserving the seal between the compressed vapor above the piston and the crankcase. This is extremely relevant as leakage past the piston rings was identified as having the bigger impact on compressor performance by Süss et al. [103]. Many of the papers reviewed suggested that leakage influence on a CO_2 compressor is extremely small (about 1 %) when working with properly designed. Furthermore, they are well suited for high-pressure differentials with a very small displacement [31, 52]. Taking the aforementioned characteristics into account, reciprocating compressors are the most versatile and are typically regarded as the current finest solution for a transcritical CO_2 heat pump [106].

4.2. Heat exchangers

In comparison to systems using traditional refrigerants, the CO_2 system uses both heat exchangers at greater levels of operation. Although the required component thickness is increased

as a result, the flow velocity can also be increased. Higher Reynolds numbers in the heat exchangers as a result enhance the rate of heat transfer [52].

It is also relevant to recognize that the gas cooler and evaporator must have different designs. This is due to the fluids that they are exchanging heat with. While the evaporator exchanges heat with ambient air, the gas cooler heats DHW. This implies that the considerations for both heat exchangers will be significantly different. Further details are given below.

4.2.1. Gas cooler

Gas cooler performance has an essential impact on many variables responsible for the performance of the system, such as gas cooler refrigerant and water outlet temperature, and high-side pressure. Determined the gas cooler pressure at the outlet of the compressor, the gas cooler may be dimensioned using the desired inlet and outlet temperatures and either the heat load or the mass flow rates. Moreover, regarding the gas cooler design, it is known that the heat exchanger should allow counterflow configuration as that is extremely important to take advantage of the high refrigerant temperature glide [52].

The plate and frame heat exchanger, which is shown in Figure 4.2, consists of a set of thin metal plates with rectangular geometry and a pattern of corrugations. The corrugations are normally described as herringbone indentations and aim at promoting the turbulent circulation of the fluids and also at increasing the effective area for heat exchange. Thus, this type of heat exchanger is able to achieve high heat transfer rates while occupying small spaces. Because the hot and cold fluids move in opposite directions and alternate channels, each cold fluid stream is surrounded by two hot fluid streams, providing exceptionally efficient heat transfer. The heat load may be increased by installing more plates [40]. Dimension of the plates and number of passes may also be altered to adapt to certain applications. Current heat exchanger producers, such as SWEP, use brazed plate heat exchangers (BPHE) which eliminate the necessity for the use of gaskets as in the traditional plate to frame heat exchangers, thus maximizing energy transfer efficiency (95 % of its content) and reducing material use. BPHEs have stainless steel plates with a copper coating applied to one side. These plates go through a vacuum-brazing process that melts the cooper, forming a brazed joint at every contact point. This type of heat exchanger configuration is also known as a plate to plate heat exchanger [31, 107]. It is also relevant to state that since the heat exchanger is designed to achieve a specific temperature differential, the log mean temperature difference ($LMTD$) method is more appropriate than the effectiveness-NTU method [40].

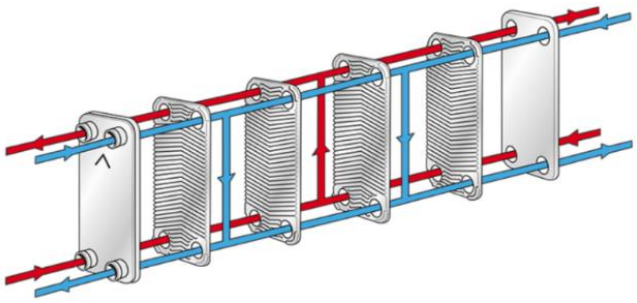


Figure 4.2: SWEP brazed plate heat exchanger configuration [107].

The arrangement of the plates may be changed depending on the required heat transfer rate and pressure drop. As seen in Figure 4.3, the plates are normally rectangular with four circular openings through which the two exchanging fluids can enter and exit. Usually, the plates are manufactured in the chevron corrugation shape. This implies that these plates are normally offered with two or more inclination angles (θ pattern), for the same pattern. Up to 45º (low θ pattern), plates assure lower pressure drop thus being named soft plates. Angles higher than 45º and up to 90º (high θ pattern) cause significantly higher pressure drops and are, therefore, called hard plates. The conjugation of two plates can be made as desired [42, 108]. For example, a high θ pattern plate can be used with a low θ pattern plate, resulting in the M type plate displayed in Figure 4.3.

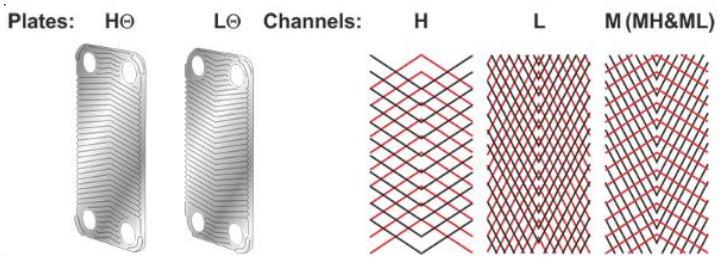


Figure 4.3: Plates with low theta pattern ($L\theta$) and high theta pattern ($H\theta$) and the different possible plate pattern conjugations [42].

The design of the gas cooler assumes great importance mainly due to its impact on the gas cooler outlet temperature. Minimizing this temperature is essential to achieve significant improvements in heat pump performance. Three main impacts should be considered from decreasing the refrigerant gas cooler outlet temperature [55]:

- Reduction of throttling loss on the expansion device due to the reduction of the optimum gas cooler pressure;
- Maximizing the heat rejection on the gas cooler;

- Reduction of compressor work input due to reduction of the optimum gas cooler pressure.

It has been also observed by various studies that the water inlet temperature has a significant impact on the performance of the HPWH. Yamaguchi et al. [109] concluded that an increase in water inlet temperature leads to a degradation of the performance of the heat pump. These results were corroborated by Stene et al. [43], which showed that increasing water inlet temperature from 5 ºC to 15 ºC causes a COP reduction of 10 %. Finally, Paniagua et al. [110] stated that the heat exchange at the gas cooler increases for lower water inlet temperature due to the increase in enthalpy difference and a better fit between the CO_2 and water temperature profiles. It was also concluded that the effect of water inlet temperature variation on compressor work is negligible.

4.2.2. Evaporator

In a typical CO_2 cycle, the evaporator serves two crucial functions: it ensures that CO_2 is completely vaporized prior to the compressor's suction by allowing heat transfer from the surrounding air to the refrigerant at the proper temperature. An accumulator and an IHX, however, mean that the second function is no longer entirely required. The IHX will make sure that CO_2 enters the compressor completely vaporized. Depending on how the fluid flows through it, the evaporator can operate in one of two ways. A receiver can be used to allow the fluid to flow completely liquid into the evaporator, separating the gas from the liquid. This results in a vapor-liquid mixture at the evaporator outlet (usually 50 to 80 % vapor). The alternative setup, named direct expansion (DX) allows the fluid to continuously run through the evaporator while completely evaporating and even being superheated at the evaporator exit [31, 42].

Other classification may be done depending on its design. In this heat pump configuration, the evaporator exchanges heat with ambient air, which is naturally at a higher temperature. This implies that the heat exchanger is differently designed from both the gas cooler and the IHX, which were defined as BPHE. As the heat transfer coefficient of the air side is very small, finned tubes are increasingly used nowadays in order to increase heat transfer effective area and have balanced thermal conductance on both sides. The EcoCute units, referenced before, use finned-tube air to refrigerant evaporators with copper tubes and aluminum fins. In essence, these evaporators are similar to the evaporators used for HFC refrigerants. They need, however, special considerations considering CO_2 unique features, such as thicker tubes and specific circuitry.

It is commonly assumed that the working fluid, coming for the expansion valve in a two-phase regime, either is heated to saturated vapor at the evaporator exit or is superheated. However, since the adopted configuration uses an IHX, the working may not be superheated and even display a quality less than 1.

CO_2 flows in a controlled manner, unlike the fluid with which it exchanges heat, in this case, air at atmospheric pressure. Thus, the evaporator shall consist of a cross-flow heat exchanger with a single tube and be configured as illustrated in Figure 4.4. The configuration must be the plate finned-tube type as it allows easy flow of the atmospheric air. Air circulation may be by natural convection or forced circulation using a fan to the evaporator system. This implies that the work input for the fan is added to the compressor work input, thus affecting the global system COP value. As for the material, copper is usually used for the tubes and stainless steel or aluminum for the fins [31, 42]. These materials are displayed in the example shown in Figure 4.5.

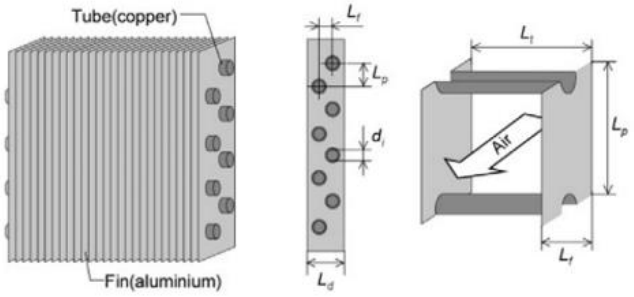


Figure 4.4: Schematic of the finned tube evaporator [109].



Figure 4.5: Finned-tube evaporator with aluminum fins and copper tubes.

The evaporator accounts for one of the inconveniences of a working heat pump. The noise of the fans, in some cases, can be somewhat loud leading to some discomfort, especially in domestic applications. In this specific application, since a residential building is being considered, the evaporator can easily be placed in some compartment separate from any inhabitants, therefore avoiding this discomfort. Still, an axial fan with low speed ensures a quieter operation [102].

4.2.3. Internal heat exchanger

As was previously mentioned, the IHX has the function of superheating the fluid to prevent any liquid drops from entering the compressor and degrading its performance. The IHX can be

introduced as a BPHE, much as the gas cooler, to boost efficiency. Most of the research regarding the use of the IHX in a CO_2 transcritical heat pump was already presented in Chapter 3.3.1.

4.3. Expansion device

The expansion and throttling process of the working fluid is performed by an expansion valve. The expansion valve is used to attain the necessary operating temperatures of the CO_2 in the evaporator after heat rejection in the gas cooler. Therefore, it must be installed at the outlet of the gas cooler. However, as in this heat pump configuration, an IHX is used, and the expansion valve will only be put after the IHX. In addition, it helps to achieve the desired pressure differential between the low side and the high side of the cycle [69]. For this specific heat pump, the evaporation temperature defines the low side pressure, and the gas cooler optimal pressure, as a result of the desired water outlet temperature, defines the high side pressure. Finally, it is able to restrict the flow of the CO_2 around the heat pump, controlling the refrigerant charge to an adequate amount to overcome the heat load in the evaporator.

A variety of types of expansion devices can be used to achieve these goals in the transcritical cycle. The following are the primary types of valves utilized in this process [111]:

- Capillary tube or orifice;
- Mechanic expansion valve (MEV);
- Thermostatic expansion valve (TEV);
- Electronic expansion valve (EEV).

Both capillary tube and MEVs are not capable of operating efficiently as their mechanism is extremely simplified. A TEV can be used to manage refrigerant flow as it allows precise refrigerant flow control for a wide range of inlet temperatures. By controlling the level of vapor superheating at the evaporator outlet, this kind of valve enables the entire surface of the evaporator to be utilized for evaporation. Still, EEVs are increasingly employed today, providing flow control with even greater accuracy and performance [112]. To achieve dynamic matching of the CO_2 system, the EEV, operating via a controlling algorithm, is precisely controlled for accurate opening based on the load demand of the system. This allows a quick and precise reaction of the mechanism to load changes, considerably boosting the unit's operational energy efficiency [113]. Furthermore, the possibility of linking components electrically allows for more freedom in the system layout,

which is vital to designing compact systems [31]. Finally, it eliminates the need for a separate shut-off solenoid valve, as this type of valve can close when the system is turned off.

4.4. Accessories

4.4.1. Suction line accumulator

The use of suction line accumulator (SLA) is aimed at mainly three purposes [114]: (1) protecting compressors functioning, avoiding liquid refrigerant to enter its crankcase, (2) assure that the oil return is made a adequate rate to the compressor, (3) store excess system charge.

After consulting with various manufacturers, since it has been added an IHX that significantly superheats the fluid, the utility of a SLA was questioned regarding this specific application. The use of the SLA in this configuration would only be useful to store the liquid that did not fully evaporate, i.e. an unused portion of the system charge [115]. However, even with a heat exchanger mounted on the suction line, it is recommended to mount a suction accumulator. When starting or restarting the installation, liquid hammer is common. In short, liquid hammer causes a significant pressure rise owing to the stopping of the flow caused by the operation of components such as valves. This leads to high pressure shockwaves traveling through the piping system, frequently resulting in pipe pipes and damage to valves [42]. Furthermore, at the start-up, the heat exchanger is not capable of giving enough power to vaporize the liquid. Therefore, the appropriate SLA and its associated cost have been ascertained.

4.4.2. Oil separator

As it is known, oil serves a crucial function of lubrication in the compressor. Thus, the use of oil is significantly important to achieve sufficient efficiency in the compressor. However, it affects negatively if present in the heat transfer components, as it increases pressure drop and reduces heat transfer performance [116]. In order to avoid this to happen, oil separators can be installed at the high pressure side, at the discharge of the compressor. When the refrigerant fluid mixed with some oil enters the separator, due to the expansion, the fluid separates from the oil, rising towards the outlet connection, while the oil heads to the bottom of the separator. The oil can then also be recovered back from the separator and returned to the compressor through a dedicated connection. Hence, the refrigerant follows to the gas cooler without almost any oil mixed, increasing the heat transfer efficiency and increasing the lifetime of the system [42, 117].

Inevitably, some oil will always mix with the refrigerant because no oil separator is 100% effective. It is significant to note that at lower temperatures, the issue of oil carry-over becomes more significant. This happens as a result of the oil having a bigger impact on heat transmission as viscosity also rises [42]. The oil separator is even more crucial in cycles that require high oil concentrations, such as ammonia systems, or in large capacity systems [116].

4.4.3. Oil receiver

An oil receiver must be used when compressors are operating in parallel and are capable of starting and stopping independently. Maintaining the right oil level for the various working scenarios is one of the trickiest parts of this kind of system. This is because when the compressor is stopped, the oil level in the compressor crankcase may decrease, making it difficult for the compressor to start when it is required [118].

4.4.4. Filters

It is critical to reduce pollutants to a minimal in order to achieve long-term system life. This especially necessary for a heavy-duty application like a heat pump. Poor initial system cleaning, poor oil, and refrigerant quality, or even oil deterioration might result in contaminants. As a result, every heat pump should have at least one filter drier. Two normal filter are normally desired, however if this causes a piping issue, a single reversing filter-drier will suffice [119]. Filter driers are typically installed in the liquid line of the heat pump or refrigeration cycle, where they serve two purposes. To protect the expansion valve from particle contamination and to absorb any moisture present in the system. Both these functions are essential. In one hand, moisture can freeze in the expansion valve orifice, corrode metal components, and wet the motor windings of a semi hermetic compressor, such as the one used in this specific application. This could eventually result in motor burnout and oil sludge. On the other side, foreign particles can contaminate the compressor oil and get stuck in the expansion valve's parts, turning them inoperable. Additionally, since there is a filter in the liquid line, it is simple to determine if it has clogged because a pressure drop results in the refrigerant liquid boiling and producing flash gas. This will inevitably result in the expansion valve failing. Filters can also be inserted, though less frequently, in the suction line prior to the compressor input to protect the compressor from potential pollution. If there are many compressors, it is ideal to place filters in both the liquid line and each suction line. Finally, oil filters are frequently used between the oil separator and the compressor in the oil return line.

Excessive oil carry-over can result if this filter is clogged, negatively affecting heat transfer in the evaporator [42, 120].

4.4.5. Check valves

Check valves guarantee a one-way flow of refrigerant in the installations with high working pressures. To stop the refrigerant return, they can be put on the liquid, suction, discharge, or hot gases defrost lines [121].

4.4.6. Sight glass

Even though they can be fitted at any desired location, sight glasses are usually inserted into the liquid line of the heat pump and refrigerating systems immediately after the filter drier to monitor flow, condition, and moisture changes before entering the expansion process. It generally serves two purposes. It checks whether the refrigerant moisture content is within permissible limits through a color code and whether the expansion valve only receives liquid refrigerant. The first function can be performed via a humidity indicator. A green color indicates that the moisture content is fine, and no action is necessary. However, if the color starts to change to yellow, there are problems regarding the humidity of the system and the filter drier must be substituted. The second function can be controlled directly through the viewing of flow. If frothing is detected in the sight glass, then either there is a shortage of refrigerant, or the refrigerant is a gas/liquid mixture. This may be due to insufficient subcooling, high-pressure drop in the liquid line, or heat transfer throughout the liquid line to the surrounding environment [42, 120, 122].

4.5. Issues related to component design

4.5.1. Throttling loss

The throttling loss is mainly affected by the gliding heat rejection process at the gas cooler. An adequate design of the gas cooler can minimize these losses. By reducing the temperature of the outlet supercritical gas cooler as much as feasible, throttling losses can be significantly decreased. This is due to the decrease in the optimum gas cooler pressure. However, it is important to bear in mind that the high specific heat near the critical region is also a factor that increases throttling loss. For subcritical heat rejection, this loss would be significantly lower [49, 55].

4.5.2. Pressure drop

When designing a transcritical CO_2 heat pump, pressure drop via the heat exchange components should be a key issue. For example, compared to the conventional refrigerant R134a, R744 has an estimated pressure drop of 0.9 bar/K in the evaporator at 0 ºC. A R134a heat pump shows a pressure drop of only 0.1 bar/K in the same conditions [55].

5. Simulation of cycles

The following assumptions were assumed to simplify the modeling of the heat pump:

- Steady-state operation;
- Changes in kinetic and potential energy are negligible;
- Compressor and heat exchanger operates adiabatically;
- Heat loss in connecting piping is negligible;
- The expansion process is isenthalpic.

Note that after analyzing the market and studying the desired application it is the author's opinion that the lower heating capacity would be sufficient for a heat pump with DHW applications. Still, the results from the thermodynamic EES simulations for higher heat loads can be found in Appendix F. Therefore, further work is only made for the lower heating capacity. Also note that all pressure values presented in this work will be treated as absolute pressures.

5.1. CO_2 thermodynamic model

5.1.1. Compressor

The compressor is assumed to be operating adiabatically, thus, the heat loss factor is considered zero. Therefore, the compressor power input can be calculated as shown in the following equation:

$$\dot{W}_{comp} = \frac{\dot{m}_r}{\eta_{s,comp}} \times \left(h_{disch,is} - h_{suc}\right) = \dot{m}_r \times \left(h_{disch} - h_{suc}\right) \tag{5.1}$$

$$\dot{m}_r = \rho_{suc} \times \eta_v \times V_{disp} \times \left(\frac{N}{60}\right) \tag{5.2}$$

where ρ_{suc} is the density of the fluid at the compressor inlet (kg/m^3), V_{disp} is displacement volume (m^3), and N is the number of rotations per minute (RPM).

Both volumetric and isentropic efficiencies are functions of the pressure ratio p_r and can be estimated by a variety of correlations that have been developed by manufacturers or in technical literature.

The thermodynamic study also assumes that the refrigerant flows continuously throughout the system. As a result, the input and output flow rates for all components are the same:

$$\dot{m}_{comp,r} = \dot{m}_{gc,r} = \dot{m}_{ev,r} = \dot{m}_{valve,r} = \dot{m}_r \tag{5.3}$$

5.1.2. Gas cooler

The following equations establish energy balance equations for the refrigerant and water sides:

$$\dot{Q}_{gc} = \dot{m}_r \times \left(h_{gc,i} - h_{gc,o}\right) = \dot{m}_w \times \left(h_{w,o} - h_{w,i}\right) \tag{5.4}$$

$$\dot{Q}_{gc} = \dot{m}_w \times c_w \times \left(T_{gc,w,o} - T_{gc,w,i}\right) \tag{5.5}$$

It is important to state that, when possible, the use of the specific heat for CO_2 should be avoided. This is due to the very significant variations that, as it was explained in Chapter 2.3, happen near the critical point, which can lead to less accurate results.

The gas cooler is designed as a counterflow heat exchanger. Therefore, the heat transfer rate can also be defined through the logarithmic mean temperature difference method [47]:

$$\dot{Q}_{gc} = U_{gc} \times A_{gc} \times LMTD_{gc} \tag{5.6}$$

$$LMTD_{gc} = \frac{\left(T_{gc,r,i} - T_{gc,w,o}\right) - \left(T_{gc,r,o} - T_{gc,w,i}\right)}{\ln\left(\left(T_{gc,r,i} - T_{gc,w,o}\right)/\left(T_{gc,r,o} - T_{gc,w,i}\right)\right)} \tag{5.7}$$

In a refrigerant-to-water heat exchanger it is typically the case that $h_w > h_r$.This implies that the overall heat transfer coefficient for the gas cooler is mainly determined by the heat transfer

coefficient of the refrigerant. Specifically, for this application, the heat transfer coefficient for the CO_2 side is the main parameter that determines U_{gc} [47]. A schematic of the gas cooler model is shown in Figure 5.1.

5.1.3. Evaporator

Similar to the gas cooler, two energy balance equations can be established for the evaporator. In this case for the ambient air and the refrigerant:

$$\dot{Q}_{evap} = \dot{m}_r \times \left(h_{evap,r,o} - h_{evap,r,i}\right) \tag{5.8}$$

$$\dot{Q}_{evap} = \dot{m}_{air} \times c_{p,air} \times \left(T_{amb} - T_{evap,air,o}\right) \tag{5.9}$$

The temperature differences between the evaporator and the gas cooler are different from a general perspective. The exponential nature of temperature variation in the gas cooler does not occur in the evaporator, as the heat transferred from the ambient air to the CO_2 is first promoting phase change rather than temperature increase. When considering the superheat happening at the evaporator after the complete phase change, the evaporator heat transfer can be divided into two separate regions: the two-phase region and the superheating region [123]. Since the CO_2 configuration implies that an IHX is inserted after the evaporator, there is no need to superheat the fluid and, therefore, only the two-phase region is considered. A schematic of the gas cooler model is shown in Figure 5.2.

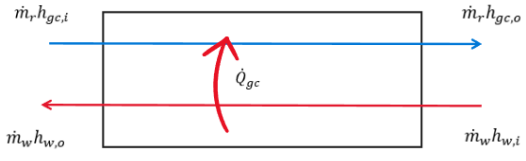


Figure 5.1: Schematic of the gas cooler model.

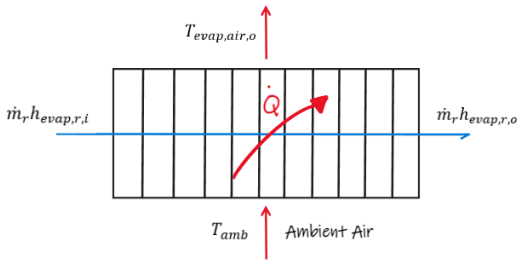


Figure 5.2: Schematic of the evaporator model.

Unlike the gas cooler, the evaporator is designed as an air-to-refrigerant heat exchanger. The typical case is that $h_{air} < h_r$. As a result, it may be noted that the overall heat transfer

coefficient of the evaporator U_{evap}, is more sensitive to the heat transfer coefficient of the air side h_{air} [47].

5.1.4. Expansion valve

This work admits the expansion process as isenthalpic, meaning that,

$$h_{o,EEV} = h_{i,EEV} \tag{5.10}$$

In the conventional cycle, the CO_2 state at the exit of the gas cooler is considered to be the inlet to the EEV, whereas in the cycle with the IHX, the exit of the high-pressure side of the IHX is considered the entrance to the EEV. In both cycles, the outlet of the EEV indicates the state of the refrigerant at the input of the evaporator.

5.1.5. Internal heat exchanger

The IHX configuration is very similar to the gas cooler design. Both are designed as counterflow heat exchangers. The main distinction of the IHX is that the heat exchange happens internally in the cycle. Two heat exchanges can be defined through the IHX:

$$\dot{Q}_{IHX,hp} = \dot{m}_r \times \left(h_{hp,i} - h_{hp,o}\right) \tag{5.11}$$

$$\dot{Q}_{IHX,lp} = \dot{m}_r \times \left(h_{lp,o} - h_{lp,i}\right) \tag{5.12}$$

The IHX effectiveness ε_{IHX} is defined as [124]:

$$\varepsilon_{IHX} = \frac{T_{lp,o} - T_{lp,i}}{T_{hp,i} - T_{lp,i}} \tag{5.13}$$

After reviewing previous studies, this value was taken as $\varepsilon_{IHX} = 0.60$ [124].

Moreover, the IHX is assumed to be externally adiabatic, i.e. there is no heat loss to the environment. This implies that:

$$h_{hp,i} - h_{hp,o} = h_{lp,o} - h_{lp,i} \quad (5.14)$$

5.1.6. Perfomance

The performance of the heat pump is measured by COP value, which is the ratio between the heat output to heated fluid and the need for compressor work input:

$$COP_{hp} = \frac{\dot{Q}_{gc}}{\dot{W}_{comp}} \quad (5.15)$$

Another relevant measuring property is the pressure ratio p_r as it highly influences the compressor isentropic efficiency and, consequently, the compressor work input. The p_r is the ratio between the heat rejection pressure and the evaporation pressure:

$$p_r = \frac{P_{gc}}{P_{evap}} \quad (5.16)$$

5.2. CO_2 conventional cycle

Following the adoption of the internal heat exchanger configuration, it is important to prove that there are improvements over the conventional cycle. For that, various calculations were made using the EES software for both systems. For comparison purposes, before component selection, standard inputs, shown in Table 5.1, were defined:

- Two ambient air temperatures, T_{amb}, were considered, regarding the summer and winter conditions in Porto city (Pedras Rubras). For winter $T_{amb} = 0$ °C. For summer $T_{amb} = 30$ °C. However, for the simulation, it was considered an intermediate situation of $T_{amb} = 10$ °C. After the selection of the components, these two extreme situations will be analyzed with the designed heat pump;
- A difference of 10 ℃ was established between ambient air temperature and evaporation temperature, thus, $T_{evap} = 0$ °C;

- The temperature of CO_2 at the gas cooler exit was defined as $T_{gce} = 35$ °C. Although it is a defined input of the simulation, it is, however, important to understand that T_{gce} is not an independent variable. It is determined by the refrigerant and water mass flow rates, the design of the gas cooler, and the evaporation temperature. Because of this complexity, the optimum pressure correlations will most likely change for each system according to the size and design of the parts of the heat pump. Thus, this value serves as a mere approximation;
- Compressor isentropic efficiency was estimated to be 70 % using heat rejection pressure at the gas cooler P_{gc} and evaporation pressure P_{evap}. The correlation presented in Equation (5.17) was developed by Danfoss A/S for their CO_2 compressors [125]:

$$\eta_{s,comp} = 1.003 - 0.121 \times \left(\frac{P_{gc}}{P_{evap}}\right) = 1.003 - 0.121 \times \left(\frac{8600}{3485}\right) = 0.7044 \qquad (5.17)$$

- Superheating was defined as 5 K;
- No subcooling was needed since CO_2 is in a supercritical state;
- Gas cooler pressure was put at 86 bar. This value was determined using an equation developed by Sakar et. al [124], which allows the optimal heat rejection pressure, $P_{gc,opt}$, to be calculated based on the values of the gas cooler and evaporation temperatures:

$$P_{gc,opt} = 4{,}9 + 2.256 \times T_{gce} - 0{,}17 \times T_{evap} + 0.002 \times T_{gce}^2 = 86.31 \text{ bar} \qquad (5.18)$$

This correlation is valid for evaporation temperatures between -10 and 10 ºC and gas cooler exit temperatures between 30 and 50 ºC.

- Heating rejected at the gas cooler to the DHW, $\dot{Q}_{gc}$, was defined as a constant for the simulation in order to establish the necessary sizing of the components. Thus, for each of the different heating solutions, $\dot{Q}_{gc}$ was the only variable input which was changed in order to achieve the desired heating output.

The conventional CO_2, shown in the plots presented in Figure 5.3, is a standard vapor compression cycle with a gas cooler replacing the condenser. The cycle is composed of the thermodynamic evolutions between the following reference points:

1. Evaporator outlet and compressor inlet;
2. Compressor outlet and gas cooler inlet;
3. Gas cooler outlet and expansion valve inlet;
4. Expansion valve outlet and evaporator inlet.

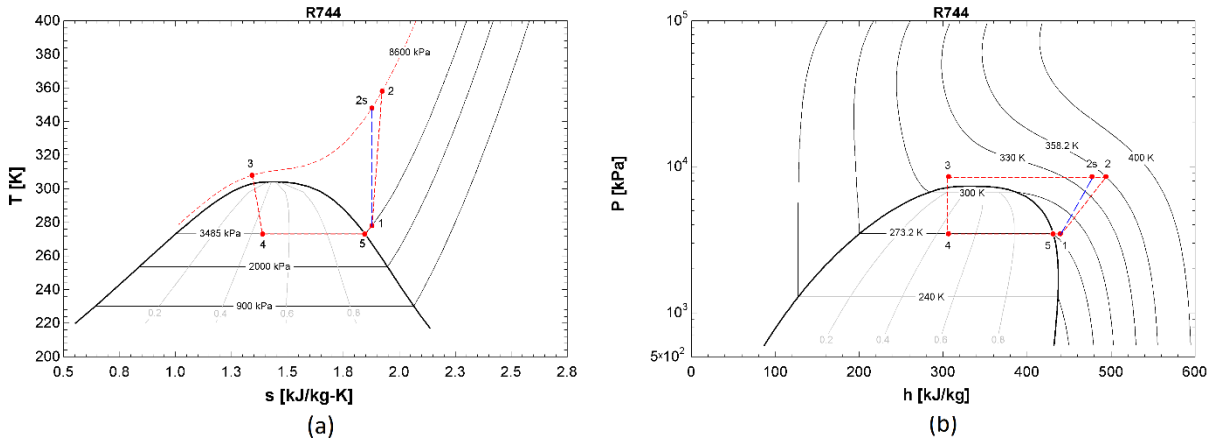


Figure 5.3: Conventional CO_2 cycle: (a) *T-s* diagram (b) *P-h* diagram.

In order to analyze the performance of the heat pump, various thermodynamic simulations via the EES software were made. The codes regarding these simulations are presented in Appendix J.

Table 5.1: 50 kW simulation inputs

Inputs	Value
T_{amb}	10 ℃
T_{evap}	0 ℃
T_{gce}	35 ℃
T_{sh}	5 ℃
T_{sc}	0 ℃
P_{gc}	8600 kPa
$\eta_{s,comp}$	70.00 %
$\dot{Q}_{gc}$	50 kW

Table 5.2: 50 kW simulation outputs

Outputs	Value
COP_{HP}	3.468
COP_{LZ}	7.353
η_{HP}	47.16 %
P_{evap}	3485 kPa
p_r	2.468
$\dot{m}_{CO2}$	0.2668 kg/s
$\dot{Q}_{evap}$	35.58 kW
$\dot{W}_{comp}$	14.42 kW

Table 5.3: State points simulation results (50 kW configuration)

State, i	T_i [K]	P_i [kPa]	s_i [kJ/(kg · K)]	h_i [kJ/kg]
1	278	3485	1.877	439.6
2	358	8600	1.923	493.6
2s	348	8600	1.877	477.4
3	308	8600	1.341	306.2
4	273	3485	1.389	306.2
5	273	3485	1.845	430.9

5.3. CO_2 cycle with IHX

When compared to the conventional system, the CO_2 cycle with IHX takes advantage of the added component to recover some of the high-pressure heat, superheating the CO_2 before entering the compressor. The placement of the IHX is shown in the heat pump schematic in Figure 5.4. The thermodynamic cycle is now composed of six evolutions:

1. Low-pressure side of the IHX outlet and compressor inlet;
2. Compressor discharge state and gas cooler inlet;
3. Gas cooler outlet and high-pressure side of the IHX inlet;
4. High-pressure side of the IHX outlet and expansion valve inlet;
5. Expansion valve outlet and evaporator inlet;
6. Evaporator/accumulator outlet and low-pressure side of the IHX inlet.

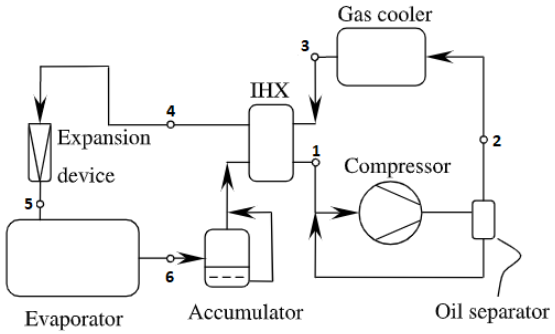


Figure 5.4: Schematic of the transcritical CO_2 cycle with the IHX addition [89].

This cycle also considers the addition of a SLA between the evaporator and the IHX. This component guarantees that only saturated vapor enters the compressor. However, this may still, in

practice, let a few drops of liquid enter sporadically. With the IHX, the vapor enters somewhat superheated, increasing the likelihood that no liquid drops will enter.

Figure 5.5 shows the diagrams *T-s* and *P-h* for the CO_2 transcritical cycle with the addition of the IHX. The results are explicit in Table 5.4 and Table 5.5. The presented results were also corroborated by software developed by IPU, "Simple CO2 one stage cycle", as is shown in Figure B.1 in Appendix B.

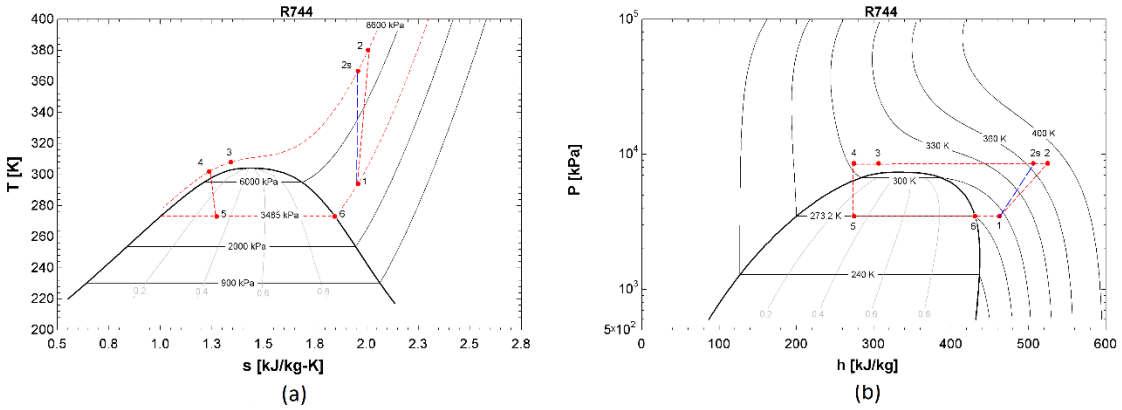


Figure 5.5: Transcritical CO_2 cycle with IHX: (a) *T-s* diagram (b) *P-h* diagram.

Table 5.4: 50 kW with IHX simulation inputs

Inputs	Value
T_{amb}	10 ℃
T_{evap}	0 ℃
T_{gce}	35 ℃
T_{sh}	0 ℃
T_{sc}	0 ℃
P_{gc}	8600 kPa
$\eta_{s,comp}$	70.00 %
ε_{IHX}	60.00 %
$\dot{Q}_{gc}$	50 kW

Table 5.5: 50 kW with IHX simulation outputs

Outputs	Value
COP_{HP}	3.513
COP_{LZ}	6.296
η_{HP}	55.79 %
P_{evap}	3485 kPa
p_r	2.468
$\dot{m}_{CO2}$	0.2811 kg/s
$\dot{Q}_{evap}$	43.99 kW
$\dot{Q}_{IHX}$	8.94 kW
$\dot{W}_{comp}$	17.51 kW

Table 5.6: State points simulation results (50 kW with IHX configuration)

State, i	T_i [K]	P_i [kPa]	s_i [kJ/(kg · K)]	h_i [kJ/kg]
1	294.2	3485	1.958	462.7
2	380.3	8600	2.008	525.0
2s	366.8	8600	1.958	506.2
3	308.2	8600	1.341	306.2
4	302.0	8600	1.237	274.4
5	273.2	3485	1.272	274.4
6	273.2	3485	1.845	430.9

5.4. CO_2 cycles simulation analysis

5.4.1. Gas cooler optimal pressure

As was stated previously, the gas cooler working pressure should be adjusted to achieve the best system performance. The optimum value is heavily dependent on the exit temperature of CO_2 at the gas cooler, as can be seen in Figure 5.6 that displays $P_{gc,opt}$ values for five different T_{gce}. The optimum discharge pressure increases with an increase in gas cooler exit temperature. It can also be concluded that for higher gas cooler exit temperatures, the perfomance of the system is less susceptible to variations in the gas cooler pressure. For example, in Figure 5.6, at 50 °C, it can be seen that the COP value is practically constant after the optimal value.

The influence of the discharge pressure on the COP value for five different evaporation temperatures is presented in Figure 5.7. Firstly, it can be seen that as the evaporation temperature increases, the same variation of 5 °C achieves a greater COP increase. It is shown that a decrease in the evaporation temperature lowers the discharge optimal pressure, even though that effect is not as significant as the effect of the refrigerant at the exit of the gas cooler. Furthermore, it can be concluded that to improve the COP, the system must be designed for the lowest feasible gas cooler exit temperature and the highest possible evaporator temperature.

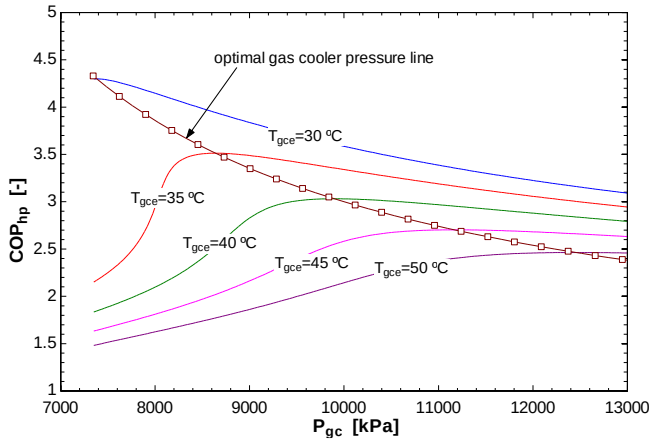


Figure 5.6: Effect of gas cooler pressure on COP of the IHX cycle at various gas cooler CO_2 exit temperatures T_{gce}.

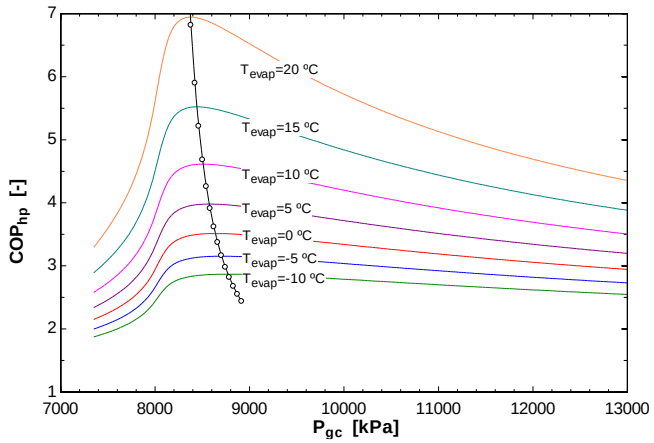


Figure 5.7: Effect of gas cooler pressure on *COP* of the IHX cycle at various evaporation temperatures T_{evap}.

Besides the gas cooler outlet temperature and the evaporator temperature, the compressor design and the degree of superheat both should have some impact on the optimal discharge pressure. However, several studies have shown that their effect is seen to be relatively unimportant when compared to the other two variables [86]. These conclusions are reflected in Equation (5.18) which was used previously used to determine the theoretical $P_{gc,opt}$. The graph shown in Figure 5.8 confirms that the gas cooler outlet temperature has a much more significant impact on the optimum discharge pressure than evaporation temperature. In addition to that equation, Sarkar also developed a correlation that allows the maximum COP value to be determined:

$$COP_{max} = 48.2 + 0.21 \times T_{evap} + 0.05 \times T_{gce} \times \left(T_{gce} - 50\right) - 0.0004 \times T_{gce}^{3} \qquad (5.19)$$

This equation is defined for the temperatures in °C and pressures in bar can be used for $-10\ °C < T_{evap} < 10\ °C$ and $30\ °C < T_{gce} < 50\ °C$. If one determines the maximum COP value with the standard variable inputs defined previously:

$$COP_{max} = 48.2 + 0.21 \times 0 + 0.05 \times 35 \times (35 - 50) - 0.0004 \times 35^3 = 4.8 \qquad (5.20)$$

From the simulations, the obtained COP value was slightly lower, which is understandable since the IHX did not represent the highest improvement in the performance of the heat pump. Therefore, the other solutions presented previously would lead to values closer to 4.8. It may be noted that all values were reached considering the effectiveness of 60 % for the IHX.

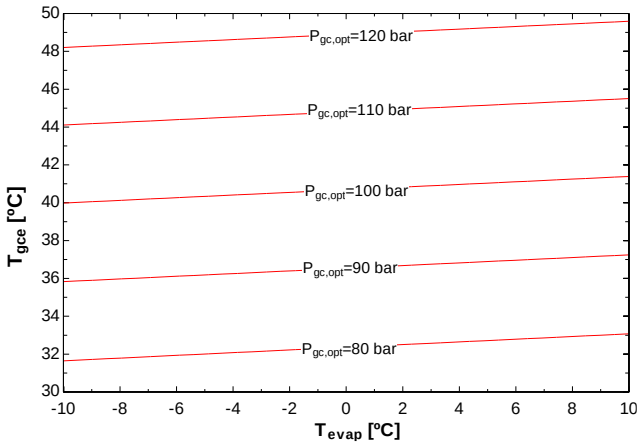


Figure 5.8: Influence of T_{gce} and T_{evap} on the optimal gas cooler pressure according to Equation (5.16).

Results in Table 5.7 show that the effect of the IHX on system perfomance and optimum discharge pressure is reduced for $T_{gce} = 35$ ℃. However, the influence of the IHX increases for higher CO_2 gas cooler outlet temperatures. If a gas cooler pressure is maintained at 86 bar, while for $T_{gce} = 35$ ℃, the COP increases by 1.30 % and optimum discharge pressure decreases by 1.20 %, for $T_{gce} = 40$ ℃, the COP increases by 10.50 % and optimum discharge pressure decreases by 2.27 %. Moreover, for $T_{gce} = 45$ ℃, the COP increases by 22.41 % and optimum discharge pressure decreases by 3.64 percentage points. Finally, for $T_{gce} = 50$ ℃, the COP increases by 35.96 % and optimum discharge pressure decreases by 5.31 %. However, if the gas cooler pressure is controlled to be at the optimal value for all configurations, then the influence in the COP is smaller. While for $T_{gce} = 35$ ℃, the COP increases by 1.12 %, for $T_{gce} = 40$ ℃, the COP increases by 2.02 %, for $T_{gce} = 45$ ℃ the increase is 3.01 %, for $T_{gce} = 50$ ℃, the COP

increases by 4.06 %. Thus for each 5 ºC that gas cooler exit temperature increases, the increase in COP improvement with the IHX are approximately 1 %. It can then be assumed that the optimum pressure optimization is more influential in the conventional configuration. Figure 5.9 corroborates that IHX influence increases with an increase in T_{gce} since the gap between the two solutions curves grows increasingly larger. However, when comparing the evolution of both optimal gas cooler pressure lines it can be concluded that there is little difference. This is in line with the results presented in Table 5.7. Still, in both configurations optimal pressure significantly increases the COP value and, thus, it is extremely important to be able to control P_{gc} depending essentially on T_{gce}. Figure 5.10 confirms that the impact of the IHX does not alter considerably with evaporation temperature. Furthermore, it demonstrates that the optimal gas cooler pressure line has become more vertical, implying that the inclusion of the IHX helps to a more consistent optimal gas cooler pressure.

Table 5.7: Optimal gas cooler pressure results from the simulation iteration (T_{evap} = 0 ºC)

T_{gce} [ºC]	COP (for optimal pressure)			$P_{gc,opt}$ [kPa]		
	Conventional	With IHX	Change	Conventional	With IHX	Change
30	4.285	4.299	+ 0.33 %	7418	7382	-0.49 %
35	3.474	3.513	+ 1.12 %	8744	8639	-1.20 %
40	2.971	3.031	+ 2.02 %	10127	9897	-2.27 %
45	2.624	2.703	+ 3.01 %	11590	11168	-3.64 %
50	2.367	2.463	+ 4.06 %	13152	12454	-5.31 %

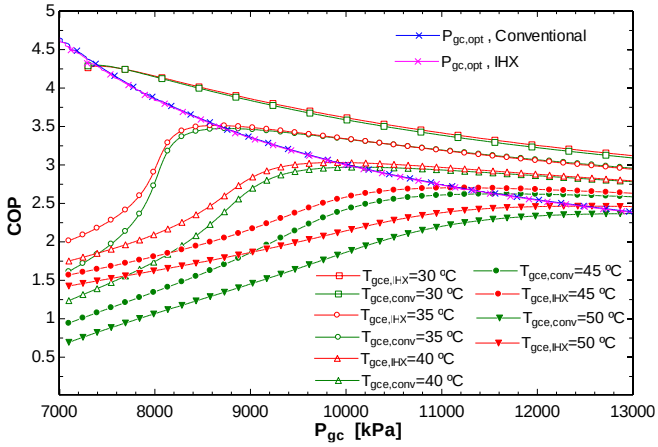


Figure 5.9: Gas cooler outlet temperature T_{gce} influence on gas cooler optimal pressure ($P_{gc,opt}$) and COP with the addition of the IHX.

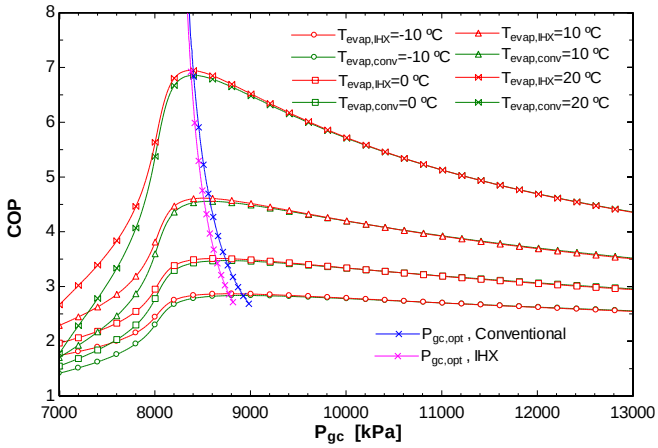


Figure 5.10: Evaporation temperature (T_{evap}) influence on gas cooler optimal pressure $P_{gc,opt}$ and *COP* with the addition of the IHX.

From Table 5.7 and Figure 5.9 and Figure 5.10, an analysis of the effect of both T_{evap} and T_{gce} can be made. As shown in Figure 5.6 and Figure 5.9, increased temperature output from the gas cooler leads to degraded heat pump performance. Also, COP values experience bigger fluctuations according to the gas cooler pressure for T_{gce} closer to the critical point. The influence of T_{gce} on the COP is significantly higher for pressures below the optimal pressure, after which the COP of all curves converges to approximately the same value. An evaluation of the influence of the ambient air temperature can be made thorough T_{evap} since the difference of -10 ºC is maintained constant for all configurations. Therefore, it can be concluded that even though it does not show great influence on $P_{gc,opt}$, it has a bigger impact on the heat pump performance than T_{gce}.

Figure 5.10 demonstrates that for greater T_{evap}, the same temperature difference increases double the previous increase. This implies that in Summer, for higher temperatures, the heat pump performance will suffer more variations although performing at higher COP.

Table 5.8: Different parameters values for different gas cooler pressures and IHX efficiencies

	P_{gc} [bar]	75	86	95	105	115	125
$\varepsilon_{IHX} = 0.40$	$\dot{m}_{CO2}$ [kg/s]	0.4908	0.2433	0.2188	0.2020	0.1887	0.1772
	T_{suc} [ºC]	14.00	14.00	14.00	14.00	14.00	14.00
	T_{disch} [ºC]	82.12	97.45	109.7	123.2	136.8	150.9
	p_r	2.152	2.468	2.726	3.013	3.300	3.587
	$\eta_{s,comp}$	0.7426	0.7044	0.6732	0.6384	0.6037	0.5690
	$\dot{W}_{comp}$ [kW]	22.75	14.24	15.06	16.32	17.66	19.03
	COP	2.198	3.511	3.321	3.063	2.831	2.628
$\varepsilon_{IHX} = 0.60$	$\dot{m}_{CO2}$ [kg/s]	0.4384	0.2290	0.2066	0.1911	0.1787	0.1679
	T_{suc} [ºC]	21.00	21.00	21.00	21.00	21.00	21.00
	T_{disch} [ºC]	90.95	106.8	119.5	133.6	147.9	162.7
	p_r	2.152	2.468	2.726	3.013	3.300	3.587
	$\eta_{s,comp}$	0.7426	0.7044	0.6732	0.6384	0.6037	0.5690
	$\dot{W}_{comp}$ [kW]	21.49	14.17	15.03	16.32	17.67	19.05
	COP	2.327	3.529	3.326	3.064	2.829	2.624
$\varepsilon_{IHX} = 0.80$	$\dot{m}_{CO2}$ [kg/s]	0.3985	0.2170	0.1964	0.1819	0.1703	0.1601
	T_{suc} [ºC]	28.00	28.00	28.00	28.00	28.00	28.00
	T_{disch} [ºC]	99.60	116.0	129.1	143.7	158.5	174.0
	p_r	2.152	2.468	2.726	3.013	3.300	3.587
	$\eta_{s,comp}$	0.7426	0.7044	0.6732	0.6384	0.6037	0.5690
	$\dot{W}_{comp}$ [kW]	20.52	14.10	15.01	16.31	17.68	19.07
	COP	2.437	3.545	3.332	3.065	2.828	2.623

From

Table 5.8, it can be concluded that the needed mass flow rate of CO_2 to achieve a defined output heat is highly dependent on both ε_{IHX} and P_{gc}, decreasing with an increase for both variables. This decrease is mainly connected to the higher discharge temperature achieved via the increase of the superheat achieved by the IHX. A higher discharge temperature allows for a greater enthalpy difference, which implies that less flow rate is needed to achieve the same heat output. However, this extra superheat may lead to temperatures that the components are not prepared to sustain. Also, to achieve these values a very efficient heat exchanger would be needed to be designed, increasing the cost of the system. Nonetheless, the superheating degree should be high

enough because it has little influence on the refrigerant density at the compressor intake and since the evaporating pressure should be regulated. Higher superheating allows for a lower refrigerant mass flow rate [126].

A greater subcooling means greater cooling effect and equal compressor work, thus greater efficiency. The problem resides in the superheating, which causes a great increase in the compression work. However, superheating is necessary to avoid drops of liquid entering the compressor. This would lead to a great increase in the isentropic performance of the compressor. Therefore, superheating is done to ensure that the fluid at the compressor inlet is fully in the vapor phase. Subcooling, on the other hand, is used to ensure that at the inlet of the expansion valve the fluid is in the liquid phase. However, in the case of the supercritical cycle the question of subcooling is not relevant because, in the heat exchange with the hot source, CO_2 is always supercritical.

5.5. NH_3 conventional cycle

For the NH_3, such as for the CO_2, both configurations were simulated in the EES software to understand if the addition of an IHX brings improvements to the heat pump performance. Moreover, the simulation of a configuration using NH_3 allows the analysis of possible future use of this refrigerant for heat pumps, replacing CO_2. Thus, a comparison between the four configurations will also be made.

The cycle for an NH_3 heat pump obeys the conventional vapor compression refrigeration cycle, previously explained, since NH_3 will be working in the subcritical area, contrary to CO_2. The NH_3 vapor contains significant superheat above saturated condensing temperatures. This is the maximum attainable temperature in the NH_3 heat pump system and is utilized to produce DHW without needing to increase the condensing temperature. Thus, the gas that exits the compressor is cooled in a separate heat exchanger known as a desuperheater so that the heat from gas cooling may be used to provide DHW. However, since this component represents an additional investment, it must be studied if the slight increase in COP justifies the additional cost. If not, then desuperheating and condensing may be merged into one exchanger. The heat extracted from condensation can either be used to provide other heating services, such as a floor heating system or provide heat to DHW, simultaneously with the desuperheater, thus, decreasing water mass flow rate necessity. The refrigerant is subcooled in the condenser and expanded in an expansion device, keeping the superheat value within the appropriate range. Finally, the two-phase fluid exiting the

expansion valve is heated in the evaporator before entering the compressor as superheated gas [72, 127]. Thus, seven different reference points will be considered:

1. Evaporator outlet and compressor inlet;
2. Compressor outlet and desuperheater inlet;
3. Desuperheater outlet and condenser inlet;
4. Condenser outlet and expansion valve inlet;
5. Expansion valve outlet and evaporator inlet.

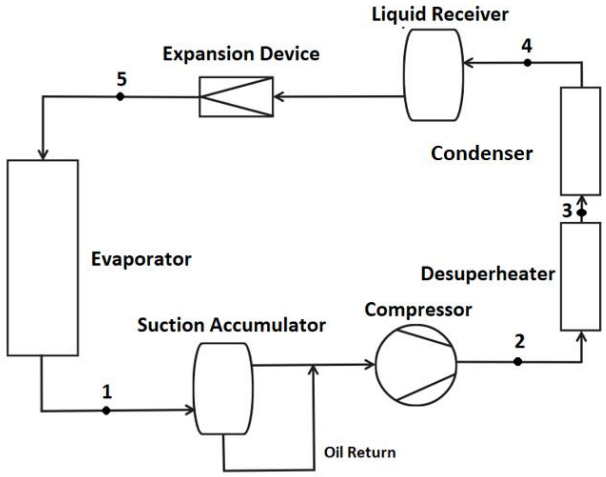


Figure 5.11: Schematic of the conventional NH_3 cycle.

Contrary to the supercritical CO_2 cycles, there is no need to optimize the condenser pressure as it is defined as a function of the condensation temperature. Moreover, heat rejection for the NH_3 cycle will be separated into two different components: the condenser and the desuperheater. The desuperheater rejects heat at higher temperatures until the fluid reaches the saturated vapor state. The following considerations were done for the NH_3 conventional cycle:

- The same average temperature as for the CO_2 cycle was taken for ambient air;
- A difference of 10 ℃ was established between air temperature and evaporation temperature to achieve a reasonable comparison with the CO_2 system. Thus, $T_{evap} = 0$ ℃;
- The condensation temperature was defined at $T_{cond} = 40$ ℃ so that, with the subcooling of 5 ℃, the temperature at the entrance of the expansion component was 35 ℃. This way, a comparison between the NH_3 and CO_2 conventional configurations can be more accurately made. Moreover, the floor heating temperature requirement is between 35 and

45 ºC. This way, the condensation process can be used for a secondary floor heating system [43];

- When using the same compressor efficiency as for the CO_2 configuration (70 %), simulations showed that the discharge temperature was about 130 ℃. According to Stene et al. [128], the temperature of the lubricant and ammonia should not exceed 130 ℃ and 160 ℃, respectively. Therefore, a slightly higher compressor efficiency needed to be considered. This is one of the reasons why regular compressors should not be used when working with ammonia [71]. To predict the higher compressor efficiency, two correlations formed by Granryd for ammonia compressors et al [129] were used:

$$\eta_{v,comp} = 1.02 \times \exp(-0.063 \times p_r) \tag{5.21}$$

$$\frac{\eta_{v,comp}}{\eta_{s,comp}} = \exp\left[-1.69 \times \left(\frac{T_{cond}}{T_{evap}}\right) + 1.97\right] \tag{5.22}$$

Using the values displayed in Table 5.9 and Table 5.10, the corresponding efficiencies can be defined:

$$\eta_{v,comp} = 0.812 \tag{5.23}$$

$$\eta_{s,comp} = 0.786 \tag{5.24}$$

- Superheating was defined as $T_{sh} = 5$ ℃.

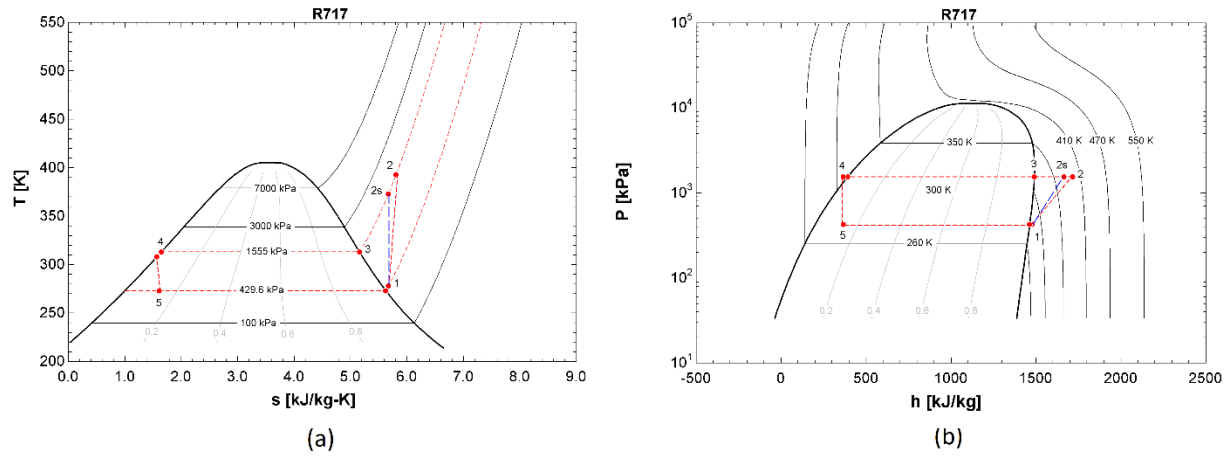


Figure 5.12: Conventional NH_3 cycle: (a) *T-s* diagram (b) *P-h* diagram.

Table 5.9: Conventional NH_3 cycle 50 kW simulation inputs

Inputs	Value
T_{amb}	10 °C
T_{evap}	0 °C
T_{cond}	40 °C
T_{sh}	5 °C
T_{sc}	5 °C
$\eta_{s,comp}$	78.60 %
$\dot{Q}_{heat}$	50 kW

Table 5.10: Conventional NH_3 cycle 50 kW simulation outputs

Outputs	Value
COP_{HP}	5.599
COP_{Carnot}	7.829
η_{HP}	71.52 %
P_{evap}	429.6 kPa
P_{cond}	1555 kPa
p_r	3.621
x_5	13.17 %
$\dot{m}_{NH3}$	0.03702 kg/s
$\dot{W}_{comp}$	8.931 kW
$\dot{Q}_{evap}$	41.07 kW
$\dot{Q}_{dsh}$	8.395 kW
$\dot{Q}_{cond}$	41.61 kW

Table 5.11: NH_3 cycle state points simulation results (50 kW configuration)

State, i	T_i [K]	P_i [kPa]	s_i [kJ/(kg · K)]	h_i [kJ/kg]
1	278.2	429.6	5.669	1476
2	392.9	1555	5.804	1717
2s	373.1	1555	5.669	1665
3	313.2	1555	5.155	1490
4	308.2	1555	1.566	366.3
5	273.2	429.6	1.609	366.3

5.6. NH_3 cycle with IHX

Such as it was made for the CO_2 configuration, and simulations regarding the addition of an IHX to the conventional NH_3 cycle were done. In this way, the NH_3 cycle with IHX can be divided similarly into:

1. Low-pressure side of the IHX outlet and compressor inlet;
2. Compressor discharge state and desuperheater inlet;
3. Desuperheater outlet and condenser inlet;
4. Condenser outlet and high-pressure side of the IHX inlet;
5. High-pressure side of the IHX outlet and expansion valve inlet;
6. Expansion valve outlet and evaporator inlet;
7. Evaporator outlet and low-pressure side of the IHX inlet.

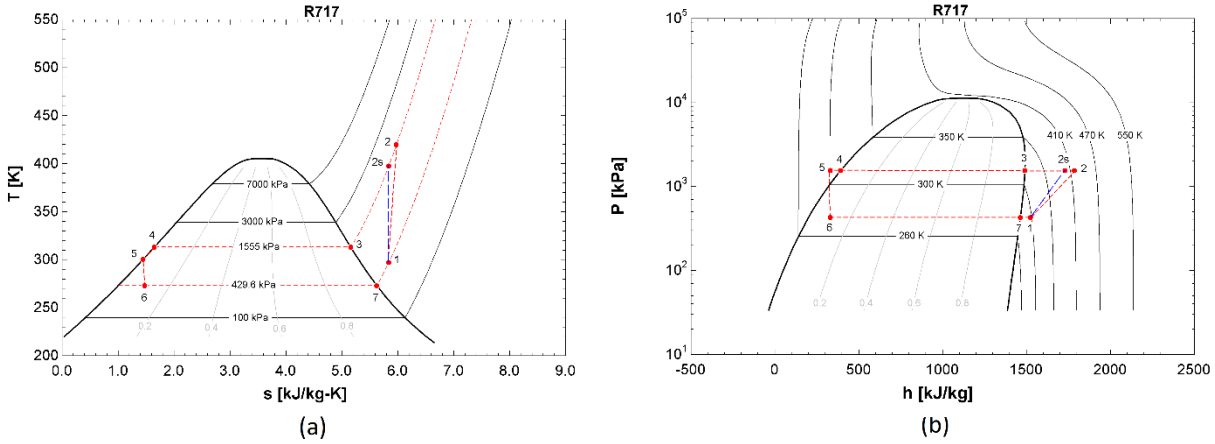


Figure 5.13: NH_3 cycle with IHX: (a) *T-s* diagram (b) *P-h* diagram.

Table 5.12: Conventional NH_3 cycle 50 kW with IHX simulation inputs

Inputs	Value
T_{amb}	10 ℃
T_{evap}	0 ℃
T_{cond}	40 ℃
$\eta_{s,comp}$	78.60 %
ε_{IHX}	60.00 %
$\dot{Q}_{heat}$	50 kW

Table 5.13: Conventional NH_3 cycle 50 kW with IHX simulation outputs

Outputs	Value
COP_{hp}	5.325
COP_{carnot}	7.829
η_{HP}	68.01 %
P_{evap}	429.6 kPa
P_{cond}	1555 kPa
p_r	3.621
x_6	10.27 %
$\dot{m}_{NH3}$	0.03585 kg/s
$\dot{W}_{comp}$	9.39 kW
$\dot{Q}_{evap}$	40.61 kW
$\dot{Q}_{dsh}$	10.59 kW
$\dot{Q}_{cond}$	39.41 kW

Table 5.14: NH_3 cycle state points simulation results (50 kW with IHX configuration)

State, i	T_i [K]	P_i [kPa]	s_i [kJ/(kg · K)]	h_i [kJ/kg]
1	297.2	429.6	5.836	1523
2	419.8	1555	5.973	1785
2s	397.8	1555	5.836	1729
3	313.2	1555	5.155	1490
4	313.2	1555	1.645	390.7
5	300.6	1555	1.446	329.7
6	273.2	429.6	1.475	329.7
7	273.2	429.6	5.621	1462

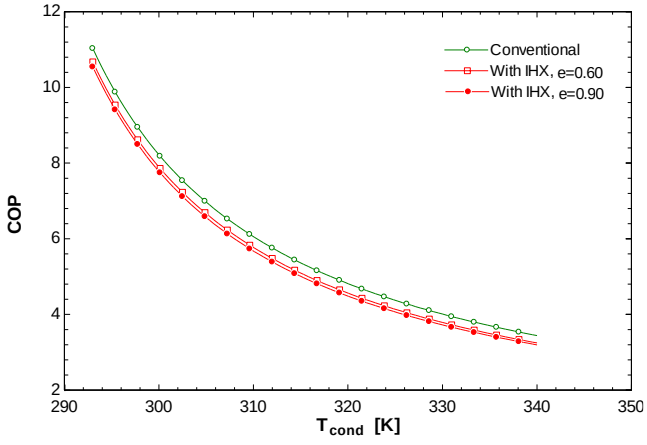


Figure 5.14: COP dependence of T_{cond} for different IHX efficiencies and the conventional configuration.

5.7. NH_3 cycles simulation analysis

Figure 5.15 demonstrates that the addition of an IHX to the conventional NH_3 cycle decreases COP value. In addition, it also shows that the lower the efficiency of the IHX the greater the COP. Thus, it can be concluded that besides the inclusion of the IHX not improving the performance of the system, it may even harm it. This is largely related to the fact that, contrary to what happens with most refrigerants, increasing superheat for the NH_3 cycle decreases its COP. Results from the simulation show that when increasing $T_{sh} = 0$ ℃ to $T_{sh} = 24$ ℃, which is the superheat that it receives if $\varepsilon_{IHX} = 0.60$, the COP suffers a decrease of 4.2 %. As a result, it is beneficial to use an evaporator followed by a liquid separator to ensure that no drops of ammonia enter the compressor, while still allowing the suction gas to be as near the saturated vapor state as possible. Still, the use of IHX can also be justified via practical reasons. Because the superheating added by the IHX ensures that only superheated vapor enters the compressor, the isentropic efficiency of this component should increase when the IHX is installed. To analyze if a slightly increased $\eta_{s,comp}$ would increase the benefit of the IHX, a comparison simulation considering $\eta_{s,comp} = 0.850$ for the cycle with IHX, and $\eta_{s,comp} = 0.786$ for the conventional cycle was made. According to the findings in Figure 5.15, adding the IHX does not represent a significant improvement over the traditional cycle, even when considering a significant increase in isentropic efficiency. This is consistent with the findings of Mastrullo et al. [130], who came to the conclusion that the inclusion of the IHX is unfavorable for the R717 under all scenarios studied, which included evaporation temperatures from -40 to 10 °C and condensation temperatures from 25 to 50 °C. Furthermore, the installation of the IHX results in discharge temperatures that are higher than those recommended for an NH_3 system. As previously stated, the lubricant and NH_3 temperatures should not exceed 130 and 160 ºC, respectively. However, the discharge temperature climbs to near 150 ºC for an exchanger efficiency of 60 % and ambient temperature of 10 ºC, as shown in Table 5.14. This value will increase even more if the ambient temperature lowers from 10 ºC, exceeding the permissible limit of 160 ºC. For example, for an ambient temperature of 0 ºC, discharge temperature will further increase to 185 ºC. This can be countered by lowering the condenser outlet temperature [89]. In this way, in order to avoid the additional cost of the IHX, the conventional configuration will be adopted for the NH_3 heat pump.

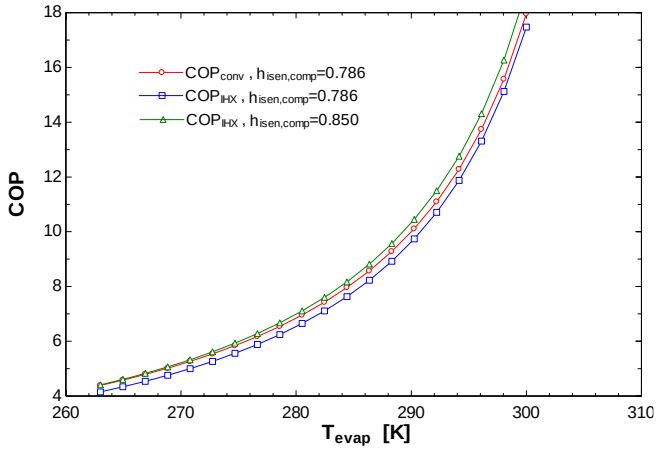


Figure 5.15: *COP* dependence on T_{evap} for the conventional and the IHX configurations.

5.8. Comparison between CO_2 and NH_3 simulations

The first analysis should be made regarding the heat pump performance with the different fluids. Figure 5.16 shows a significant difference in the COP values of both heat pumps. For $T_{evap} = 0$ ℃, the COP value for the NH_3 heat pump is 52 % higher than COP value for the CO_2 heat pump.

Results, displayed in Table 5.5 and Table 5.10, demonstrate that, when compared to the result for CO_2 mass flow rate, a significantly lower NH_3 mass flow rate is needed to achieve the same power output. Specifically, for the standard inputs and the conventional configurations, the NH_3 mass flow rate is 86 % lower than the CO_2 mass flow rate. This corroborates with what was previously stated regarding NH_3 properties. Due to the high vaporization latent heat and low vapor-specific volume of ammonia, lower compressor displacement and mass flow rate are required [72]. The higher NH_3 compressor efficiency furthermore increases this difference. Figure 5.16 validates this information, furthermore, shows that the CO_2 mass flow rate is highly dependent on the evaporation temperature, increasing with it. The same does not happen for the NH_3 mass flow rate, which is maintained practically constant. If there is the need to increase the heating load, without increasing the mass flow rate of the refrigerant, that can be achieved by reducing the evaporation temperature and, consequently, boosting the discharge temperature. Naturally, that means that the compressor work will need to increase. Increased superheat can also be used to achieve the same suction temperature [36].

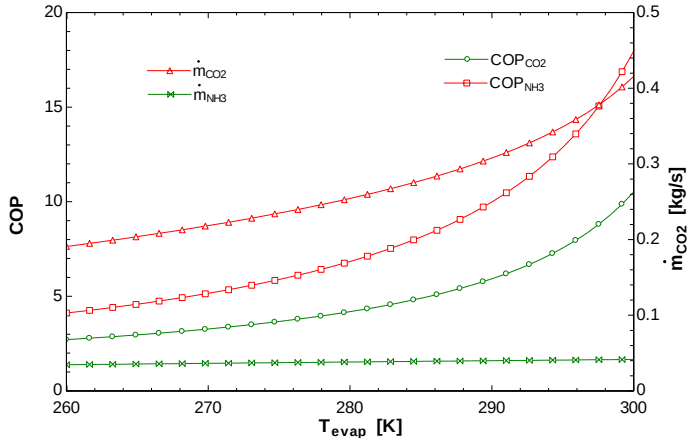


Figure 5.16: *COP* and mass flow rate dependence of the evaporation temperature for the NH_3 and CO_2 configurations.

Another significant dissimilarity is the difference in working pressures that the heat pump is required to work to obtain the same heating power. While the gas cooler at the transcritical CO_2 heat pump works at 86 bar for optimal performance, the condenser at the subcritical NH_3 heat pump only needs to go up to 15.5 bar to reach the $T_{cond} = 40$ °C.

Finally, discharge temperatures also vary considerably from one configuration to another. Since the superheat in the CO_2 heat pump will be significantly higher and dependent on the IHX, the NH_3 heat pump does not have an IHX, and its superheat value should be as low as possible. This implies that the temperature at the compressor exit will be significantly higher in the CO_2 configuration. Figure 5.17 shows that discharge temperature suffers the same evolution for both systems, maintaining a constant difference of 35 ºC. However, it demonstrates that, for the NH_3 heat pump, for very high superheat values, discharge temperatures reach non-recommended values. Additionally, Figure 5.17 also corroborates that COP value of the NH_3 heat pump is harmed for increasing superheat, while the COP value for the CO_2 heat pump is slightly increased.

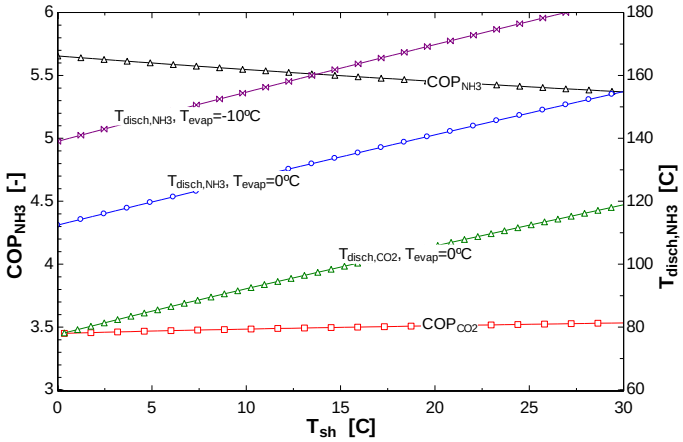


Figure 5.17: *COP* and T_{disch} values for different superheat and evaporation temperatures.

6. Component selection

6.1. Transcritical CO_2 system

In this chapter, the selection of the components for the CO_2 heat pump with the lower heat load solution will be presented. The complete reports of the selected components are available in Appendix C.

6.1.1. Compressor

For this specific application, semi-hermetic reciprocating was considered the best option for a transcritical CO_2 heat pump. The selected compressor defines the CO_2 mass flow rate and the possible heat output at the gas cooler. Thus, even though the EES simulation was made with the input of 50 kW to heat domestic water, the values obtained serve only as a guide to dimension the following components, as it is the availability of the compressor that mainly defines the outputs of the heat pump and its components.

The compressor selection was done using the BITZER software available online [131]. It is relevant to notice that the software considers the CO_2 cycle with the IHX. The first step was to choose the suitable type of compressor for a CO_2 heat pump application. A semi-hermetic reciprocating compressor was chosen. This type of compressor is the most used in transcritical CO_2 applications as it allows for achieving better leak tightness, efficiency, size, and weight, leading to a compact system [132]. To be able to select the appropriate compressor, it was necessary to supply the software with the inputs provided in Table 6.1. These inputs were based on the results of the simulations shown previously.

Table 6.1: Compressor inputs in the BITZER software

Software necessary inputs	Values
$\dot{Q}_{evap}$	36 kW
T_{evap}	0 ℃
P_{gc}	86 bar
T_{gce}	35 ℃
T_{sh}	21 ℃

After supplying the inputs, the software returned the compressor 4GTE-20-40P with an external frequency inverter from the series ECOLINE+ manufactured by BITZER as being the

most appropriate for the intended operation of the heat pump. An example of the configuration of the compressors belonging to this series is displayed in Figure 6.1. Its main properties, such as power input and gas cooler capacity that it allows, provided by the software, are displayed in Figure 6.2. The software results show that the nominal heating capacity at $P_{gc} = 86$ bar, $T_{evap} = 0$ ℃ and $T_{gce} = 35$ ℃ is 61.5 kW. It may be noted that, this heating capacity is superior to the 50 kW of the EES simulation. This implies that the results obtained in the simulation will also differ from these results. If we change the value on the EES simulation to $\dot{Q}_{heat} = 61.5$ kW, then the remaining main values of the simulation will change to rather similar values to those given by the BITZER software.



Figure 6.1: BITZER ECOLINE+ compressor [133].

Compressor	4GTE-20K-40P
Capacity steps	100%
Cooling capacity	44,0 kW
Cooling capacity *	43,5 kW
Evaporator capacity	44,0 kW
Power input	17,52 kW
Current (400V)	29,5 A
Voltage range	380-420V
Gas cooler capacity	61,5 kW
COP/EER	2,51
Mass flow	1013 kg/h
Discharge gas temp. w/o cooling	107,1 °C
optimal high pressure	86,0 bar(a)

Figure 6.2: BITZER software selection output [131].

Besides these values, it is also relevant to state the geometry parameters of the chosen compressor, which are displayed in the compressor report shown in Figure C.2 of Appendix C:

- Nº of cylinders = 4 cylinders;
- Bore = 38 mm;
- Stroke = 38 mm;
- Displacement volume, $V_{disp} = \pi \times (0.038/2)^2 \times 0.038 \times 4 = 0.0001724$ m^3;
- Displacement (1450 RPM, 50 Hz) = 15.0 m^3/h;
- Displacement (1750 RPM, 60 Hz) = 18.1 m^3/h.

Since this application requires very high temperatures, correct lubrification becomes critical. The standard oil type recommended for the chosen compressor is BSE85K. This oil is a polyolester oil (POE). Polyalkylene glycol oil can also be used if different advantages are desired.

In that case, the recommended oil would be BSG68K [134]. Both lubrication oils are supplied by BITZER.

Regarding compressor efficiency, it was previously stated previously that the use of CO_2 allows for lower pressure ratios than usual for conventional HFC refrigerants. This allows for CO_2 compressors to display higher compressor isentropic efficiencies, thus, reducing the input power and increasing COP [135]. This value is usually given by the manufacturer. However, as in the BITZER software used information was not available, and the compressor efficiency was calculated via Equation (5.17). The value obtained was 0.70. When making the comparison of the heating load, cooling load, work input, discharge temperature, and CO_2 mass flow rate of the compressor, obtained in the EES simulation, these values matched the values obtained in the BITZER software. Therefore, the estimated compressor efficiency obtained from Equation (5.17) has been admitted was appropriate.

As it can be seen in Figure 6.2, the BITZER software also presented the high-pressure value for an optimal compressor and cycle functioning. Comparing that value with the obtained previously, using both Equation (5.18) and the EES simulation, it can be determined that that value is consensual and that the gas cooler should be working at approximately 86 bar for optimal conditions at the design parameters.

Using Equation (5.2), the mass flow rate given by the software allows the determination of the volumetric efficiency, $\eta_{v,comp}$, which measures the quality of the compressor work:

$$\eta_{v,comp} = \frac{\dot{m}_{CO2}}{\left(\frac{N}{60}\right) \times V_{disp} \times \rho_{suc}} = \frac{1013/3600}{(1450/60) \times 0.0001724 \times 79.79} \tag{6.1}$$

$$\Leftrightarrow \eta_{v,comp} = 0.6876 \tag{6.2}$$

6.1.2. System piping

Following the selection of the compressor, it is now necessary to scale the installation pipes, as these may influence the choice of other components due to their connections with the tubing. These pipes connect all the equipment, making the refrigerant continuously go through the

cycle. The piping must be designed to account for the fluid speed, the loss of load, and the associated costs. The greater the speed of the fluid passing through the piper, the greater the loss of the system load, but the smaller the diameter of the pipe. This implies lower associated costs, but that does not mean they are preferable, because they imply higher load losses, which means higher compressor consumption, resulting in higher energy costs that, in many circumstances, may not compensate for the material savings.

- Line 1: IHX to compressor;
- Line 2: compressor to gas cooler;
- Line 3: gas cooler to IHX;
- Line 4: IHX to expansion valve;
- Line 5: expansion valve to evaporator;
- Line 6: evaporator to IHX.

Each line that connects different components demands different piping diameters. Table 6.2 shows the minimum and maximum values that should be considered for the velocity of the different piping lines in the heat pump. Knowing the maximum mass flow rate intrinsic to the compressor and defining the desired velocity, the appropriate diameter can be determined via Equations (6.3) and (6.4). However, it is very unlikely that the exact calculated internal diameter matches with an existing nominal diameter of an existing piping line. Thus, the velocity of must is recalculated using the existing diameters.

$$\dot{V} = \frac{\dot{m}}{\rho} \tag{6.3}$$

$$\dot{V} = A \times u_{rec} \leftrightarrow D = \sqrt{\frac{4 \times \dot{V}}{u_{rec} \times \pi}} \tag{6.4}$$

In the equations above $\dot{V}$ is the volumetric flow rate in the pipeline (m^3/s) ; $\dot{m}$ is the mass flow rate in the pipeline; ρ is the density of the fluid (kg/m^3); A is the section of the tube (m^2); D is the inner diameter of the tube (m); u_{rec} is the defined fluid velocity between the recommended limits (m/s).

After the selection of the most appropriate diameter, the remaining properties must be calculated to determine pressure drop. Using Equations (6.5) and (6.7), Reynolds number Re and Darcy friction factor f can be, respectively, determined. Finally, using the Darcy-Weisbach equation (6.6), pressure drop throughout the tube line is calculated.

$$Re = \frac{\rho \times u \times d}{\mu} \tag{6.5}$$

$$\frac{\Delta P}{L} = \frac{f}{D} \times \frac{\rho \times u^2}{2} \tag{6.6}$$

$$\frac{1}{\sqrt{f}} = -2 \times \log_{10}\left(\frac{\varepsilon/_D}{3.7} + \frac{2.51}{Re \times \sqrt{f}}\right) \tag{6.710}$$

In the equations above u is the velocity of the fluid for the chosen diameter $(\mathrm{m/s})$; μ is the kinematic viscosity of the fluid $(\mathrm{m^2/s})$; ΔP is the pressure drop throughout the tube line (Pa); L is the length of the tube (m); ε/D is the relative roughness.

Table 6.2: Recommended velocities for the different pipelines [118]

Line	Recommended velocities	Chosen velocities, u_{rec}
1	$3 - 12$ m/s	6.5 m/s
2	$5 - 12$ m/s	8.5 m/s
3	1 m/s	1 m/s
4	1 m/s	1 m/s
5	1 m/s	1 m/s
6	$3 - 12$ m/s	6.5 m/s

An example of the calculus method will be shown for the compressor suction line (state 1). Density and kinematic viscosity were taken for each of the CO_2 states at the beginning of the line. For example, for the suction line, both properties were taken at $T_1 = 21$ ℃ and $P_1 = 3485$ kPa. From that, it resulted in $\rho_1 = 79.76\ \mathrm{kg/m^3}$ and $\mu_1 = 1.552 \times 10^{-5}\ \mathrm{m^2/s}$. Therefore:

$$\dot{V} = \frac{\dot{m}}{\rho} = \frac{0.2814}{79.76} = 3.528 \times 10^{-3}\ \mathrm{m^3/s} \tag{6.8}$$

$$D = \sqrt{\frac{4 \times \dot{V}}{u_{rec} \times \pi}} = \sqrt{\frac{4 \times 3.528 \times 10^{-3}}{6.5 \times \pi}} = 0.02629 \text{ m} \quad (6.9)$$

After consulting the existing piping diameter, the closest defined sizes were $D = 0.0223$ m and $D = 0.0285$ m. This resulted in $u = 9.033$ m/s and $u = 5.531$ m/s, respectively. The first criterion was to choose the closest diameter that allowed a slightly higher fluid velocity. If the smaller diameter allowed much higher velocities than the established, then the greater diameter was chosen. Still, in all piping lines, for this specific application, the smaller inner diameter and therefore the higher velocities were chosen. Thus, the suction line $D = 0.0223$ m was chosen. The type of pipe corresponding to this diameter is DIN-EN SS 20.

After the inner diameter of the piping line was chosen, the pressure drop calculation followed as can be seen below. The material used for the piping will be stainless steel as they are recommended for hot water systems pipes. Thus, ε was taken as 0.015×10^{-3} m.

$$Re = \frac{\rho \times u}{\mu} = \frac{79.76 \times 9.033}{1.552 \times 10^{-5}} = 1035527 \quad (6.10)$$

$$\frac{1}{\sqrt{f}} = -2 \times \log_{10}\left(\frac{\varepsilon/D}{3.7} + \frac{2.51}{Re \times \sqrt{f}}\right) \therefore f = 0.0183 \quad (6.11)$$

$$\frac{\Delta P}{L} = \frac{f}{D} \times \frac{\rho \times u^2}{2} = \frac{0.0183}{0.0223} \times \frac{79.76 \times 9.033^2}{2} = 2670 \text{ Pa/m} = 0.02670 \text{ bar/m} \quad (6.12)$$

The remaining piping lines follow the same approach and method, and their chosen piping sizes are displayed in Table 6.3.

Table 6.3: CO_2 heat pump piping selection

Line	Piping type	Inner diameter (m)	Re	f	Pressure drop (bar/m)
1	DIN-EN SS 20	0.0223	1035527	0.0183	0.02670
2	DIN-EN SS 15	0.0167	1021920	0.0195	0.06480
3	DIN-EN SS 20	0.0223	341092	0.0190	0.00355
4	DIN-EN SS 20	0.0223	345095	0.0200	0.00301
5	DIN-EN SS 50	0.0545	444508	0.0162	0.00022
6	DIN-EN SS 20	0.0223	1086580	0.0182	0.02171

6.1.3. Gas cooler

As heat exchangers often run for extended periods with no change in working conditions, they may be represented as steady-state devices. As a result, the mass flow rate of both fluids stays unchanged, as do fluid parameters like temperature and velocity at the inlet and outlet [40]. Therefore the compressor defines the CO_2 mass flow as its property. Thus, that was the value input into the software instead of the desired heat load $\dot{Q}_{gc}$. However as the results will show, the same output would result from the use of heat load. The software used was the SSP G8 developed by SWEP for advanced heat exchange calculations [136]. The necessary software inputs are displayed in Table 6.4. A member of SWEP team was also consulted and advised the same heat exchanger.

Table 6.4: Gas cooler SWEP software inputs

Software inputs	Value
Fluid side 1	CO_2
$\boldsymbol{P_{CO2}}$	86 bar
Fluid side 2	Water
$\boldsymbol{T_{CO2,i} = T_{disch}}$	107.1 ℃
$\boldsymbol{T_{CO2,o} = T_{gce}}$	35.0 ℃
$\boldsymbol{T_{w,i}}$	10.0 ℃
$\boldsymbol{T_{w,o}}$	60.0 ℃
$\boldsymbol{\dot{m}_{CO2}}$	0.2813 kg/s
$\boldsymbol{Max\ PD_{CO2}}$	50 kPa
$\boldsymbol{Max\ PD_{w}}$	50 kPa

Table 6.5: Gas cooler SWEP software outputs

Software outputs	Value
Model	B4THx90
$\boldsymbol{\dot{Q}_{gc}}$	61.46 kW
$\boldsymbol{\dot{m}_{w}}$	0.2942 kg/s
$\boldsymbol{A_{gc}}$	1.06 m^2
$\boldsymbol{PD_{CO2}}$	17.0 kPa
$\boldsymbol{PD_{w}}$	7.46 kPa

This exchanger consists of 90 plates with a total effective area of 1.06 m^2. The 90 plates form 89 channels, 45 of which is intended for the circulation of water and the remaining 44 for the circulation of the refrigerant. The distance between each plate is between 0.4 and 0.5 mm. Stainless

steel is used for the plates and copper is used as braze material. Figure 6.3 illustrates a plate constituting the exchanger used. The remaining data, both geometrical and thermodynamic, is available in the manufacturer's report in Appendix C.



Figure 6.3: SWEP B4TH gas cooler.

6.1.4. Evaporator

The evaporator selection was not done the same way as the IHX and gas cooler selection. Since SWEP does not manufacture finned tube heat exchangers, Alfa Laval was the manufacturer chosen for the evaporator design. After contacting Alfa Laval team members, it was recommended to use an evaporator from CABERO. The complete report of the selected evaporator is available in Figure C.6 of Appendix C. The chosen evaporator is model CO2-ACHSSD097C1. The evaporator consists of stainless steel tubes and aluminum fins, and it has a maximum operating pressure of 120 bar and a maximum heat capacity of 106.4 kW.

The evaporator is equipped with a ventilator of 50 Hz with a nominal velocity of 885 RPM and a motor capacity of 2.1 kW.

6.1.5. Internal heat exchanger (IHX)

The used IHX, similar to the gas cooler, was selected using SWEP software and with the help of a member of the SWEP team. The necessary inputs are displayed in Table 6.6 and their outputs in Table 6.7.

Table 6.6: IHX SWEP software inputs

Software inputs	Value
Fluid side 1	CO_2
$\boldsymbol{P_{CO2,1}}$	86.0 bar
Fluid side 2	CO_2
$\boldsymbol{P_{CO2,2}}$	34.9 bar
$\boldsymbol{T_{CO2,1,in}}$	35.0 ℃
$\boldsymbol{T_{CO2,1,out}}$	28.9 ℃
$\boldsymbol{T_{CO2,1,in}}$	0.0 ℃
$\boldsymbol{T_{CO2,1,out}}$	21.0 ℃
$\boldsymbol{\dot{m}_{CO2,1}}$	0.2814 kg/s
$\boldsymbol{Max\ PD_{CO2,1}}$	20 kPa
$\boldsymbol{Max\ PD_{CO2,2}}$	20 kPa

Table 6.7: IHX SWEP software outputs

Software outputs	Value
Model	SWEP B18Lx30
$\boldsymbol{\dot{Q}_{IHX}}$	8.997 kW
$\boldsymbol{\dot{m}_{CO2,2}}$	0.2809 kg/s
$\boldsymbol{A_{IHX}}$	1.15 m^2
$\boldsymbol{PD_{CO2}}$	17.7 kPa
$\boldsymbol{PD_{w}}$	8.07 kPa

This exchanger consists of 30 plates with a total effective area of 1.15 m^2. The 30 plates form 29 channels, 14 of which are for the circulation of high-pressure CO_2 and the remaining 15 for the circulation of low-pressure CO_2. The distance between each plate is between 0.4 and 0.5 mm. Stainless steel is used for the plates and copper is used as brazing material. The remaining data, both geometrical and thermodynamic, are available in the manufacturer's report in Appendix C.

6.1.6. Expansion valve

Following a review of the available EEVs on the market and recommendations from the compressor manufacturer, and EEV from Danfoss was chosen. The selection of the EEV was made using Danfoss software Coolselector 2 [137]. It is important to state that this software was designed mainly for refrigeration purposes. Thus, the values calculated for the functioning of the EEV, shown in Figure 6.4, are not completely accurate. Still, for the input $\dot{Q}_{gc} = 61.5$ kW, the software calculated $\dot{Q}_{evap} = 45.2$ kW and $\dot{m}_{CO2} = 0.2266$ kg/s . Even though these values slightly differentiate from the previously calculated for this configuration, they are still close enough to assume the correct functioning of this valve. Besides that, the calculated load percentage sits at 47%, which ensures that for higher heat loads the EEV will still operate correctly. Furthermore, the CCMT model valves are designed specifically by Danfoss for transcritical CO_2 applications as they can be used in flash gas bypass, parallel compression, or standalone configurations. Comparing the different designs of this valve series, the model CCMT 4, whose main operating properties associated with this valve are displayed in Figure 6.5, is illustrated in Figure 6.6

and Figure 6.7. It was chosen as it allows for the desired heating capacity and working pressure while maintaining a low load rate.

```
Capacity
  Cooling capacity [W] ..................................=   45230
  Specific cooling capacity [J/kg] ......................=  199600
  Heating capacity [W] ..................................=   61500
  Specific heating capacity [J/kg] ......................=  271500
  Compressor mass flow [kg/s] ...........................=  0.2266
  Evaporator mass flow [kg/s] ...........................=  0.2266
Evaporation
  Evaporating temperature [K] ...........................=     273
  Evaporating dew point temperature [K] .................=     273
  Evaporating bubble point temperature [K] ..............=     273
  Evaporating pressure [Pa] .............................= 3471000
  Useful superheat [K] ..................................=    21.0
  Additional superheat [K] ..............................=    21.0
Compressor discharge
  Discharge temperature [K] .............................=     380
Condensation
  Condensing temperature [K] ............................=     303
  Condensing dew point temperature [K] ..................=     303
  Condensing bubble point temperature [K] ...............=     303
  Condensing pressure [Pa] ..............................= 7200000
  Subcooling [K] ........................................=     6.0
  Additional subcooling [K] .............................=       0
Additional
  Max liquid line pressure drop (before flashing) [Pa] =  924400
```

Figure 6.4: EEV software system results [137].

```
Additional:
  Maximum opening pressure differential [Pa] =  9000000
  Max. working pressure (PS/MWP) gauge [Pa] .= 14000000
  Maximum operating temperature [K] .....=      333
  Minimum operating temperature [K] .....=      233
  Opening degree [%] ....................=    65.17
  Choked ................................=    False
  Valve state ...........................=     Open
  Capacity [%] ..........................=    47.07
  Maximum capacity [W] ..................=    96090
  Nominal size inlet [mm] ...............=    15.00
  Nominal size inlet [inch] .............=     0.50
  Inlet diameter [mm] ...................=    16.70
  Nominal size outlet [mm] ..............=    15.00
  Nominal size outlet [inch] ............=     0.50
  Outlet diameter [mm] ..................=    16.70
Available connections:
  DIN-EN Butt weld.     Size: 15 t=2.3 mm
  DIN-EN SS butt weld.  Size: 15 t=2.3 mm
  DIN-EN soldering ODF. Size: 15
  DIN-EN soldering ODF. Size: 16
  ANSI soldering ODF.   Size: 5/8"
Suggested connection:
  DIN-EN Butt weld. Size: 15 t=2.3 mm
```

Figure 6.5: CCMT4 mechanical and geometric properties [137].



Figure 6.6: Danfoss CCMT 4 expansion valve [138].

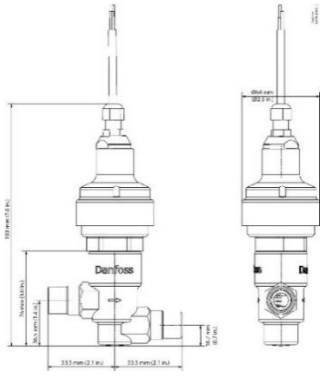


Figure 6.7: Technical drawing of the Danfoss CCMT 4 expansion valve [138].

6.1.7. Accessories

Suction line accumulator

After contacting many manufacturers, ESK manufacturer suggested the use of their FA-22U-CDH based on the given data. That SLA has an associated cost of approximately 150 €. This SLA is a 2.3 l vessel. Both the inlet and outlet connections have an OD of 22 mm. According to the manufacturer report, the maximum operating pressure of the SLA is 100 bar and the maximum operating temperature is 100 ºC. These characteristics were taken from the manufacturer report shown in Figure 6.8. Assemblage must be done only in a vertical position, as near to the compressor as feasible and at the same height. Moreover, the inlet must be connected to the side inlet of the SLA and the outlet must be connected to the top outlet. Finally, the charge capacity of the SLA must be 50 % higher than the total load of the heat pump system [106]. In addition, Figure 6.9, Figure 6.10, and Figure 6.11 show the design of the SLA, its technical drawing, and its dimensions, respectively.

Technische Daten / Technical data

Flüssigkeits-abscheider Suction line accumulator	Lötanschluss innen Solder conn. ODS		Inhalt Volume	Kälteleistung Q_0 [kW] bei –10°C Verflüssigungstemperatur Ref. capacity Q_0 [kW] at –10°C condensing temperature			Kälteleistung Q_0 [kW] bei 90 bar Hochdruck, 35°C Gaskühler-Austrittstemp., 10 K Überhitzung Ref. capacity Q_0 [kW] at 90 bar high pressure, 35°C gas cooler outlet temp., 10 K superheat							Gewicht Weight	Heizband erforderlich Heater band necessary	DGRL PED
Typ Type	mm	inch	l	Verdampfungstemperatur / Evaporating temperature [°C] –30	–35	–40	10	5	0	–5	–10	–15	–20	kg	Stck./pcs.	Kategorie Category
FA-12U-CDH	12	–*	0,8	Opt. 10 Min. 3	9 2,5	7 2,1	19,0 5,0	16,0 4,5	14,0 4,0	12,0 3,5	11,0 3,1	9,2 2,6	7,9 2,3	3,0		I
FA-16U-CDH	16	5/8	2,0	Opt. 20 Min. 5,8	17 5	14 4,1	36,0 10,0	32,0 9,0	28,0 8,0	24,0 7,0	21,0 6,0	18,0 5,0	15,0 4,0	5,8	**HB-30/100** 2x	II
FA-22U-CDH	22	7/8	2,5	Opt. 41 Min. 12,1	35 10,2	29 8,4	74,0 21,0	65,0 19,0	57,0 16,0	50,0 14,0	43,0 12,0	37,0 11,0	32,0 9,0	7,5	**HB-30/100** 2x	II

Figure 6.8: ESK technical data report for FA-CDH suction line accumulators [139].



Figure 6.9: FA-CDH prototype [139].

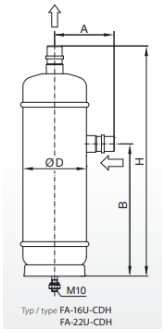


Figure 6.10: FA-CDH technical drawing [139].

Abmessungen / Dimensions

Abb./Typ Fig./Type		ØD mm	H mm	A mm	B mm
a	**FA-12U-CDH**	76,1	290	78	175
b	**FA-16U-CDH**	114,3	326	87	188
b	**FA-22U-CDH**	114,3	414	107	238

Figure 6.11: Dimension represented in Figure 6.10 [139].

Oil separator

After contact with the company Temprite and the use of their software [140], a coalescent oil separator was selected. Specifically, the model 135A with a maximum working pressure of 140 bar was considered the adequate choice when considering the inputs in Table 6.8. This model, besides separating the oil from the R744, also filters dirt out of both the refrigerant and the oil [141]. The diameter of this model is 102 mm (G in Figure 6.13) and its height is 545 mm (D Figure 6.13). The remaining data can be found in the manufacturer report in Appendix C. Moreover, the discharge line header size asked was 1/2 in nominal diameter. However, the connection available for this model is 3/4 in. Since the connection on the oil separator must be the same size or larger than the discharge line size it can still be used [141]. Also, the oil outlet must be connected to the suction line after the SLA. Finally, it is indicated by both the software and the company assistant that model 135A will be at approximately 34 % of its capacity. After consulting the manufacturer, the price given for this oil separator was approximately 800 €. Figure 6.12 and Figure 6.13 show the design of the oil separator and its respective technical drawing.

Table 6.8: Temprite software inputs for the selection of the oil separator

Software necessary inputs	Values
Fluid	CO_2
Type of system	DX
Type of compressor	Reciprocating
$\dot{Q}_{evap}$	44 kW
T_{evap}	0 ℃
T_{gce}	35.0 ℃

There are some important considerations for the correct functioning of the oil separator. Similar to the SLA, it must be mounted vertically as close as possible to the compressor. In addition, it must be thermally insulated so that no refrigeration condensation is possible [106].



Figure 6.12: Temprite oil separator model 135A [141].

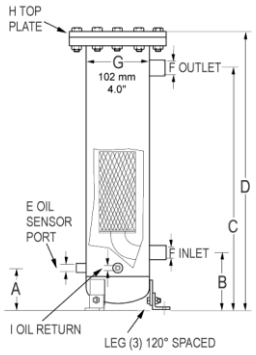


Figure 6.13: Technical drawing of model 135A with the respective components [141].

Oil receiver

As it was stated in Chapter 4.4.2, an oil receiver is only completely necessary when compressors are working in parallel and can stop independently. Since this configuration only uses one compressor, there is no necessity to choose an oil receiver. However, for the configurations with higher heating capacities, multi-compressors are used. This implies that, for those configurations, an oil receiver must be accounted for.

Even though no oil receiver was selected, Tecnac manufacturer was contacted and confirmed that there are available oil separators for this type of application. Tecnac provides oil separators up to 130 bar.

Filter drier

Filters consist of a housing and a core acting as a filtering load. Thus, in comparison to other components, the filer selections are distinctive. The chosen filters must allow for the core to be changed when it is no longer functional and must be able to be disassembled. Carly manufacturer has distinct cores for different functions. On the one hand, for the suction line, two functional cores must be arranged in a specific order before the permanent core can be inserted. First, an “F” type core. It is used to start up the system and has the filtering of pollutants as its primary duty. After that, the “F” type core is replaced with an “N” type core, and the system is decontaminated, dried and acid neutralized. The type “I” is the final core added. This core is the permanent one and serves to preserve the system from the remaining pollutants [142]. On the other hand, for the liquid line, the “F” and “I” core types cannot be used. This implies that cleaning core

"N" is used first. After that, either an "HP" or a "Platinium" core is used permanently until saturation. The permanent filter serves mainly drying purposes.

The chosen manufacturer for the filter driers was Carly. After consulting the manufacturer catalog, the selected filter drier shell is the BCY-P14 487. It is suitable for transcritical CO_2 systems as its maximum operating temperature and pressure are 100 ºC and 140 bar, respectively [143]. The chosen filter BCY-P14 487 has 22 mm connections available, which is the size of the liquid line and suction line pipe. The remaining technical dimensions are shown in Figure 6.14 and Figure 6.15.

CARLY references	Connection types (1)	Filtering surface cm²	Dimensions mm Ø1	Ø2 (2)	Ø3	L1	L2	E1	E2
BCY-P14 485 S/MMS	5	420	141	146	215	263	210	129	98
BCY-P14 487 S/MMS	5	420	141	146	215	277	210	143	115

Figure 6.14: Carly's table of dimensions for the filter drier BCY-P14 487 [143].

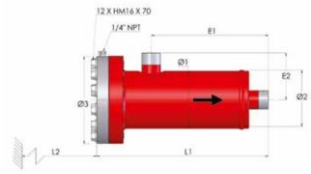


Figure 6.15: Technical dimensions of the filter drier [143].

For the selected filter shell BCY, Figure 6.16 shows that the core reference (size) to be used is CCY 48 or Platinium 48. After consulting the catalog for the drying, filtering, and cleaning cores from Carly (Figure D.1 of Appendix D), the selection was made as shown in Table 6.9. Note that different cores need to be selected for the suction line and liquid line.

Shell reference	Core reference (size)
BDCY	CCY 42
BCY / BCY-HP / ACY	CCY 48 / PLATINIUM 48
BCY-P6 / BCY-P14	PLATINIUM 48 / CCY 48
BBCY / BACY	CCY 100 / PLATINIUM 100

Figure 6.16: Core reference for the chosen shell [142].

Table 6.9: Chosen cores for the filters [142]

Line	Features	Core
Suction line	Reinforced filtration	CCY 48 F
	Burnout decontamination, reinforced drying, reinforced acid neutralization, wax, and resin binding	CCY 48 N
	Filtering	CCY 48 I
Liquid Line	Burnout decontamination, reinforced drying, reinforced acid neutralization, wax, and resin binding	CCY 48 N
	Optimum drying	PLATINIUM 48

Check valves

Carly offers check valves with maximum operating pressure up to 90 bar for CO_2. The available models are displayed in Figure 6.17.

CARLY references	Connections To solder ODF inch	CARLY references	Connections To solder ODF mm	Δ P (1) bar	kv (2) m³/h
CRCY-P9 2 S	1/4	CRCY-P9 2 MMS	6	0,06	0,69
CRCY-P9 3 S	3/8	CRCY-P9 3 MMS	10	0,06	1,75
CRCY-P9 4 S	1/2	CRCY-P9 4 MMS	12	0,05	3,27
CRCY-P9 5 S/MMS	5/8	CRCY-P9 5 S/MMS	16	0,05	3,64

Figure 6.17: ESK catalog for available check valves for transcritical CO_2 operation [144].

6.1.8. Economic analysis

After the selection of the main components of the heat pump, it is relevant to proceed with economic analysis in order to understand the estimated cost of the design of a CO_2 transcritical HPWH. Note that the cost of piping is excluded, as well as the accumulator tank cost that will be discussed further.

A CO_2 heat pump manufactured by Mitsubishi with a heating capacity of 40 kW was estimated to cost 18000 € [118]. Comparing the two values, it can be concluded that the designed heat pump is slightly more expensive. Since the heating capacity is also higher (61.5 kW) the

estimated cost seems reasonable. A lower heating capacity would lead to a general decrease in the cost of the components, mainly the compressor and the evaporator. For example, the cost of a BITZER compressor 4JTE-10K that allows a 40 kW heat load is 8000 €. This would mean a decrease of 3000 € in the estimated cost of the heat pump.

Note that the evaporator cost represents a high parcel of the investment. Therefore, since this component is over-dimensioned, a smaller evaporator can be used in order to diminish the estimated cost. Moreover, the manufacturer of the evaporator also informed that the material cost has risen by 25 % from October 2021 due to the Russia invasion on Ukraine. This has also an effect on the increased transportation cost that is already included in the evaporator cost. Finally, the evaporator cost could be highly decreased using copper tubes instead of stainless steel.

Table 6.10: Economical analysis for the CO_2 transcritical heat pump

Component	Compressor	Gas cooler	Evaporator	EEV	SGHX	SLA	Oil separator	Filter
Model	4GTE-20K	B4TH x90	CO2-ACHS	CCMT 4	B18Lx30	FA-22U-CDH	135A	BCY-P14 487
Cost (€)	10927	640	8200	1247	1851	150	800	400
Total cost (€)	24215							

6.2. Subcritical NH_3 system

A selection of the components will be shown below, similar to the CO_2 configuration. However, since the selection process was already heavily covered for the CO_2 heat pump, it was the author's decision to not go into as much detail for the NH_3 heat pump component selection. The complete manufacturer reports of each component are shown in Appendix C.

6.2.1. Compressor

Previous studies showed that compressors that are not specifically designed for heat pumps working with R717 will not survive more than a few days. Thus, it has been concluded that the best construction for compressors destined for ammonia systems is an open type or separated hood [71]. As for the type of compressor, screw-type compressors were considered an option, however, they are best fitted for applications with higher refrigeration capacity. Therefore, similar to the CO2 configuration, a reciprocating compressor was chosen.

For the selection of the compressor, once again the BITZER software was used. The software indicated compressor W4NA as the best selection.



Figure 6.18: BITZER model W4NA.

Compressor	W4NA
Capacity steps	100%
Cooling capacity	47,8 kW
Cooling capacity *	46,7 kW
Evaporator capacity	47,8 kW
Shaft power	10,57 kW
Condenser capacity	58,4 kW
COP/EER	4,52
COP/EER *	4,42
Mass flow	155,1 kg/h
Operating mode	Coupling (1:1)
Compr. speed	1450 /min
Recommended driving motor	15,00 kW
Discharge gas temp. w/o cooling	121,5 °C

Figure 6.19: Bitzer software outputs for the NH_3 compressor.

Similar to what happens for the CO_2 configuration, the available compressor allows a system with a higher heating capacity than the 50 kW previously defined. Figure 6.19 shows that the W4NA compressor when working at 100 % of its capacity can feed a system with a condenser capacity of 58.4 kW. Since the designed configuration also uses an extra heat exchanger, these values will be divided by the condenser capacity and the desuperheater capacity. To calculate how the heating output is divided by each heat exchanger and calculate the isentropic efficiency of the compressor, the heating power input in the simulation was changed to $\dot{Q}_{heat} = 58.4$ kW. The results are available in Table 6.11.

Table 6.11: EES simulation results for the NH_3 configuration with a heat load of 58.4 kW

NH_3 HPWH variable	Values
$\dot{Q}_{cond}$	48.45 kW
$\%_{cond}$	82.96 %
$\dot{Q}_{dsh}$	9.951 kW
$\%_{dsh}$	17.04 %
$\eta_{comp,s}$	77.3 %
$\dot{m}_{NH3}$	0.04311 kg/s

6.2.2. Piping

The suggested flow velocity for the NH_3 system is quite similar to the values established for CO_2. Since pressure drop calculation was already carried out for the CO_2 system, for the NH_3,

Danfoss Coolselector 2 software was used to determine the recommended piping sizes. The software selection report is shown from Figure E.1 to Figure E.6 in Appendix E. The results given by the software are shown in Table 6.12.

- Line 1: evaporator to compressor (suction line);
- Line 2: compressor to condenser (discharge line);
- Line 3: condenser to expansion valve (liquid line);
- Line 4: expansion valve to evaporator (liquid line).

Table 6.12: NH_3 heat pump piping selection (Coolselector 2)

Line	Piping type	Inner diameter (m)	Velocity (m/s)	Pressure drop (bar/m)
1	DIN-EN SS 32	0.0372	11.86	0.00130
2	DIN-EN SS 20	0.0223	12.91	0.00718
3	DIN-EN SS 8	0.0089	1.18	0.01348
4	DIN-EN SS 8	0.0089	1.18	0.01348

6.2.3. Condenser

The selection process was equal to what was done for the CO_2 plate exchangers. Following the mass flow rate and heat load available in Table 6.11, the selection was made using SWEP selection software and consulting SWEP team. The heat exchanger that was recommended to use was model B10TSHx40.

The condenser was designed to allow water to heat from the network temperature of 10 ºC to 35 ºC. This implies that the outlet temperature of the NH_3 of the condenser needs to be higher than the previously defined 35 ºC. Therefore, subcooling was reduced to 3 ºC and the outlet temperature of the condenser was increased to 37 ºC. In addition, it was defined that the NH_3 enters the condenser at 45 ºC. This is 5 ºC above the condensation temperature (40 ºC), which is needed to assure that no vapor is condensed previously to the inlet of the condenser.

6.2.4. Evaporator

The evaporator selected for the NH_3 heat pump was the same as the one selected for the CO_2 heat pump configuration since aluminum and stainless steel are safe working materials for ammonia.

6.2.5. Desuperheater

The desuperheater is a component that is not present in the CO_2 heat pump configuration. However, the selection was persecuted the same way as for the remaining plate heat exchangers, this is using SWEP software and consulting SWEP team.

Since the condenser was designed for the fluid to enter it at 45 ºC, the designed desuperheater must allow a decrease from the discharge temperature to that temperature. The indicated heat exchanger was model SWEP B5THx42 as the best candidate for the required desuperheater application. Moreover, as it was also defined by the condenser selection, the desuperheater must be designed to allow an increase from the water condenser outlet temperature (35 ºC) to the set DHW temperature (60 ºC).

It is relevant to note that SWEP advises installing the desuperheater so that gas enters the top of the BPHE so that if condensation occurs it is easily removable.

6.2.6. Expansion valve

The expansion valve was chosen in the same way as it had been for CO_2, using Danfoss Coolselector 2 software. Thus, the Danfoss expansion valve AKVA 10-7 was selected for this application. The AKVA is a model of electronic expansion valve specifically built for ammonia refrigeration/heat pump systems.

6.2.7. Accessories

Liquid receiver

ESK was the manufacturer chosen to evaluate the liquid receiver options. After consulting the product sheet for NH_3 compatible liquid receivers shown in Figure D.2 of Appendix D, the model SGS-32-FL1 was selected. This liquid receiver offers a capacity of storage of 32 l of NH_3 fluid, maximum working pressure of 25 bar, and maximum operating temperature of 100 ºC.

Suction line accumulator

Similar to the CO_2 SLA, ESK was contacted to choose a compatible SLA for NH_3 operation. It was recommended to use model FA-42. The catalog report of other possible models is available in Figure D.3 of Appendix D.

Oil separator

After consulting the catalog shown in Figure D.4 of Appendix D, the selected oil separator was 924 from the manufacturer Temprite. This selection was made considering the refrigerating capacity of the designed NH_3 heat pump. In order to confirm this selection, Temprite selection software was also used.

6.2.8. Economic analysis

Table 6.13 presents the individual estimated cost of each component, together with the estimated total cost of the NH_3 heat pump. Note that, similar to the CO_2 analysis, both the piping system and the water storage costs are excluded.

When comparing the estimated total cost, it can be concluded that the NH_3 heat pump represents a lower cost than the CO_2 heat pump. This difference is mainly due to the significantly higher cost of the compressor used in the CO_2 configuration. All the remaining components are within the same range.

Table 6.13: Economic analysis for the NH_3 heat pump

Component	Compressor	Condenser	Desuperheater	Evap.	EEV	Liquid receiver	SLA	Oil separator	**Filter**
Model	W4NA	B10TSHx 40	B5THx18	CO2-ACHS	AKVA 10-7	SGS-32-FL1	FA-42	924R	BCY-P14 487
Cost (€)	6198	939	321	8200	301	1006	351	950	400
Total cost (€)	18648								

6.3. Dimensions and refrigerant charge

Refrigerant charge optimization is essential for correct system performance. The capacity, reliability, and efficiency of a system are reduced when it is undercharged or overcharged. This implies that various methods for determining refrigerant charge levels in heat pump systems are known. However, the implementation might be difficult due to the needed measurements. For the correct calculation of refrigerant charge for both configurations, a definitive installation layout would have to be made since the length of the piping is necessary.

6.3.1. CO_2 heat pump

After analyzing different available market heat pumps, an estimative of 11 to 12 kg of CO_2 was made. This was estimated based on the analysis of the CO_2 HPWH EcoCute manufactured by Itomic [145]. Since the heating capacity, the compressor work input, and the considered temperatures were similar, this was considered a viable comparison point. The technical report of the EcoCute HPWH is available in Appendix H.

An example of an application for the designed heat pump can be found in Figure 6.20. In the figure, both the HPWH and the water storage tank can be seen. Via this example, it was also possible to estimate the necessary dimensions of the designed HPWH. These are shown in Figure 6.21 and Table 6.14. The Y-frame allows for installations in a limited space and for multiple HPWH to be put together if necessary.

Table 6.14: CHP-80Y EcoCute model dimensions and characteristics [145]

Model	CHP-80Y
Dimension	1790 mm × 1990 mm × 1010 mm
Weight	680 kg
Fan	Properller fan 300W x 2 units
CO_2 (R744) charge	11.3 kg
Sound level	60 dB



Figure 6.20: Example of a multiple EcoCute HPWH installation for a dormitory [145].

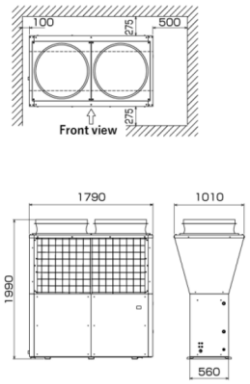


Figure 6.21: Dimension of Y-Frame EcoCute HPWH [145].

6.3.2. NH_3 heat pump

Refrigerant charge is a critical concern in an NH_3 system. The previous safety problems regarding the toxic nature of NH_3 make the smallest leak in the system a serious problem. Naturally, the higher the NH_3 charge better the performance of the heat pump. However, the risk in the event of a leak is also increased. As a result, an optimal relation between these two factors must be achieved. Currently, a low-charge ammonia system is considered by diverse manufacturers as a system that doesn't require more than 1.3 kg per kW of refrigeration capacity [146]. In the configuration presented in this work, this would lead to 62 kg. To estimate the needed refrigerant charge, the various configurations of the HeatPAC NH_3 heat pump, previously referred to in Table 3.1, were studied. Based on the heating capacity from various heating capacities a linear regression was made in Excel to estimate the charge needed for the heating capacity of the configuration in this work. Considering the significantly higher heating output of this model, it is expected that the value needed is lower than the calculated. For the heating capacity of 58.4 kW, a 21 kg refrigerant charge was estimated based on the HeatPAC example. However, current studies show that ammonia systems can work with no more than 0.065 kg per kW [146]. This value would evaluate a total of 3.12 kg, which would lead to significantly lower risk. NH_3 refrigerant charge was taken as the average of these two values, thus being 12 kg. Further studies would be needed to evaluate the optimum value.

6.4. Control system

It is crucial for a complex system such as a heat pump to be efficiently optimized through capacity control. System control done properly can lead to improved efficiency, fewer starters, and longer running times. The many features and refrigerant thermodynamic states of a heat pump and its cycle are controlled by a variety of components that compose the heat pump, such as the compressor, responsible for enthalpy increase, and the expansion valve, responsible for achieving pressure difference between the low and high-pressure sides. Outside the primary loop, the mass flow rate of water through the gas cooler is determined by the water pump, which influences the heat transfer rate transferred from the refrigerant to the DHW. Likewise, by altering the mass flow rate over the evaporator coils, the evaporator fan determines the rate of heat output to the refrigerant from the air [69, 147].

Considering the effect that the gas cooler pressure on the performance of the heat pump and COP values, it is important, if possible, to install a control mechanism over the heat rejection pressure. This way, it would be possible to maximize the performance based on the variable conditions such as T_{amb} and T_{gce}. Kim et. al [74] stated three distinct mechanisms that can be utilized to control gas cooler pressure:

- Control the refrigerant charge on the high-pressure side by varying the expansion valve opening;
- Control the volume on the high side (gas cooler);
- Allow the refrigerant temperature to pressure control.

The 61.5 kW heat pump designed in this project is operated constantly at 86 bar. However, that is the pressure adopted for the boundary conditions initially defined, such as T_{evap} and T_{gce}. However, both these temperatures may suffer variations throughout the working process of the heat pump. Therefore, if a controller is installed to adjust the gas cooler pressure based on the operating conditions, mainly heat source temperature, COP value can be maintained maximum throughout the year [135]. The controller can be for example adjusted to obey the correlation presented in Equation (5.18).

Most current heat pumps are controlled to maintain constant heat output, even when there are ambient air or water inlet temperature changes. Therefore, for cases where ambient air

temperature decreases or water inlet temperature increases, the compressor work and speed have to increase to achieve the same heat load. This translates into a decrease in COP.

7. CO_2 heat pump simulation with selected components

Naturally, the designed heat pumps will not work at the selected inputs throughout the whole operation. Inputs, such as T_{evap} and $T_{network}$, may change depending on the daytime and season. Thus, it is relevant to simulate the operation of the designed heat pumps in order to establish operation limits. As previously said, the compressor is the most significant component of a heat pump, and its nominal mass flow rate is a key parameter. Thus, in all cases, the previously selected compressor specifies the flow rate of the refrigerant, and the remaining simulations will be based on this input. This implies that, in contrast to what occurred in the prior simulations, the thermal power outputs, such as $\dot{Q}_{evap}$ or $\dot{Q}_{gc}$, will vary according to the change in temperature.

Another parameter that is not constant is T_{gce}. This temperature is dependent on all of the main characteristics of the system. These include pressure differentials, flow rates, inlet water temperature, and discharge temperature.

It is also noteworthy that the evaporation temperature is subject to great change for the duration of the year is the evaporation temperature, due to the variations of the ambient air temperature. Besides T_{evap}, $T_{w,i}$ may sometimes suffer variations in its temperature, even though it will be minimal compared to ambient air temperature. Another parameter that is not constant is T_{gce}. This temperature is dependent on all of the main characteristics of the system. Therefore, it is relevant to study how this variation may affect heat pump performance.

7.1. Gas cooler

The heat output to the water in the gas cooler needed to achieve the desired water temperature increase from 10 to 60 ºC can be defined using its specific heat:

$$\dot{Q}_{gc} = \dot{m}_w \times c_{p,w}\left(T_{w,o} - T_{w,i}\right) \tag{7.1}$$

Moreover, for the gas cooler, since it is designed as a counter-flow, the LMTD can be defined with the following equations:

$$\Delta T_{1,gc} = T_{disch} - T_{w,o} = 107.1 - 60 = 47.1\ ℃ \tag{7.2}$$

$$\Delta T_{2,gc} = T_{gce} - T_{w,i} = 35 - 10 = 25\ ℃ \tag{7.3}$$

$$LMTD_{gc} = \frac{\Delta T_1 - \Delta T_2}{\ln\left(\frac{\Delta T_1}{\Delta T_2}\right)} = \frac{47.1 - 25}{\ln\left(\frac{47.1}{25}\right)} = 34.9\ ℃ \tag{7.4}$$

Using the LMTD method in Equation (5.6), U_{gc} can be determined as follows:

$$U_{gc} = \frac{\dot{Q}_{gc}}{A_{gc} \times LMTD_{gc}} = \frac{61.5}{1.06\ \times 34.9} = 1.66\ \mathrm{kW/(m^2℃)} \tag{7.5}$$

As was stated previously. T_{gce} is not constant throughout the functioning of the heat pump. All of the system essential properties affect this temperature. These include pressure differentials, flow rates, inlet water temperature, and discharge temperature. To determine the outlet temperature at the gas cooler, the equality between Equations (5.5) and (7.1) can be used. This determines a relationship between the waterside and the refrigerant side:

$$T_{gce} = T_{w,i} + \frac{T_{disch} - T_{w,o}}{\exp\left(\frac{\left(T_{disch} - T_{w,o} - T_{gce} + T_{w,i}\right) \times A_{gc} \times U_{gc}}{\dot{m}_w \times c_w \times \left(T_{w,o} - T_{w,i}\right)}\right)} \dot{Q}_{gc} \tag{7.5}$$

For the simulation U_{gc} will be treated as constant. This is not completely accurate since changes in flow rate and temperatures in the gas cooler lead to changes in the overall heat transfer coefficient. Still, it can be considered an acceptable approximation. In addition, the value of A_{gc} is given in Table 6.5.

As means to determine the necessary water mass flow rate to achieve the temperature increase from 10 to 60 ºC, an energy balance can be made using Equations (5.4) and (7.1). This results in the following equation:

$$\dot{m}_w = \frac{\dot{m}_{CO2} \times \left(h_{disch} - h_{gce}\right)}{c_{p,w} \times \left(T_{w,o} - T_{w,i}\right)} \tag{7.6}$$

7.2. Results and discussion

The complete EES simulation results for water inlet temperatures from 10 to 25 ºC and ambient temperatures from -10 ºC to 25 ºC are displayed in Table G.1 and Table G.2 of Appendix G. Additionally, the used EES code is available in Appendix J.

7.2.1. Water inlet temperature

The water inlet temperature is a crucial factor for the heat pump performance since it influences the amount of heat rejected by the CO_2 to the DHW. A higher $T_{w,i}$ leads to a smaller enthalpy difference at the entrance of the gas cooler, thus reducing $\dot{Q}_{gc}$ and, subsequently, COP value. This was concluded by various papers mentioned in Chapter 4.2.1. This is proven by the results of the simulation as shown in Figure 7.1. For nominal operation, i.e. $T_{evap} = 0$ ℃ and $P_{gc} = 86$ bar, $\dot{Q}_{gc}$ decreases 20 % and COP decreases 21 % when increasing $T_{w,i}$ from 10 ºC to 25 ºC. Further details are shown in Table G.2 from Appendix G.

Based on Equation (7.5), if $T_{w,i}$ varies, assuming that U_{gc} is constant, then there will be a consequent increase in the CO_2 outlet temperature of the gas cooler. Accordingly, there will a greater temperature difference between the high and low-pressure CO_2 in the IHX. This leads to a significant increase in the suction temperature and, consequently, increased discharge temperature. These effects are shown by the values presented in Figure 7.2.

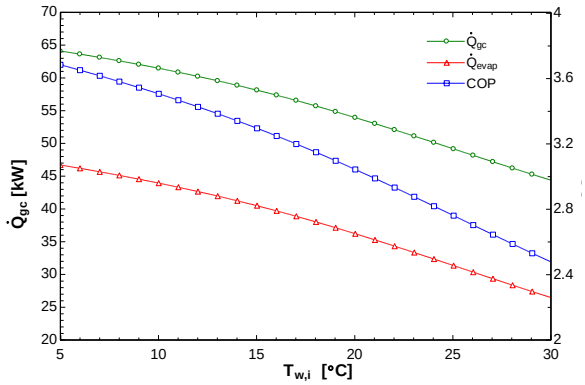


Figure 7.1: $\dot{Q}_{gc}$ and *COP* dependence on $T_{w,i}$ (T_{evap} = 0 °C and P_{gc} = 86 bar).

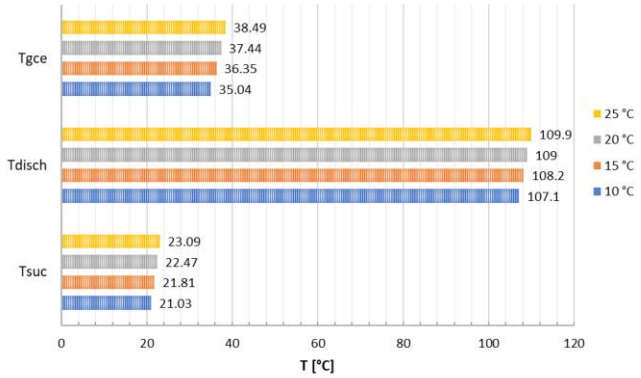


Figure 7.2: T_{gce}, T_{disch}, T_{suc} for four different $T_{w,i}$ (T_{evap} = 0 °C and P_{gc} = 86 bar).

Note that if $T_{evap} = 0$ °C, for $T_{w,in} = 10$ °C, the work input of the compressor is already at its nominal maximum value of 17.52 kW. If $T_{w,i}$ increases and CO_2 mass flow rate is maintained at its nominal value this would demand extra power from the compressor. As a result, $\dot{m}_{CO2}$ must decrease when increasing $T_{w,i}$. Also, since the heating output decreases both water and CO_2 flow rates allow lower values. This consequence is demonstrated in Figure 7.3.

Finally, there is a significant effect on optimum gas cooler pressure $P_{gc,opt}$. When considering Equation (5.18) and the results of the simulation, it can be concluded that the increase in T_{gce} leads to an increase in $P_{gc,opt}$, as shown in Figure 7.3. Therefore, for increasing $T_{w,in}$, the characteristic pressure of 86 bar is further and further away from the optimal value. The same can be concluded in Figure 7.4 which shows the effect of $T_{w,in}$ on both COP and $P_{gc,opt}$.

It is important to state that, even tough $T_{w,in}$ is subject to change due to mixing in the accumulation tanks and variations in network capacity, it is highly unlikely that water inlet temperature reaches more than 15 ºC.

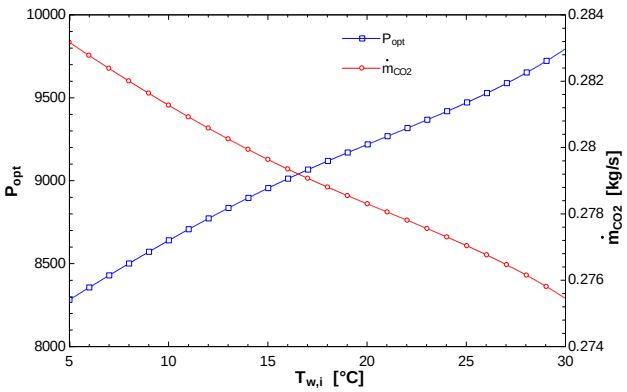


Figure 7.3: $P_{gc,opt}$ and $\dot{m}_{CO2}$ dependence on $T_{w,i}$ (T_{evap}=0 °C).

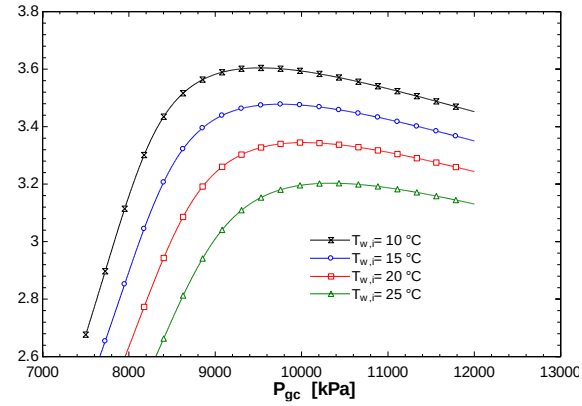


Figure 7.4: COP dependence on P_{gc} for four different $T_{w,i}$ (T_{evap}=0 °C).

7.2.2. Ambient air temperature

The ambient air temperature plays a crucial role in heat pump operation. Because all heat to the fluid is provided by the environment, temperature changes must be heavily considered as they cause the heat pump to operate outside of its nominal values. Considering that the heat pump was designed for $T_{amb} = 10$ °C ($T_{evap} = 0$ °C), if T_{amb} is higher the heat pump will have better performance, while for lower T_{amb} its performance will be degraded.

For $T_{amb} = 10$ °C, heat pump operation will obey the design conditions. When ambient temperature increases, as shown in the graph of Figure 7.5, COP benefits highly and increases from 3.508 up to a maximum of 4.597 at $T_{amb} = 25$ °C, when P_{gc} is maintained constant at 86 bar. The graph also depicts that $\dot{Q}_{gc}$ suffers a decrease. This is mainly an effect of the decrease that the discharge temperature suffers from the higher evaporation temperature and subsequently the higher suction temperature at the compressor. Since the decrease in the discharge temperature is significantly higher than the increase in the gas cooler outlet temperature, as shown in Figure 7.6, the enthalpy values of these states will be closer and less heating output to the DHW will be needed.

Moreover, it can be concluded through Figure 7.5 that compressor work input can be lowered from its maximum of 17.52 kW when T_{amb} is higher than 10 ºC. This is a viable result because (1) the temperature difference between the inlet and outlet decreases, and (2) the higher evaporation temperature increases the evaporation pressure, which leads to a lesser pressure ratio, thus, increasing compressor efficiency. This second reason is shown in Figure 7.7. Compressor

efficiency is estimated to grow up to 17 % when increasing from T_{amb} increases from 10 ºC to 30 ºC.

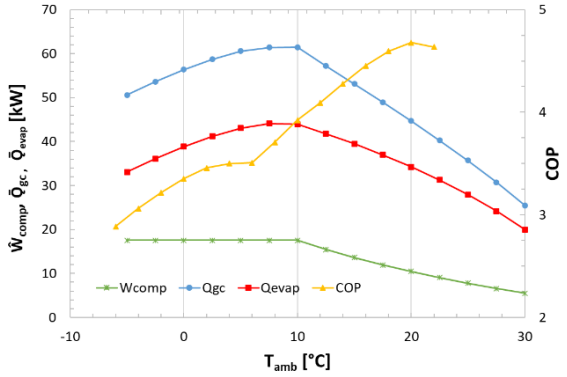


Figure 7.5: $\dot{Q}_{gc}$, $\dot{Q}_{evap}$, $\dot{W}_{comp}$ and COP dependence on T_{amb} (P_{gc} = 86 bar).

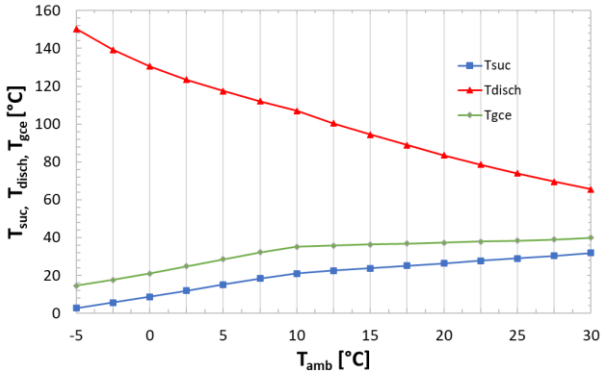


Figure 7.6: T_{gce}, T_{disch}, T_{suc} dependence on T_{amb} (P_{gc} = 86 bar).

The results above are simulated for a constant $P_{gc} = 86$ bar. However, as it was concluded previously, the changes in T_{evap} and T_{gce} highly influence the pressure at which heat pump performance is optimum and COP is at its highest possible value. When comparing the results from the performance at variable pressure and constant pressure, the efficiency benefits are clear. Analyzing the graph in Figure 7.8, it can be deduced that $\dot{Q}_{gc,opt}$ decreases at a much slower rate. This allows that COP value can increase at a much higher rate when T_{amb} increases, extending its possible maximum value to 5.567 with $P_{gc} = 97$ bar for $T_{amb} = 30$ ºC, instead of the 4.637 at $P_{gc} = 86$ bar. Thus, it is highly beneficial to have a control system that allows for P_{gc} to vary to the optimum pressure throughout heat pump functioning. This was previously also concluded in Chapter 5.4.1.

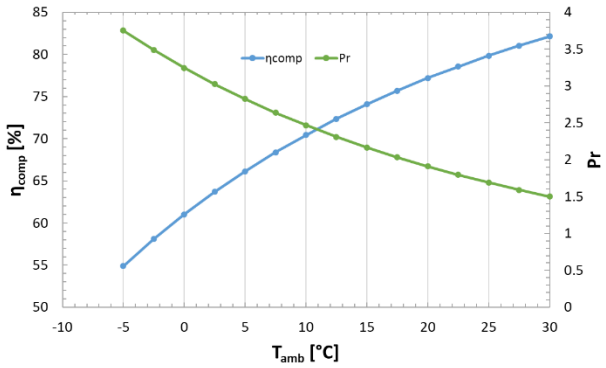


Figure 7.7: p_r and η_{comp} dependence on T_{amb} (P_{gc} = 86 bar).

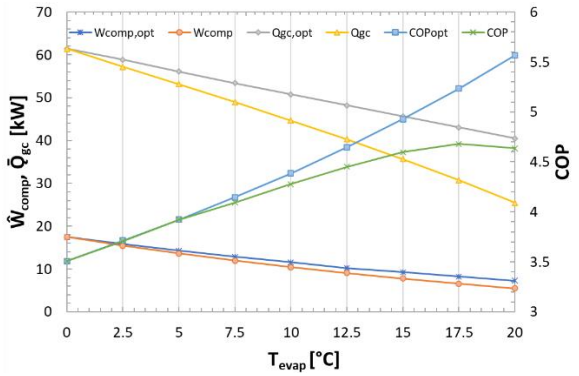


Figure 7.8: Difference between the values of $\dot{Q}_{gc}$, $\dot{Q}_{evap}$, $\dot{W}_{comp}$ and COP at different T_{amb} at optimal P_{gc} and at (P_{gc} = 86 bar) for different evaporation temperatures.

7.3. Comparison with NH_3 heat pump

The adopted configuration for the NH_3 heat pump, as previously explained in Chapter 5.5, includes a condenser and a desuperheater instead of the gas cooler of the CO_2 heat pump. Thus, a similar simulation was made using the components selected for the NH_3 heat pump. The complete EES code is available in Figure J.6 in Appendix J. Moreover, the values that will be presented are displayed in the complete result table for the interval of T_{amb}= -5 ºC to 25 ºC. in Appendix G.

This comparison is mainly made with a focus on ascertaining the potential performance upside that the NH_3 heat pump can have on the CO_2 heat pump and confirming the previous analysis done in Chapter 5.8. Figure 7.9 shows that COP value evolution according to the ambient temperature is significantly different for both heat pumps. Even though CO_2 HPWH shows COP improvement for higher T_{amb}, the NH_3 system reveals remarkable performance for the ambient temperatures studied. On top of that, the difference in performance is increasingly more noticeable while increasing air temperature. For example, COP value is 56 % higher for $T_{amb} = 10$ ºC and 96 % higher for $T_{amb} = 10$ ºC. Table 7.1 shows the improvement that an NH_3 HPWH may offer over the CO_2 configuration. This is mainly due to the lower work input needed at the compressor. At $T_{evap} = 0$ ºC, for a heat load of 61.5 kW, the CO_2 compressor needs 17.52 kW, while, under the same conditions, for a heat load of 58.0 kW, the NH_3 compressor only requires a power input of 10.58 kW.

Table 7.1: *COP* value for the CO_2 and NH_3 and the calculated improvement

T_{amb}	-5	-0	5	10	15	20	25
COP_{CO2}	2.886	3.218	3.457	3.508	3.923	4.279	4.597
COP_{NH3}	3.892	4.315	4.833	5.483	6.321	7.44	9.011
Diff. [%]	34.86	34.09	39.80	56.30	61.13	73.87	96.02

Another very significant value difference can be found when analyzing the refrigerant mass flow rate. This is in line with was stated previously in Chapter 5.8. The needed NH_3 mass flow rate was found to be 80 % lower than the CO_2 mass flow rate at $T_{amb} = 10$ ℃.

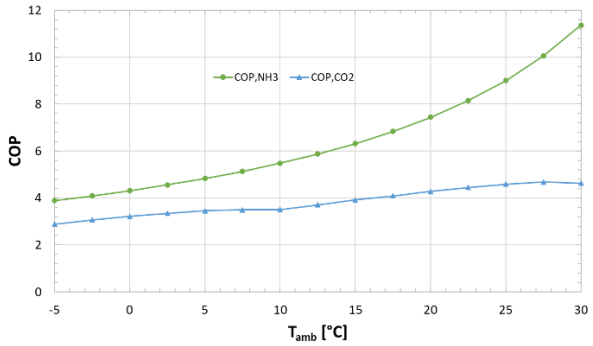


Figure 7.9: *COP* dependence on ambient temperature for the NH_3 and CO_2 configurations.

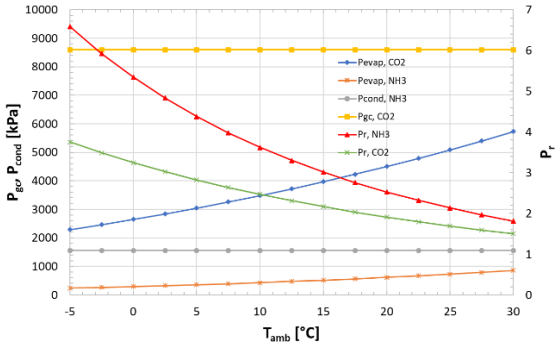


Figure 7.10: P_{evap}, P_{cond}, p_r dependence on ambient temperature for NH_3 and CO_2 configurations.

Finally, another main difference can be found in Figure 7.10. The working pressures for the NH_3 system are much lesser than those presented in the CO_2 configuration. While the CO_2 HPWH heat rejection occurs at a constant 8600 kPa, the NH_3 condensation happens at 1555 kPa (almost six times lower). It can also be concluded that evaporation pressure at the NH_3 system is much more subject to variation of T_{amb}. While for NH_3, it was found that evaporation increases 3.6 times from 236.2 kPa at $T_{amb} = -5$ ℃ to 728.8 at 25 ºC, for CO_2 only increases by 2.5 times from 2291 to 5089 kPa. This leads to a close approximation of both pressure ratio values when increasing T_{amb}. This highly impacts compressor efficiency as this parameter is extremely dependent on the pressure ratio value.

8. Domestic hot water heating

8.1. CO_2 heat pump water storage

The interaction between the heat pump, the storage tank, and the DHW consumption is an essential aspect of the study. Because they affect the compressor's on/off periods of the compressor, it is critical to design the proper volume of the storage tanks. Small water tanks cause the compressor to cycle on and off frequently, shortening its lifespan. A water tank that is too large will result in higher installation costs. The price of electricity, which might display fluctuations during the day, has a significant impact on tank size [112].

The temperature that water is stored is also extremely important due to mainly health concerns. The following criteria must be used to determine the value [148]:

- When stored water surpasses 60-65 ºC, these phenomena, such as corrosion and limestone deposition, become faster and more aggressive;
- The use of low stored water temperatures significantly increases the size of the accumulators;
- Bacteria can generally endure temperatures of up to 50 ºC for an extended period. However, they are quickly eliminated above 55 ºC.

Considering these factors, holding hot water in the 60 to 65 ºC range is usually a reasonable solution that is also compatible with current standards.

As means to achieve the desired storage temperature, two strategies can be followed: mixing or stratification. Mixing inside the tank occurs when the water flow rate is high due to the use of a water pump. A variable speed pump, which regulates water flow, is used to achieve a full temperature increase to the desired 60 ºC through one pass on the gas cooler. This method allows water inlet temperature at the gas cooler to increase gradually, which decreases the heat pump COP. Then, the storage water tank gradually increases temperature until it reaches the set point. Subsequently, various studies, such as Checchinato et al. [149], showed that the best energy efficiency is obtained via stratification since it allows constant water inlet temperature and water outlet temperature very close to the desired output. In this case, the water temperature lift across the gas cooler is much higher [69]. This requires thermosyphon flow, meaning that the water flow rate is sufficiently low avoiding any mixing in the storage tank. In this case, no water pump is

required, and all the heat transfer is through natural convection. However, when thermosyphon flow through the gas cooler is not achievable, accumulator tanks can be equipped with diffusers at their inlet and outlet to decrease water velocity, thus, minimizing the mixing of the hot and cold water [150].

When analyzing the flow rates calculated previously in Chapter 4, the flow rate necessary to achieve a single pass temperature increase from 10 ºC to 60 ºC is too high to be possible to have stratification. Thus, there will be a mixing problem at the beginning of the filling of the water tanks. This will lead to worse performance as the water inlet temperature increases due to mixing the water that exits the gas cooler at 60 ºC. The thermodynamic losses will be more significant at the charging stage of the tank when the temperature difference between the DHW and the tank water is higher.

The system charging works as follows: cold water is drawn from the cold water network system to fill the DHW tanks. The valves between the DHW tanks and the heat pump are then closed. The HPWH would then be turned on and water would be pumped through the gas cooler from the bottom of the last DHW tank. Water is heated and returned to the top of the first DHW water tank. When the water stored in the final tank hits 60 ºC, it switches off. The storage tank must have a highly insulated design and be put atop an insulation block to reduce heat losses to the floor. All water tanks must be equipped with temperature sensors. Finally, the hot water that is drawn to the users must be mixed with network water so that the desired supply tap water temperature is achievable.

It is beneficial to have multiple small water tanks instead of a few large tanks. Large water tanks lead to higher heat conductions between the hot and cold water during the charging of the tanks.

Besides the heat pump heating capacity, the water storage tanks must be equipped with backup electric water heaters. In case of incapacity from the HPWH, the electric water heaters must be able to heat the water in the final tank to the set point temperature. This can happen if there is excessive time with no draw, which will eventually lead to the temperature dropping due to standby losses [151]. This implies that a controller is programmed so that, the water pump, the HPWH, and the electrical heating element can maintain the desired water outlet temperature.

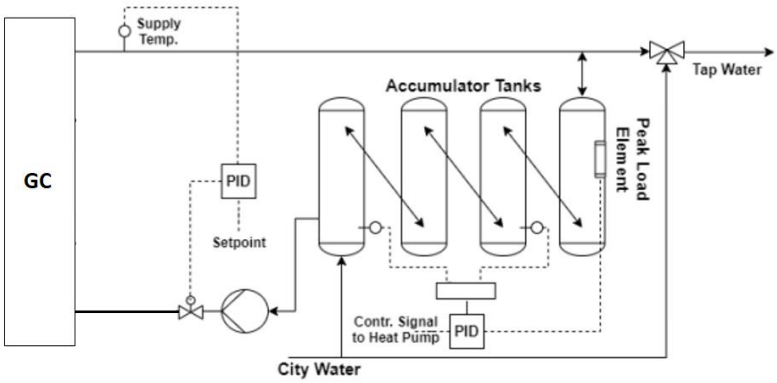


Figure 8.1: Schematic diagram of the system of DHW accumulation [150].

Another option that is increasingly efficient and therefore more widely used is the use of phase change materials (PCMs). Currently, the main candidate is paraffin wax (RT 60), specifically due to its significant melting temperature range (55 to 61 ºC), which adapts very well to the desired outlet water temperature. When compared to the water storage method, using PCMs as storage materials allow significantly higher heat capacity (four to five times), occupying less volume. This is especially important for solutions that are placed inside a building. Moreover, there is no danger to health, and it is 100 % recyclable. Naturally, these advantages are accompanied by a higher cost. The estimation is that PCMs (with RT 60) are up to 4 times more expensive than the water solution [152].

8.2. DHW requirements

For service buildings such as hotels, residential buildings, hospitals, etc. the installed system must meet the adequate supply of hot water. The correct sizing of the heat pump requires an understanding of the type of building and its main characteristics, such as the number of lavatories, bathtubs, basins, etc. Thus, proper sizing and design lead to customer satisfaction and, therefore, a successful dimensioning of the heat pump water heater. Still, an adequate hot water supply must be achieved at the lowest cost of installation and maintenance possible.

For this report, ASHRAE recommendations were considered in order to determine DHW requirements and, with that, the necessary storage tank volumes. Considering a small residential building with the following characteristics:

- 20 apartments

- 20 basins: $20 \times 7{,}6 \ = \ 152$ L/h
- 10 foot basins: $10 \times 11 \ = \ 110$ L/h
- 15 bathtubs: $15 \times 76 \ = 1140$ L/h
- 10 showers: $10 \times 114 \ = \ 1140$ L/h
- 20 dishwashers: $20 \times 57 \ = \ 1140$ L/h
- 20 kitchen sinks: $20 \times 38 \ = \ 760$ L/h
- 10 laundry tubs: $10 \times 76 \ = \ 760$ L/h

Then it is possible, following ASHRAE recommendations [153] to estimate the maximum demand for hot water service:

- Possible maximum demand = 5202 L/h
- Probable maximum demand = Possible max. demand x Demand factor = $5202 \times 0{,}30 \ = \ 1561$ L/h
- Storage tank capacity = Heat pump capacity x Storage capacity factor = $1561 \times 1.25 = \ 1952$ L/h

9. CO_2 system diagram

After selecting the components, it is possible through AutoCAD to establish an approximate design of the CO_2 system. Figure 9.1 shows a schematic with the main components that compose the designed heat pump. Together with the refrigerant side, it was also designed the accumulation tanks and the respective water pump. Note that the figure can be seen in more detail in Appendix I.

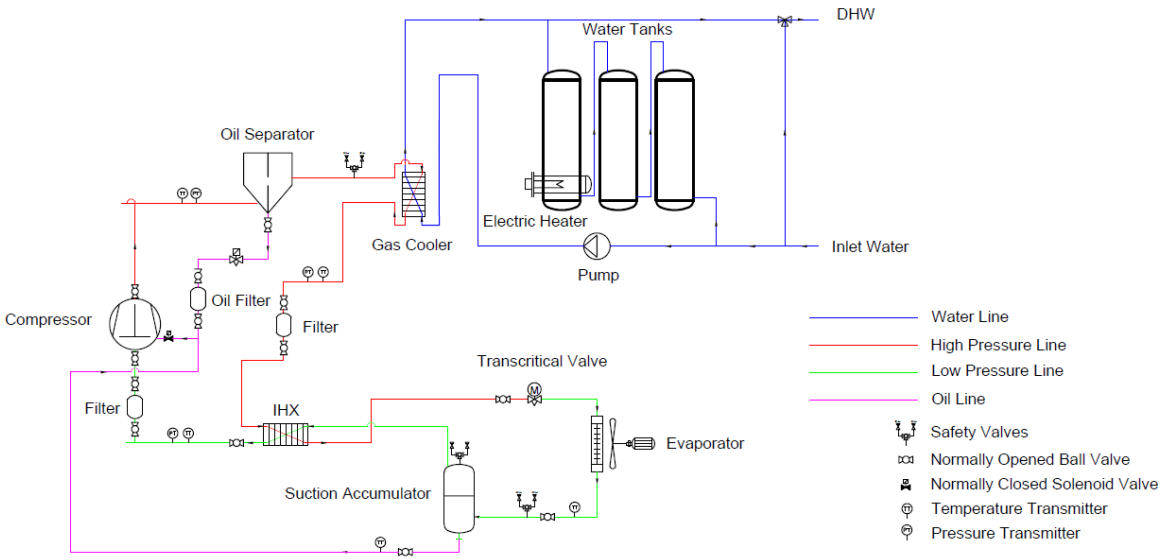


Figure 9.1: Schematic of the CO_2 heat pump with the designed components (AutoCAD software).

10. Conclusions

For the EES simulations, the evaporation was defined as having a 10 ºC difference from the ambient air temperature, as this would allow sufficient heat exchanger between both fluids. As for the design ambient air temperature, it was considered as an average of the city temperature (10 ºC). Therefore, the design evaporation temperature was 0 ºC.

A simulation for 50 kW heat load was made, which allowed a study on the influence of the various design parameters, mainly the gas cooler optimum pressure. The gas cooler outlet temperature was revealed to have the highest influence on the optimum pressure. Specifically, the optimum discharge pressure increases very significantly for higher gas cooler exit temperatures. Even though the evaporation temperature also showed some influence, results showed that it is considerably lower and almost minimal when compared to the gas cooler outlet temperature impact.

After exploring possible modifications to the transcritical cycle that would improve COP value for the heat pump cycle, it was concluded that only the addition of the IHX would be simulated. Even though it found that the IHX configuration offered the lowest COP improvement, the remaining modifications represented significantly higher investments and are not as well optimized as the addition of the IHX. In addition, various studies also reported that the IHX allowed sufficient optimal discharge pressure reduction. The IHX effectiveness was put at 60 %. The result comparison between the CO_2 cycle with IHX and the conventional CO_2 cycle showed that the COP improvement in the IHX cycle over the COP for the conventional cycle is very low at lower gas cooler outlet temperatures (0.33 % for 30 ºC). However, the improvement gets more noticeable for higher outlet temperatures (4.05 % for 50 ºC). The same trend was found for the optimum gas cooler pressure. The reduction in optimum gas cooler pressure was found to be higher for the higher gas cooler outlet temperatures. Moreover, it was concluded that the addition of the IHX helps the optimum gas cooler pressure to be more constant. Therefore, in a system without variable gas cooler pressure this would lead to the system being closer to the optimum performance. The benefits of the IHX are mainly due to the reduction of expansion losses.

Moreover, the results of the simulation also allowed analyzing the effect of the efficiency of the internal heat exchanger on the CO_2 heat pump cycle. Efficiency varied from 40 to 60 %. Results showed that higher efficiency allows for higher superheating of the fluid, enhancing

suction temperature at the entrance of the compressor. This led to higher discharge temperature and, consequently, lower refrigerant mass flow rate needed for the desired heat load.

Regarding the NH_3 cycle, simulation results showed that, when considering the addition of the IHX, the effect was the inverse of the desired. For higher IHX efficiencies, the COP value decreased, which was sufficient to conclude that the IHX configuration does not benefit the NH_3 cycle. This was justified by the fact that, contrary to most working fluids, increasing the superheat in an NH_3 cycle is prejudicial, degrading the performance of the system. Therefore, the following work was done considering the NH_3 conventional cycle.

The simulation for the 50 kW heat load also allowed us to determine the needed capacity for the remaining components. The main determining component was the compressor. For the CO_2 heat pump, the compressor selected was found to allow a 61.5 kW heat load, higher than the 50 kW previously defined. Moreover, the nominal flow rate was defined at 0.2813 kg/s. The remaining components were selected using the nominal CO_2 flow rate of the compressor. The optimal gas cooler pressure for this design was found to be 86 bar which led to a COP value of 3.513 at design conditions.

The component selection was made according to the design conditions and the nominal operation parameters of the compressor. Regarding the heat exchangers for the CO_2 heat pump, the gas cooler and the IHX were selected as plate heat exchangers from SWEP, while the evaporator was selected as a finned tube heat exchanger due to exchanging heat with ambient air. The expansion device was selected as an electronic expansion valve from Danfoss. Various extra components were also selected, such as a suction line accumulator, filters, and oil separators. It was concluded that even though an IHX was added to the CO_2 heat pump, a suction line accumulator was still useful to decrease the liquid hammer phenomenon. For the NH_3 heat pump, component selection occurred similarly, apart from the selection of a liquid receiver, which the CO_2 heat pump didn't need due to the fact that CO_2 exits the gas cooler in a supercritical state.

Economic analysis showed that the estimated cost of the designed CO_2 heat pump is within range of other currently commercially available heat pumps. However, it also showed that the estimated cost of the NH_3 heat pump is significantly lower than the CO_2 heat pump.

Finally, other simulations were made using the geometric and thermodynamic parameters of the heat exchangers selected in order to access the performance of the heat pumps throughout

variable ambient air and water conditions. It was found that water inlet temperature has a very significant influence on the performance of the heat pump. An increasing water inlet temperature leads to a decrease in enthalpy difference that, as a result, diminishes the heat load transferred to the water. As a result, COP value lowers significantly. Moreover, it increases the optimum gas cooler pressure due to the increase of the gas cooler outlet temperature.

In these simulations, the ambient air temperature was also varied. Results show that COP value increases significantly from 3.508 at 10 ºC to 4.597 at 25 ºC and compressor efficiency increases from 70 to 80 % due to the pressure ratio decrease.

Finally, the comparison with the NH_3 heat pump showed that the use of ammonia as a working fluid brings many benefits to the performance of the heat pump. Results show that, under the same design conditions, COP value is 35 % higher in the NH_3 configuration. This value increases up to 96 % when considering higher ambient air temperatures such as 25 ºC. Thus, it can be concluded that NH_3 can be turned into a valuable option as a working fluid for DHW heat pumps if the correct safety measures are taken.

11. Further studies

After the conclusion of this work, there are now a few suggestions for further studies that can add value to this project. The big goal would be to initiate the assembly of the heat pumps as means to achieve experimental results that would enable the model to be validated and the system to be optimized to the best performance. Before taking that action, though, some additional in-depth research would need to be done.

A more complete investigation of the heat transfer on the designed heat exchanger. The project used previously designed heat exchangers. This can be researched and optimized for the needed application. To increase the effectiveness of heat transfer, it is possible to study and assess the effects of many aspects, such as the length, number of plates or tubes of the heat exchanger, etc.

Additional studies of the control system should be done to combine control possibilities by both time and temperature parameters.

Finally, it would be useful then to design the heat pump for a realistic scenario with DHW heating needs where an assessment of needs and costs could be made. This would allow a comparison of the annual cost of a conventional heating system such as a boiler with the potential costs of installation and operation costs of a heat pump.

References

[1] bp, " bp Statistical Review of World Energy 2021," Statistical Review of World Energy, 2021.

[2] J. M. Calm, "Refrigerants Transition... Again," in *ASHRAE/NIST Conference*, Gaithersburg, MD, USA, 2012.

[3] A. Grübler and N. Nakicenovic, "Decarbonizing the Global Energy System," *Technological Forecasting and Social Change*, vol. 53, no. 1, pp. 97-110, September 1996.

[4] H. Tian, Z. Yang, M. Li and Y. Ma, "Research and application of CO 2 refrigeration and heat pump cycle," *Science in China Series E Technological Sciences*, vol. 52, no. 6, pp. 1563-1575, 2009.

[5] European Comission, "Climate Action - Paris Agreement," [Online]. Available: https://ec.europa.eu/clima/eu-action/international-action-climate-change/climate-negotiations/paris-agreement_pt. [Accessed 15 March 2022].

[6] S. Sorrell, "Reducing energy demand: A review of issues, challenges and approaches," *Renewable and Sustainable Energy Reviews*, vol. 47, pp. 74-82, 2015.

[7] R. Clémençon, "The Two Sides of the Paris Climate Agreement: Dismal Failure or Historic Breakthrough?," *Journal of Environment & Development*, vol. 25, no. 1, pp. 3-24, 2016.

[8] bp, "bp Energy Outlook: 2022 edition," 2022. [Online]. Available: https://www.bp.com/content/dam/bp/business-sites/en/global/corporate/pdfs/energy-economics/energy-outlook/bp-energy-outlook-2022.pdf. [Accessed 15 March 2022].

[9] I. E. Agency, "World Energy Outlook 2021," October 2021. [Online]. Available: https://www.iea.org/reports/world-energy-outlook-2021. [Accessed 15 March 2022].

[10] G. Zachmann, F. Holz, B. McWilliams, F. Meissner, A. Roth, R. Sogalla and C. Kemfert, "Decarbonisation of Energy," November 2021. [Online]. Available: https://www.europarl.europa.eu/RegData/etudes/STUD/2021/695469/IPOL_STU(2021)695469_EN.pdf. [Accessed 16 March 2022].

[11] P. Tschakert, J. Roy, H. Waisman, S. A. Halim, P. Antwi-Agyei, P. Dasgupta, B. Hayward, M. Kanninen, D. Liverman, C. Okereke, P. F. Pinho, K. Riahi and A. G. Rodriguez, "Sustainable Development, Poverty Eradication and Reducing Inequalities," *Global Warming of 1.5°C. An IPCC Special Report*, pp. 445-538, 2018.

[12] UNESCO, "Sustainable Development," UNESCO, [Online]. Available: https://en.unesco.org/themes/education-sustainable-development/what-is-esd/sd. [Accessed 20 March 2022].

[13] United Nations, "Transforming our world: the 2030 Agenda for Sustainable Development," 25 September 2015. [Online]. Available: https://www.un.org/ga/search/view_doc.asp?symbol=A/RES/70/1&Lang=E. [Accessed 20 March 2022].

[14] United Nations, "Transforming our world: the 2030 Agenda for Sustainable Development," United Nations, 21 October 2015. [Online]. Available: https://sdgs.un.org/2030agenda. [Accessed 20 March 2022].

[15] United Nations, "The 17 Goals," [Online]. Available: https://sdgs.un.org/goals. [Accessed 20 March 2022].

[16] United Nations, "Goal 7: Ensure access to affordable, reliable, sustainable and modern energy," [Online]. Available: https://unric.org/en/sdg-7/. [Accessed 21 March 2022].

[17] International Energy Agency, "Universal Access to Sustainable Energy Will Remain Elusive Without Addressing Inequalities," 7 June 2021. [Online]. Available: https://www.iea.org/news/universal-access-to-sustainable-energy-will-remain-elusive-without-addressing-inequalities. [Accessed 22 March 2022].

[18] IEA, IRENA, UNSD, WB and WHO, "Tracking SDG 7: The Energy Progress Report 2019," Washigton DC, 2019.

[19] European Environment Agency, "Energy intensity," 16 December 2016. [Online]. Available: https://www.eea.europa.eu/data-and-maps/indicators/total-primary-energy-intensity-3. [Accessed 25 March 2022].

[20] Internation Energy Agency, "Energy intensity," [Online]. Available: https://www.iea.org/reports/sdg7-data-and-projections/energy-intensity. [Accessed 25 March 2022].

[21] International Energy Agency, "Energy Efficiency 2021 - Executive Summary," 2021. [Online]. Available: https://www.iea.org/reports/energy-efficiency-2021/executive-summary. [Accessed 25 March 2022].

[22] U.S Energy Information Administration, "Link between growth in economic activity and electricity use is changing around the world," 20 November 2017. [Online]. Available: https://www.eia.gov/todayinenergy/detail.php?id=33812. [Accessed 24 March 2022].

[23] G. Szustak, P. Dąbrowski, W. Gradoń and Ł. Szewczyk, "The Relationship between Energy Production and GDP: Evidence from Selected European Economies," *Energies,* vol. 15, no. 1, 2022.

[24] United Nations Environment Programme, " 2020 Global Status Report for Buildings and Construction: Towards a Zero-emission, Efficient and Resilient Buildings and Construction Sector," 2020. [Online]. Available: https://wedocs.unep.org/bitstream/handle/20.500.11822/34572/GSR_ES.pdf. [Accessed 26 March 2022].

[25] European Comission, "Energy use in buildings," [Online]. Available: https://ec.europa.eu/energy/eu-buildings-factsheets-topics-tree/energy-use-buildings_en. [Accessed 26 March 2022].

[26] Direção-Geral de Energia e Geologia, "Edifícios," [Online]. Available: https://www.dgeg.gov.pt/pt/areas-setoriais/energia/eficiencia-energetica/edificios/. [Accessed 26 March 2022].

[27] U.S. Department of Energy , "QUADRENNIAL TECHNOLOGY REVIEW: AN ASSESSMENT OF ENERGY TECHNOLOGIES AND RESEARCH

OPPORTUNITIES," *Chapter 5: Increasing Efficiency of Building Systems and Technologies,* 2015.

[28] E. Papadis and G. Tsatsaronis, "Challenges in the decarbonization of the energy sector," *Energy,* vol. 205, 2020.

[29] International Energy Agency, "World Energy Model Documentation," October 2021. [Online]. Available: https://iea.blob.core.windows.net/assets/932ea201-0972-4231-8d81-356300e9fc43/WEM_Documentation_WEO2021.pdf. [Accessed March 28 2022].

[30] P. Neksa, H. Rekstad, G. R. Zakeri and P. A. Schiefloe, "CO2-heat pump water heater: characteristics, system design and experimental results," *International Journal of Refrigeration,* vol. 21, no. 3, pp. 172-179, 1998.

[31] G. Hundy, A. Trott and T. Welch, Refrigeration, Air Conditioning and Heat Pumps, Oxford: Butterworth-Heinemann, 2016.

[32] G. Lorentzen, "Trans-critical Vapour Compression Cycle Device". USA Patent PCT/NO89/00089, 6 September 1989.

[33] G. Lorentzen and J. Pettersen, "New possibilities for non-CFC refrigeration," Refrigeration, energy and environment, Norway, 1992.

[34] SWEP, "Heat Pumps," [Online]. Available: https://www.swep.net/applications/residential-heating/heat-pumps/. [Accessed 2 June 2022].

[35] P. Neksa and K. Stenstadvold, "TRANSCRITICAL CO 2 HEAT PUMPING SYSTEMS," SINTEF Energy Research, Norway.

[36] S. Smitt, I. Tolstorebrov and A. Hafner, "Integrated CO2 system with HVAC and hot water for hotels: Field measurements and performance evaluation," *International Journal of Refrigeration,* vol. 116, no. 1, pp. 59-69, 2020.

[37] T. Stausholm, "Sabroe Launches High-Temperature Ammonia Heat Pump," Ammonia21, 10 February 2022. [Online]. Available: https://ammonia21.com/sabroe-launches-high-temperature-ammonia-heat-pump/. [Accessed 1 June 2022].

[38] "RACE - Refrigeration & Air Conditioning Engineering," [Online]. Available: https://www.race.com.pt/pt.

[39] Michael J. Moran, Howard N. Shapiro, Daisie D. Boettner and Margaret B. Bailey, Fundamentals of Engineering Thermodynamics, John Wiley & Sons, 2010.

[40] Y. Çengel and M. Boles, Thermodynamics: An Engineering Approach, McGraw-Hill Education, 2015.

[41] A. Kornhauser, "The Use of an Ejector as a Refrigerant Expander," in *International Refrigeration and Air Conditioning Conference,* 1990.

[42] SWEP, "Refrigeration handbook," [Online]. Available: https://www.swep.net/refrigerant-handbook/refrigerant-handbook/. [Accessed 20 May 2022].

[43] J. Stene, "Residential CO2 Heat Pump System for Combined Space Heating and Hot Water Heating," NTNU - Norwegian University of Science and Technology, 2004. [Online]. Available: https://www.osti.gov/etdeweb/servlets/purl/20559406.

[44] American Society of Heating and Refrigerating and Air-Conditioning Engineers, Inc., 2018 ASHRAE Handbook - Refrigeration (I-P Edition), American Society of Heating, Refrigerating and Air-Conditioning Engineers, Inc. (ASHRAE), 2018.

[45] R. U. Rony, H. Yang, S. Krishnan and J. Song, "Recent Advances in Transcritical CO2 (R744) Heat Pump System: A Review," *Energies,* vol. 12, no. 3, 2019.

[46] Z. Ye, Y. Wang, Y. Song, X. Yin and F. Cao, "Optimal discharge pressure in transcritical CO2 heat pump water heater with internal heat exchanger based on pinch point analysis," *International Journal of Refrigeration,* vol. 118, pp. 12-20, 2020.

[47] B. S. K. Austin, "Transcritical carbon dioxide heat pump systems: A review," *Renewable and Sustainable Energy Reviews,* vol. 15, no. 8, pp. 4013-4029, 2011.

[48] EPRI, "Perfomance Assessment of an Eco-Cute Heat Pump Water Heater," Palo Alto, CA, 2008.

[49] A. Cavallini and C. Zilio, "Carbon dioxide as a natural refrigerant," *International Journal of Low Carbon Technologies,* vol. 2, no. 3, pp. 225-249, July, 2007.

[50] ASHRAE and UNEP, "Update on New Refrigerants Designations and Safety Classifications," April 2020. [Online]. Available: https://www.ashrae.org/file%20library/technical%20resources/refrigeration/factsheet_ashrae_english_20200424.pdf. [Accessed 3 April 2022].

[51] F. Bruno, M. Belusko and E. Halawa, "CO2 Refrigeration and Heat Pump Systems—A Comprehensive Review," *Energies,* vol. 12, no. 15, 2019.

[52] J. Sarkar, "Transcritical carbon dioxide based heat pumps for simultaneous cooling and heating applications," *Ph.D. dissertation, Indian Institute of Technology,* January 2005.

[53] C. Afonso, Sistemas Frigoríficos, Porto: Efeitos Gráficos, 2019.

[54] Emerson Climate Technologies, "CO2 as a Refrigerant — Properties of R744," [Online]. Available: https://emersonclimateconversations.com/2015/05/14/co2-as-a-refrigerant-properties-of-r744/. [Accessed 1 April 2022].

[55] A. G. M. Ibrahim, "A Study of a Transcritical Multi-Stage Carbon Dioxide Heat Pump," *Ph.D. dissertation,* 2004.

[56] I. Pioro and S. Mokry, "Thermophysical Properties at Critical and Supercritical Conditions," in *Heat Transfer - Theoretical Analysis, Experimental Investigations and Industrial Systems,* Canada, University of Ontario Institute of Technology, 2011, pp. 573-592.

[57] S.M. Liao and T. Zhao, "Measurements of Heat Transfer Coefficients From Supercritical Carbon Dioxide Flowing in Horizontal Mini/Micro Channels," *Journal of Heat Transfer* , vol. 124, pp. 414-420, 2002.

[58] F-Chart Software, "EES: Engineering Equation Solver".

[59] Danfoss, "Refrigerant trends - The 7 Force Model: a path to sustainability," [Online]. Available: https://www.danfoss.com/en/about-danfoss/our-businesses/cooling/refrigerants-and-energy-efficiency/refrigerants-from-a-danfoss-perspective/7-forces-model/. [Accessed 2 April 2022].

[60] G. Poongavanam, V. Sivalingam, R. Prabakaran, M. Salman and S. C. Kim, "Selection of the best refrigerant for replacing R134a in automobile air conditioning system using different MCDM methods: A comparative study," *Case Studies in Thermal Engineering,* vol. 27, 2021.

[61] B. Thonon, "Transcritical R744 (CO2) heat pumps," 2007.

[62] S. Gupta, N. K. Karanam, R. Konijeti and A. Dasore, "Thermodynamic Analysis and Effects of Replacing HFC by Fourth-Generation Refrigerants in VCR Systems," *International Journal of Air-Conditioning and Refrigeration,* vol. 26, no. 1, 2018.

[63] C. Arpagaus, F. Bless, M. Uhlmann, J. Schiffmann and S. Bertsch, "High temperature heat pumps: Market overview, state of the art, research status, refrigerants, and application potentials," *Energy,* vol. 152, pp. 985-1010, 2018.

[64] J. W. Elkins, "Chlorofluorocarbons (CFCs)," 1999. [Online]. Available: https://gml.noaa.gov/hats/publictn/elkins/cfcs.html. [Accessed 20 May 2022].

[65] M. Longhini, "Martina Longhini," MSc Thesis, Lisbon, Portugal, 2015.

[66] M. Razzaq, J. Ahamed and A. Hossain, "A REVIEW ON HYDROCARBON (HCs) AS AN ALTERNATIVE REFRIGERANT: BASED ON THERMODYNAMIC AND ENVIRONMENTAL APPROACH," *Mechanical Engineering Research Journal,* vol. 11, pp. 86-96, 2018.

[67] A. Hafner, "The advantages of natural working fluids," in *25th IIR International Congress of Refrigeration*, Montreal, Canada, August 24-30, 2019.

[68] Linde Gas, "Natural Refrigerants," [Online]. Available: https://www.linde-gas.com/en/products_and_supply/refrigerants/natural_refrigerants/index.html. [Accessed 4 April 2022].

[69] P. Murray, "Performance Analysis of a Transcritical CO2 Heat Pump Water Heater Incorporating a Brazed-Plate Gas Cooler," *M.S. thesis,* 2014.

[70] O. Bamigbetan, T. Eikevik, P. Nekså and M. Bantle, "Review of Vapour Compression Heat Pumps for High Temperature Heating using Natural Working Fluids," *International Journal of Refrigeration,* vol. 80, pp. 197-211, 2017.

[71] A. Zajacs, A. Lalovs, A. Borodinecs and R. Bogdanovics, "Small ammonia heat pumps for space and hot tap water heating," *Energy Procedia,* vol. 122, pp. 74-79, September 2017.

[72] B. Monfared, "Design and Construction of a Small Ammonia Heat Pump," KTH Industrial Engineering and Management, Master of Science Thesis EGI, 2010.

[73] H. Liu, Z. Gu and Y. Li, "Simulation of NH3/CO2 Two-Stage Low Temperature Refrigeration System," in *International Refrigeration and Air Conditioning Conference*, 2002.

[74] M.-H. Kim, J. Pettersen and C. W. Bullard, "Fundamental process and system design issues in CO2 vapor compression systems," *Progress in Energy and Combustion Science,* vol. 30, pp. 119-174, 2004.

[75] DENSO, "Bomba de calor a CO2 residencial," DENSO, [Online]. Available: https://www.denso-am.eu/pt/other/bomba-de-calor-a-co2-residencial. [Accessed 3 May 2022].

[76] Viessman, "Vitocal 252-A," [Online]. Available: https://www.viessmann.pt/pt/residencial/bombas-de-calor/bombas-de-calor-de-aragua-split/vitocal-252-a.html. [Accessed 10 June 2022].

[77] Mayekawa, "unimoAW," [Online]. Available: https://mayekawa.com.au/494/wp-content/uploads/2013/07/unimoAW_Flyer100713.pdf. [Accessed 10 June 2022].

[78] Automatic Heating, "REVERE CO_2 Air to Water Heat Pump," [Online]. Available: https://www.automaticheating.com.au/product/revere-co2-air-to-water-heat-pump/#tab-4-3. [Accessed 10 June 2022].

[79] Mayekawa, "Heat pumps," [Online]. Available: https://mayekawa.com/products/heat_pumps/. [Accessed 10 June 2022].

[80] Mitsubishi, "CO2 heat pump Q-TON series," [Online]. Available: https://www.mitsubishi-termal.it/wp-content/uploads/2018/02/Q-TON_en.pdf. [Accessed 10 June 2022].

[81] Sabroe, "SABROE HeatPAC heat pumps," [Online]. Available: https://www.johnsoncontrols.com/fi_fi/-/media/jci/be/finland/heat-pumps/files/bts_sabroe_heatpac_en_eu.pdf. [Accessed 10 June 2022].

[82] Z. Wang, M. B. Luther, M. Amirkhani, C. Liu and P. Horan, "State of the Art on Heat Pumps for Residential Buildings," *Buildings*, vol. 11, no. 8, p. 350, 2021.

[83] M. Marcic, "Long-term performance of central heat pumps in Slovenian homes," *Energy and Buildings*, vol. 36, pp. 185-193, 2004.

[84] G. Lorentzen, "Revival of carbon dioxide as a refrigerant," *International Journal of Refrigeration*, vol. 17, no. 5, pp. 292-301, January 1994.

[85] J.-y. Mu, J.-p. Chen and C. Zhi-jiu, "System design and analysis of the trans-critical carbon-dioxide automotive air-conditioning system," *Journal of Zhejiang University SCIENCE*, vol. 4, no. 3, pp. 305-308, 2003.

[86] J. Sarkar, "Review on Cycle Modifications of Transcritical CO2 Refrigeration and Heat Pump Systems," *Journal of Advanced Research in Mechanical Engineering*, vol. 1, no. 1, pp. 22-29, 2010.

[87] C. Aprea and A. Maiorino, "An experimental evaluation of the transcritical CO2 refrigerator performances using an internal heat exchanger," *International Journal of Refrigeration*, vol. 31, pp. 1006-1011, 2008.

[88] D. Boewe, C. Bullard, J. Yin and P. Hrnjak, "Contribution of Internal Heat Exchanger to Transcritical R-744 Cycle Performance," *HVAC&R Research*, vol. 7, no. 2, pp. 155-168, 2001.

[89] Y. Chen and J. Gu, "The optimum high pressure for CO2 transcritical refrigeration systems with internal heat exchangers," *International Journal of Refrigeration*, vol. 28, pp. 1238-1249, 2005.

[90] P. Neksa, J. Pettersen and G. Skaugen, "CO2 Refrigeration, Air Conditioning and Heat Pump Technology," SINTEF Energy Research, Norwegian University of Science and Technology (NTNU), Trondheim, Norway.

[91] D. Yang, Y. Li, J. Xie and J. Wang, "Research and application progress of transcritical CO2 refrigeration cycle system: a review," *International Journal of Low-Carbon Technologies,* vol. 17, pp. 245-256, 2021.

[92] E. A. Groll and J.-H. Kim, "Review of Recent Advances toward Transcritical CO2 Cycle Technology," *HVAC&R Research,* vol. 13, no. 3, pp. 499-520, 2007.

[93] S. Lecompte, E. Ntavou, B. Tchanche, G. Kosmadakis, A. Pillai, D. Manolakos and M. De Paepe, "Review of Experimental Research on Supercritical and Transcritical Thermodynamic Cycles Designed for Heat Recovery Application," *Applied Sciences,* vol. 9, no. 12, p. 2571, 2019.

[94] J. Ma, A. Mhanna, N. Juan, M. Brands and A. S. Fung, "Effects of Intercooling and Inter-Stage Heat Recovery on the Performance of Two-Stage Transcritical CO2 Cycles for Residential Heating Applications," *Energies,* vol. 12, no. 24, p. 4763, 2019.

[95] D. M. C. Santosa, "Optimisation of Gas Coolers for CO2 Refrigeration Application," *Ph.D. dissertation, Brunel University London,* 2015.

[96] C. Arpagaus, F. Bless, J. Schiffmann and S. S. Bertsch, "Multi-temperature heat pumps: A literature review," *International Journal of Refrigeration,* vol. 69, pp. 437-465, 2016.

[97] L. Zheng, J. Deng, Y. He and P. Jiang, "Dynamic model of a transcritical CO2 ejector expansion refrigeration system," *International Journal of Refrigeration,* vol. 60, pp. 247-260, 2015.

[98] A. N. U. Shan, "A Review of Trans-critical CO2 refrigeration cycle," in *International Conference on Industrial & Mechanical Engineering and Operations Management*, Dhaka, Bangladesh, December 2020.

[99] D. M. Robinson and E. A. Groll, "Efficiencies of transcritical CO2 cycles with and without an expansion turbine," *International Journal of Refrigeration,* vol. 27, no. 2, pp. 577-589, 1998.

[100] J. L. Yang, Y. T. Ma, M. X. Li and H. Q. Guan, "Exergy analysis of transcritical carbon dioxide refrigeration cycle with an expander," *Energy,* vol. 30, no. 7, pp. 1162-1175, 2005.

[101] T. Hua, M. Yitai, L. Minxia and W. Wei, "Study on expansion power recovery in CO2 trans-critical cycle," *Energy Conversion and Management,* vol. 51, pp. 2516-2522, 2010.

[102] I. Sarbu and C. Sebarchievici, Ground-Source Heat Pumps, Timisoara, Romania: Academic Press, 2016.

[103] J. Süβ and H. Kruse, "Efficiency of the indicated process of CO2-compressors," *International Journal of Refrigeration,* vol. 21, no. 3, pp. 194-2011, 1998.

[104] J. Fleming, "Carbon Dioxide as the Working Fluid in Heating and/or Cooling Systems," University of Strathclyde, Glasgow, Scotland, 2003.

[105] D. H. Robinson and P. J. Beaty, "Compressor Types, Classifications, and Applications," Texas A&M University, 1992.

[106] Tecnalia, "Detailed Design of the High Temperature Heat Pump Laboratory Prototype," Chester, Spain, 2019.

[107] SWEP, "Brazed plate heat exchangers," 2019. [Online]. Available: https://www.swep.net/technology/brazed-plate-heat-exchangers/. [Accessed 20 June 2022].

[108] H. Martin, "N6 Pressure Drop and Heat Transfer in Plate Heat Exchangers," in *VDI Heat Atlas*, Springer Science & Business Media, 2016, pp. 1515-1522.

[109] S. Yamaguchi, D. Kato, K. Saito and S. Kawai, "Development and validation of static simulation model for CO2 heat pump," *International Journal of Heat and Mass Transfer*, vol. 54, no. 9-10, pp. 1896-1906, 2011.

[110] I. L. Paniagua, Á. J. Álvaro, J. R. Martín, C. G. Fernández and R. N. Carlier, "Comparison of Transcritical CO2 and Conventional Refrigerant Heat Pump Water Heaters for Domestic Applications," *Energies*, vol. 12, no. 3, p. 479, 2019.

[111] F. Kasap, H. Acul, H. Canbaz and S. Erbil, "R744 (CO2) Refrigerant Cooling Systems, the Finned Tube R744 (CO2) Evaporator and Gas Cooler Design Principles," 16 05 2011. [Online]. Available: http://www.frigoristes.fr/static/telechargement/CO2/pdf_748.pdf. [Accessed 20 June 2022].

[112] A. Lalovs, "Optimizing a Small Ammonia Heat Pump with Accumulator Tank for Space and Hot Tap Water Heating," NTNU, 2015.

[113] Mayekawa, "Natural Refrigerant CO2 Heat Pump High Temperature Hot Water Unit," [Online]. Available: https://tica.pro/wp-content/uploads/2021/03/heat-pump-co2-english.pdf. [Accessed 20 June 2022].

[114] Emerson Climate, "Suction Line Accumulators," March 2014. [Online]. Available: https://climate.emerson.com/documents/a-as-suction-accumulators-pa-00307-en-2884336.pdf. [Accessed 1 July 2022].

[115] Parker, "Accumulators and Receivers, Catalog C-1," May 2016. [Online]. Available: https://sporlanonline.com/literature/misc/parker/Catalog%20C-1%20Accumulators%20and%20Receivers.pdf. [Accessed 25 May 2022].

[116] M. Zehnder, "Efficient Air-Water Heat Pumps for High Temperature Lift Residential Heating, including Oil Migration Aspects," *Ph.D. dissertation*, 2004.

[117] Castel Italian Technology, "Oil Separator," [Online]. Available: https://www.castel.it/wp-content/uploads/2021/07/Oil_Separators.pdf. [Accessed 25 May 2022].

[118] RACE SA, "Apontamentos Internos," 2022.

[119] G. Steinkoenig, "HVACR Tech Tip: How to Apply Filter-Driers on Heat Pumps for System Protection," Parker, 2021. [Online]. Available: https://blog.parker.com/site/usa/en-US/details-home-page/hvacr-tech-tip-how-to-apply-filter-driers-on-heat-pumps-for-system-protection-us. [Accessed 20 June 2022].

[120] Danfoss, "Filter driers and sight glasses," 2011. [Online]. Available: https://www.danfoss.com/en/service-and-support/case-stories/dcs/filter-driers-and-sight-glasses/. [Accessed 24 May 2022].

[121] Carly, "Check Valves," 2018. [Online]. Available: https://www.carly-sa.com/wp-content/uploads/2018/09/CARLY-DTEN-CRCY-P9.pdf. [Accessed 25 May 2022].

[122] Carly, "Filtering - Drying - Decontamination," [Online]. Available: https://www.carly-sa.com/family/filtration-deshydratation-decontamination/vcyl/. [Accessed 25 May 2022].

[123] Y. Dazhang, L. Jing, H. Zhebin and H. Xiuzhi, "Simulation and Analysis of fin-tube Evaporator for Carbon dioxide heat pump," in *International Conference on Energy and Environment Technology*, Shangai, China, 2009.

[124] J. Sarkar, S. Bhattacharyya and M. Gopal, "Optimization of a transcritical CO2 heat pump cycle for simultaneous cooling and heating applications," *International Journal of Refrigeration,* vol. 27, no. 8, pp. 830-838, 2004.

[125] X. Zhang, X. Fan, F. Wang and H. Shen, "Theoretical and experimental studies on optimum heat rejection pressure for a CO2 heat pump system," *Applied Thermal Engineering,* vol. 30, no. 16, pp. 2537-2544, 2010.

[126] B. C. Neto, S. Abreu, M. J. Gonçalves and B. Noni, "A Simulation Model for CO2 Solar-Assisted Heat Pumps," in *IEA SHC International Conference on Solar Heating and Cooling for Buildings and Industry*, Brazil, 2019.

[127] B. Palm, "Ammonia in low capacity refrigeration and heat pump systems," *International Journal of Refrigeration,* vol. 31, no. 4, pp. 709-715, June 2008.

[128] J. Stene, "Design and Application of Ammonia Heat Pump Systems for Heating and Cooling of Non-Residential Buildings," SINTEF Energy Research, Trondheim, Norway, January 2008.

[129] E. Granryd, Refrigerating engineering, Stockholm: Royal Institute of Technology, 2005.

[130] R. Mastrullo, A. W. Mauro, S. Tino and G. P. Vanoli, "A chart for predicting the possible advantage of adopting a suction/liquid heat exchanger in refrigerating system," *Applied Thermal Engineering*, vol. 27, no. 14-15, pp. 2443-2448, 2007.

[131] BITZER, "BITZER Software v6.17.8," 2022.

[132] Y. Hwang and R. Radermacher, "Development of Hermetic Carbon Dioxide Compressor," in *International Refrigeration and Air Conditioning Conference*, University of Maryland, 1998.

[133] Bitzer, "SÉRIE ECOLINE+ (TRANSCRÍTICO CO_2)," 2022. [Online]. Available: https://www.bitzer.de/pt/pt/compressores-alternativos/ecoline-transcritico/. [Accessed 10 May 2022].

[134] BITZER, "Oils for refrigerant R744 (CO2)," June 2021. [Online]. Available: https://www.bitzer.de/shared_media/html/kt-500/en-GB/26559348326559719 5.html. [Accessed 1 June 2022].

[135] J. Stene and M. J. Alonso, "Field Measurements - Heat Pump Systems in NZEB," SINTEF Academic Press and Norwegian University of Science and Technology , Trondheim, 2016.

[136] SWEP, "SSP G8," 2022.

[137] Danfoss, "Coolselector®2".

[138] Danfoss, "Electric regulating valve CCMT 4," [Online]. Available: https://store.danfoss.com/en/Climate-Solutions-for-cooling/Valves/Control-and-Regulating-Valves/Motor-Operated-Valves/Electric-regulating-valve%2C-CCMT-4/p/027H7201. [Accessed 1 June 2022].

[139] ESK Schultze, "ESK Schultze," [Online]. Available: https://www.esk-schultze.de/. [Accessed 30 May 2022].

[140] Temprite, "Product Selector," 2022. [Online]. Available: https://temprite.com/home/product-selector/.

[141] Temprite, "130 Series for CO2," [Online]. Available: https://temprite.com/products/coalescent-oil-separators/130series/#1512424177873-a59f2519-1096. [Accessed 30 May 2022].

[142] Carly Sa, "Drying, filtering and cleaning cores," June 2018. [Online]. Available: https://www.carly-sa.fr/wp-content/uploads/2018/09/CCY_DOCTEC_12_07_GB.pdf. [Accessed 30 May 2022].

[143] Carly Sa, "Replaceable core filter drier shells," June 2018. [Online]. Available: https://www.carly-sa.com/wp-content/uploads/2018/09/CARLY-DTEN-BCY-P14.pdf. [Accessed 30 May 2022].

[144] Carly Sa, "Check valves," February 2018. [Online]. Available: https://www.carly-sa.com/wp-content/uploads/2018/09/CARLY-DTEN-CRCY-P9.pdf. [Accessed 30 May 2022].

[145] Itomic, "Industrial-use Eco-Cute Y-Fame," [Online]. Available: https://www.itomic.co.jp/en-category/ecocute_y-frame_english/. [Accessed 25 June 2022].

[146] ATMOsphere, "What is low-charge ammonia?," Ammonia21, [Online]. Available: https://ammonia21.com/what-is-low-charge-ammonia/. [Accessed 30 June 2022].

[147] P. Fahlén, "Capacity control of heat pumps," *REHVA Journal,* 2012.

[148] M. Doninelli, "Produção de Água Quente por Acumulação," *Hidráulica*, vol. 19, 2002.

[149] L. Cecchinato, M. Corradi, E. Fornasieri and L. Zamboni, "Carbon dioxide as refrigerant for tap water heat pumps: A comparison with the traditional solution," *International Journal of Refrigeration,* vol. 28, no. 8, pp. 1250-1258, December 2005.

[150] J. C. Rømcke, "Performance Analysis of Prototype Residential CO2 Heat Pump," *Master's thesis in Energy and Environmental Engineering,* June 2020.

[151] A. Banks, C. Grist and J. Heller, "CO2 Heat Pump Water Heater Multifamily Retrofit: Elizabeth James House," Emerging Technologies, Seattle WA, May 2020.

[152] S. Dharkar, "CO2 HEAT PUMPS FOR COMMERCIAL BUILDING APPLICATIONS WITH SIMULTANEOUS HEATING AND COOLING DEMAND," 2015. [Online]. Available: https://docs.lib.purdue.edu/open_access_theses/1104. [Accessed 20 June 2022].

[153] ASHRAE, "Service Water Heating," in *ASHRAE Handbook - HVAC Applications*, 2003.

[154] IPU, "Simple one-stage CO2," February 2022. [Online]. Available: https://www.ipu.dk/products/simple-one-stage-co2/.

[155] K. Cleary, "Electrification 101," Resources for the Future, 5 December 2019. [Online]. Available: https://www.rff.org/publications/explainers/electrification-101/. [Accessed 17 March 2022].

[156] Danfoss, "Carbon dioxide (CO_2)," [Online]. Available: https://www.danfoss.com/en/about-danfoss/our-businesses/cooling/refrigerants-and-energy-efficiency/refrigerants-for-lowering-the-gwp/carbon-dioxide-co2/#/. [Accessed 2 April 2022].

[157] BITZER, "Transcritical CO2 applications," September 2020. [Online]. Available: https://www.bitzer.de/shared_media/html/a-540/en-GB/160684299161565835.html. [Accessed 6 April 2022].

[158] X. Liu, C. Liu, Z. Zhang, L. Chen and Y. Hou, "Experimental Study on the Performance of Water Source Trans-Critical CO2 Heat Pump Water Heater," *Energies,* vol. 10, no. 6, p. 810, 2017.

Appendices

A. Comparison with other refrigerants

Refrigerants	Category	Formula	Critical Temp.	Critical Pressure	Saturated Pressure	Liquid Density	Vapor Density	Lat. Heat of Vaporization	Thermal Conductivity of Liquid	Viscosity of Liquid	ODP Rel. R11	GWP_{100} Rel. CO_2	Toxicity and Flammability
-		-	°C	bar	bar	kg m^{-3}	kg m^{-3}	kJ kg^{-1}	W.m.k^{-1}	µPa.s		100 year	-
R290	HC	C_3H_8	96.7	42.5	5.51	521.8	11.98	367.5	0.105	121.8	0	0.072	A3
R600a	HC	C_4H_{10}	134.6	36.5	1.88	575	5.07	346	0.114	193.6	0	3	A3
R717	Inorganic	NH_3	132.3	113.3	5.16	631.7	4.12	1244	0.544	161.2	0	0	B2L
R744	Inorganic	CO_2	31.0	73.8	39.70	896	114.60	215	0.102	90.8	0	1	A1
R1234ze	HFO	$C_3F_4H_2$	109.4	36.3	2.61	1226	14.15	180.9	0.082	242	0	7	A2L
R22	HCFC	$CHClF_2$	96.1	49.9	5.84	1265	24.80	200.9	0.094	200.2	0.055	1760	A1
R245fa	HFC	$C_3H_3F_5$	154.0	36.5	0.66	1391	3.99	201.7	0.087	537.6	0	858	B1
R32	HFC	CH_2F_2	78.1	57.8	9.52	1038	25.89	307.3	0.141	147.4	0	677	A2L
R134a	HFC	CH_2FCF_3	101.0	40.6	0.66	1278	17.14	194.7	0.092	249.2	0	1300	A1
Objective		**-**	**High**	**Low**	**Low**	**Low**	**High**	**High**	**High**	**Low**	**Low**	**Low**	**Low**

Figure A.1: Properties of the most used refrigerants in heat pumps.

B. Other software results

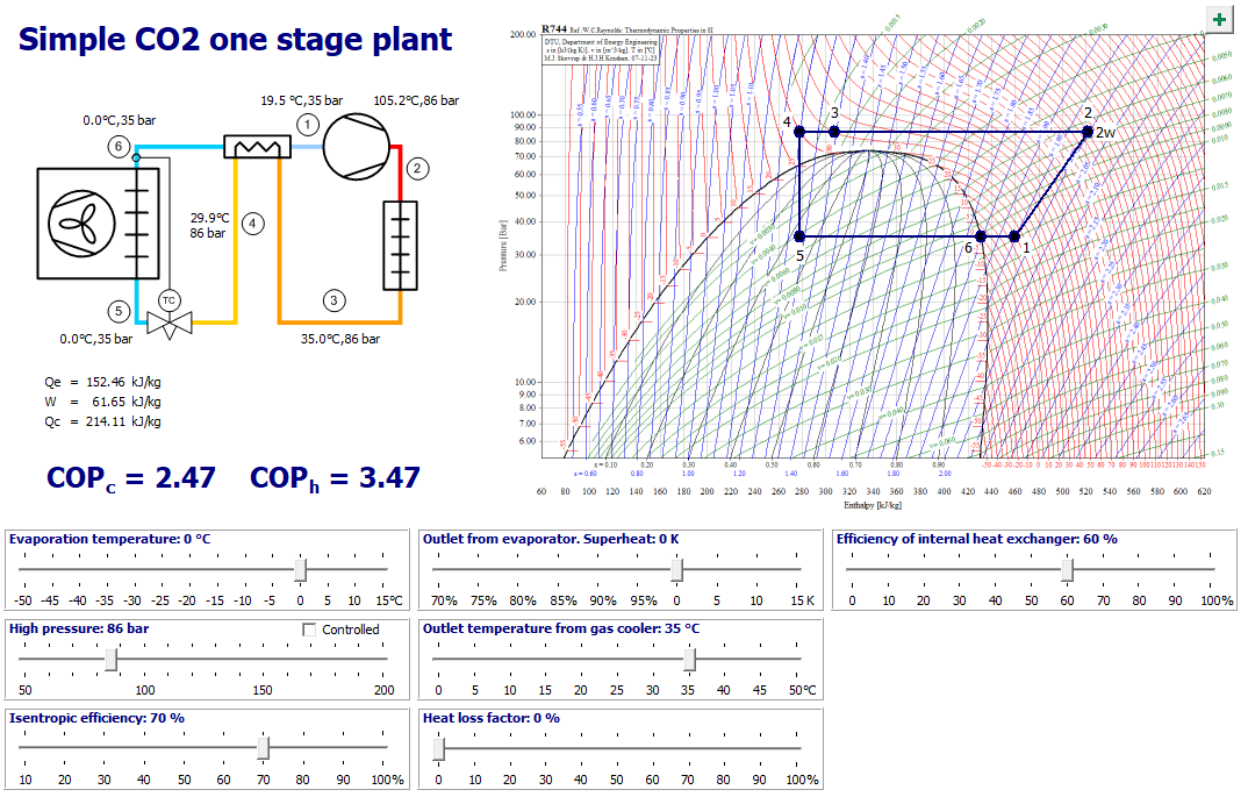
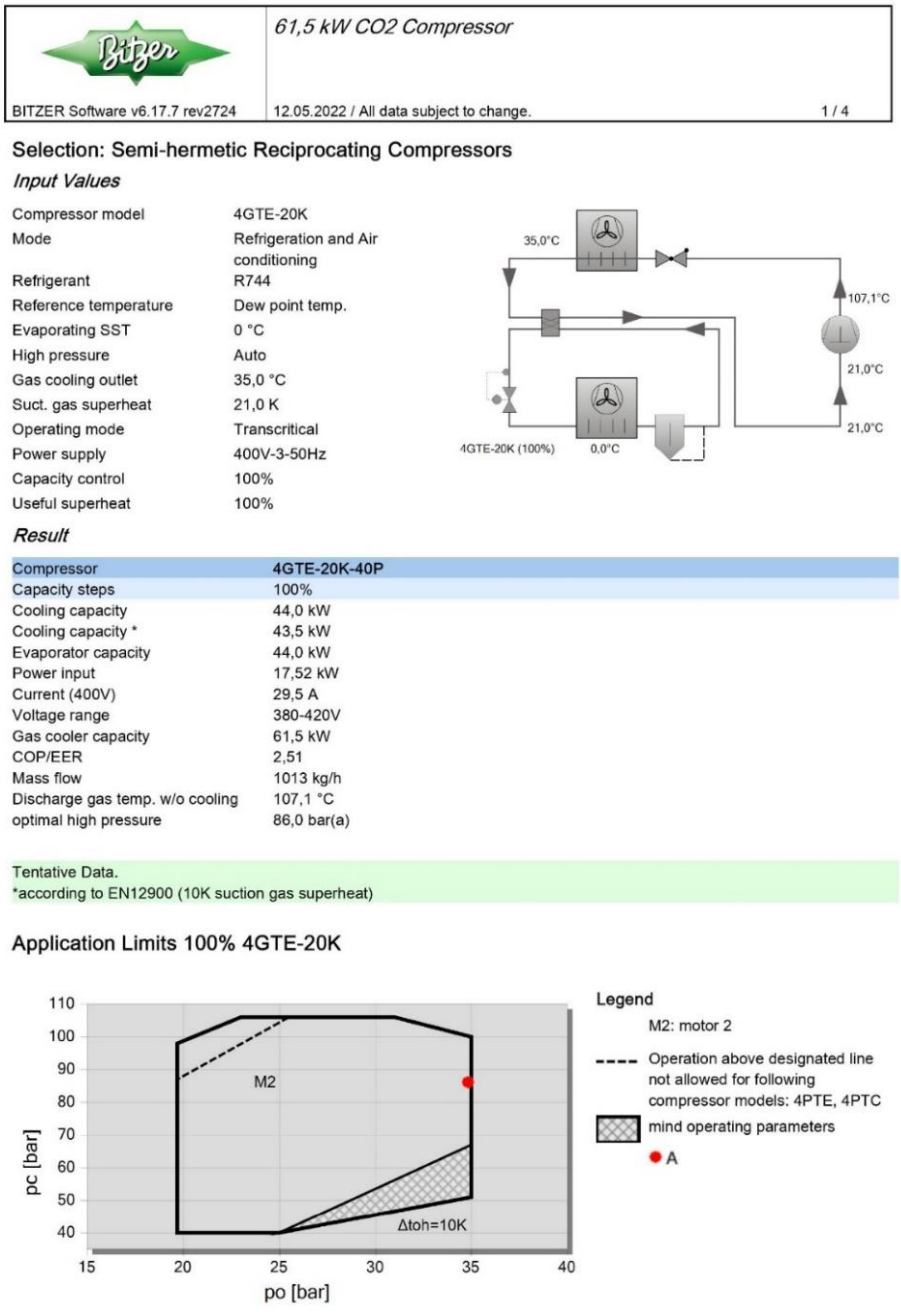


Figure B.1: Simple CO_2 one-stage plant software results [154].

C. Components full reports

This section serves as a complement to the selection of the components presented in Chapter 6. The component report allows a deeper understanding of the parameters used in each selection and the characteristics of the compressors, heat exchanger, expansion valves, and the remaining components.



61,5 kW CO2 Compressor

BITZER Software v6.17.7 rev2724 | 12.05.2022 / All data subject to change. | 1 / 4

Selection: Semi-hermetic Reciprocating Compressors

Input Values

Compressor model	4GTE-20K
Mode	Refrigeration and Air conditioning
Refrigerant	R744
Reference temperature	Dew point temp.
Evaporating SST	0 °C
High pressure	Auto
Gas cooling outlet	35,0 °C
Suct. gas superheat	21,0 K
Operating mode	Transcritical
Power supply	400V-3-50Hz
Capacity control	100%
Useful superheat	100%

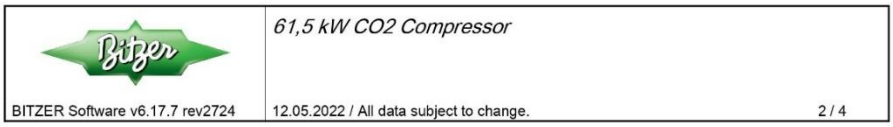
Result

Compressor	4GTE-20K-40P
Capacity steps	100%
Cooling capacity	44,0 kW
Cooling capacity *	43,5 kW
Evaporator capacity	44,0 kW
Power input	17,52 kW
Current (400V)	29,5 A
Voltage range	380-420V
Gas cooler capacity	61,5 kW
COP/EER	2,51
Mass flow	1013 kg/h
Discharge gas temp. w/o cooling	107,1 °C
optimal high pressure	86,0 bar(a)

Tentative Data.
*according to EN12900 (10K suction gas superheat)

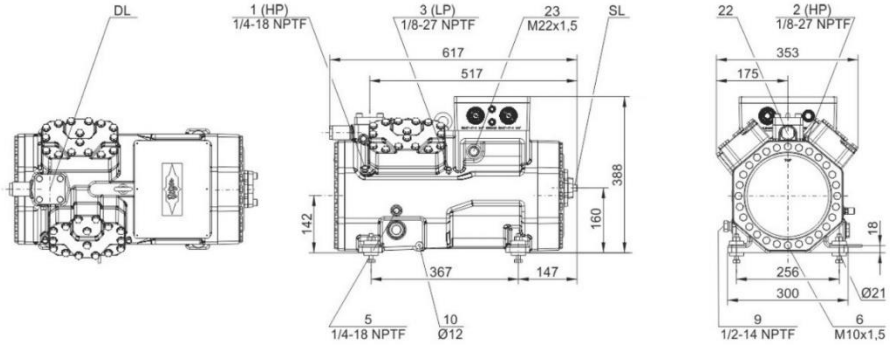
Application Limits 100% 4GTE-20K

Figure C.1: CO_2 BITZER compressor 4GTE-20K (page 1/2).



Technical Data: 4GTE-20K

Dimensions and Connections



Technical Data

Technical Data	
Displacement (1450 RPM 50Hz)	15,0 m3/h
Displacement (1750 RPM 60Hz)	18,1 m3/h
No. of cylinder x bore x stroke	4 x 38mm x 38mm
Weight	187 kg
Max. pressure (LP/HP)	100/160 bar
Connection suction line	28 mm - 1 1/8"
Connection discharge line	18 mm - 3/4"
Oil type R744 (CO2)	BSE85K (Standard), BSG68K (Option)
Motor data	
Motor version	2
Motor voltage (more on request)	380-420V PW-3-50Hz
Max operating current	36.2 A
Winding ratio	50/50
Starting current (Rotor locked)	97.0 A Y / 158.0 A YY
Max. Power input	20.7 kW
Extent of delivery (Standard)	
Motor protection	SE-B3(Standard), SE-B2(Option)
Enclosure class	IP65
Vibration dampers	Standard
Oil charge	2,60 dm³
Crankcase heater	0..140 W PTC (Standard)
Available Options	
Connection suction line	Option
Discharge shut-off valve	Option
Oil level monitoring	OLC-K1 (Option)
Sound measurement	
Sound power level (-10°C / 90bar)	80 dB(A) @ 60Hz
Sound pressure level @ 1m (-10°C / 90bar)	72 dB(A) @ 60Hz

Figure C.2: CO_2 BITZER compressor 4GTE-20K (page 2/2).

SWEP International AB
Box 105, Hjalmar Brantings väg 5
SE-261 22 Landskrona, Sweden
www.swep.net

SINGLE PHASE - RATING

SWEP SSP G8 2022.421.1.0

HEAT EXCHANGER: B4THx90/1P-NC-U (B4TH/1P-NC-U 4x3/4"&16)

Date: 23/05/2022

Art No: 19222-090

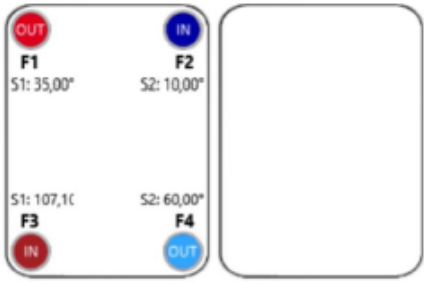
SSP Alias: B4TH

CONNECTION DATA

Port	NND	Denomination
F1	18	ISO-G 3/4" & SOLDER 16 (20)
F2	18	ISO-G 3/4" & SOLDER 16 (20)
F3	18	ISO-G 3/4" & SOLDER 16 (20)
F4	18	ISO-G 3/4" & SOLDER 16 (20)

CONNECTION LOCATION	Side 1 (S1)	Side 2 (S2)
Inlet	F3	F2
Outlet	F1	F4

PORT FLOW CONFIGURATION



F - Side P - Side

DUTY REQUIREMENTS		Side 1	Side 2
Fluid		R744 (Carbon Dioxide) (86,0 bar)	Water
Flow type		Counter-Current	
Circuit		Inner	Outer
Heat load	kW	61,46	
Inlet temperature	°C	107,10	10,00
Outlet temperature	°C	35,00	60,00
Flow rate	kg/s	0,2814	0,2942
Thermal length		2,066	1,433

PLATE HEAT EXCHANGER		Side 1	Side 2
Total heat transfer area	m²	1,06	
Heat flux	kW/m²	58,2	
Mean temperature difference	K	34,89	
O.H.T.C. (available/required)	W/m²,°C	3200/3160	
Pressure drop - total	kPa	17,0	7,46
- in ports	kPa	2,49	1,03
- inlet connections	kPa	0,000	0,000
- outlet connections	kPa	0,000	0,000
Port diameter (up/down)	mm	17,5/17,5	17,5/17,5
Number of channels per pass		44	45
Number of plates		90	
Oversurfacing	%	1	
Fouling factor	m²,°C/kW	0,003	
Reynolds number		8035	253,7
Port velocity (up/down)	m/s	3,10/3,10	1,24/1,24
Channel velocity	m/s	0,595	0,118
Shear stress	Pa	30,3	13,4
Average wall temperature	°C	42,62	41,70
Largest wall temperature difference	K	1,53	
Min./Max. wall temperature	°C	23,67/68,26	22,17/66,75

Figure C.3: CO_2 SWEP gas cooler B4THx90 (page 1/2).

SWEP International AB
Box 105, Hjalmar Brantings väg 5
SE-261 22 Landskrona, Sweden
www.swep.net

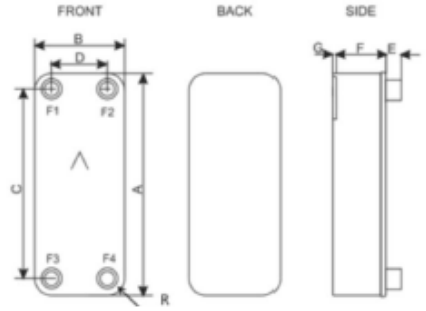
NOTES

! *For a desuperheater installation it is recommended to have the gas enter in the top of the BPHE, etiher in F1 or F2. The reason is to easily remove possible condensate from the BPHE*

PHYSICAL PROPERTIES		Side 1	Side 2
Reference temperature	°C	46,22	33,81
Dynamic viscosity	cP	0,0206	0,720
Dynamic viscosity - wall	cP	0,0244	0,633
Density	kg/m³	191,8	994,1
Heat capacity	kJ/kg,°C	1,774	4,178
Thermal conductivity	W/m,°C	0,02995	0,6233
Film coefficient	W/m²,°C	5460	10600

TOTALS		Side 1	Side 2
Total weight empty	kg	4,42	
Total weight filled	kg	4,95	
Hold-up volume (Inner Circuit)	dm³	0,41	
Hold-up volume (Outer Circuit)	dm³	0,42	
Port size F1/P1	mm	17,5	
Port size F2/P2	mm	17,5	
Port size F3/P3	mm	17,5	
Port size F4/P4	mm	17,5	
Carbon footprint	kg	31,07	
Plate material		AISI304 Stainless Steel	
Braze material		Copper	
Max operating pressure 20°C	bar(g)	140	140
Max operating pressure 225°C	bar(g)	117	117
Test pressure	bar(g)	201	201
Minimal/Maximal working temperature	°C	NaN/225	

DIMENSIONS



**This is a schematic sketch. For correct drawings please use the order drawing function or contact your SWEP representative.*

A	mm	194,5 ±2
B	mm	76,9 ±1
C	mm	154 ±1
D	mm	40 ±1
E	mm	20 ±1
F	mm	103,4
G	mm	4 ±1
R	mm	18

Disclaimer:
Data used in this calculation is subject to change without notice. SWEP strives to use "best practice" for the calculations leading to the above results. Calculation is intended to show thermal and hydraulic performance, no consideration has been taken to mechanical strength of the product. Product restrictions - such as pressure, temperatures and corrosion resistance- can be found in SWEP product sheets and other technical documentation. SWEP may have patents, trademarks, copyrights or other intellectual property rights covering subject matter in this document. Except as expressly provided in any written license agreement from SWEP, the furnishing of this document does not give you any license to these patents, trademarks, copyrights, or other intellectual property. To the maximum extent permitted by applicable law, the software, the calculations and the results are provided without warranties of any kind, whether express or implied. No advice or information obtained through use of the software (including information provided in the results), will create any warranty not expressly stated in the applicable license terms. Without limiting the foregoing, SWEP does not warrant that the content (including the calculations and the results) is accurate, reliable or correct. SWEP does not warrant that any system comprising heat exchanger and other components, installed on the basis of calculations in this software, will meet your requirements or function to your satisfaction or expectations.

Figure C.4: CO_2 SWEP gas cooler B4THx90 (page 2/2).

CABERO
HEAT EXCHANGER

Cliente		Atención	
Pais			
Proyecto		Numero de cotización	
Fecha consulta		Referencia	
Fecha	26/06/2022	Persona de contacto	
Version Sw	220609 [2CBEC8A28]	Contacto teléfonico	

CONDENSADOR REMOTO	**CO2-ACHSSD097C1x1-1.4-40-L D SFD3 (eb) EC**		Numero de pasos	**20**	
Capacidad requerida	**90,0**	kW	Temp. condensacion	**17,7**	°C
Capacidad efectiva	**106,4**	kW	Temp. condensacion	**20,0**	°C
Margen de seguridad	**18,2**	%	**Refrigerante (1)**	**R744**	
Caudal de aire	**28000,0**	m³/h	Temp. Gas caliente	**70**	°C
Velocidad del aire	**2,52**	m/s	Flujo de masas	**1567,04**	kg/h
Presión atmosferica/Altitud	**1013/0**	mbar/m	Coeff. De trans. De calor (*)	**16,9**	W/(m² K)
Entrada aire/Temp. salida	**5,0/15,7**	°C	Coeff. De trans. De calor (**)	**55,2**	W/(m² K)
Presión adicional externa del aire	**0**	Pa	Perdida de carga	**0,1/10**	K/kPa

Cant. de ventilador(es)	**1 (400V/3/50Hz) (eb) EC - Operación nominal (3)**		Rango de Temp. ventilador	**-25/60**	°C
Velocidad ventilador	**885**	RPM	Nivel de presión sonora (2)	**49**	dB(A)
Capacidad por motor/total	**2,1/2,1**	kW	A la distancia de	**10**	m
Intensidad por motor/ total	**3,2/3,2**	A	Nivel de poder sonoro	**80,4**	dB(A)
Cap. Servicio motor /total	**1,55/1,55**	kW	Clase de eficiencia energetica	**C**	
Construccion					
Carroceria	**FeZn (Casing)**		Aletas	**Aluminium**	
Barnizado	**Polvo cubierto RAL 9010**		Superficie	**225,9**	m²
Peso seco (4)	**362**	kg	Paso de aleta	**3**	mm
Presion operativa max.	**120**	bar	Tubos	**Stainless Steel**	
Longitud (L)	**1700**	mm	Volumen tubo	**51,0**	dm³
Amplitud (D)	**2240**	mm	Cabezales	**1 x 54x2,7 / 1 x 35x1,5**	
Altura (A)	**1565**	mm	Posición de los colectores	**Mismo lado**	
Nº suspensiones			Material cabezales	**Stainless Steel**	

(*) Considerar la Temp. del gas caliente
(**) Considerar solo la Temp. de condensacion

Nuestros terminos generales de ventas y entrega se aplican

La capacidad y la temperatura están de acuerdo con EN327, EN328 y EN1048, temperaturas de la tolerancia 0.2K
(1) grupo 1 fluido deacuerdo con la directiva 67/548/EWG
(2) Por usar el desarrollo el metodo acc. De EN 13487. Nota: tolerancia de emision sonora de los ventiladores + 2 dB
(3) El consumo de intensidad puede variar dependiendo de la Temp. del aire y de las variaciones del sistema de voltaje según la direccion VDE
Para los puntos de operación del ventilador (carga completa y parcial), se aplica el estándar del fabricante del ventilador según DIN 24166 clase 3.
Los datos son para el punto de operación. Solo los datos de sello de los ventiladores son relevantes para los fusibles de la planta. Esto se comunicará en el diagrama del circuito.
Solo a partir de los diagramas de circuitos confirmados son vinculantes.
(4) La dimension y el peso no son validos para todas las opciones posibles! Para el pedido por favor referirse al dibujo de conformidad

CABERO Wärmetauscher GmbH & Co. KG - Jesenwanger Strasse 50 - 82284 Grafrath, Germany
Phone: +49 8144 20 400-0 - Fax: +49 8144 20 400-900 - E-mail: info@cabero.de | www.cabero.de

Figure C.5: CABERO evaporator CO2-ACHS S (page 1/2).

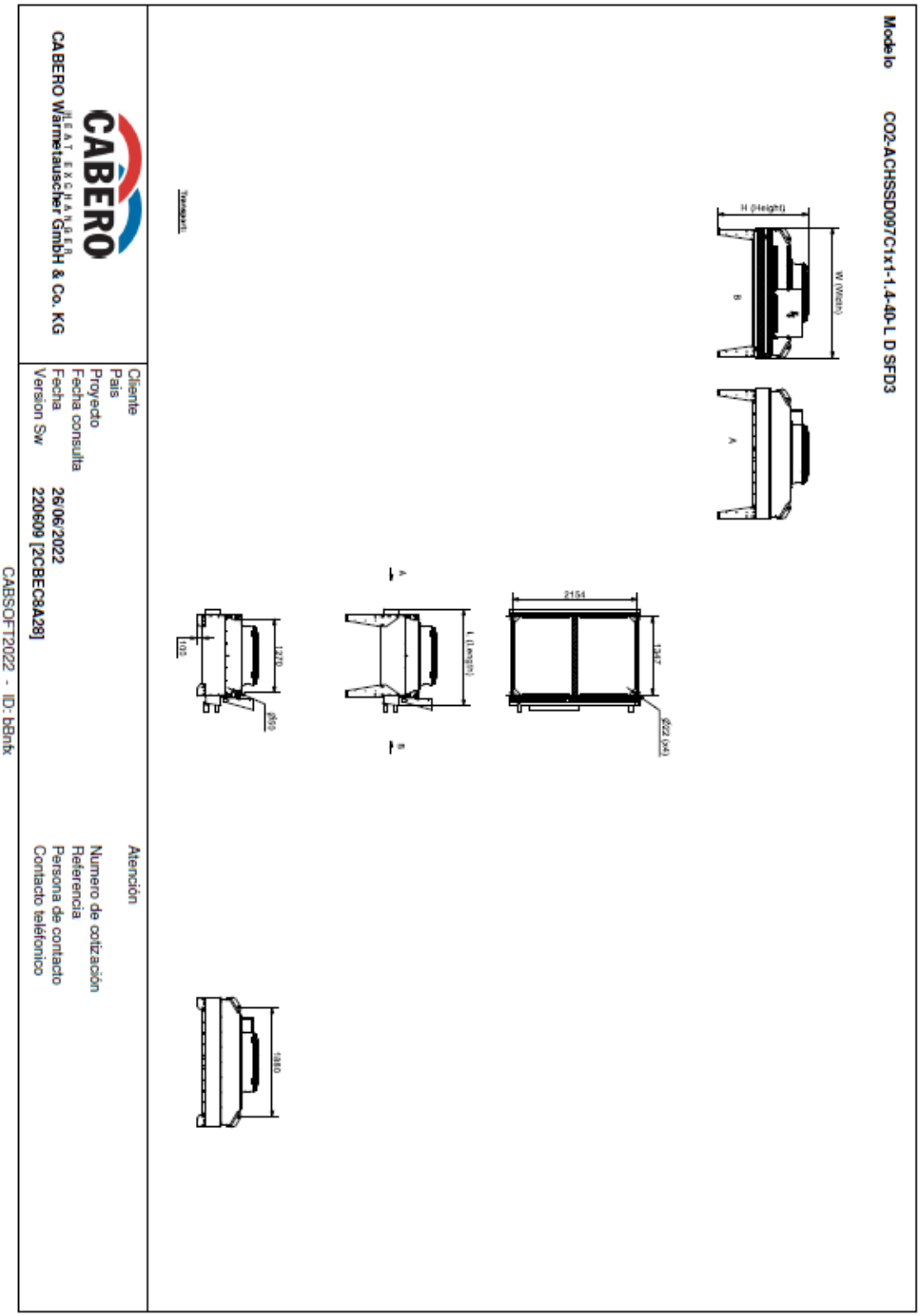


Figure C.6: CABERO evaporator CO2-ACHS S (page 2/2).

SWEP International AB
Box 105, Hjalmar Brantings väg 5
SE-261 22 Landskrona, Sweden
www.swep.net

SINGLE PHASE - RATING

SWEP SSP G8 2022.421.1.0

HEAT EXCHANGER: B18Lx30/1P-SC-U (B18L/1P-SC-U 4xS28.58&W35.1)

Date: 23/05/2022

Art No: 5000017-030

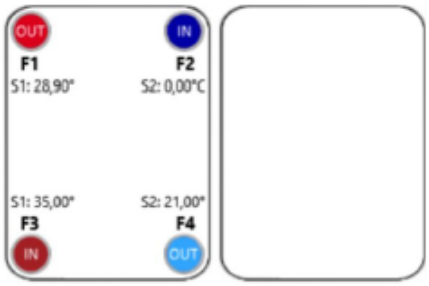
SSP Alias: B18L

CONNECTION DATA

Port	NND	Denomination
F1	27	SOLDER 28.58 & WELD 35.1 & G 1 1/2" A for UHP test (45)
F2	27	SOLDER 28.58 & WELD 35.1 & G 1 1/2" A for UHP test (45)
F3	27	SOLDER 28.58 & WELD 35.1 & G 1 1/2" A for UHP test (45)
F4	27	SOLDER 28.58 & WELD 35.1 & G 1 1/2" A for UHP test (45)

CONNECTION LOCATION	Side 1 (S1)	Side 2 (S2)
Inlet	F3	F2
Outlet	F1	F4

PORT FLOW CONFIGURATION



F - Side P - Side

DUTY REQUIREMENTS		Side 1	Side 2
Fluid		R744 (Carbon Dioxide) (86,0 bar)	R744 (Carbon Dioxide) (34,0 bar)
Flow type		Counter-Current	
Circuit		Inner	Outer
Heat load	kW	8,941	
Inlet temperature	°C	35,00	0,00
Outlet temperature	°C	28,90	21,00
Flow rate	kg/s	0,2814	0,2890
Thermal length		0,297	1,022

PLATE HEAT EXCHANGER		Side 1	Side 2
Total heat transfer area	m²	1,15	
Heat flux	kW/m²	7,79	
Mean temperature difference	K	20,56	
O.H.T.C. (available/required)	W/m²,°C	711/375	
Pressure drop - total	kPa	1,47	9,83
- in ports	kPa	0,271	2,33
- inlet connections	kPa	5,14e-3	0,0362
- outlet connections	kPa	4,75e-3	0,0483
Port diameter (up/down)	mm	24,0/24,0	24,0/24,0
Number of channels per pass		14	15
Number of plates		30	
Oversurfacing	%	90	
Fouling factor	m²,°C/kW	1,263	
Reynolds number		6494	22790
Port velocity (up/down)	m/s	0,907/0,907	7,52/7,52
Channel velocity	m/s	0,170	1,36
Shear stress	Pa	2,72	16,9
Average wall temperature	°C	26,64	26,16
Largest wall temperature difference	K	0,64	
Min./Max. wall temperature	°C	19,79/31,47	19,15/31,15

Figure C.7: CO_2 SWEP IHX B18Lx30 (page 1/2).

SWEP International AB
Box 105, Hjalmar Brantings väg 5
SE-261 22 Landskrona, Sweden
www.swep.net

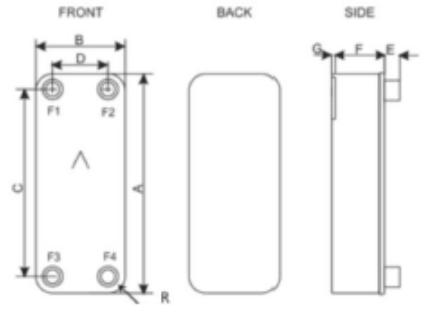
NOTES

! *For a desuperheater installation it is recommended to have the gas enter in the top of the BPHE, etiher in F1 or F2. The reason is to easily remove possible condensate from the BPHE*

PHYSICAL PROPERTIES		Side 1	Side 2
Reference temperature	°C	32,32	9,17
Dynamic viscosity	cP	0,0557	0,0151
Dynamic viscosity - wall	cP	0,0663	0,0157
Density	kg/m³	698,2	84,11
Heat capacity	kJ/kg,°C	4,918	1,447
Thermal conductivity	W/m,°C	0,07736	0,01897
Film coefficient	W/m²,°C	2610	1010

TOTALS		Side 1	Side 2
Total weight empty	kg	12,956	
Total weight filled	kg	13,586	
Hold-up volume (Inner Circuit)	dm³	0,81	
Hold-up volume (Outer Circuit)	dm³	0,87	
Port size F1/P1	mm	24	
Port size F2/P2	mm	24	
Port size F3/P3	mm	24	
Port size F4/P4	mm	24	
Carbon footprint	kg	81,23	
Plate material		AISI316 Stainless Steel	
Braze material		Copper	
Max operating pressure 20°C	bar(g)	140	107
Max operating pressure 225°C	bar(g)	117	89
Test pressure	bar(g)	201	154
Minimal/Maximal working temperature	°C	NaN/225	

DIMENSIONS



A	mm	377 ±2
B	mm	119,5 ±1
C	mm	329 ±1
D	mm	72 ±1
E	mm	45 (opt. 81) ±1
F	mm	72
G	mm	2 ±1
R	mm	23,5

**This is a schematic sketch. For correct drawings please use the order drawing function or contact your SWEP representative.*

Disclaimer:
Data used in this calculation is subject to change without notice. SWEP strives to use "best practice" for the calculations leading to the above results. Calculation is intended to show thermal and hydraulic performance, no consideration has been taken to mechanical strength of the product. Product restrictions - such as pressure, temperatures and corrosion resistance- can be found in SWEP product sheets and other technical documentation. SWEP may have patents, trademarks, copyrights or other intellectual property rights covering subject matter in this document. Except as expressly provided in any written license agreement from SWEP, the furnishing of this document does not give you any license to these patents, trademarks, copyrights, or other intellectual property. To the maximum extent permitted by applicable law, the software, the calculations and the results are provided without warranties of any kind, whether express or implied. No advice or information obtained through use of the software (including information provided in the results), will create any warranty not expressly stated in the applicable license terms. Without limiting the foregoing, SWEP does not warrant that the content (including the calculations and the results) is accurate, reliable or correct. SWEP does not warrant that any system comprising heat exchanger and other components, installed on the basis of calculations in this software, will meet your requirements or function to your satisfaction or expectations.

Figure C.8: CO_2 SWEP IHX B18Lx30 (page 2/2).

Coolselector2

Project information

Project name:	
Comments:	
Created by:	
Coolselector2 version:	4.8.2. Database: 86
Printed:	Tuesday, July 5, 2022
Preferences used:	All applications

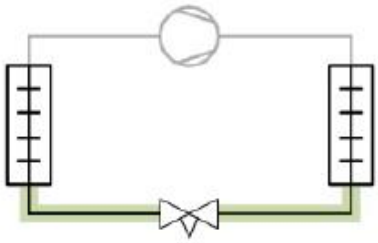
Electronic expansion valve: CO2 EEV

Operating conditions

Refrigerant:	R744		Heating capacity:	61500	W
Cooling capacity:	45230	W	Mass flow in line:	0.2266	kg/s
Evaporating temperature:	273	K	Condensing temperature:	303	K
Evaporating pressure:	3471000	Pa	Condensing pressure:	7200000	Pa
Useful superheat:	21.0	K	Subcooling:	6.0	K
Additional superheat:	21.0	K	Additional subcooling:	0	K
Discharge temperature:	380	K			

System and line: *Dry expansion system. Liquid line*

Selection criteria: *Load: 80 %. Distributor pressure drop: 0 Pa*



Selection: CCMT 4



Type	CCMT 2	CCMT 4	CCMT 8	CCMT 16
NS	15	15	15	25

Page 1/4

Figure C.9: CO_2 EEV Danfoss CCMT 4 (page 1/2).

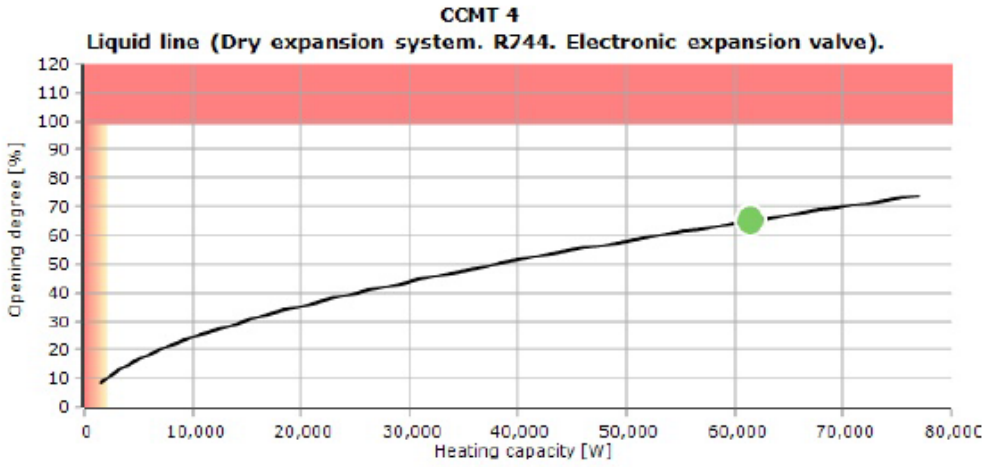
Coolselector2

Max. capacity [W]	36280	96090	171100	341800
Min. capacity [W]	570	1509	2683	16240
Load [%]	125	47	26	13
DP [Pa]	3729000	3729000	3729000	3729000
Velocity, in [m/s]	1.35	1.35	1.35	0.46

Selected code number for CCMT 4

CCMT 4. Electric regulating valve: *027H7201*

Performance curve



Page 2/4

Figure C.10: CO_2 EEV Danfoss CCMT 4 (page 2/2).

5/16/22, 10:54 PM Model 135A: Accessible - Temprite



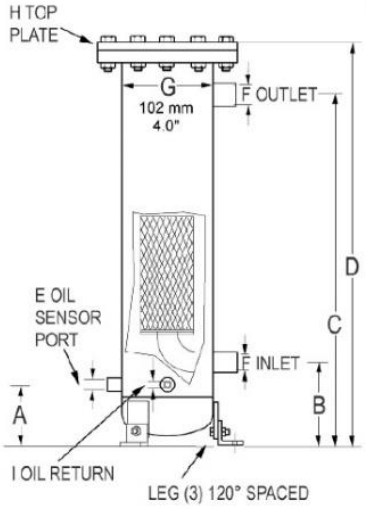
Model 135A: Accessible

Product Info Technology

Compatible with traditional refrigerants, new blends and natural refrigerants.*

PRINT





* Traditional refrigerants such as R-22 and blends like R-404a; new blends such as R-427a and R-448a; and natural refrigerants such as ammonia (NH_3) and CO_2.

Connection options available: ODS, BW or MPT.

Connection options: ODS/Butt Weld/MPT Connections

Metric sizes also available: contact us.

Part #	Model #	Max. Working Press.	A Dim.	B Dim.	C Dim.	D Dim.	E Dim.	F Dim.	G Dim.	H Dim.	I Dim.
			Sensor/Oil Loc.	Inlet Loc.	Outlet Loc.	Height	Sensor	Inlet/Outlet	Dia.	Dia.	Oil Return
013501350	135A	140 bar 2030 PSI	118 mm 4.6"	152 mm 6"	433 mm 17.1"	545 mm 21.4"	3/4" FPT*	3/4" MPT*	102 mm 4.0"	176 mm 6.9"	1/4" FP

https://temprite.com/products/coalescent-oil-separators/130series/model-135a-accessible/ 1/2

Figure C.11: CO_2 oil separator Temprite 135A (page 1/2).

013501351	135A	140 bar 2030 PSI	118 mm 4.6″	152 mm 6″	433 mm 17.1″	545 mm 21.4″	3/4″ FPT*	3/4″ BW*	102 mm 4.0″	176 mm 6.9″	1/4″ FPT*
013504352	135A	140 bar 2030 PSI	118 mm 4.6″	152 mm 6″	433 mm 17.1″	545 mm 21.4″	3/4″ FPT*	7/8″ ODS*	102 mm 4.0″	176 mm 6.9″	1/4″ FPT*

*FPT=Female Pipe Thread, MPT=Male Pipe Thread, BW=Butt Weld, ODS = Outside Diameter Solder

THE CONNECTIONS ON THE OIL SEPARATOR MUST BE THE SAME SIZE AS (OR LARGER THAN) THE DISCHARGE LINE SIZE.

Temprite's 920 & 920R Series of products are suitable for CO_2 subcritical applications up to 44.8 bar (650 PSI) and ammonia (NH_3).



Choose the right Temprite conventional or coalescent oil separator using the Product Selector. Fill in the blanks with your system specifications and the Selector does the work. Selector results include details on the specifications input, allowing you to save and print your work. Temprite's Quick Sizing Charts can be printed and downloaded.

Resource Documents:

Installation Instructions for Model 131 and all 300 Series Hermetic Coalescent Oil Separators
Installation Instructions for 133A, 135A, 137A, 138A, 139A Accessible Coalescent Oil Separators
Standard Filter Replacement Instructions for 130 Series Accessible Coalescent Oil Separators
Clean-Up® Filter Replacement Instructions for 130 Series
130 Series, 920 and 920R Series Filter Access Clearance Chart
Torque Specifications
Oil Pre-charge
Installation Instructions for All Oil Reservoirs
Sizing Chart: 130 Series for Natural Refrigerants: Transcritical & Subcritical CO_2, kW
Sizing Chart: 130 Series for Natural Refrigerants: Transcritical & Subcritical CO_2, Tons
Sizing Chart: 130 Series for Natural Refrigerants: Transcritical CO_2 Gas Cooler Outlet, Tons & kW

Temprite Customer or Technical Support: Contact Us.

Contact
Privacy & Legal
Site Map

Product Catalog (PDF)
Emerson Report (PDF)

Product Selector
Savings Calculator

This site is protected by reCAPTCHA and the Google Privacy Policy and Terms of Service apply.

Copyright Temprite 2022 All Rights Reserved

Figure C.12: CO_2 oil separator Temprite 135A (page 2/2).

BITZER Software v6.17.8 rev2725

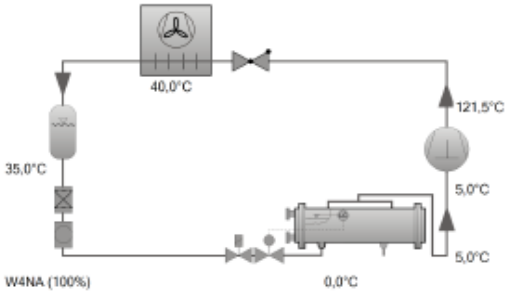
NH3 Compressor

05.07.2022 / All data subject to change. 1 / 1

Selection: Open-Type Reciprocating Compressors

Input Values

Compressor model	W4NA-K
Refrigerant	R717
Reference temperature	Dew point temp.
Evaporating SST	0 °C
Condensing SDT	40,0 °C
Liq. subc. (in condenser)	5,00 K
Suct. gas superheat	5,00 K
Useful superheat	100%
Motor speed	1450 /min
Drive	Coupling (1:1)
Capacity control	100%



Result

Compressor	W4NA
Capacity steps	100%
Cooling capacity	47,8 kW
Cooling capacity *	46,7 kW
Evaporator capacity	47,8 kW
Shaft power	10,57 kW
Condenser capacity	58,4 kW
COP/EER	4,52
COP/EER *	4,42
Mass flow	155,1 kg/h
Operating mode	Coupling (1:1)
Compr. speed	1450 /min
Recommended driving motor	15,00 kW
Discharge gas temp. w/o cooling	121,5 °C

Starting point for motor selection see T. Data/ Notes
*According to EN12900 (5K suction gas superheat, 0K liquid subcooling)

Application Limits Standard

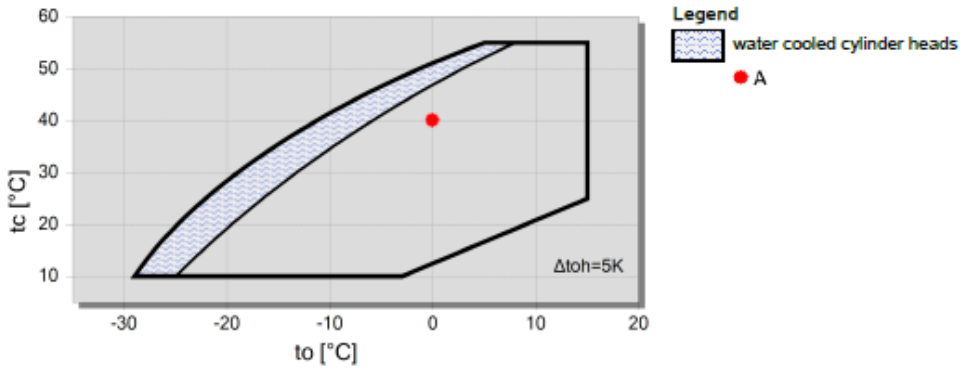
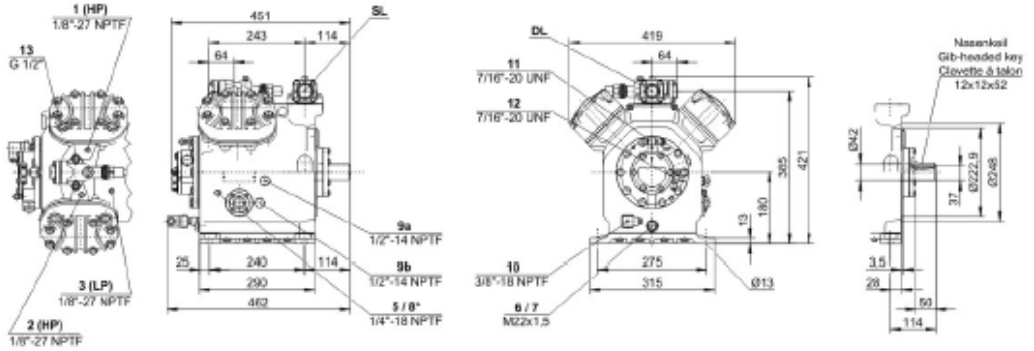


Figure C.13: NH_3 compressor Bitzer W4NA-K (page 1/2).

BITZER Software v6.17.8 rev2725 | 05.07.2022 / All data subject to change. | 2 / 4

Technical Data: W4NA-K

Dimensions and Connections



Technical Data

Technical Data	
Displacement (1450 RPM 50Hz)	56,1 m3/h
Displacement (1750 RPM 60Hz)	67,7 m3/h
No. of cylinder x bore x stroke	4 x 60 mm x 57 mm
Allowed speed range	750 .. 1750 1/min
Weight	77 kg
Max. pressure (LP/HP)	19 / 25 bar
Connection suction line	NW 32
Connection discharge line	NW 25
Oil type NH3	Reniso KC68 (Standard)
Extent of delivery (Standard)	
Oil charge	4,0 dm3
Protective charge	Standard
Suction shut-off valve	Standard
Discharge shut-off valve	Standard
Water-cooled cylinder heads	Standard
Available Options	
Coupling (..-K) w. A/C + medium	KK411 [<11kW] / KK420 [<22kW] (Option)
Coupling (..-K) w. low temp.	KK415 [<7.5kW] / KK425 [<22kW] (Option)
Coupling housing	Option
Motor pulley (..-S)	190, 210, 230 mm (Option)
V-belts	3 x SPA (Option)
Discharge gas temperature sensor	Option (incl. INT69VS)
Start unloading	Option
Connection cooling water	R 1/2"
Capacity control	100-50% (Option)
Oil service valve	Option
Crankcase heater	100 W (Option)
Oil pressure monitoring	MP55A (Option)

Figure C.14: NH_3 compressor BITZER W4NA-K (page 2/2).

SWEP International AB
Box 105, Hjalmar Brantings väg 5
SE-261 22 Landskrona, Sweden
www.swep.net

CONDENSER - RATING

SWEP SSP G8 2022.620.1.0

HEAT EXCHANGER: B10TSHx40/1P-SPS-S (B10TSH/1P-SPS-S 4x1"&22U)

Date: 22/06/2022

Art No: 17314-040

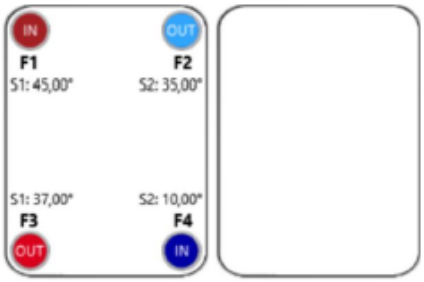
SSP Alias: B10TS All-Stainless

CONNECTION DATA

Port	NND	Denomination
F1	27	ISO-G 1" A&SOLDER 22U (20)
F2	27	ISO-G 1" A&SOLDER 22U (20)
F3	27	ISO-G 1" A&SOLDER 22U (20)
F4	27	ISO-G 1" A&SOLDER 22U (20)

CONNECTION LOCATION	Side 1 (S1)	Side 2 (S2)
Inlet	F1	F4
Outlet	F3	F2

PORT FLOW CONFIGURATION



F - Side P - Side

CONNECTIONS NOTES

F3: Outlet connection velocity lower than the recommended value of 0.5-2 m/sec

DUTY REQUIREMENTS		Side 1		Side 2
Fluid		R717 (Ammonia)		Water
Flow type			Counter-Current	
Circuit		Inner		Outer
Heat load	kW		48,77	
Inlet vapor quality		1,000		
Outlet vapor quality		0,000		
Inlet temperature	°C	45,00		10,00
Condensation temperature (dew)	°C	40,00		
Subcooling	K	3,00		
Outlet temperature	°C	37,00		35,00
Flow rate	kg/s	0,04310		0,4664
Fluid condensed	kg/s	0,04310		

PLATE HEAT EXCHANGER		Side 1		Side 2
Total heat transfer area	m²		1,18	
Heat flux	kW/m²		41,4	
Mean temperature difference	K		14,76	
O.H.T.C. (available/required)	W/m²,°C		3310/2800	
Pressure drop - total	kPa	0,536		2,60
- in ports (Inlet/Outlet)	kPa	-0,216/9,61e-3		0,513
- inlet connections	kPa	0,0940		0,129
- outlet connections	kPa	1,46e-3		0,101
Operating pressure (outlet)	kPa	1560		
Number of channels per pass		19		20
Number of plates			40	
Oversurfacing	%		18	
Fouling factor	m²,°C/kW		0,055	
Port diameter (up/down)	mm	24,0/24,0		24,0/24,0
Recommended inlet connection diameter	mm	13,5 - 30,2		
Recommended outlet connection diameter	mm	6,88 - 13,8		

Figure C.15: NH_3 condenser SWEP B10TSHx40 (page 1/3).

SWEP
A DOVER COMPANY

SWEP International AB
Box 105, Hjalmar Brantings väg 5
SE-261 22 Landskrona, Sweden
www.swep.net

PLATE HEAT EXCHANGER		Side 1		Side 2
Reynolds number				437,1
Inlet Port velocity	m/s	7,92		1,03
Channel velocity	m/s	0,834		0,103
Shear stress	Pa			7,63
Largest wall temperature difference	K		1,65	
Min./Max. wall temperature	°C	17,92/38,14		17,10/37,74

NOTES

! *Very high heat flux not experimentally certified (41,40 kW/m²).*
! *Secondary side port pressure drop is high in relation to total pressure drop. This could cause secondary side maldistribution*
i *Condenser performance prediction does not use two phase correction factors.*

PHYSICAL PROPERTIES		Side 1	Side 2
Reference temperature	°C	40,01	22,49
Liquid • Dynamic viscosity	cP	0,110	0,944
• Density	kg/m³	579,6	997,6
• Heat capacity	kJ/kg,°C	4,933	4,181
• Thermal conductivity	W/m,°C	0,4361	0,6028
Vapor • Dynamic viscosity	cP	0,0104	
• Density	kg/m³	12,03	
• Heat capacity	kJ/kg,°C	3,518	
• Thermal conductivity	W/m,°C	0,03093	
• Latent heat	kJ/kg	1100	
Film coefficient	W/m²,°C	9610	6460

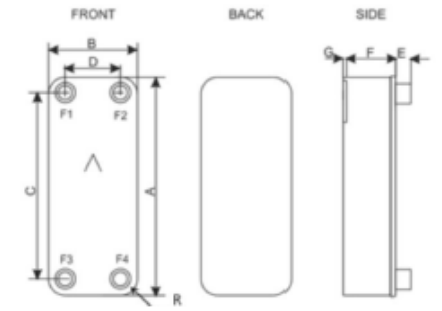
TOTALS		Side 1		Side 2
Total weight	kg		6,08	
Hold-up volume (Inner Circuit)	dm³		1,16	
Estimated refrigerant charge	kg		0,09	
Hold-up volume (Outer Circuit)	dm³		1,22	
Port size F1/P1	mm		24	
Port size F2/P2	mm		24	
Port size F3/P3	mm		24	
Port size F4/P4	mm		24	
Carbon footprint	kg		42,71	
Plate material			AISI316 Stainless Steel	
Braze material			Stainless Steel	
Max operating pressure 20°C	bar(g)	37		37
Max operating pressure 225°C	bar(g)	23		23
Test pressure	bar(g)	53		53
Minimal/Maximal working temperature	°C		-196/350	

DIMENSIONS

Figure C.16: NH_3 condenser SWEP B10TSHx40 (page 2/3).

SWEP International AB
Box 105, Hjalmar Brantings väg 5
SE-261 22 Landskrona, Sweden
www.swep.net

DIMENSIONS



A	mm	289 ±2
B	mm	119 ±1
C	mm	243 ±1
D	mm	72 ±1
E	mm	20 (opt. 27) ±1
F	mm	99,6
G	mm	6 ±1
R	mm	23

**This is a schematic sketch. For correct drawings please use the order drawing function or contact your SWEP representative.*

Disclaimer:
Data used in this calculation is subject to change without notice. SWEP strives to use "best practice" for the calculations leading to the above results. Calculation is intended to show thermal and hydraulic performance, no consideration has been taken to mechanical strength of the product. Product restrictions - such as pressure, temperatures and corrosion resistance- can be found in SWEP product sheets and other technical documentation. SWEP may have patents, trademarks, copyrights or other intellectual property rights covering subject matter in this document. Except as expressly provided in any written license agreement from SWEP, the furnishing of this document does not give you any license to these patents, trademarks, copyrights, or other intellectual property. To the maximum extent permitted by applicable law, the software, the calculations and the results are provided without warranties of any kind, whether express or implied. No advice or information obtained through use of the software (including information provided in the results), will create any warranty not expressly stated in the applicable license terms. Without limiting the foregoing, SWEP does not warrant that the content (including the calculations and the results) is accurate, reliable or correct. SWEP does not warrant that any system comprising heat exchanger and other components, installed on the basis of calculations in this software, will meet your requirements or function to your satisfaction or expectations.

Figure C.17: NH_3 condenser SWEP B10TSHx40 (page 3/3).



SWEP International AB
Box 105, Hjalmar Brantings väg 5
SE-261 22 Landskrona, Sweden
www.swep.net

SINGLE PHASE - DESIGN
HEAT EXCHANGER: B5THx42/1P

SWEP SSP G8 2022.629.1.0
Date: 06/07/2022

SSP Alias: B5T All-Stainless

DUTY REQUIREMENTS		Side 1	Side 2
Fluid		R717 (Ammonia) (15.5 bar)	Water
Flow type		Counter-Current	
Circuit		Outer	Inner
Heat load	kW	9.196	
Inlet temperature	°C	**121.50**	**35.00**
Outlet temperature	°C	**45.00**	**60.00**
Flow rate	kg/s | l/min	**0.04310**	5.337
Pressure drop (Design PD)	kPa	4.02 **(20.00)**	0.221 **(20.00)**
Thermal length		2.698	0.882

PLATE HEAT EXCHANGER		Side 1	Side 2
Total heat transfer area	m²	0.480	
Heat flux	kW/m²	19.2	
Mean temperature difference	K	28.35	
O.H.T.C. (available/required)	W/m²,°C	721/734	
Pressure drop - total*	kPa	4.02	0.221
- in ports	kPa	2.35	0.0962
Port diameter (up/down)	mm	16.0/16.0	16.0/16.0
Number of channels per pass		21	20
Number of plates		42	
Oversurfacing	%	0	
Fouling factor	m²,°C/kW	-0.023	
Reynolds number		4698	209.0
Port velocity (up/down)	m/s	21.3/21.3	0.443/0.443
Channel velocity	m/s	1.44	0.0305
Shear stress	Pa	8.69	0.649
Average wall temperature	°C	49.14	48.84
Largest wall temperature difference	K	0.68	
Min./Max. wall temperature	°C	37.98/70.75	37.86/70.07

**Excluding pressure drop in connections.*

NOTES

! *For a desuperheater installation it is recommended to have the gas enter in the top of the BPHE, etiher in F1 or F2. The reason is to easily remove possible condensate from the BPHE*

PHYSICAL PROPERTIES		Side 1	Side 2
Reference temperature	°C	79.00	46.89
Dynamic viscosity	cP	0.0121	0.571
Dynamic viscosity - wall	cP	0.0107	0.558
Density	kg/m³	9.755	989.2
Heat capacity	kJ/kg,°C	2.725	4.180
Thermal conductivity	W/m,°C	0.03492	0.6405
Film coefficient	W/m²,°C	904	3790

TOTALS		Side 1	Side 2
Total weight empty (no connections)*	kg	2.28 - 2.72	
Total weight filled (no connections)*	kg	2.78 - 3.22	
Hold-up volume (Inner Circuit)	dm³	0.48	
Hold-up volume (Outer Circuit)	dm³	0.5	



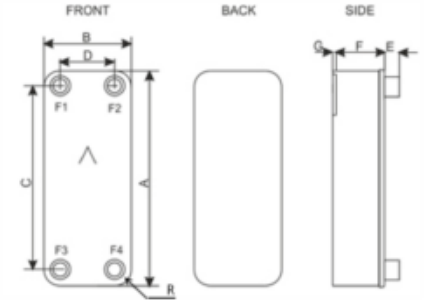
Figure C.18: NH_3 desuperheater SWEP B5THx18 (page 1/2).

SWEP International AB
Box 105, Hjalmar Brantings väg 5
SE-261 22 Landskrona, Sweden
www.swep.net

TOTALS		Side 1	Side 2
Port size F1/P1	mm		16
Port size F2/P2	mm		16
Port size F3/P3	mm		16
Port size F4/P4	mm		16
Carbon footprint	kg		16.47

*Weight depends on the selected product.

DIMENSIONS



*This is a schematic sketch. For correct drawings please use the order drawing function or contact your SWEP representative.

A*	mm	192.8 - 193 ±2
B*	mm	75.4 - 76 ±2
C	mm	154 ±1
D	mm	40 ±1
E	mm	20 ±1
F*	mm	98.08 - 102.08 ±3%
G*	mm	6.2 - 7.4 ±2.1
R*	mm	17.7 - 18

*Dimensions depend on the selected product.

Disclaimer:
Data used in this calculation is subject to change without notice. SWEP strives to use "best practice" for the calculations leading to the above results. Calculation is intended to show thermal and hydraulic performance, no consideration has been taken to mechanical strength of the product. Product restrictions - such as pressure, temperatures and corrosion resistance- can be found in SWEP product sheets and other technical documentation. SWEP may have patents, trademarks, copyrights or other intellectual property rights covering subject matter in this document. Except as expressly provided in any written license agreement from SWEP, the furnishing of this document does not give you any license to these patents, trademarks, copyrights, or other intellectual property. To the maximum extent permitted by applicable law, the software, the calculations and the results are provided without warranties of any kind, whether express or implied. No advice or information obtained through use of the software (including information provided in the results), will create any warranty not expressly stated in the applicable license terms. Without limiting the foregoing, SWEP does not warrant that the content (including the calculations and the results) is accurate, reliable or correct. SWEP does not warrant that any system comprising heat exchanger and other components, installed on the basis of calculations in this software, will meet your requirements or function to your satisfaction or expectations.

Figure C.19: NH_3 desuperheater SWEP B5THx18 (page 2/2).

Coolselector2

Project information

Project name:	
Comments:	
Created by:	
Coolselector2 version:	4.8.2. Database: 86
Printed:	Tuesday, July 5, 2022
Preferences used:	All applications

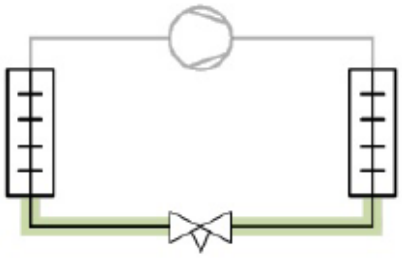
Electronic expansion valve: NH3 EEV

Operating conditions

Refrigerant:	R717		Mass flow in line:	0.04324	kg/s
Cooling capacity:	48040	W	Heating capacity:	58460	W
Evaporating temperature:	273	K	Condensing temperature:	313	K
Evaporating pressure:	426800	Pa	Condensing pressure:	1548000	Pa
Useful superheat:	5.0	K	Subcooling:	5.0	K
Additional superheat:	0	K	Additional subcooling:	0	K
Discharge temperature:	393	K			

System and line: *Dry expansion system. Liquid line*

Selection criteria: *Load: 80 %. Distributor pressure drop: 0 Pa*



Selection: AKVA 10-7



Figure C.20: NH_3 EEV Danfoss AKVA 10-7 (page 1/2).

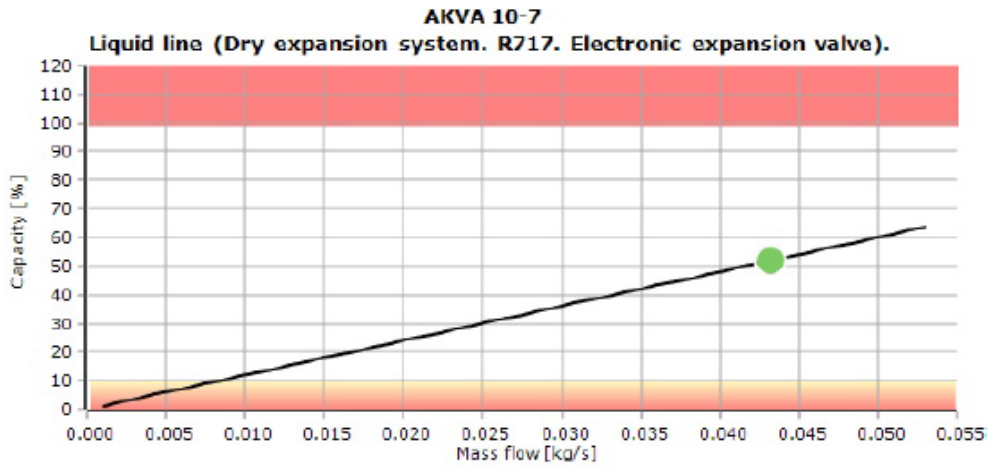
Coolselector2

Type	AKVA 10-5	AKVA 10-6	AKVA 10-7	AKVA 15-1	AKVA 10-8
NS	10	10	15	20	15
Max. capacity [W]	31360	58740	92380	142600	143000
Min. capacity [W]	3136	5874	9238	14260	14300
Load [%]	153	82	52	34	34
DP [Pa]	1121000	1121000	1121000	1121000	1121000
Velocity, in [m/s]	0.59	0.59	0.34	0.19	0.34

Selected code number for AKVA 10-7

AKVA 10-7. Electric expansion valve: *068F3267*

Performance curve



Page 2/4

Figure C.21: NH_3 EEV Danfoss AKVA 10-7 (page 2/2)

D. Catalogs

CTCY-EN – 8.1-6 / 06-2018

Drying, filtering and cleaning cores

→ CCY / PLATINIUM

■ Functional features

CARLY References	To be used with							Use			Filtration	Composition	Features
	BDCY	BCY BCY-HP	BCY-P6 BCY-P14	BBCY	ACY	BACY	HCYBF	On suction line	On liquid line	On oil line	microns		
Felt cores													
CCY 42 F	X							Temporary a few days			10	Felt	For CFC, HCFC, HFC, CO_2 Reinforced filtration
CCY 48 F			X										
CCY 100 F						X							
Stainless steel cores													
CCY 42 I	X							Permanent			140	Stainless steel mesh cloth and screen	For CFC, HCFC, HFC, CO_2 Filtering
CCY 48 I			X		X								
CCY 100 I						X							
High efficiency drying cores													
CCY 42 HP	X							Temporary a few days	Permanent until saturation		50	Chemical agents	For CFC, HCFC, HFC, CO_2 Reinforced drying acid neutralization
CCY 48 HP		X	X		X								
CCY 100 HP				X		X							
Very hich efficiency drying cores													
PLATINIUM 48		X	X		X			Temporary a few days	Permanent until saturation		50	Chemical agents	For CFC, HCFC, HFC, CO_2 Optimum drying
PLATINIUM 100				X		X							
Cleaning cores													
CCY 42 N	X							Temporary a few days	Temporary a few days		50	Chemical agents	For CFC, HCFC, HFC, CO_2 Burnout decontamination, reinforced drying, reinforced acid neutralization, wax and resin binding
CCY 48 N		X	X		X								
CCY 100 N				X		X							
Oil cores													
CCY 48 HU							X			Permanent until saturation	30	Filtrating cellulose, glued, pleated	For refrigerating oil filtering

Figure D.1:Carly catalog for the selection of the cores for the filter drier.

Für brennbare Kältemittel: Baureihe SGS-FL1

Die ESK-Flüssigkeitssammler der Serie SGS-FL1 werden speziell für den Einsatz mit brennbaren Kältemitteln (Fluide der Gruppe 1 nach DGRL) angeboten und sind für R290, R600a, R717, R723, R1150 und R1270 freigegeben. Die Sammler sind standardmäßig mit Schweißstutzen, mit zwei (bzw. drei) Schaugläsern und einem Anschluss für ein Sicherheitsventil ausgestattet.

For hazardous refrigerants: Series SGS-FL1

The ESK SGS-FL1 series liquid receivers are specially designed for use with hazardous refrigerants (fluids of group 1 according to PED) and are approved for R290, R600a, R717, R723, R1150 and R1270.
The receivers are equipped as standard with weldable connectors, with two (or three) sight glasses and a connection for a safety valve.

Technische Spezifikation

Max. zulässiger Betriebsüberdruck (Ps max) im Temperaturbereich:
[1] Zul. Betriebstemperatur: 100 ... –10 °C → Ps1 = 25 bar
[2] Zul. Betriebstemperatur: –10 ... –40 °C → Ps2 = 10 bar
Max. zulässige Temperatur: 90 °C (grüne Schauglas-Schwimmerkugel)

Technical specification

Max. allowable operating pressure (Ps max) according to the temp. range:
[1] Allow. operating temperature: 100 ... –10 °C → Ps1 = 25 bar
[2] Allow. operating temperature: –10 ... –40 °C → Ps2 = 10 bar
Max. allowable temperature: 90 °C (green sight glass float ball)

Technische Daten / **Technical data**

	Sammler / Receiver	Inhalt / Volume Vt l	V1 l	V2 l	V3 l	Anschluss Eintritt / Connection inlet ØOL mm	Ø OL inch	Anschluss Austritt / Connection outlet ØOL mm	ØOL inch	Abmessungen / Dimensions ØD mm	A mm	H mm	E mm	D mm	C mm	Gewicht / Weight kg	FL1
a	SGS-7,5-FL1	7,5	2,9	5,6	–	16 LF	5/8 LF	16 LF	5/8 LF	198	70	360	74	134	224	5,8	●
	SGS-11-FL1	10,5	3,0	8,4	–	16 LF	5/8 LF	16 LF	5/8 LF	198	70	459	74	134	321	7,8	●
	SGS-18-FL1	18,0	6,0	12,0	–	16 LF	5/8 LF	16 LF	5/8 LF	302	75	396	83	135	225	14,0	●
b	SGS-32-FL1	32,0	6,0	15,0	25,5	22 LF	7/8 LF	22 LF	7/8 LF	273	120	807	230	400	591	36,2	●

Vt = Volumen gesamt / Vt = Total volume
Ø OL = Ölleitung Außendurchmesser / Ø OL = Oil line outside diameter
Anschluss ..LF = Schweißadapter mit Rotalockmutter / Conn. ..LF = Welding adapters with rotalock nuts

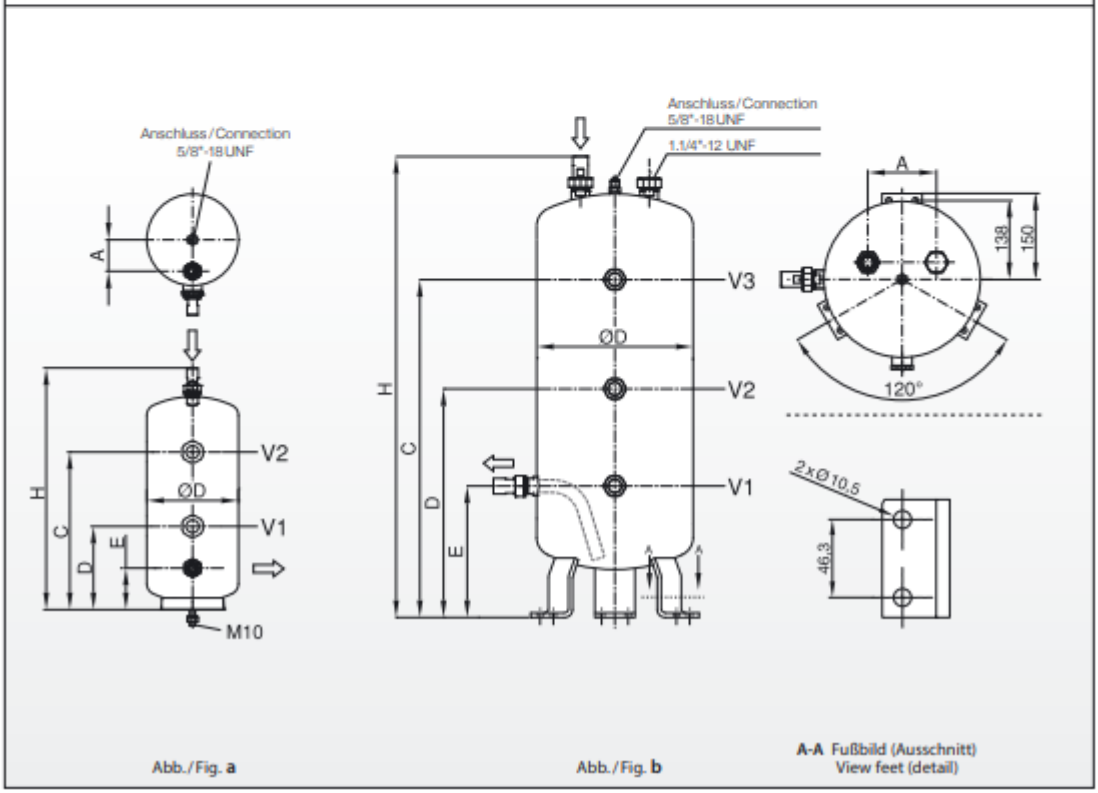


Figure D.2: ESK catalog for NH_3 liquid receivers.

Auslegungsdaten — **Selection data**

Flüssigkeits-abscheider Anschlussgröße / Suction line-accumulator connection size				Kälteleistung Q_0 [kW] bei 40 °C Verflüssigungstemperatur und 25 °C Sauggastemperatur, Verdampfungstemperatur [°C], einstufiger Betrieb / Ref. capacity Q_0 [kW] at 40 °C condensing temperature and 25°C suctiongas temperature, Evaporating temperature [°C], single stage operation																	Effektives Förder-volumen / Effective displace-ment
ØSL mm	ØSL inch	Typ / Type		R404A, R407A, R407C, R507, R22 +5	0	−5	−10	−15	−20	−25	−30	−35	−40	R410A +5	−5	−15	−25	R134a +5	−10	−20	−30	V_0 m³/h
12	–	FA-12/15	Opt.	4,3	3,8	3,2	2,6	2,1	1,7	1,4	1,2	1,0	0,7	6,0	4,4	3,0	2,0	2,8	1,6	1,0	0,6	4,0
			Min.	2,2	1,9	1,6	1,3	1,1	0,9	0,7	0,6	0,5	0,4	3,0	2,2	1,5	1,0	1,4	0,8	0,5	0,3	2,0
15	–	FA-12/15	Opt.	7,1	6,2	5,4	4,6	3,5	2,9	2,4	1,9	1,6	1,2	10,4	7,4	5,2	3,6	4,7	2,6	1,8	1,1	6,6
			Min.	3,6	3,1	2,7	2,3	1,8	1,5	1,2	1,0	0,8	0,6	5,2	3,7	2,6	1,8	2,4	1,3	0,9	0,5	3,3
16	5/8	FA-16...	Opt.	8,4	7,6	6,4	5,2	4,1	3,3	2,8	2,3	2,0	1,4	12,0	8,6	6,0	4,0	5,5	3,0	2,0	1,2	7,8
			Min.	4,2	3,8	3,2	2,6	2,1	1,7	1,4	1,2	1,0	0,7	6,0	4,3	3,0	2,0	2,8	1,5	1,0	0,6	3,9
18	–	FA-18...	Opt.	10,9	9,0	7,4	6,0	4,9	4,0	3,2	2,5	2,2	1,6	15,6	10,8	7,4	5,0	7,0	3,8	2,4	1,5	10,2
			Min.	5,5	4,5	3,7	3,0	2,5	22,0	1,6	1,3	1,1	0,8	7,8	5,4	3,7	2,5	3,5	1,9	1,2	0,8	5,1
22	7/8	FA-22...	Opt.	17,0	15,0	12,6	10,6	8,3	7,0	5,5	4,6	3,8	2,9	25,0	18,0	12,0	8,4	10,2	5,6	3,6	2,4	15,8
			Min.	8,5	7,5	6,3	5,3	4,2	3,6	3,0	2,3	1,9	1,5	12,5	9,0	6,0	4,2	5,1	2,8	1,8	1,2	7,9
28	1-1/8	FA-28...	Opt.	26,7	23,0	19,0	16,0	13,0	11,0	8,8	7,2	5,8	4,5	38,4	28,0	20,0	13,0	17,5	9,8	6,4	4,0	24,8
			Min.	13,4	11,5	9,5	8,0	6,5	5,5	4,5	3,6	2,9	2,3	19,2	14,0	10,0	6,5	8,7	4,9	3,2	2,0	12,4
35	1-3/8	FA-35...	Opt.	44	36	32	26	22	18	14,0	12	10	8	64	46	32	22	26,8	15,0	9,8	6,2	40,6
			Min.	22	18	16	13	11	9	7,0	6	5	4	32	23	16	11	13,4	7,5	4,9	3,1	20,3
42	1-5/8	FA-42...	Opt.	62	52	46	36	30	25	20	16	14	10	94	66	46	32	40	22	14	9,0	57,2
			Min.	31	26	23	18	15	13	10	8	7	5	47	33	23	16	20	11	7	4,5	28,6
54	2-1/8	FA-54...	Opt.	107	92	76	64	52	43	35	28	24	18	154	110	76	52	70	40	26	16	99,0
			Min.	53	46	38	32	26	22	18	14	12	9	77	55	38	26	35	20	13	8	49,5
64	2-1/2	FA-67/64...	Opt.	153	128	108	90	75	62	50	42	34	26	220	158	110	76	100	56	36	24	142
			Min.	77	64	54	45	38	31	25	21	17	13	110	79	55	38	50	28	18	12	71
67	2-5/8	FA-67...	Opt.	168	142	122	100	84	72	58	48	38	30	244	174	122	84	108	62	40	26	148
			Min.	84	71	61	50	42	36	29	24	19	15	122	87	61	42	54	31	20	13	74
70	2-3/4	FA-67/70...	Opt.	180	154	132	108	90	76	62	50	40	32	268	192	134	92	114	66	44	28	163,0
			Min.	90	77	66	54	45	38	31	25	20	16	134	96	67	46	57	33	22	14	81,5
80	3-1/8	FA-80...	Opt.	240	208	176	146	124	104	84	70	56	44	356	254	178	122	158	89	58	36	218
			Min.	120	104	89	73	62	52	42	35	28	22	178	127	89	61	79	45	29	18	109
89	3-1/2	FA-80/89...	Opt.	310	266	226	188	158	132	108	88	72	56	444	318	222	152	202	114	74	48	270
			Min.	155	133	113	94	79	66	54	44	36	28	222	159	111	76	101	57	37	24	135
104	4-1/8	FA-104...	Opt.	430	360	304	256	210	172	140	116	92	73	600	430	300	200	270	152	98	62	400
			Min.	215	180	152	128	105	86	70	58	46	37	300	215	150	100	135	76	49	31	200

Ø SL = Saugleitungs-Außendurchmesser / Suction line outside diameter

Einsatz nur mit Wärmeübertrager oder Heizelementen / Application with heat exchanger or heater elements only

Figure D.3: ESK catalog for NH_3 suction line accumulators.

	Model	922 922R	923 923R	924 924R	925 925R	926 926R	927 927R	928 928R	930 930R
	Connection Size	5/8"	7/8"	1-1/8"	1-3/8"	1-5/8"	2-1/8"	2-5/8"	3-1/8"
Refrigerant	Temp °C	**kW @ 37.8°C Condensing 5.6°C Superheat 0°C Subcooling**							
R-290 Propane C_3H_8	4.4	26.4	36.8	66.2	100.6	172.2	234.7	470.3	392.2
	-1.1	22.0	30.6	55.1	83.7	143.3	195.3	391.6	326.4
	-6.7	18.2	25.3	45.5	69.2	118.4	161.4	312.9	269.7
	-12.2	15.0	20.9	37.6	57.2	97.9	133.4	252.2	222.9
	-17.8	12.1	16.9	30.4	46.2	79.1	107.8	201.5	180.1
	-23.3	9.8	13.6	24.5	37.3	63.8	87.0	159.4	145.3
	-28.9	7.8	10.9	19.6	29.8	51.0	69.5	124.8	116.1
	-34.4	6.2	8.6	15.5	23.6	40.3	55.0	96.5	91.8
	-40	4.8	6.7	12.1	18.4	31.5	42.9	73.7	71.7
R-600a Butane C_4H_{10}	4.4	10.7	14.9	26.8	40.8	69.8	95.2	159.1	270.4
	-1.1	8.7	12.1	21.7	33.1	56.6	77.2	128.9	219.2
	-6.7	7.0	9.7	17.5	26.6	45.5	62.0	103.5	176.0
	-12.2	5.6	7.7	13.9	21.1	36.2	49.3	82.4	140.1
	-17.8	4.4	6.1	10.9	16.6	28.5	38.8	64.9	110.3
	-23.3	3.4	4.7	8.5	13.0	22.2	30.3	50.6	85.9
	-28.9	2.6	3.6	6.6	10.0	17.1	23.3	38.9	66.1
	-34.4	2.0	2.8	5.0	7.6	13.0	17.7	29.5	50.2
	-40	1.5	2.1	3.7	5.7	9.7	13.3	22.1	37.6
R-717 NH_3	4.4	34.6	48.2	86.7	131.9	225.7	307.7	514.1	873.9
	-1.1	28.4	39.5	71.0	108.0	184.8	251.9	420.9	715.5
	-6.7	23.0	32.0	57.6	87.6	150.0	204.4	341.5	580.6
	-12.2	18.5	25.7	46.3	70.4	120.5	164.3	274.5	466.7
	-17.8	14.7	20.5	36.8	56.0	95.9	130.7	218.4	371.3
	-23.3	11.6	16.1	29.0	44.1	75.4	102.8	171.8	292.1
	-28.9	9.0	12.5	22.5	34.3	58.6	79.9	133.5	227.0
	-34.4	7.4	10.3	18.5	28.2	48.2	65.7	109.8	186.6
	-40	5.2	7.3	13.1	19.9	34.0	46.4	77.5	131.7
	Model	**922 922R**	**923 923R**	**924 924R**	**925 925R**	**926 926R**	**927 927R**	**928 928R**	**930 930R**
	Connection Size	5/8"	7/8"	1-1/8"	1-3/8"	1-5/8"	2-1/8"	2-5/8"	3-1/8"
Refrigerant	Temp °C	**kW @ -3.88°C Condensing 5.6°C Superheat 0°C Subcooling**							
R-744 CO_2 Subcritical (650 PSI max)	4.4	103.7	144.2	259.5	394.6	675.4	920.6	1538.2	2614.9
	-1.1	88.5	123.1	221.6	337.0	576.7	786.2	1313.6	2233.1
	-6.7	75.3	104.8	188.6	286.7	490.7	668.9	1117.7	1900.0
	-12.2	63.7	88.6	159.4	242.4	415.0	565.7	945.1	1606.7
	-17.8	53.7	74.7	134.4	204.4	349.9	477.0	796.9	1354.8
	-23.3	45.0	62.5	112.6	171.1	292.9	399.3	667.2	1134.2
	-28.9	37.4	52.0	93.6	142.3	243.5	332.0	554.7	943.0
	-34.4	30.8	42.9	77.2	117.4	200.9	273.9	457.6	777.9
	-40	25.2	35.1	63.1	96.0	164.3	224.0	374.2	636.2

SELECT OIL SEPARATOR WITH CONNECTION SIZE NO LESS THAN DISCHARGE LINE SIZE.

920 and 920R Series for Natural Refrigerants, Tons and kW Notes:

1. Tons = Capacity in evaporator (12,000 BTUH/Hr/Ton), based on Condensing Temperature stated in the chart, 10°F Superheat, 0°F Subcooling.
2. kW = Capacity based on Condensing Temperature stated in the chart, 5.6°C Superheat, 0°C Subcooling.
3. For applications other than reciprocating compressors, (scroll, screw type, 2-stage) please contact Temprite engineering at temprite@temprite.com.

Figure D.4: Temprite catalog for the selection of NH_3 oil separator.

E. Pressure drop

In this section are presented the results from the calculation of the diameter that allowed to determine the necessary piping size for the CO_2 heat pump. For the NH_3 heat pump, these calculations were not made and Danfoss software Coolselector was used. The reports from the software are also presented.

Table E.1: Selection of piping sizes for CO_2 heat pump

Line	$\boldsymbol{m}$ **(kg/s)**	$\boldsymbol{\dot{V}}$ **(m^3/s)**	$\boldsymbol{D_{calc}}$ **(m)**	Available diameters **(m)**	Velocity **(m/s)**
1	0.2814	0.003528	0.02629	0.0223	9.033
				0.0285	5.531
2		0.001893	0.01684	0.0167	8.640
				0.0223	4.846
3		0.0004511	0.02397	0.0223	1.155
				0.0285	0.707
4		0.0003771	0.02191	0.0167	1.722
				0.0223	0.966
5		0.002884	0.06060	0.0545	1.236
				0.0703	0.743
6		0.002884	0.02377	0.0223	7.384
				0.0285	4.520

Coolselector2

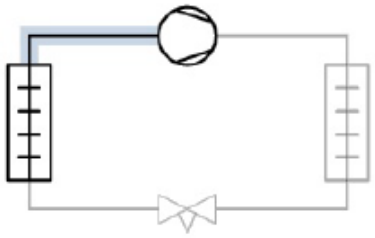
Piping: Suction Line NH3

Operating conditions

Refrigerant:	R717		Mass flow in line:	0.04324	kg/s
Cooling capacity:	47490	W	Heating capacity:	58460	W
Evaporating temperature:	273	K	Condensing temperature:	313	K
Evaporating pressure:	426800	Pa	Condensing pressure:	1548000	Pa
Useful superheat:	0	K	Subcooling:	5.0	K
Additional superheat:	5.0	K	Additional subcooling:	0	K
Discharge temperature:	393	K			

System and line: *Dry expansion system. Suction line*

Selection criteria: *Velocity: 12.00 m/s. Length: 10.00 m*



Selection: Stainless steel pipe DIN-EN SS 32

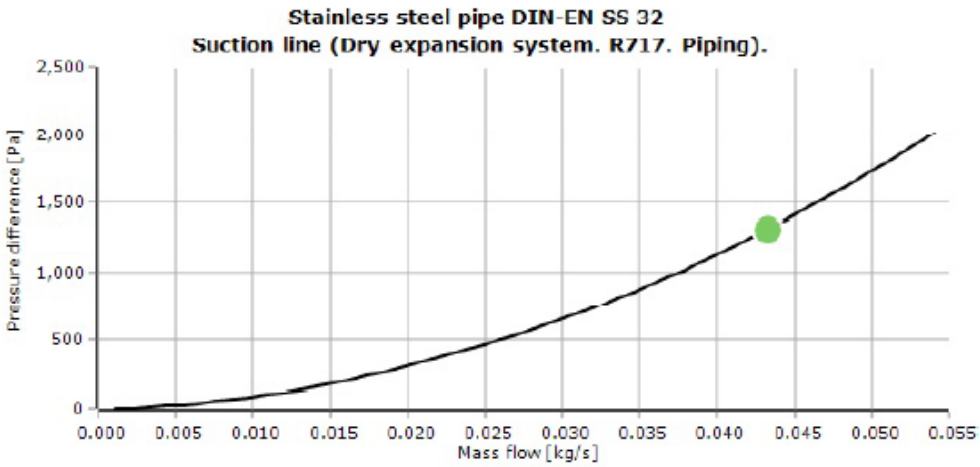
Type	DIN-EN SS 20	DIN-EN SS 25	DIN-EN SS 32	DIN-EN SS 40	DIN-EN SS 50
DT_sat [K]	1.2	0.3	0.1	0.0	0.0
NS	20	25	32	40	50
Diameter, in [m]	0.0223	0.0285	0.0372	0.0431	0.0545
Diameter, out [m]	0.0223	0.0285	0.0372	0.0431	0.0545
DP [K/m]	0.117	0.032	0.008	0.004	0.001
DP [Pa]	18390	5117	1307	619.8	190.8
Velocity, in [m/s]	33.00	20.20	11.86	8.83	5.52
Velocity, out [m/s]	34.49	20.45	11.89	8.85	5.53

Page 3/8

Figure E.1: Danfoss Coolselector2 NH_3 piping selection report (page 1/6).

Coolselector2

Performance curve



Page 4/8

Figure E.2: Danfoss Coolselector2 NH_3 piping selection report (page 2/6).

Coolselector2

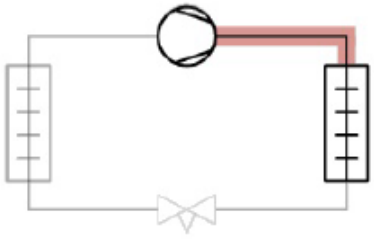
Piping: Discharge Line NH3

Operating conditions

Refrigerant:	R717		Mass flow in line:	0.04324	kg/s
Cooling capacity:	47490	W	Heating capacity:	58460	W
Evaporating temperature:	273	K	Condensing temperature:	313	K
Evaporating pressure:	426800	Pa	Condensing pressure:	1548000	Pa
Useful superheat:	0	K	Subcooling:	5.0	K
Additional superheat:	5.0	K	Additional subcooling:	0	K
Discharge temperature:	393	K			

System and line: *Dry expansion system. Discharge line*

Selection criteria: *Velocity: 15.00 m/s. Length: 10.00 m*



Selection: Stainless steel pipe DIN-EN SS 20

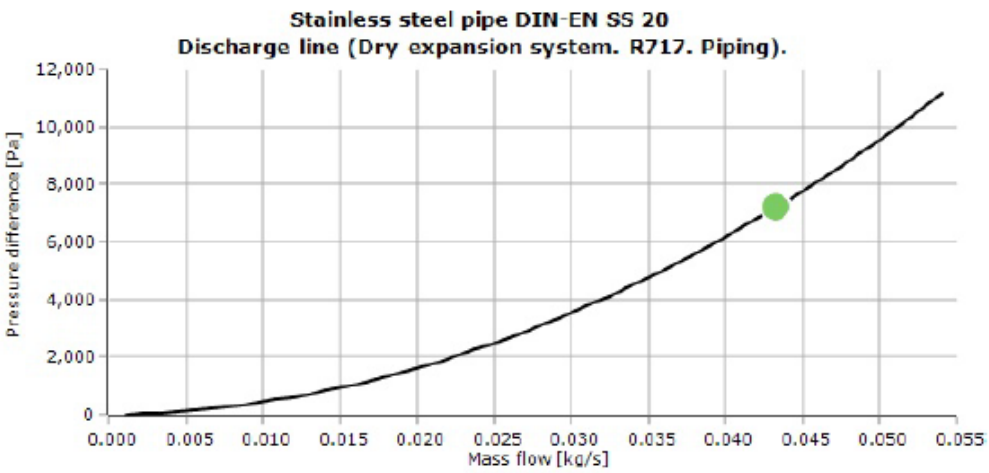
Type	DIN-EN SS 10	DIN-EN SS 15	DIN-EN SS 20	DIN-EN SS 25	DIN-EN SS 32
DT_sat [K]	3.5	0.8	0.2	0.0	0.0
NS	10	15	20	25	32
Diameter, in [m]	0.0126	0.0167	0.0223	0.0285	0.0372
Diameter, out [m]	0.0126	0.0167	0.0223	0.0285	0.0372
DP [K/m]	0.352	0.076	0.017	0.005	0.001
DP [Pa]	145700	32380	7195	2043	529.1
Velocity, in [m/s]	40.45	23.03	12.91	7.91	4.64
Velocity, out [m/s]	44.70	23.53	12.98	7.92	4.64

Page 5/8

Figure E.3: Danfoss Coolselector2 NH_3 piping selection report (page 3/6).

Coolselector2

Performance curve



Page 6/8

Figure E.4: Danfoss Coolselector 2 NH_3 piping selection report (page 4/6).

Coolselector2

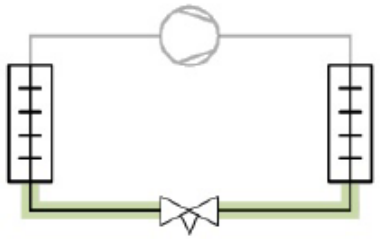
Piping: Liquid Line NH3

Operating conditions

Refrigerant:	R717		Mass flow in line:	0.04324	kg/s
Cooling capacity:	47490	W	Heating capacity:	58460	W
Evaporating temperature:	273	K	Condensing temperature:	313	K
Evaporating pressure:	426800	Pa	Condensing pressure:	1548000	Pa
Useful superheat:	0	K	Subcooling:	5.0	K
Additional superheat:	5.0	K	Additional subcooling:	0	K
Discharge temperature:	393	K			

System and line: *Dry expansion system. Liquid line*

Selection criteria: *Velocity: 1.00 m/s. Length: 10.00 m*



Selection: Stainless steel pipe DIN-EN SS 8

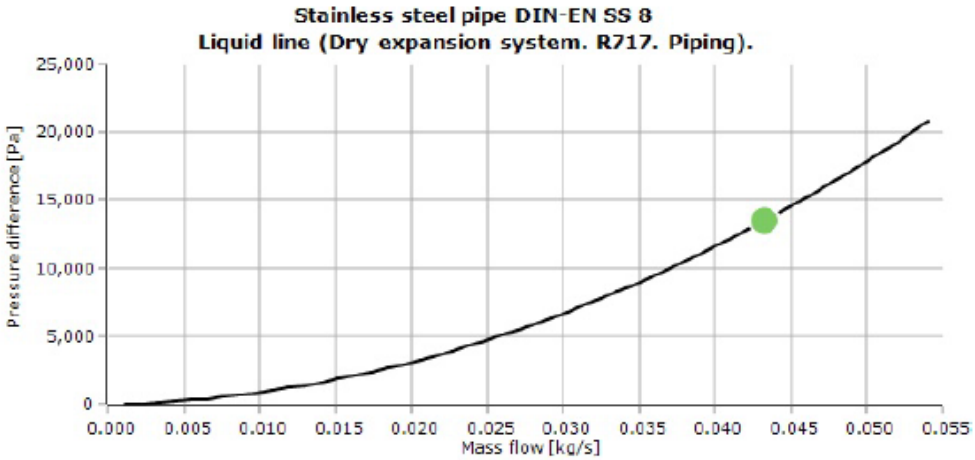
Type	DIN-EN SS 6	DIN-EN SS 8	DIN-EN SS 10	DIN-EN SS 15
DT_sat [K]	3.6	0.3	0.1	0.0
NS	6	8	10	15
Diameter, in [m]	0.0056	0.0089	0.0126	0.0167
Diameter, out [m]	0.0056	0.0089	0.0126	0.0167
DP [K/m]	0.363	0.031	0.005	0.001
DP [Pa]	150000	13480	2280	553.2
Velocity, in [m/s]	2.98	1.18	0.59	0.34
Velocity, out [m/s]	2.98	1.18	0.59	0.34

Page 7/8

Figure E.5: Danfoss Coolselector 2 NH_3 piping selection report (page 5/6).

Coolselector2

Performance curve



Page 8/8

Figure E.6: Danfoss Coolselector 2 NH_3 piping selection report (page 6/6).

F. EES simulation results for the thermodynamic cycles

This section presents the thermodynamic results from varying the heat load given by the gas cooler in the CO_2 heat pump EES simulations.

Table F.1: Parameters results from the EES simulations of different gas cooler capacities

	1st	**2nd**	**3rd**	**4th**	**5th**
$\dot{Q}_{gc}$ **[kW]**	61.5	107.9	157.5	202	253
$\dot{Q}_{evap}$ **[kW]**	44.0	76.4	112.1 kW	143.2	178.0
$\dot{m}_{CO2}$ **[kg/s]**	0.2814	0.4866	0.7128	0.9094	1.1306
P_{gc} **[bar]**	86.0	86.2	86.3	86.4	86.4
$\dot{W}_{comp}$ **[kW]**	17.52	31.5	45.4	58.7	75.5
T_{disch} **[ºC]**	107.1	109.1	108.3	109.0	110.7
η_{comp}	0.700	0.675	0.687	0.680	0.655
COP	3.513	3.423	3.467	3.441	3.352

G. Results for EES simulations with components properties

Table G.1: EES simulation results for $T_{w,i}$ =10, 15, 20 and 25 ℃

$T_{w,i}$ [ºC]	10	15	20	25
T_{suc} [ºC]	21.03	21.81	22.47	23.09
T_{disch} [ºC]	107.1	108.2	109	109.9
T_{gce} [ºC]	35.04	36.35	37.44	38.49
$\dot{Q}_{gc}$ [kW]	61.48	58.01	53.79	48.96
$\dot{Q}_{evap}$ [kW]	43.95	40.49	36.27	31.44
$\dot{W}_{comp}$ [kW]	17.52	17.52	17.52	17.52
$\dot{m}_{CO2}$ [kg/s]	0.2813	0.2796	0.2783	0.2770
$\dot{m}_{w}$ [kg/s]	0.2936	0.3079	0.3212	0.3341
COP	3.508	3.297	3.046	2.764

Table G.2: CO_2 heat pump simulation results for ambient temperatures from -5 to 25 ºC

T_{amb} [ºC]	-5.0	-2.5	0.0	2.5	5.0	7.5	10.0	**12.5**	15.0	17.5	20.0	22.5	25
T_{evap} [ºC]	-15	-12.5	-10	-7.5	-5.0	-2.5	0	2.5	5.0	7.5	10.0	12.5	15.0
P_{evap} [kPa]	2291	2465	2649	2842	3045	3260	3485	372	3969	4230	4503	4788	5089
P_{gc} [kPa]	8600	8600	8600	8600	8600	8600	8600	8600	8600	8600	8600	8600	8600
p_r	3.754	3.489	3.247	3.026	2.824	2.638	2.468	2.311	2.167	2.033	1.91	1.796	1.69
T_{suc} [ºC]	2.746	5.521	8.596	11.84	15.12	18.29	21.02	22.43	23.79	25.11	26.4	27.68	28.98
T_{disch} [ºC]	150.3	139.3	130.6	123.5	117.5	112.1	107.1	100.4	94.43	88.84	83.57	78.6	73.93
T_{gce} [ºC]	14.58	17.54	20.99	24.74	28.54	32.15	35.04	35.72	36.31	36.85	37.33	37.8	38.31
$\dot{Q}_{gc}$ [kW]	50.57	53.65	56.39	58.73	60.56	61.4	61.47	57.22	53.13	48.97	44.7	40.29	35.68
$\dot{Q}_{evap}$ [kW]	33.05	36.13	38.87	41.21	43.04	44.12	43.94	41.79	39.51	37	34.25	31.24	27.92
η_{is}	54.87	58.08	61.01	63.69	66.13	68.38	70.44	72.34	74.08	75.7	77.19	78.57	79.84
$\dot{W}_{comp}$ [kW]	17.52	17.52	17.52	17.52	17.52	17.52	17.52	15.43	13.62	11.96	10.45	9.047	7.761
$\dot{m}_{w}$ [kg/s]	0.2416	0.2563	0.2694	0.2806	0.2893	0.293	0.2937	0.2733	0.2538	0.2339	0.2135	0.1924	0.1704
$\dot{m}_{CO2}$ [kg/s]	0.1451	0.1639	0.1837	0.205	0.228	0.2536	0.2813	0.2813	0.2813	0.2813	0.2813	0.2813	0.2813
$P_{gc,opt}$	-	-	-	-	-	-	86.4	87.62	88.61	89.46	90.2	90.91	91.7
COP	2.886	3.062	3.218	3.352	3.457	3.5	3.508	3.709	3.901	4.093	4.279	4.453	4.597

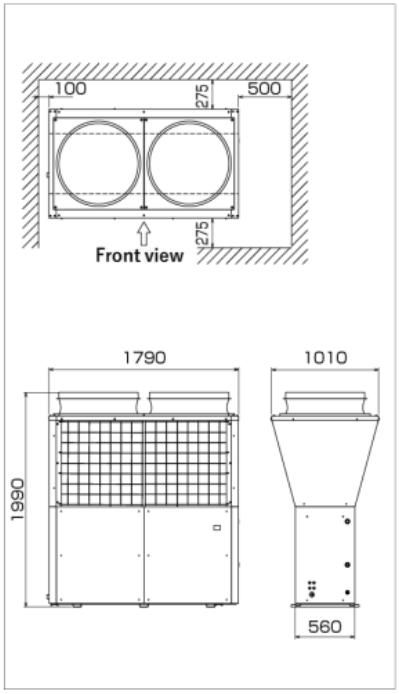
Table G.3: NH_3 heat pump simulation results for ambient temperatures from -5 to 25 ºC

T_{amb} [ºC]	-5.0	-2.5	0.0	2.5	5.0	7.5	10.0	12.5	15.0	17.5	20.0	22.5	25
T_{evap} [ºC]	-15	-12.5	-10	-7.5	-5.0	-2.5	0	2.5	5.0	7.5	10.0	12.5	15.0
P_{evap} [ºC]	236.2	262.4	290.8	321.6	354.9	390.8	429.6	471.2	516	563.9	615.3	670.2	728.8
P_{cond} [ºC]	1555	1555	1555	1555	1555	1555	1555	1555	1555	1555	1555	1555	1555
p_r	6.583	5.926	5.347	4.835	4.382	3.979	3.619	3.300	3.013	2.758	2.527	2.320	2.134
T_{suc} [ºC]	-10	-7.5	-5.0	-2.5	0.0	2.5	5.0	7.5	10.0	12.5	15.0	17.5	20.0
T_{disch} [ºC]	164.5	156.6	149.1	141.8	134.7	127.9	121.4	115	108.9	103.1	97.41	91.97	86.74
T_3 [ºC]	39.80	39.49	40.40	41.42	42.55	43.77	45.07	44.87	44.72	44.58	44.48	44.42	44.41
T_4 [ºC]	37.0	37.0	37.0	37.0	37.0	37.0	37.0	37.0	37.0	37.0	37.0	37.0	37.0
$\dot{Q}_{dsh}$ [kW]	6.02	9.552	9.685	9.608	9.506	9.377	9.21	8.529	7.871	7.23	6.603	5.988	5.384
$\dot{Q}_{cond}$ [kW]	41.22	43.35	45.70	48.29	51.19	54.43	58.03	57.27	56.59	55.93	55.29	54.67	54.06
$\dot{Q}_{evap}$ [kW]	30.63	32.76	35.1	37.7	40.59	43.83	47.44	47.52	47.64	47.75	47.86	47.96	48.06
η_{is}	72.98	74.58	75.88	76.9	77.67	78.23	78.6	78.8	78.86	78.8	78.63	78.37	78.03
$\dot{W}_{comp}$ [kW]	10.58	10.58	10.58	10.58	10.58	10.58	10.58	9.75	8.95	8.18	7.43	6.71	6.00
$\dot{m}_{w,dsh}$ [kg/s]	0.05752	0.09126	0.09253	0.09179	0.09082	0.08958	0.08799	0.08148	0.0752	0.06907	0.06308	0.05721	0.05143
$\dot{m}_{w,cond}$ [kg/s]	0.3363	0.3229	0.3440	0.3696	0.3982	0.4303	0.4664	0.4657	0.4655	0.4653	0.4652	0.4651	0.465
$\dot{m}_{NH3}$ [kg/s]	0.02834	0.03022	0.03228	0.03457	0.03712	0.03997	0.04311	0.04311	0.04311	0.04311	0.04311	0.04311	0.04311
COP	3.892	4.093	4.315	4.56	4.833	5.139	5.483	5.874	6.321	6.837	7.44	8.154	9.011

H. EcoCute technical report

CO2 Heat pump water heater :::Eco-Cute::: (CHP-80Y2)

CHP-80Y2 Specification table (380V)



Model		CHP-80Y
Dimension		W 1,790mm×H 1,990mm×D 1,010mm
Weight		Basic mass : 680 kg / Operating mass : 700 kg
Installation		Outdoor
Power		3Φ 380V 50/60 Hz
Operating temp range	Ambient temperature	Standard : -5~43℃, Antifreeze : -15~43℃, Cold district : -20~43℃
	Supply water temperature	Std : 5℃~50℃, Circ heating·HP independent(High temp supply water): 5~63℃
	Output temperature	60~90℃
Output flow rate		150 L/min
Refrigerant design pressure		High pressure side 14.0 MPa/Low pressure side 7.5 MPa
Decompression valve (Customer prepare)		Standard tank : 170 kPa Others : Please consult
Pressure relief valve		Standard tank : 190 kPa Others : Please consult
Comp-ressor	Model	Semi-hermetic reciprocating compressor
	Electric motor type	Inverter drive, 3 Φ induction motor
	Rated output	15.8 kW
	Refrigerating capacity	9.6 ton/day
Crankcase heater		140W
Fan		Properller fan 300W ×2 units
Pump		Seal- less DC282V-140W (Pressure resistance 490 kPa)
Heat ex-changer	Air	Forced air-cooling cross fin
	Output hot water	Forced circulation double-tube
Protection devices		High pressure switch, High/Low pressure sensor, Compressor decompression valve, Overcurrent relay(fan) , Overcurrent protection(compresor)
Refrigerant/filling amount		CO_2 (R744) / 11.3 kg
Performance		Heating ability : 65 kW
Piping connec-tion	SW·HW·Air HEX (room drain)	Rc 1 (25A) female screw
	Drain	Rc 3/4 (20A) female screw
Accesorries		Remote control
Paint color		Ivory white (Japan reg. 2.5Y 8/1)
seismic strengthening		1.5 G
Sound level		60dB (regula season) /61dB (winter season)

Figure H.1: EcoCute technical report [145].

I. CO_2 system diagram

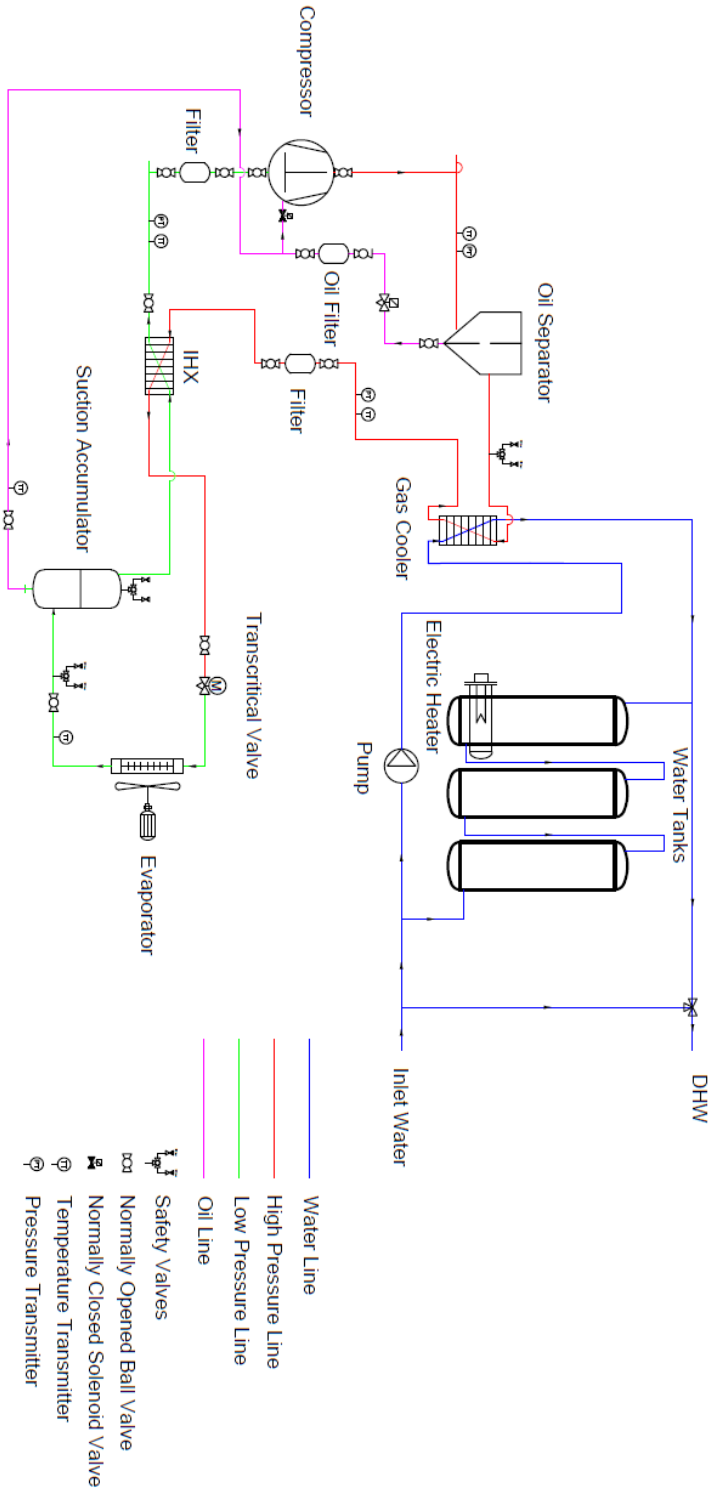


Figure I.1: CO_2 system diagram with the selected components.

J. EES simulation codes

This section presents the codes used for the EES simulation of the heat pump cycles.

Air-to-Water Transcritical CO2 Heat Pump - Conventional Configuration

1: Evaporator outlet and compressor inlet
2: Compressor outlet and gas cooler inlet
3: Gas cooler outlet and expansion valve inlet
4: Expansion valve outlet and evaporator inlet

Input temperatures

T_{amb} = **ConvertTemp** (C, K, 10)

T_{evap} = T_{amb} − 10 [K]

P_{evap} = P_{sat} (R744, T = T_{evap})

T_{sh} = 5 [K]

T_{sc} = 0 [K]

Compressor information

$\eta_{s,comp}$ = 0.7

Gas Cooler Information

Gas Cooler Pressure Calculation

P_{gc} = 8600 [kPa]

T_{gce} = **ConvertTemp** (C, K, 35)

State Point 1 -

Set Variables

T_1 = T_{evap} + T_{sh}

P_1 = P_{evap}

Calculated Variables

h_1 = **h** (R744, T = T_1, P = P_1)

s_1 = **s** (R744, T = T_1, h = h_1)

v_1 = **v** (R744, T = T_1, h = h_1)

State Point 2

Set Variables

P_2 = P_{gc}

Isentropic Conditions (6=2s)

h_6 = **h** (R744, s = s_{2i}, P = P_2)

s_6 = s_{2i}

T_6 = **T** (R744, s = s_{2i}, P = P_2)

P_6 = P_{gc}

s_{2i} = s_1

h_{2i} = **h** (R744, s = s_{2i}, P = P_2)

Calculated Variables

$$\eta_{s,comp} = \frac{h_{2i} - h_1}{h_2 - h_1}$$

$T_2 = \mathbf{T}(R744, P = P_2, h = h_2)$

$s_2 = \mathbf{s}(R744, P = P_2, h = h_2)$

$v_2 = \mathbf{v}(R744, P = P_2, h = h_2)$

State Point 3

Set Variables

$P_3 = P_2$

$T_3 = T_{gce} - T_{sc}$

Calculated Variables

$h_3 = \mathbf{h}(R744, T = T_3, P = P_3)$

$s_3 = \mathbf{s}(R744, T = T_3, P = P_3)$

$v_3 = \mathbf{v}(R744, T = T_3, P = P_3)$

State Point 4

Set Variables

$h_4 = h_3$

$P_4 = P_{evap}$

Calculated Variables

$T_4 = \mathbf{T}(R744, P = P_4, h = h_4)$

$s_4 = \mathbf{s}(R744, P = P_4, h = h_4)$

$v_4 = \mathbf{v}(R744, P = P_4, h = h_4)$

State Point 5 - Evaporator saturated vapor

Set Variables

$T_5 = T_{evap}$

$P_5 = P_{evap}$

Calculated Variables

$h_5 = \mathbf{h}(R744, P = P_5, x = 1)$

$s_5 = \mathbf{s}(R744, P = P_5, x = 1)$

$v_5 = \mathbf{v}(R744, P = P_5, x = 1)$

Energy balance

$\dot{Q}_{gc} = 50$ [kW] Desired power output

$\dot{W}_{comp} = \dot{m}_{CO2} \cdot (h_2 - h_1)$

$\dot{Q}_{gc} = \dot{m}_{CO2} \cdot (h_2 - h_3)$

$\dot{Q}_{evap} = \dot{m}_{CO2} \cdot (h_1 - h_4)$

Perfomance

$$p_r = \frac{P_{gc}}{P_{evap}}$$

$$COP_{HP} = \frac{h_2 - h_3}{h_2 - h_1}$$

$$COP_{LZ} = \frac{T_6 - T_3}{T_6 - T_3 - T_{amb} \cdot \ln\left[\frac{T_6}{T_3}\right]}$$

$$\eta_{HP} = \frac{COP_{HP}}{COP_{LZ}}$$

Figure J.1: EES simulation code for the CO_2 conventional heat pump cycle.

Air-to-Water Transcritical CO2 Heat Pump - IHX configuration

1: Low-pressure side of the IHX exit and compressor inlet
2: Compressor discharge state and gas cooler inlet
3: Gas cooler exit and high-pressure side of the IHX inlet
4: High-pressure side of the IHX exit and expansion valve inlet
5: Expansion valve exit and evaporator inlet
6: Evaporator exit and low-pressure side of the IHX inlet

Inputs temperatures

$T_{amb} = \mathbf{ConvertTemp}(C, K, 10)$

$T_{evap} = T_{amb} - 10$ [K]

$P_{evap} = \mathbf{P}_{sat}(R744, T = T_{evap})$

Compressor information

$$p_r = \frac{P_2}{P_1}$$

$\eta_{s,comp} = 0.7$

$\eta_{s,t} = 1.003 - 0.121 \cdot p_r$

Volumetric efficiency

$$\eta_{v,comp} = \frac{\dot{m}_{CO2}}{\frac{N}{60} \cdot V_{comp} \cdot \rho_{suc}}$$

$\rho_{suc} = \rho(R744, T = T_1, P = P_1)$

$$V_{comp} = \pi \cdot \left[\frac{0.038}{2}\right]^2 \cdot 0.038 \cdot 4$$

$N = 1450$ [RPM]

IHX Information

$$\varepsilon_{IHX} = \frac{T_1 - T_6}{T_3 - T_6}$$

$\varepsilon_{IHX} = 0.6$

$h_3 - h_4 = h_1 - h_6$

Gas cooler Information

$P_{gc} = 8600$ [kPa]

$P_{gc,t} = (4.9 + 2.256 \cdot (T_{gce} - 273.15) - 0.17 \cdot (T_{evap} - 273.15) + 0.002 \cdot (T_{gce} - 273.15)^2) \cdot 10^2$

$T_{gce} = \mathbf{ConvertTemp}(C, K, 35)$

State Point 1

Set Variables

$P_1 = \mathbf{P}(R744, T = T_{evap}, x = 1)$

$T_1 = T_{evap} + \delta T_{IHX}$

Calculated Variables

$h_1 = \mathbf{h}(R744, T = T_1, P = P_1)$

$s_1 = \mathbf{s}(R744, h = h_1, P = P_1)$

State Point 2

Set Variables

$P_2 = P_{gc}$

Isentropic Conditions

$s_{2i} = s_1$

$h_{2i} = \mathbf{h}(R744, s = s_{2i}, P = P_2)$

State 7=2s

$s_7 = s_{2i}$

$h_7 = \mathbf{h}(R744, s = s_7, P = P_7)$

$T_7 = \mathbf{T}(R744, P = P_7, h = h_7)$

$P_7 = P_{gc}$

Calculated Variables

$$\eta_{s,comp} = \frac{h_{2i} - h_1}{h_2 - h_1}$$

$T_2 = \mathbf{T}(R744, P = P_2, h = h_2)$

$s_2 = \mathbf{s}(R744, T = T_2, P = P_2)$

State Point 3

Set Variables

$P_3 = P_2$

$T_3 = T_{gce}$

Calculated Variables

$h_3 = \mathbf{h}(R744, T = T_3, P = P_3)$

$s_3 = \mathbf{s}(R744, T = T_3, P = P_3)$

State Point 4

Set Variables

$P_4 = P_3$

Calculated Variables

$T_4 = \mathbf{T}(R744, h = h_4, P = P_4)$

$s_4 = \mathbf{s}(R744, T = T_4, P = P_4)$

State Point 5

Set Variables

$h_5 = h_4$ Isenthalpic expasion

$P_5 = P_1$

$T_5 = T_{evap}$

Calculated Variables

$s_5 = \mathbf{s}(R744, T = T_5, h = h_5)$

State Point 6

Set Variables

$P_6 = P_1$

$T_6 = T_{evap}$

Calculated Variables

$h_6 = \mathbf{h}(R744, P = P_6, x = 1)$

$s_6 = \mathbf{s}(R744, T = T_6, h = h_6)$

Energy Balance

$\dot{Q}_{gc} = 61.5$ [kW]

$\dot{Q}_{gc} = \dot{m}_{CO2} \cdot (h_2 - h_3)$

$\dot{W}_{comp} = \dot{m}_{CO2} \cdot (h_2 - h_1)$

$\dot{Q}_{evap} = \dot{m}_{CO2} \cdot (h_6 - h_5)$

$\dot{Q}_{IHX} = \dot{m}_{CO2} \cdot (h_1 - h_6)$

Perfomance

$$COP_{HP} = \frac{h_2 - h_3}{h_2 - h_1}$$

$$COP_{LZ} = \frac{T_7 - T_3}{T_7 - T_3 - T_{amb} \cdot \ln\left[\frac{T_7}{T_3}\right]}$$

$$\eta_{HP} = \frac{COP_{HP}}{COP_{LZ}}$$

Figure J.2: EES simulation code for the CO_2 with IHX heat pump cycle.

Air-to-Water NH3 Heat Pump - Conventional Configuration

1: Evaporator outlet and compressor inlet
2: Compressor outlet and desuperheater inlet
3: Desuperheater and condenser inlet
4: Condenser outlet and expansion valve inlet
5: Expansion valve outlet and evaporator inlet

Input temperatures

$T_{amb} = \mathbf{ConvertTemp}(C, K, 10)$

$T_{evap} = T_{amb} - 10$

$T_{cond} = \mathbf{ConvertTemp}(C, K, 40)$

$P_{evap} = \mathbf{P_{sat}}(R717, T = T_{evap})$

$P_{cond} = \mathbf{P_{sat}}(R717, T = T_{cond})$

$T_{sh} = 5$ [K]

$T_{sc} = 5$ [K]

Compressor information

$$p_r = \frac{P_2}{P_1}$$

$$\eta_{v,comp} = 1.02 \cdot \mathbf{exp}(-0.063 \cdot p_r)$$

$$\frac{\eta_{v,comp}}{\eta_{s,comp}} = \mathbf{exp}\left[-1.69 \cdot \frac{T_{cond}}{T_{evap}} + 1.97\right]$$

State 1

Set Variables

$T_1 = T_{evap} + T_{sh}$

$P_1 = P_{evap}$

$h_1 = \mathbf{h}(R717, P = P_1, T = T_1)$

$s_1 = \mathbf{s}(R717, P = P_1, T = T_1)$

State 2

Set Variables

$P_2 = P_{cond}$

Isentropic Conditions (6=2s

$h_6 = \mathbf{h}(R717, s = s_{2i}, P = P_2)$

$s_6 = s_{2i}$

$T_6 = \mathbf{T}(R717, s = s_{2i}, P = P_2)$

$P_6 = P_{cond}$

Calculated Variables

$s_{2i} = s_1$

$h_{2i} = \mathbf{h}(R717, s = s_{2i}, P = P_{cond})$

$\eta_{s,comp} = \frac{h_{2i} - h_1}{h_2 - h_1}$

$T_2 = \mathbf{T}(R717, P = P_2, h = h_2)$

$s_2 = \mathbf{s}(R717, T = T_2, P = P_2)$

State 3

Set Variables

$P_3 = P_{cond}$

$T_3 = \mathbf{ConvertTemp}(C, K, 40)$

Calculated Variables

$h_3 = \mathbf{h}(R717, x = 1, P = P_3)$

$s_3 = \mathbf{s}(R717, x = 1, P = P_3)$

State 4

Set Variables

$T_4 = T_{cond} - T_{sc}$

$P_4 = P_{cond}$

Calculated Variables

$h_4 = \mathbf{h}(R717, P = P_4, T = T_4)$

$s_4 = \mathbf{s}(R717, P = P_4, T = T_4)$

State 5

Set Variables

$h_5 = h_4$

$T_5 = T_{evap}$

$P_5 = P_{evap}$

Calculated Variables

$s_5 = \mathbf{s}(R717, T = T_5, h = h_5)$

$x_5 = \mathbf{x}(R717, T = T_5, h = h_5)$

Energy balance

$\dot{Q}_{heat} = 50$ [kW]

$\dot{Q}_{heat} = \dot{m}_{NH3} \cdot (h_2 - h_4)$

$\dot{Q}_{cond} = \dot{m}_{NH3} \cdot (h_3 - h_4)$

$\dot{Q}_{dsh} = \dot{m}_{NH3} \cdot (h_2 - h_3)$

$$part_{dsh} = \frac{\dot{Q}_{dsh}}{\dot{Q}_{heat}} \cdot 100$$ Part of the heat transferred in the desuperheater

$$part_{cond} = \frac{\dot{Q}_{cond}}{\dot{Q}_{heat}} \cdot 100$$ Part of the heat transferred in the condenser

$$\dot{W}_{comp} = \dot{m}_{NH3} \cdot (h_2 - h_1)$$

$$\dot{Q}_{evap} = \dot{m}_{NH3} \cdot (h_1 - h_5)$$

Perfomance

$$COP_{HP} = \frac{\dot{Q}_{heat}}{\dot{W}_{comp}}$$

$$COP_{Carnot} = \frac{T_{cond}}{T_{cond} - T_{evap}}$$

$$\eta_{HP} = \frac{COP_{HP}}{COP_{Carnot}}$$

Figure J.3: EES simulation code for the NH_3 conventional heat pump cycle.

Air-to-Water NH3 Heat Pump - IHX Configuration

1: Low pressure side of the IHX exit and compressor inlet
2: Compressor discharge state and condenser inlet
3: Saturated vapor at the condenser
4: Saturated liquid at the condenser/Condenser exit and high pressure side of the IHX inlet
5: High pressure side of the IHX exit and expansion valve inlet
6: Expansion valve exit and evaporator inlet
7: Evaporator exit/receiver exit and low pressure side of the IHX inlet

Input temperatures

$T_{amb} = \mathbf{ConvertTemp}(C, K, 10)$

$T_{evap} = T_{amb} - 10$

$T_{cond} = \mathbf{ConvertTemp}(C, K, 40)$

$P_{evap} = \mathbf{P_{sat}}(R717, T = T_{evap})$

$P_{cond} = \mathbf{P_{sat}}(R717, T = T_{cond})$

$T_{sh} = 5 \quad [K]$

$T_{sc} = 5 \quad [K]$

Compressor information

$$p_r = \frac{P_2}{P_1}$$

$$\eta_{v,comp} = 1.02 \cdot \mathbf{exp}(-0.063 \cdot p_r)$$

$$\frac{\eta_{v,comp}}{\eta_{s,comp}} = \mathbf{exp}\left[-1.69 \cdot \frac{T_{cond}}{T_{evap}} + 1.97\right]$$

Internal Heat Exchanger Information

$$\varepsilon_{ihx} = \frac{T_1 - T_7}{T_4 - T_7}$$

$\varepsilon_{ihx} = 0.6$

$h_1 - h_7 = h_4 - h_5$

State 1

Set Variables

$P_1 = \mathbf{P}(R717, T = T_{evap}, x = 1)$

$T_1 = T_{evap} + \delta T_{IHX}$

Calculated Variables

$h_1 = \mathbf{h}(R717, T = T_1, P = P_1)$

$s_1 = \mathbf{s}(R717, h = h_1, P = P_1)$

$v_1 = \mathbf{v}(R717, h = h_1, P = P_1)$

State 2

Set Variables

$P_2 = P_{cond}$

Isentropic Conditions

$h_8 = \mathbf{h}(R717, s = s_{2i}, P = P_2)$

$s_8 = s_{2i}$

$T_8 = \mathbf{T}(R717, s = s_{2i}, P = P_2)$

$P_8 = P_{cond}$

Calculated Variables

$s_{2i} = s_1$

$h_{2i} = \mathbf{h}(R717, s = s_{2i}, P = P_2)$

$\eta_{s,comp} = \frac{h_{2i} - h_1}{h_2 - h_1}$

$T_2 = \mathbf{T}(R717, P = P_2, h = h_2)$

$s_2 = \mathbf{s}(R717, T = T_2, P = P_2)$

State 3

Set Variables

$P_3 = P_{cond}$

$T_3 = T_{cond}$

Calculated Variables

$h_3 = \mathbf{h}(R717, P = P_{cond}, x = 1)$

$s_3 = \mathbf{s}(R717, P = P_{cond}, x = 1)$

State 4

Set Variables

$P_4 = P_{cond}$

$T_4 = T_{cond}$

Calculated Variables

$h_4 = \mathbf{h}(R717, P = P_{cond}, x = 0)$

$s_4 = \mathbf{s}(R717, P = P_{cond}, x = 0)$

State 5

Set Variables

$P_5 = P_{cond}$

Calculated Variables

$T_5 = \mathbf{T}(R717, h = h_5, P = P_5)$

$s_5 = \mathbf{s}(R717, T = T_5, P = P_5)$

$v_5 = \mathbf{v}(R717, h = h_5, P = P_5)$

State 6

Set Variables

$h_6 = h_5$

$T_6 = T_{evap}$

$P_6 = P_{evap}$

Calculated Variables

$s_6 = \mathbf{s}(R717, T = T_{evap}, h = h_6)$

$x_6 = \mathbf{x}(R717, T = T_{evap}, h = h_6)$

State 7 - Evaporator outlet and low pressure side of the IHX inlet

Set Variables

$P_7 = P_{evap}$

$T_7 = T_{evap}$

Calculated Variables

$h_7 = \mathbf{h}(R717, P = P_7, x = 1)$

$s_7 = \mathbf{s}(R717, T = T_7, h = h_7)$

Energy balance

$\dot{Q}_{heat} = 50$ [kW]

$\dot{Q}_{heat} = \dot{m}_{NH3} \cdot (h_2 - h_4)$

$\dot{Q}_{cond} = \dot{m}_{NH3} \cdot (h_3 - h_4)$

$\dot{Q}_{dsh} = \dot{m}_{NH3} \cdot (h_2 - h_3)$

$part_{dsh} = \frac{\dot{Q}_{dsh}}{\dot{Q}_{heat}} \cdot 100$

$part_{cond} = \frac{\dot{Q}_{cond}}{\dot{Q}_{heat}} \cdot 100$

$\dot{Q}_{IHX} = \dot{m}_{NH3} \cdot (h_1 - h_7)$

$\dot{W}_{comp} = \dot{m}_{NH3} \cdot (h_2 - h_1)$

$\dot{Q}_{evap} = \dot{m}_{NH3} \cdot (h_7 - h_6)$

Perfomance

$COP_{HP} = \frac{\dot{Q}_{heat}}{\dot{W}_{comp}}$

$COP_{Carnot} = \frac{T_{cond}}{T_{cond} - T_{evap}}$

$\eta_{HP} = \frac{COP_{HP}}{COP_{Carnot}}$

Figure J.4: EES simulation code for the NH_3 with IHX heat pump cycle.

The following figures show the EES simulation code with the geometric and thermodynamic characteristics of the heat exchangers. In order to be possible to calculate the exit temperature at the heat exchangers it was necessary to do a iteration process through the EES software. For that it was necessary to establish a Procedure control in the software. This simulations allows to establish a relationship between waterside temperatures and the working fluid temperatures.

```
Air-to-Water Transcritical CO2 Heat Pump - IHX configuration

1: Low-pressure side of the IHX exit and compressor inlet
2: Compressor discharge state and gas cooler inlet
3: Gas cooler exit and high-pressure side of the IHX inlet
4: High-pressure side of the IHX exit and expansion valve inlet
5: Expansion valve exit and evaporator inlet
6: Evaporator exit and low-pressure side of the IHX inlet
 For T_amb < 10 °C
 m_w=0.2936 [kg/s]
 W_comp=17.52
SUBPROGRAM solver (T1_guess, T_evap, T_w,i, T_w,o, P_gc : T_1, T_2, T_3, Q_gc, Q_evap, W_ccmp, m_w, COP_HP, p_r, P_opt, m_CO2)
 m_CO2 = 0.2813 [kg/s]
 η_s,comp = 0.7
 ε_ihx = 0.6
 cp_w = 4.1868 [kJ/(kg*K)]
 A_gc = 1.06 [m^2]
 U_gc = 1.66 [kW/((m^2)*C)]
 P_evap = P_sat (R744 , T = T_evap)
 T_6 = T_evap
 x_6 = 1
 P_6 = P (R744 , T = T_6, x = x_6 )
 h_6 = h (R744 , T = T_6, x = x_6 )
 s_6 = s (R744 , T = T_6, x = x_6 )
 P_5 = P_6
 T_5 = T_6
 P_2 = P_gc
 P_7 = P_gc
 P_1 = P_6
```

$$h_1 = \mathbf{h}(R744, T = T1_{guess}, P = P_1)$$

$$s_1 = \mathbf{s}(R744, T = T1_{guess}, P = P_1)$$

$$s_7 = s_1$$

$$h_7 = \mathbf{h}(R744, s = s_7, P = P_7)$$

$$T_7 = \mathbf{T}(R744, P = P_7, s = s_7)$$

$$h_2 = \frac{h_7 - h_1}{\eta_{s,comp}} + h_1$$

$$T_2 = \mathbf{T}(R744, P = P_2, h = h_2)$$

$$s_2 = \mathbf{s}(R744, T = T_2, P = P_2)$$

$$P_3 = P_{gc}$$

$$T_3 = T_{w,i} + \frac{T_2 - T_{w,o}}{\exp\left[\frac{(T_2 - T_{w,o} - T_3 + T_{w,i}) \cdot A_{gc} \cdot U_{gc}}{\dot{m}_w \cdot cp_w \cdot (T_{w,o} - T_{w,i})}\right]}$$

$$h_3 = \mathbf{h}(R744, T = T_3, P = P_3)$$

$$\dot{m}_w \cdot cp_w \cdot (T_{w,o} - T_{w,i}) = \dot{m}_{CO2} \cdot (h_2 - h_3)$$

$$h_4 = h_3 - h_1 + h_6$$

$$h_5 = h_4$$

$$P_4 = P_{gc}$$

$$T_4 = \mathbf{T}(R744, P = P_4, h = h_4)$$

$$\frac{T_1 - T_6}{T_3 - T_6} = \varepsilon_{ihx}$$

$$\dot{Q}_{gc} = \dot{m}_{CO2} \cdot (h_2 - h_3)$$

$$P_{gc,t} = 4.9 + 2.256 \cdot T_3 - 0.17 \cdot T_{evap} + 0.002 \cdot T_3^{\,2} \cdot 10^2$$

$$\dot{Q}_{evap} = \dot{m}_{CO2} \cdot (h_6 - h_5)$$

$$\dot{W}_{comp} = \dot{m}_{CO2} \cdot (h_2 - h_1)$$

$$p_r = \frac{P_2}{P_6}$$

$$P_{opt} = (4.9 + 2.256 \cdot T_3 - 0.17 \cdot T_{evap} + 0.002 \cdot T_3^{\,2}) \cdot 10^2$$

$$\eta_{s,t} = 1.003 - 0.121 \cdot p_r$$

$$COP_{HP} = \frac{\dot{Q}_{gc}}{\dot{W}_{comp}}$$

END **solver**

```
Procedure control (T1guess, Tevap, Tw,i, Tw,o, Pgc : T1, T2, T3, Q̇gc, Q̇evap, Ẇccmp ṁw, COPHP, pr, Popt, ṁCO2)
  nmax := 100
  dTmin := 0.0001
  n := 0
  T1 := T1guess
  Repeat
    Temp1 := T1
    Call solver (Temp1 , Tevap , Tw,i , Tw,o , Pgc : T1 , T2 , T3 , Q̇gc , Q̇evap , Ẇccmp , ṁw , COPHP , pr , Popt , ṁCO2 )
    n := n + 1
    dT := |Temp1 – T1 |
  Until ((n = nmax ) or (dT < dTmin ))
End control

Tevap = 0 [C]
Tw,i = 10 [C]
Tw,o = 60 [C]
Pgc = 8600 [kPa]
T1guess = 21 [C]
Call control (T1guess , Tevap , Tw,i , Tw,o , Pgc : T1 , T2 , T3 , Q̇gc , Q̇evap , Ẇccmp , ṁw , COPHP , pr , Popt , ṁCO2 )
```

Figure J.5: EES simulation code and procedure control for determination of the outlet temperature of the heat exchangers based on waterside temperatures (CO_2 IHX configuration).

SUBPROGRAM **solver** ($T3_{guess}$, T_{evap} : T_3, COP, W_{comp}, $Q_{heating}$)

T_{cond} = 40

T_{sh} = 5

T_{sc} = 3

$T_{w,i,cond}$ = 10

$T_{w,o,cond}$ = 35

$T_{w,i,dsh}$ = 35

$T_{w,o,dsh}$ = 60

$\eta_{isen,comp}$= 0.773

$\dot{m}_{w,dsh}$=0.08799 [kg/s]

$\dot{m}_{w,cond}$=0.4664 [kg/s]

W_{comp}=10.59

$\dot{m}_{NH3}$ = 0.04311

cp_w = 4.1868 [kJ/(kg*K)]

A_{cond} = 1.18

U_{cond} = 2.8

A_{dsh} = 0.48

U_{dsh} = 0.676

P_{evap} = $\mathbf{P}_{sat}$ (R717 , T = T_{evap})

P_{cond} = $\mathbf{P}_{sat}$ (R717 , T = T_{cond})

State 1 - Compressor inlet

T_1 = T_{evap} + T_{sh}

P_1 = P_{evap}

h_1 = $\mathbf{h}$ (R717 , P = P_{evap}, T = T_1)

s_1 = $\mathbf{s}$ (R717 , P = P_{evap}, T = T_1)

State 2 - Desuperheater inlet

P_2 = P_{cond}

Isentropic Conditions

s_8 = s_{2i}

h_8 = $\mathbf{h}$ (R717 , s = s_{2i}, P = P_2)

s_{2i} = s_1

h_{2i} = $\mathbf{h}$ (R717 , s = s_{2i}, P = P_{cond})

$$\eta_{isen,comp} = \frac{h_{2i} - h_1}{h_2 - h_1}$$

T_2 = $\mathbf{T}$ (R717 , P = P_{cond}, h = h_2)

```
"!State 3 - Condenser inlet"

P[3]=P_cond

T[3]=T_w_i_dsh+(T[2]-T_w_o_dsh)/(exp(((T[2]-T_w_o_dsh-T3_guess+T_w_i_dsh)*A_dsh*U_dsh)/(m_dot_w_dsh*cp_w*(T_w_o_dsh-T_w_i_dsh))))

h[3]=enthalpy(R717,T=T3_guess,P=P[3])

"!State 4 - EEV inlet"

P[4]=P_cond

T[4]=T_cond-T_sc

h[4]=enthalpy(R717,T=T[4],P=P[4])


"!State 5 - Evaporator inlet"

T[5]=T_evap
P[5]=P_evap

h[5]=h[4]

x[5]=quality(R717,h=h[5],P=P[5])

"!Energy Balance"

Q_dsh=m_dot_NH3*(h[2]-h[3])

Q_cond=m_dot_NH3*(h[3]-h[4])

m_dot_w_cond*cp_w*(T_w_o_cond-T_w_i_cond)=m_dot_NH3*(h[3]-h[4])

m_dot_w_dsh*cp_w*(T_w_o_dsh-T_w_i_dsh)=m_dot_NH3*(h[2]-h[3])

 "!Perfomance"

W_comp=m_dot_NH3*(h[2]-h[1])

Q_evap=m_dot_NH3*(h[1]-h[5])

Q_heating=Q_dsh+Q_cond

COP=Q_heating/W_comp

P_r=P_cond/P_evap

eta_v=1.02*exp(-0.063*P_r)

eta_s=eta_v/exp(-1.69*((T_cond+273.15)/(T_evap+273.15))+1.97)

End
```

```
Procedure control(T3_guess,T_evap:T[3],COP,W_comp,Q_heating)

    nmax = 100
    dTmin = 0.0001

    n:=0
    T[3] := T3_guess

    Repeat

        Temp3 = T[3]
        Call solver(Temp3,T_evap:T[3],COP,W_comp,Q_heating)
        n := n +1
        dT = abs(Temp3-T[3])

    Until ((n=nmax) or (dT < dTmin))

End

T_evap=0

T3_guess=25

Call control(T3_guess,T_evap:T[3],COP,W_comp,Q_heating)
```

Figure J.6: EES simulation code and procedure control for determination of the outlet temperature of the heat exchangers based on waterside temperatures (NH_3 conventional configuration).